Draft Report: Conceptualization, Investigation, and Sensitivity Analysis Regarding the Effects of Faults on Groundwater Flow in the Carrizo-Wilcox Aquifer in Central Texas

Prepared By

Steven Young, PhD, PE, PG
Marius Jigmond
Toya Jones, PG
Daniel Lupton, PG
INTERA Incorporated

Tom Ewing
Frontera

Bob Harden
RW Harden & Associates

March 1, 2017

This page is intentionally blank.

Executive Summary

In response to a directive from the 81st Legislature, the Texas Commission on Environmental Quality conducted a study on the characteristics and impacts of groundwater planning in the Carrizo-Wilcox Aquifer. Evaluation of the Queen City and Sparta aquifers groundwater availability models, which are the planning tools accepted by the Texas Water Development Board for the Carrizo-Wilcox Aquifer, included as part of the study identified the inclusion of faults as barriers to flow and fault locations in the central groundwater availability model as critical issues in water planning for the aquifer. The location and sealing nature of faults in the central model have a minor effect on model calibration, but have a major impact on predicted future drawdowns because future pumping is anticipated in the vicinity of the faults. Therefore, appropriate representation of fault locations and hydraulic properties in the central groundwater availability model is important for future water planning purposes.

This study provides an assessment of the impact of including faults in the central Carrizo-Wilcox Aquifer, and the conceptualization of the faults, in the groundwater availability model for the aquifer. The results of the assessment will be considered in development of an updated central Queen City and Sparta aquifers groundwater availability model, which will provide the TWDB and groundwater conservation districts in Groundwater Management Area 12 with a better tool for evaluating and selecting desired future conditions for the central Carrizo-Wilcox Aquifer. Several mini investigations were conducted as part of the assessment. These included (1) a geological investigation of the Milano Fault Zone to develop a method for mapping faults associated with the fault zone and estimating their vertical offset, (2) a modeling investigation to evaluate the sensitivity of predicted water levels to the conceptualization of faults in the Milano Fault Zone, and (3) an investigation of observed data from aquifer pumping test to determine if those data provide sufficient evidence to support representing the Milano Fault Zone in the groundwater availability model.

The geologic investigation resulted in the mapping of faults in the Milano Fault Zone based on interpretation of geophysical logs evaluated in conjunction with faults mapped at the ground surface. The results of this investigation provided evidence supporting a different conceptualization of the faults in the Milano Fault Zone than that used in the central Queen City and Sparta aquifers groundwater availability model. The current model represents the faults as long, continuous sealing faults extending across multiple counties. In contrast, this study found that the fault zone consists of four grabens and one complex, and includes areas with no faults, through which groundwater can flow more freely than in the areas with faults. In addition to the different conceptualization of the faults, the overall footprint of the faults in the Milano Fault Zone determined by this study is smaller than that in the groundwater availability model and, in two areas, evidence to support long sealing faults present in the model was not seen in our investigation.

A modeling investigation was conducted to evaluate the sensitivity of simulated historical water levels to three conceptualizations of faults in the Milano Fault Zone: the faults as represented in the current groundwater availability model, no faults, and the faults identified through our geologic investigation. The modeling indicates that the conceptualization of faults in the current

model results in simulated drawdowns that are 60 to 150 feet greater than observed drawdowns in areas of high pumping located downdip of the fault zone. The difference between simulated and observed drawdowns was much less for the model with no faults and the model with the faults from this study (root mean squared error of 25 and 37 feet, respectively) than for the model with the current fault conceptualization (root mean squared error of 97 feet). A comparison of the maximum predicted drawdown for the period from 2010 to 2070 for the three fault conceptualizations indicates that the model with the current faults predicts a drawdown 265 feet larger than that predicted by the model with no faults and the one with the faults from this study in Burleson County and more than 100 feet in Bastrop, Brazos, Lee, Milam and Robertson counties.

The Cooper-Jacob straight line method was used to interpret aquifer pumping test data for 113 tests to see if data collected in wells located near faults showed evidence of changes in aquifer transmissivity with distance from the well. A change in the slope of the semi-log plot of the time-drawdown data indicates a change in aquifer transmissivity. For tests with two slopes for wells located near faults, a transmissivity calculated from the late-time slope that is lower than the transmissivity calculated from the early-time slope provides a line of evidence that the faults were affecting groundwater flow during the test. A statistical analysis of the aquifer test interpretations demonstrated that the closer a well is located to one of the faults identified in this study, the more likely the aquifer test data indicate a region of low transmissivity located near the well.

The findings from this study indicate that the conceptualization of the Milano Fault Zone in the current Queen City and Sparta aquifers groundwater availability model is inconsistent with the results of our geological investigation; results in predicted historical water levels that are significant lower than observed water levels, especially in areas of high pumping located downdip of the fault zone; and contains a long, continuous sealing fault in Burleson and Robertson counties that is not support by the geologic evidence or observed data from aquifer pumping tests conducted in wells location near the fault. Evidence does support the presence of faults in the Milano Fault Zone that impact groundwater flow; therefore, some representation of this fault zone should be included in an updated groundwater availability model. The faults identified through this study are consistent with the available geologic and hydrogeologic data and, when incorporated in the model, provide a better match to observed water-level data than does the current groundwater availability model. This study recommends that the current conceptualization of the Milano Fault Zone in the central Queen City and Sparta aquifers groundwater availability model be abandoned ant the work begun here continue so that the faults identified through this study can be incorporated into the updated groundwater availability model.

Geoscientist and Engineering Seal

This document is released for the purpose of interim final review under the authority of Steven C. Young (P.G. 231). It is not to be used for construction, bidding, permitting, or any other purposes not specifically sanctioned by the authors.

_____ _____

Signature Date

This page is intentionally blank.

TABLE OF CONTENTS

LIST OF FIGURES

LIST OF TABLES

This page is intentionally blank.

1 Introduction

Under the Texas Water Development Board's (TWDB) Groundwater Availability Modeling Program, groundwater availability models of the northern, central, and southern portions of the Carrizo-Wilcox Aquifer were completed in 2003 by two different contractors, with one contractor developing the northern and southern models (Fryar and others, 2003; Deeds and others, 2003, respectively) and one developing the central model (Dutton and others, 2003). In 2004, three groundwater availability models for the Queen City and Sparta aquifers (northern, central, and southern), which included the underlying Carrizo-Wilcox Aquifer, were developed by Kelley and others (2004). Development of the Queen City and Sparta aquifers groundwater availability models addressed several inconsistences between the Carrizo-Wilcox Aquifer groundwater availability models, and these models are now the TWDB-accepted water planning tools for use in evaluating the groundwater resources in the Carrizo-Wilcox Aquifer as well as the Queen City and Sparta aquifers.

In 2009, the 81st Legislature directed the Texas Commission on Environmental Quality to conduct a study of the characteristics and impacts on groundwater planning in the Carrizo-Wilcox Aquifer. That study, which included evaluation of the three Queen City and Sparta aquifers groundwater availability models, identified two critical issues deserving attention: (1) whether the central portion of the aquifer should include faults as barriers to flow and (2) evaluation of the location of those faults. Although the degree to which faults in the central model are sealing has a minor effect on the model calibration, it has a major impact on predicted future drawdowns because future pumping is anticipated in the vicinity of the faults. Therefore, appropriate representation of fault locations and hydraulic properties in the central model is important for future water planning purposes.

The TWDB and several groundwater conservation districts in Groundwater Management Area 12, which is located in the boundary of the central Queen City and Sparta aquifers groundwater availability model (Figures 1-1 and 1-2), provided the funding to assess the impact of faults in the current central Queen City and Sparta aquifers groundwater availability model through (1) investigation of the faults in the central Carrizo-Wilcox Aquifer, specifically those in the Milano Fault Zone, and the most appropriate method for representing those faults in the model and (2) updating the model with historical pumping through 2010 and extending the calibration period to 2010. The updated model will provide groundwater conservation districts a better tool for evaluating and selecting desired future conditions for the Carrizo-Wilcox Aquifer.

A preliminary assessment of the faults in the central Carrizo-Wilcox Aquifer is the focus of this report. This assessment was conducted by:

- Reviewing geophysical logs to identify fault locations and offsets
- Performing model simulations with the central Queen City and Sparta aquifers groundwater availability model to investigate the sensitivity of predicted water levels to (1) the faults in the current groundwater availability model, (2) no faults, and (3) faults from this study.
- Evaluating differences between modeled and measured water levels for the three fault representations over a validation period from 2000 to 2010.

- Reviewing aquifer pumping test data to evaluate the sealing nature of the faults.

The primary objective of this report is to summarize activities associated with characterization of the faults and evaluation of the appropriateness of including the faults in the central Queen City and Sparta aquifers groundwater availability model. The final fault locations and properties, and the impact of faults on groundwater flow in the model, will be addressed in the subsequent report that documents the update to the central Queen City and Sparta aquifers groundwater availability model.

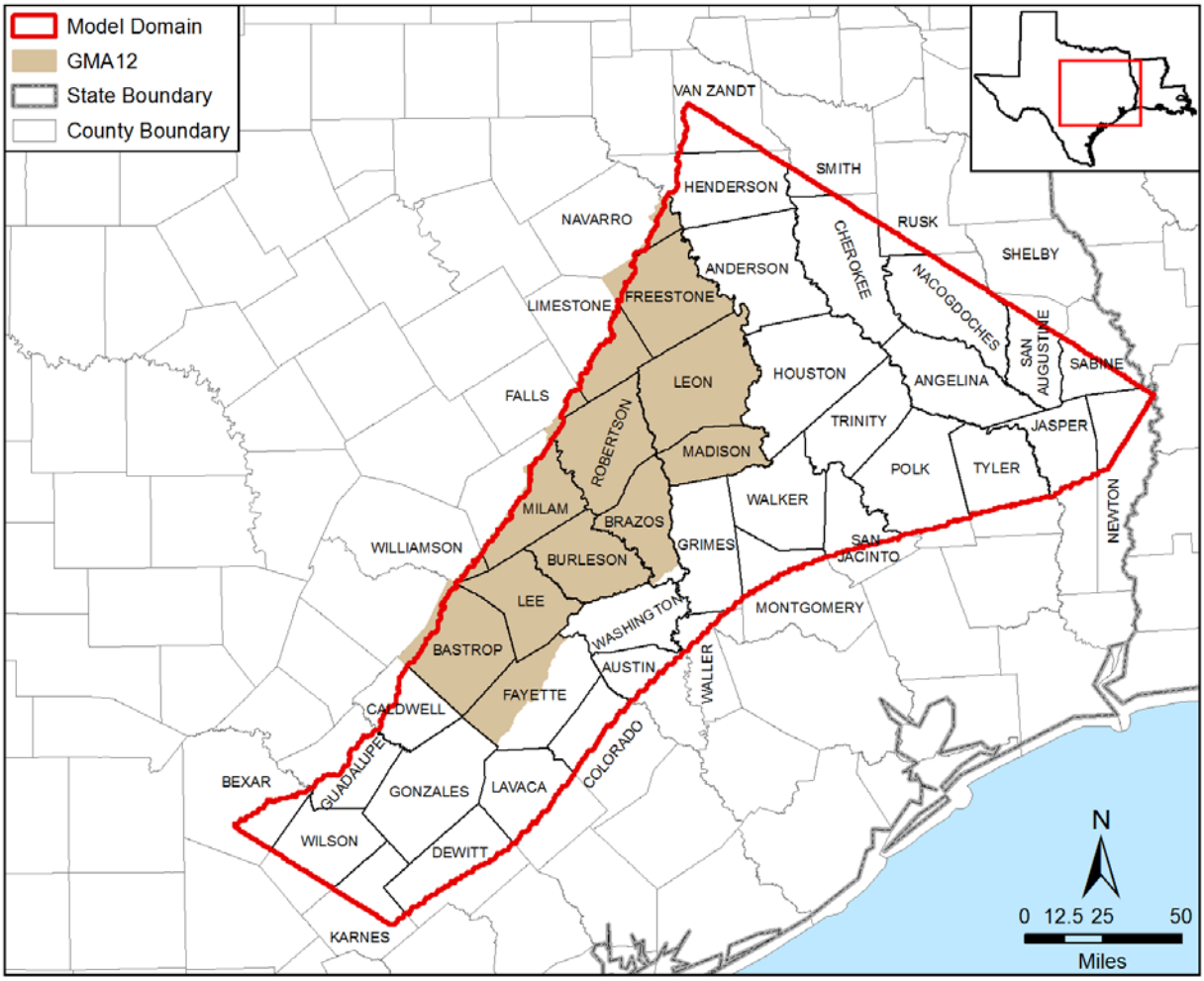

Figure 1-1. **Location of the model domain for the central Queen City and Sparta aquifers groundwater availability model (Kelley and others, 2014) and Groundwater Management Area (GMA) 12.**

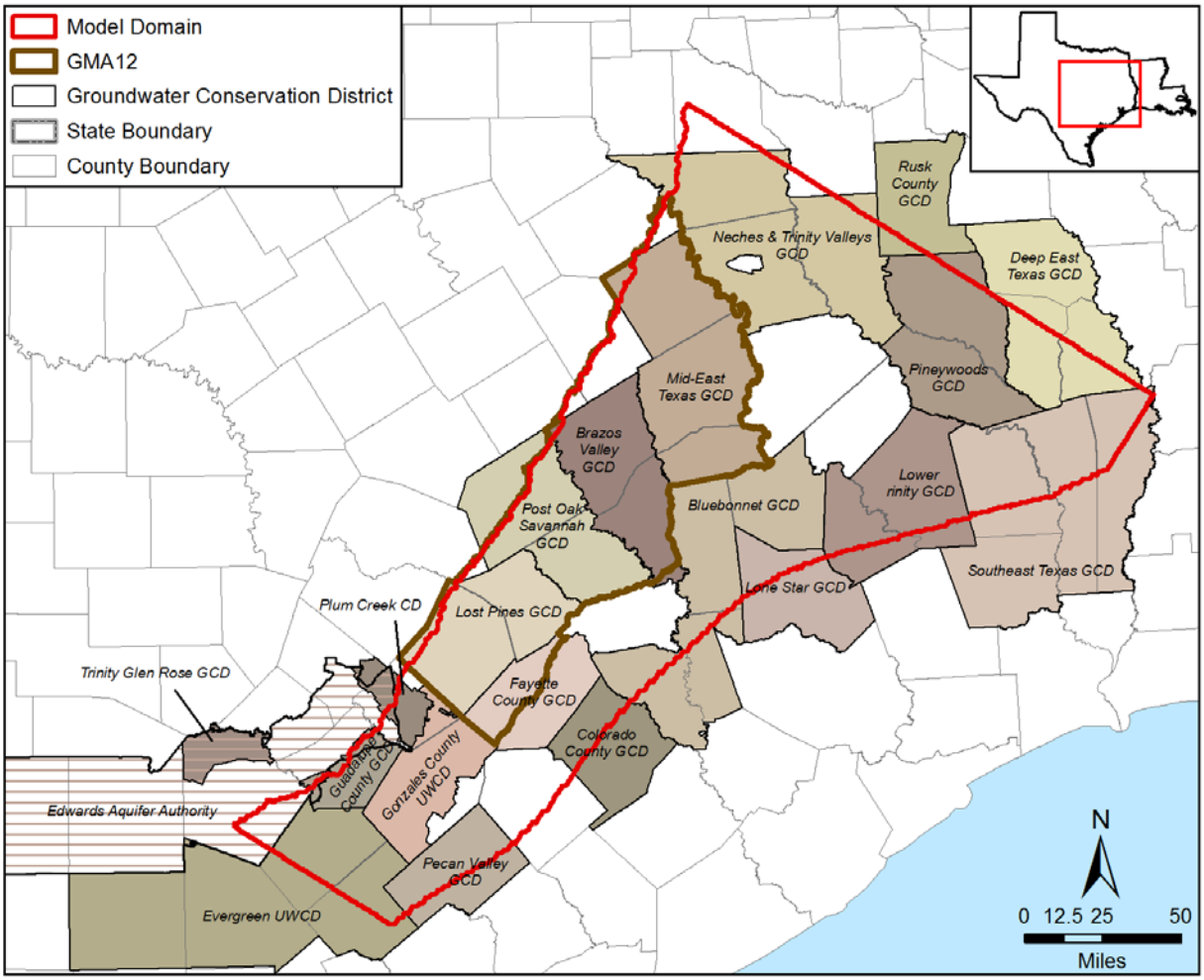

Figure 1-2. Location of the model domain for the central Queen City and Sparta aquifers groundwater availability model (Kelley and others, 2014) and Groundwater Conservation Districts (GCDs)

Note: GMA = Groundwater Management Area, UWCD = Underground Water Conservation District

2 Faults and Fault Zones in East Texas

2.1 Terms and Concepts Regarding Geologic Faults

Faults are surfaces or zones that separate two rock masses, along which one mass has slid past the other; a fault zone is a belt containing one or more faults of similar character (Ewing, 2016). To a geologist, an understanding of faults and the impacts that faults have on the occurrence and distribution of geologic units is just as important as understanding the geologic units themselves. In oil and gas, faults can serve as hydrocarbon traps in a myriad of different ways, and an understanding of how and where to drill a well is based on a complete understanding of how the faults have displaced the geologic units. For the mining geologist that is interested in following an ore seam, a single fault can make or break an entire prospect. For a hydrogeologist, faults can have a significant impact on flow in the groundwater flow system and must be accounted for when interpreting field data and developing groundwater models. .

The following explanation on faults has been adapted from the official United States Geological Survey website and is meant to be a primer on the types of faults that will be discussed in this report (USGS, 2017a). Figure 2-1 shows the major types of faults discussed in this report. Earth scientists use the angle of the fault with respect to the surface (known as the dip or the angle that a planar geologic surface is inclined from the horizontal) and the direction of slip along the fault to classify faults. Faults that move along the direction of the dip plane are known as dip-slip faults, and can be categorized as either normal or reverse (thrust) faults depending on the motion of the slip along the bedding plane. Faults that move horizontally are known as strike-slip faults, and can be classified as either right-lateral or left-lateral. Faults that show both dip-slip and strike-slip motion are known as oblique-slip faults. Within the oblique-slip fault family are the en echelon faults. En echelon faults are arranged in a staggered or overlapping manner; essentially, one fault takes over when another loses displacement, forming a ramp between them (Ewing, 2016). In summary,

- **Normal fault** - a dip-slip fault in which the hanging block above the fault has moved downward relative to the block below, called the foot block. This type of faulting, shown in Figure 2-1a, occurs in response to extension.
- **Reverse (thrust) fault** - a dip-slip fault in which the hanging block above the fault plane has moved up and over the lower block, called the foot block. This type of faulting, shown if Figure 2-1b, is common in areas of compression. is.
- **Strike-slip fault** - a fault on which the two blocks slide past one another along a horizontal plane (Figure 2-1c).
- **Graben fault** – a fault produced from parallel normal faults where the displacement of the hanging walls is upward, while that of the foot wall is downward (Figure 2-1d).
- **En echelon fault** – oblique-slip faults arranged in a staggered or overlapping manner (Figure 2-1e).

2.2 Overview of Fault Systems in East Texas

For this study, which is wholly contained within the Milano Fault Zone, we have used geophysical logs along with expert knowledge to better understand how/if faults impact the groundwater flow within the Wilcox Group. To understand the nature of the Milano Fault Zone, it is first necessary to discuss east Texas faults more generally and explain the mechanism for the various types of faults and how those mechanisms result in different fault system types. Each one is unique, yet similar enough to be classify based on location, activation, and resulting geometries. The structure of east Texas is dominated by a series of arches/uplifts and embayments, all of which are transected by faults (Figures 2-2 and 2-3). Figure 2-3e shows how the general nature and geometry of the major fault systems change from the Ouachita Front towards the Gulf of Mexico. These faults can generally be separated into four categories:

1) **Basement-Related:** these faults are related to the contemporaneous uplift of the Edwards Plateau and subsidence of the Gulf Coast Basin due to sediment loading (Ewing, 2016). The two forces acted in opposition to one another, resulting in extension of the upper crust and faulting along the paleo-Ouachita suture belt, a preexisting zone of weakness.
   - **Balcones Fault Zone:** A band of normal faults that extends from the Uvalde area in southwest Texas, north through San Antonio and Austin, and up through possibly Waco (Ewing, 2016). These faults occur landward of the pinchout of the Jurassic Louann Salt and seaward of the limit of the Ouachita thrust front and penetrate through to upper Paleozoic sediments.
   - **Luling Fault Zone:** The trend of this fault zone is similar in nature and history to that of the Balcones Fault Zone and occurs approximately 30 miles to the southeast. Towards the southwest, in the vicinity of San Antonio, it is likely that these two fault systems merge.
2) **Wilcox Fault Zone**: In the Paleocene and early Eocene, massive deltas of the Wilcox Group prograded the shelf margin, depositing large quantities of sediments on the Lower Cretaceous shelf. As the deltas prograded past the Lower Cretaceous shelf margin, deep district faults, or normal faults whose dip decreases with depth, began to form (Ewing, 1991). These faults were active during deposition of the Wilcox Group and, in some cases, resulted in deltaic sections that were five times thicker than other non-faulted areas. The Wilcox Fault Zone is essentially a zone of systematic growth faults centered on the Lower Cretaceous shelf margin.
3) **Growth Faulting**: Growth faults exist throughout the Gulf Coast Basin and are so prevalent that they were not shown on Figure 2-2. These faults occur primarily in the Tertiary section of the Gulf Coast and are related to the progradation of major sand- and mud-rich deltas across the subsiding Lower Cretaceous shelf margin and, subsequently, clastic depocenters atop the Lower Cretaceous shelf margin. Rapid deposition of deltaic sands over slope and basinal muds created an overpressuring of the deep, mud-rich units and that resulted in a mechanically unstable section (Ewing, 1991). This loading on mechanically unstable substrate resulted in prevalent syndepositional normal/growth faulting throughout the Gulf Coast Basin.
4) **Movement of Salt**: Primarily because of the relationship to the trapping of hydrocarbons, much research has been conducted on the nature of salt deposits and impacts on contacting geologic units. The following gross over simplification of salt structures in the Gulf Coast Basin was taken from Jackson (1982), Jackson and Seni (1984), and Jackson

and others (2003). These reports should be consulted for any additional information that is required. All salt related structures (domes, pillows, diapirs, etc.) in the Gulf Coast Basin are sourced through the Jurassic (Callovian) Louann Salt. The formation of salt structures from the Louann Salt by gravitationally induced flow has impacted the thickness, lithology, and structure of overlying geologic units from Late Jurassic to present. For the purposes of this study, salt related faulting can be simplified into two categories:

- **Salt anticline related faulting**: Salt domes are geologic structures that grow and develop as sediments are being deposited around them (Jackson and Seni, 1984; Halbouty, 1979). Salt, which is a low-density, ductile mineral, is gravitationally mobilized by sediment loading, forming a variety of upwelling structures. The growth of salt structures, in turn, influences the structure and stratigraphy of surrounding sediments and sedimentary rocks. The zone of uplift near the dome is surrounded by areas of subsidence and downwarping caused by salt withdrawal at depth. In addition to influencing sedimentation patterns, this subsidence and downwarping induces both syndepositional and postdepositional faulting. The geometry of faults induced by anticlinal salt structures is diverse and often specific to each structure. Anticlinal salt structures provide a variety of natural resources, including prolific petroleum reservoirs, salt and sulfur mining, and space for the storage of hydrocarbon reserves (most commonly liquefied petroleum gas) and potential disposal of chemical and radioactive wastes, although this has not been put into practice as of yet (Young and others, 2012).
- **Wedgeout of the Louann Salt**: From south to north, the Karnes, Milano, Mexia, and Talco fault zones are related to gravity/loading induced deformation of the Louann Salt (Figure 2-2). At the landward margin of the autochthonous salt basin, faulting is primarily extensional in nature, and the spatial relationship between the fault and the updip limit of the Louann Salt suggests that they accommodate a discontinuity created at the salt limit (Jackson, 1982). Essentially, these faults formed by the downdip sliding of the post-salt sedimentary column on the weak, fluid salt layer (Figure 2-4,). These systems are termed **peripheral graben systems** and are characterized by strike-parallel normal faults forming narrow grabens.

2.3 Overview of Peripheral Graben Fault Systems in East Texas

Peripheral graben systems are a distinctive feature of the Gulf Coast Basin and can be mapped continuously from Frio County, Texas northeast, north and east around the basin margin into the Texarkana area and eastward all the way to Florida. The graben systems go by various names but, in Texas, these are the Charlotte-Jourdanton Fault Zone, the Karnes Trough/Fault Zone, the Milano Fault Zone, the Mexia Fault Zone, and the Talco Fault Zone (commonly combined into the Mexia-Talco Fault Zone). Figure 2-2 shows four of these fault zones. The unifying feature of all of these fault zones in Texas is that they are full grabens bounded by normal faults on the updip and downdip side, with many of them extending tens of miles along strike. Between the full grabens are zones characterized by discontinuous, en echelon normal faults with down-to-the-basin displacement (Figure 2-3).

Relative ductility and low shear strength of the salt allowed decollement and basinward creep of the overlying strata. Where the edge of salt paralleled structural strike, the sliding column “pulls

away" from the fixed edge, where the salt is absent, a gap is formed that is filled with a relatively thickened series of sediments. Seismic and well information indicates that these fault complexes have been growing since the Late Jurassic and penetrate rocks as young as Eocene (Ewing, 1991). Where the edge of salt crosses structural strike, the fixed and moving masses sear past each other, creating the discontinuous, en echelon (stair step) structures that characterize the region between the bounding normal faults.

2.4 Previous Studies of the Milano Fault Zone

Work characterizing the geometry of peripheral fault grabens in the Gulf Coast of Texas is primarily represented by the reports Fault Tectonics of the East Texas Basin (Jackson, 1982); Tectonic Map of Texas (Ewing and others, 1990), and Salt-Related Fault Families and Fault Welds in the Northern Gulf of Mexico (Jackson and others, 2003). Other contributors to the location and stratigraphic/structural impacts of these faults on the Wilcox Group are Ayers and Lewis (1985), who drew faults at the top of the Simsboro Formation when creating contour maps of structure and thickness of the Wilcox Group and its member units and Barnes (1970; 1979; 1981), whose surface mapping showed that these peripheral fault grabens are still active in some areas.

Figure 2-5 shows faults digitized from georeferenced portable document format (PDF) copies of Ayers and Lewis (1985) in their study of lignite in the Wilcox Group. The locations of these faults were generally drawn on the base of the Wilcox Group\top of the Midway Group. Figure 2-6 shows faults taken from the digitized Geographic Information System (GIS) version of the Tectonic Map of Texas (Ewing and others, 1990). The fault locations were based on GEOMAP, a commercial mapping service and were drawn on the top of the Austin Chalk, a fairly recognizable pick on geophysical logs. Figure 2-7 shows faults from the GIS version of the Geologic Atlas of Texas (Stoeser and others, 2007) at surface.

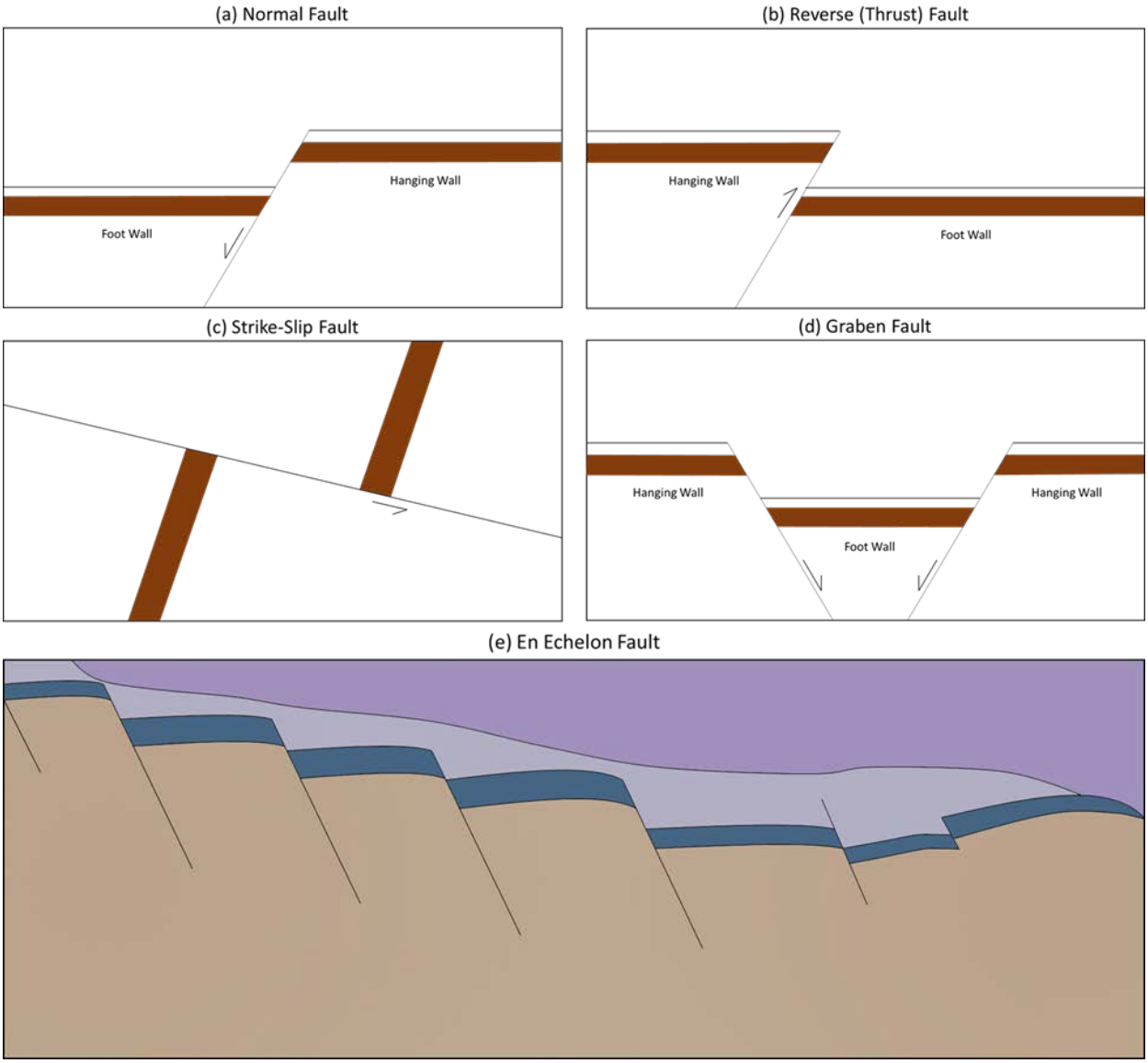

Figure 2-1. Schematics of various types of faults that occur in East Texas.

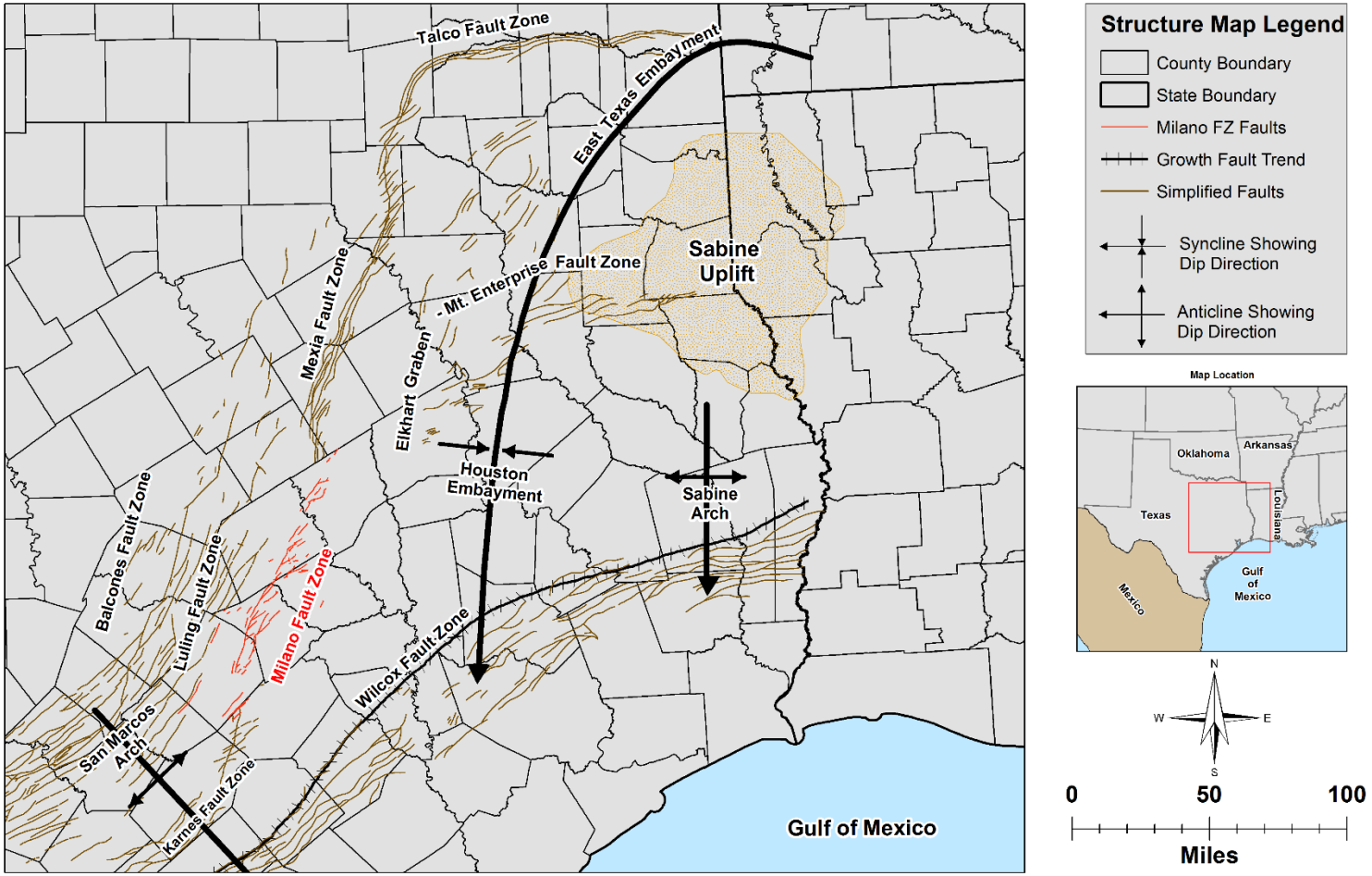

Figure 2-2. Regional structural features in east Texas. Faults modified from Ewing and others (1990). Structure axes modified from Guevara and Garcias (1972), Galloway (1982), and Galloway and others (2000). Milano Fault Zone is highlighted in red.

Note: FZ = fault zone

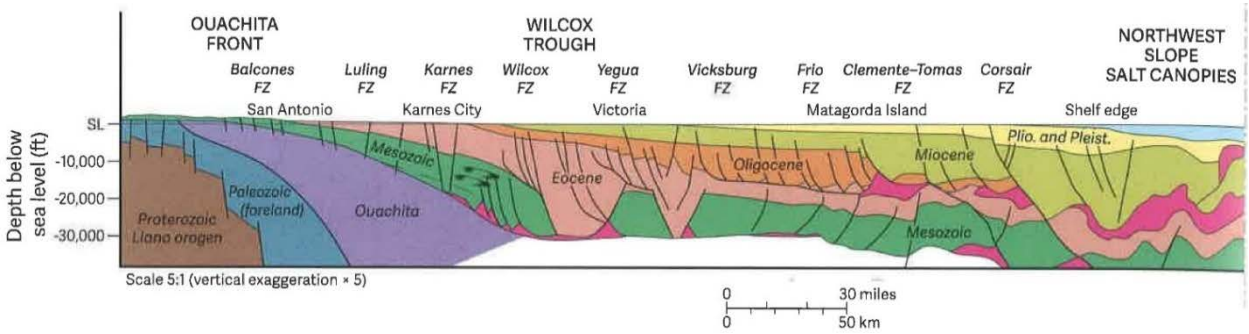

Figure 2-3. Crustal cross section of northwest margin of the Gulf of Mexico showing the main sedimentary packages and their deformation by fault systems (black lines) and mobile salt (red) (from Ewing, 2016).

Note: FZ = fault zone

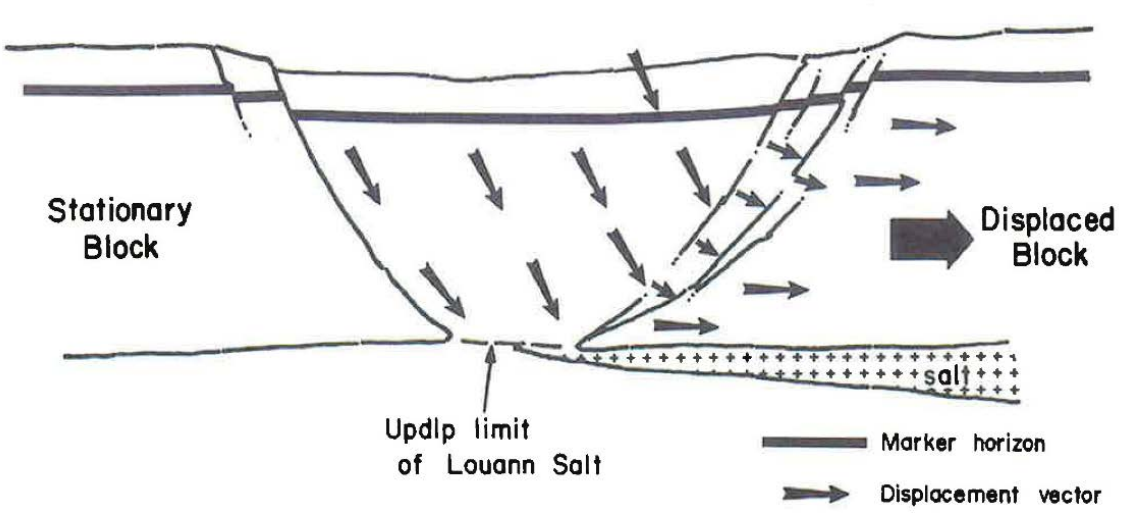

Figure 2-4. Conceptual diagram of a symmetric peripheral graben formed by extension due to gravitational sliding on a displaced block over a décollement zone of weak Louann Salt (from Jackson, 1982).

Note: FZ = fault zone

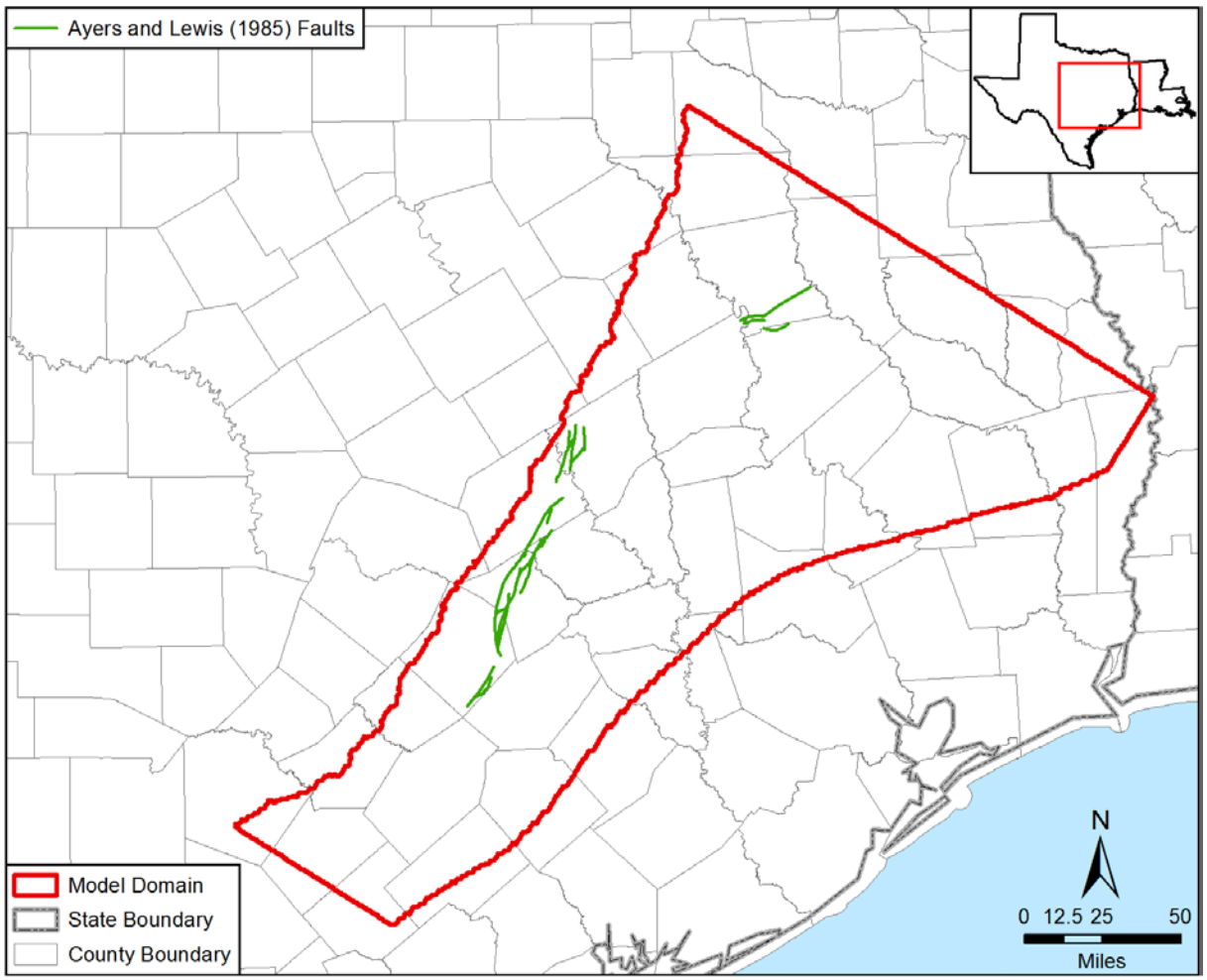

Figure 2-5. **Faults identified by Ayers and Lewis (1985) located in the model domain for the central Queen City and Sparta aquifers groundwater availability model (shown red).**

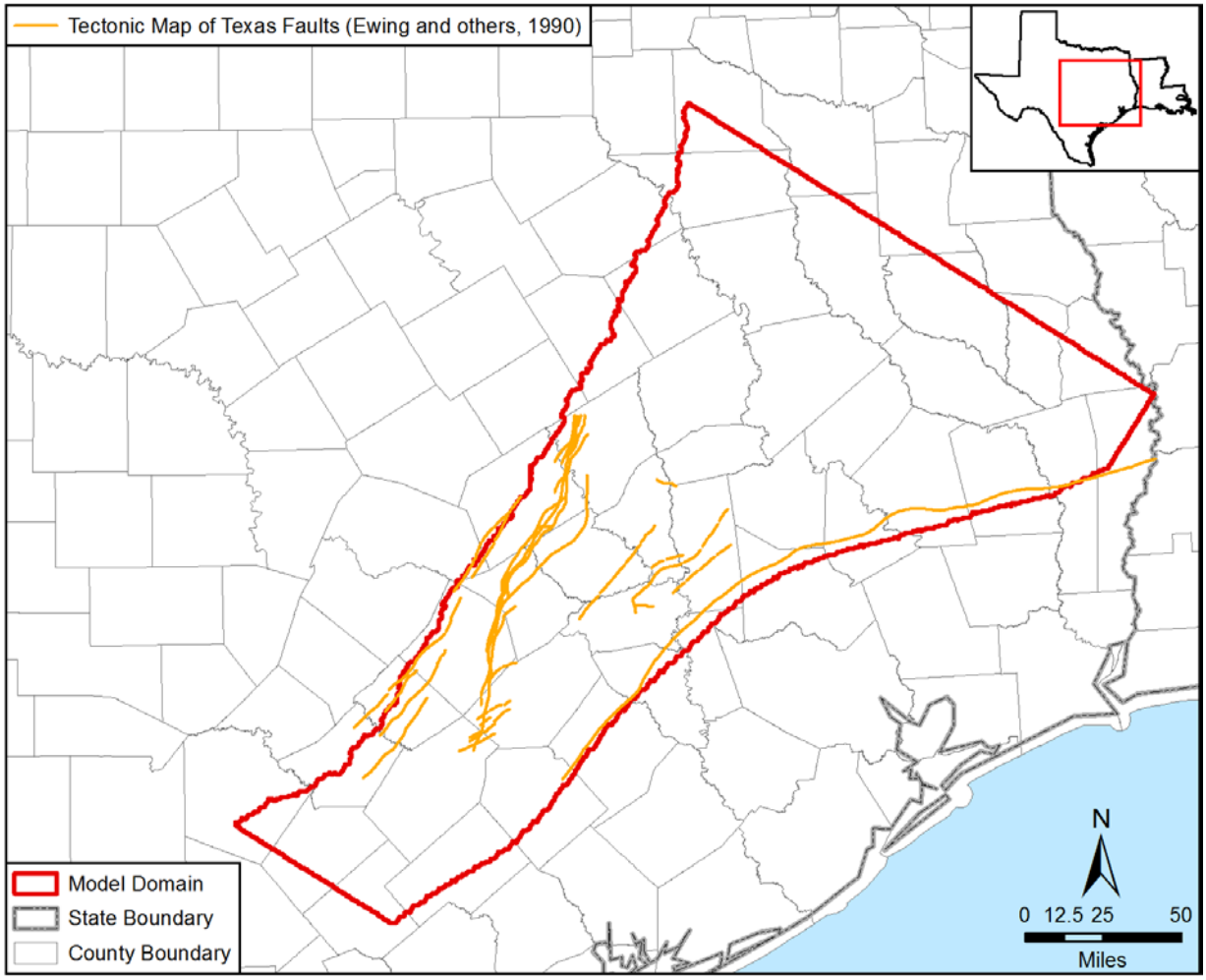

Figure 2-6. **Faults identified by Ewing and others (1990) located in the model domain for the central Queen City and Sparta aquifers groundwater availability model (shown red).**

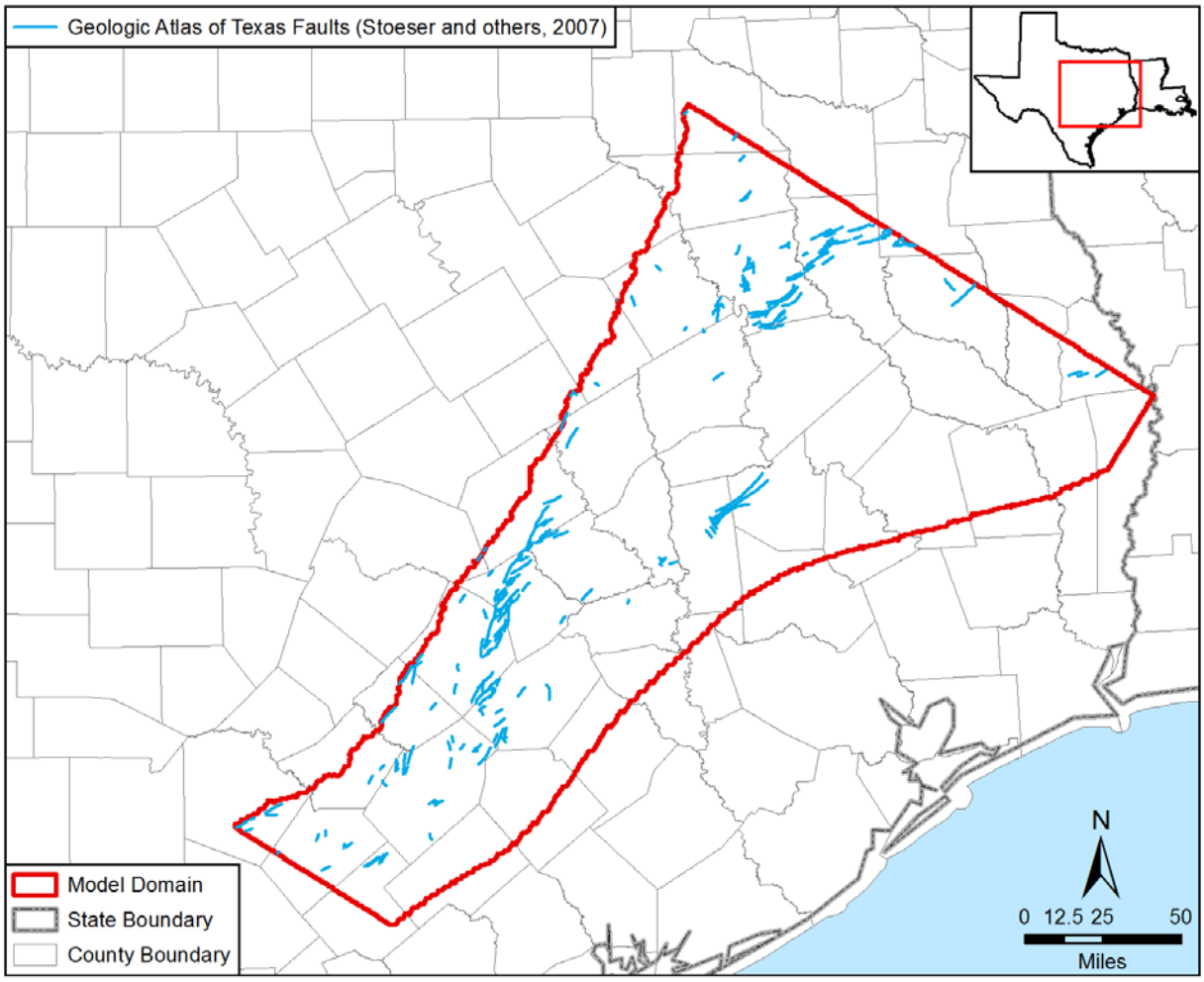

Figure 2-7. **Faults identified from the Geologic Atlas of Texas (Stoeser and others, 2007) located in the model domain for the central Queen City and Sparta aquifers groundwater availability model (shown red).**

3 Representation of Faults in the Central Queen City and Sparta Aquifers Groundwater Availability Model

This section provides an overview of the central Queen City and Sparta aquifers groundwater availability model and describes how faults are represented in that model.

3.1 Model Construction

The central Queen City and Sparta aquifers groundwater availability model consists of eight model layers. Table 3-1 lists the hydrostratigraphic unit represented by each layer. Figure 3-1 shows a conceptual schematic of the groundwater flow model for the aquifer system. Within the model domain, the Wilcox Aquifer is divided into three smaller aquifers: the Hooper (lower Wilcox), Simsboro (middle Wilcox), and Calvert Bluff (upper Wilcox) aquifers. As shown in Figure 3-1, the oldest and deepest hydrostratigraphic unit is the Hooper Formation. All the hydrostratigraphic units include an outcrop area that intersects the ground surface.

Table 3-1. Hydrostratigraphic Units Represented by the Model Layers in the Central Queen City and Sparta aquifers groundwater availability model.

Model Layer	Hydrostratigraphic Unit
1	Sparta
2	Weches
3	Queen City
4	Reklaw
5	Carrizo
6	Upper Wilcox (Calvert Bluff)
7	Middle Wilcox (Simsboro)
8	Lower Wilcox (Hooper)

Figure 3-2 shows the lateral boundaries of the central Queen City and Sparta aquifers groundwater availability model. The northwestern boundary is at the limit of the outcrop of the eight hydrostratigraphic units that comprise the groundwater availability model. The southwestern boundary lies near the San Antonio River. The northeast boundary runs from the aquifer outcrop in Van Zandt County, across part of the East Texas Basin and Sabine Uplift, and then continues to the deep part of the Carrizo-Wilcox Aquifer in Newton County. The southeastern boundary coincides with the Wilcox Fault Zone, which roughly marks the up-dip limit of geopressured conditions in the aquifer.

The central Queen City and Sparta aquifers groundwater availability model was developed from the central Carrizo Wilcox Aquifer groundwater availability model (Dutton and others, 2003). The central Carrizo-Wilcox Aquifer groundwater availability model has the same boundaries as the central Queen City and Sparta aquifers groundwater availability model and consists of six layers. The bottom four layers represent the Hooper, Simsboro, Calvert Bluff, and Carrizo aquifers. Model Layer 2 represents the Reklaw Formation, and Model Layer 1 represents all

formations younger than the Reklaw Formation. To construct the central Queen City and Sparta aquifers groundwater availability model, Kelly and others (2004) removed Model Layer 1 from the central Carrizo-Wilcox Aquifer groundwater availability model (Dutton and others, 2003) and replaced it with model layers to represent the Queen City Aquifer, the Weches Formation, and Sparta Aquifer.

The groundwater code used by Kelley and others (2004) to numerically represent the conceptual groundwater system shown in Figure 3-1 is MODFLOW-96 (Harbaugh and McDonald, 1996). MODFLOW-96 is a multi-dimensional, finite-difference, block-centered, saturated groundwater flow code which is supported by enhanced boundary condition packages to handle recharge, evapotranspiration, streams (Prudic, 1988), reservoirs (Fenske and others, 1996), and horizontal flow barriers (Hsieh and Freckleton, 1993). The model grid for the central Queen City and Sparta aquifers groundwater availability model consists of a uniform grid of square grid cells with an area of 1 square mile. Each layer represents the thickness of the aquifer or formation. The central Queen City and Sparta aquifers groundwater availability model has 48,321 grid cells per layer. The number of these grid cells that are active per layer varies and increases with the age of the hydrostratigraphic unit.

3.2 Horizontal Flow Barrier Package

The impact of geologic faults on groundwater flow in the central Queen City and Sparta aquifers groundwater availability model was implemented by using the Horizontal Flow Barrier (HFB) package of MODFLOW (Hsieh and Freckleton, 1993). The Horizontal Flow Barrier package provides the capability to place a groundwater flow barrier between two adjacent grid cells to impede groundwater flow. The key assumption underlying the Horizontal Flow Barrier package is that the width of the barrier is negligibly small in comparison with the horizontal dimensions of the cells in the grid. For the central Queen City and Sparta aquifers groundwater availability model, the horizontal leakance assigned to the horizontal flow barriers is the property that could affect groundwater flow. The horizontal leakance is defined as the horizontal flow barrier's hydraulic conductivity divided by the horizontal flow barrier's assumed width.

To illustrate the effect of a horizontal flow barrier on groundwater flow, a series of MODFLOW simulations was conducted to calculate flow through four grid cells as shown in Figure 3-3, with a horizontal flow barrier located between grid cells 2 and 3. The four grid cells have the same dimensions and properties, which are a length of 1,000 feet, a width of 100 feet, a thickness of 10 feet, and a hydraulic conductivity of 10 feet per day. Flow occurs through the four grid cells as a result of a constant head value of 200 feet mean sea level assigned to grid cell 1 and a constant head value of 100 feet mean sea level assigned to grid cell 4. The horizontal flow barrier has a length of 1 foot, but its hydraulic conductivity was varied between 1,000 and 0.0001 foot per day for the series of MODFLOW simulations. Without a horizontal flow barrier, the MODFLOW simulation produces a flow rate of 333.3 cubic feet per day.

The impact of inserting a horizontal flow barrier between grid cells 2 and 3 on the groundwater flow rate is summarized in Table 3-2. Table 3-2 shows that the hydraulic conductivity of the horizontal flow barrier needs to be less than 0.1 foot per day before the barrier decreases flow by

more than 3 percent. When the hydraulic conductivity of the horizontal flow barrier is set to 1E-5 foot per day, the flow rate is reduced to less than 1 percent of the flow rate without a horizontal flow barrier. The impact of a horizontal flow barrier on groundwater flow in a numerical model is dependent on a wide range of factors. As such, the specific relationship between reduction in groundwater flow and changes in the hydraulic conductivity of the horizontal flow barrier for the example simulations presented here cannot be applied universally throughout the groundwater availability model. What can be gleaned from the results in Table 3-2 that is of importance to using horizontal flow barriers to represent faults is that large reductions in groundwater flow across a horizontal flow barrier may not occur until the hydraulic conductivity of the barrier is lower than the hydraulic conductivity of the aquifer.

Table 3-2. Simulated impact of a horizontal flow barrier (HFB) on groundwater flow along the series of grid blocks shown in Figure 3-3 with lengths of 1,000 feet and a hydraulic conductivity of 10 feet per day.

Horizontal Flow Barrier Property			Groundwater Flow Rate (cubic feet per day)	Percent of Groundwater Flow to Base Case without HFB (percent)
Hydraulic Conductivity (feet per day)	Thickness (feet)	Horizontal Conductance (1/day)		
no HFB between the grid cells			333.3	100
1,000	1.0	1,000	333.3	100
100	1.0	100	333.3	100
10	1.0	10	333.3	100
1	1.0	1	333.3	100
0.1	1.0	0.1	322.6	97
0.01	1.0	0.01	250.0	75
0.001	1.0	0.001	76.9	23
0.0001	1.0	0.0001	9.7	3
0.00001	1.0	0.00001	1.0	<1

3.3 Representation of Faults

The central Queen City and Sparta aquifers groundwater availability model represents faults using horizontal flow barriers at the locations shown in Figure 3-4. All faults in the central Queen City and Sparta aquifers groundwater availability model are presumed to be 1 foot thick and are characterized as either sealing or non-sealing. The sealing faults are assigned a hydraulic conductivity of 0.0001 foot per day and the non-sealing faults are assigned a hydraulic conductivity of 0.9999 foot per day. The relatively high values of hydraulic conductivity assigned to the non-sealing faults prevents them from impacting groundwater flow in any meaningful way and serve primarily to indicate that a fault has been identified at that location.

In Figure 3-4, the locations of horizontal flow barriers are color-coded to indicate the model layer(s) in which the fault is presumed active. If a horizontal flow barrier penetrates from the Sparta Aquifer though the Hooper Aquifer, that barrier occurs in each of eight model layers at

the location indicated in Figure 3-4. In the up-dip portion of the model, the faults exist only in the deeper model layers, and in the down-dip region, the faults are present in all model layers.

The source for the fault locations shown in Figure 3-4 is not provided in Kelly and others (2004). Because most of the aquifer properties in the central Carrizo-Wilcox Aquifer groundwater availability model (Dutton and others, 2004) were incorporated into the central Queen City and Sparta aquifers groundwater availability model, a reasonable presumption is that the faults would be the same in the two models. However, the two models use different sets of horizontal flow barriers to represent faults. Figure 3-5 shows the location of the horizontal flow barriers in the central Carrizo-Wilcox Aquifer groundwater availability model. In Figure 3-5, the faults are categorized as sealing and non-sealing based on criteria developed by Dutton and others (2003). Although there are numerous similarities between the two sets of horizontal flow barriers in the two groundwater availability models, there are several significant differences. One significant difference is considerably more sealing faults in the Malino Fault Zone, especially in Burleson County, in the central Queen City and Sparta aquifers groundwater availability model than in the central Carrizo-Wilcox Aquifer groundwater availability model. Another significant difference is that both models have nearly identical horizontal flow barrier locations within the Mount Enterprise Fault Zone, but they represent sealing faults in the central Queen City and Sparta aquifers groundwater availability model and non-sealing faults in the central Carrizo-Wilcox Aquifer groundwater availability model.

Dutton and others (2003) attributed their fault locations in the Milano Fault Zone primarily to faults mapped by Ayers and Lewis (1984), and they explain that the criteria as to whether a fault was classified as sealing or non-sealing are based primarily on the estimated fault offset. Kelly and others (2004) do not include a discussion related to modifying the fault locations and properties from Dutton and others (2003). However, a review of the faults zones in Figure 2-6 suggests that Kelly and others (2004) used the faults from the Tectonic Map of Texas (Ewing and others, 1990) as a guide for placement of horizontal flow barriers.

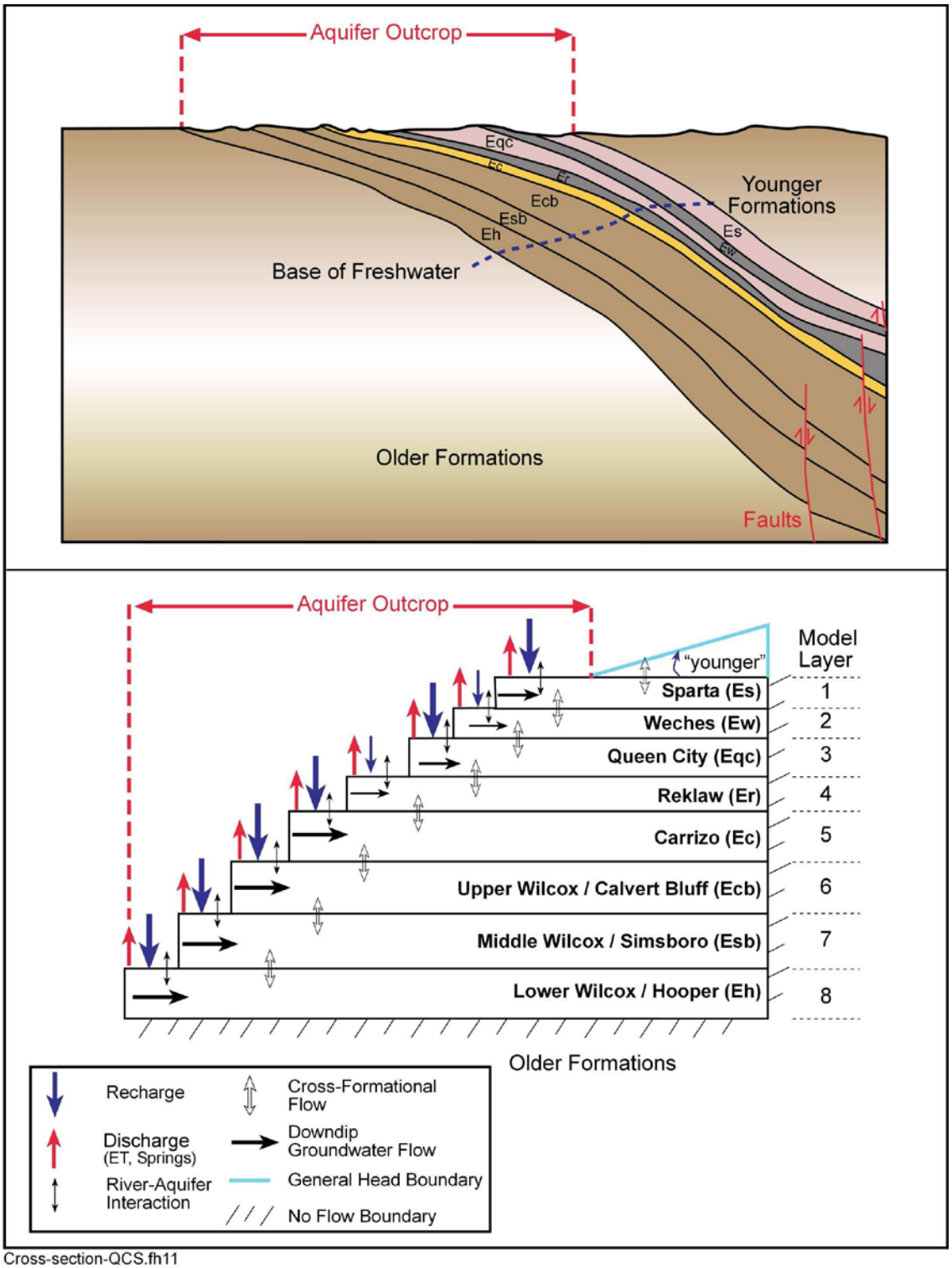

Figure 3-1. Conceptual groundwater flow model for the central Queen City and Sparta aquifers groundwater availability model (from Kelley and others, 2004).

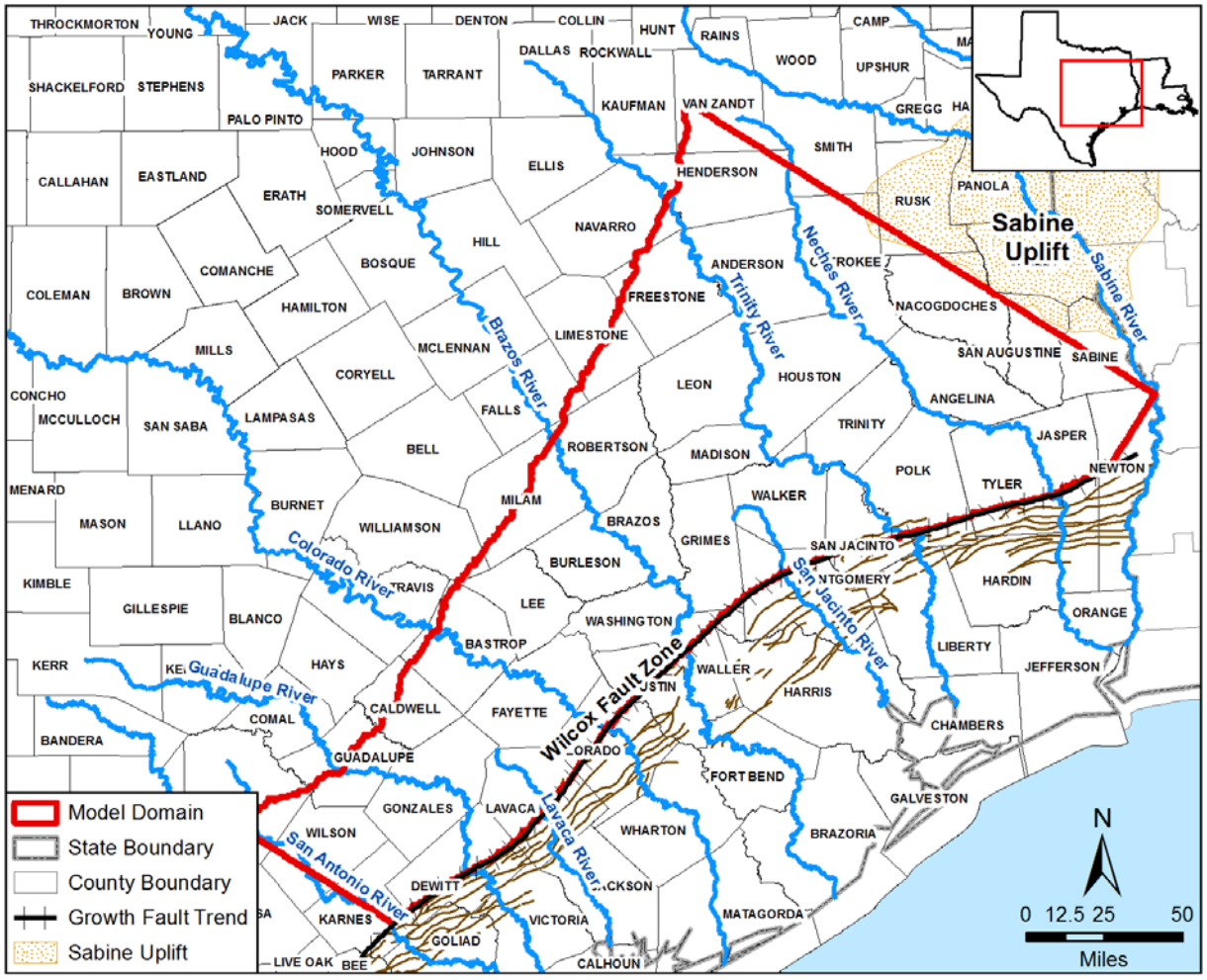

Document Path: S:\AUS\twdb_gma12\GIS\mxd\Fig_3-4_template_tyan.mxd

Figure 3-2. Lateral boundaries of the active grid cells in the central Queen City and Sparta aquifers groundwater availability model.

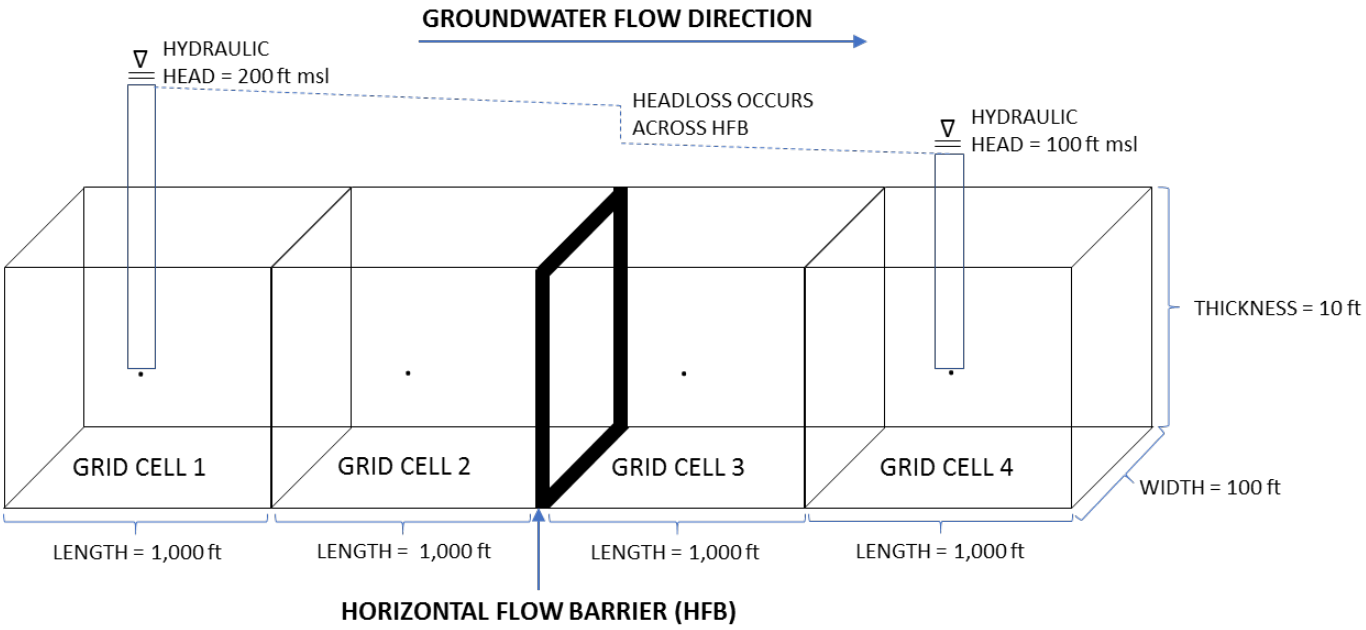

Figure 3-3. **Numerical grid consisting of a single row of four grid cells with fixed constant head boundaries used to evaluate the impact of changing the hydraulic conductivity of a horizontal flow barrier (HFB) on one-dimensional groundwater flow rates through the grid cells.**

Note: ft = feet, ft msl = feet mean sea level

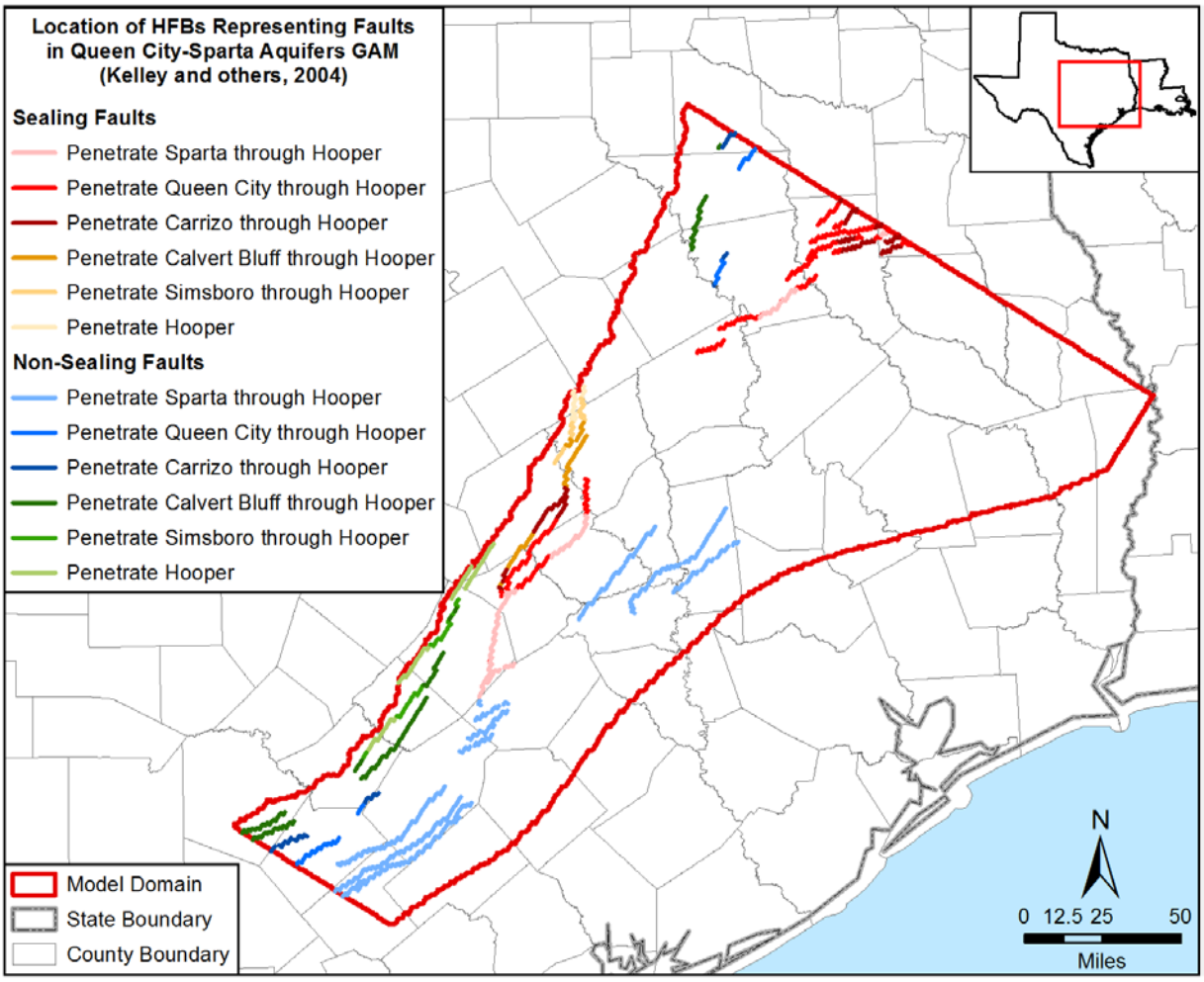

Figure 3-4. **Location of horizontal flow barriers (HFBs) used to represent sealing and non-sealing faults in the central Queen City and Sparta aquifers groundwater availability model (GAM).**

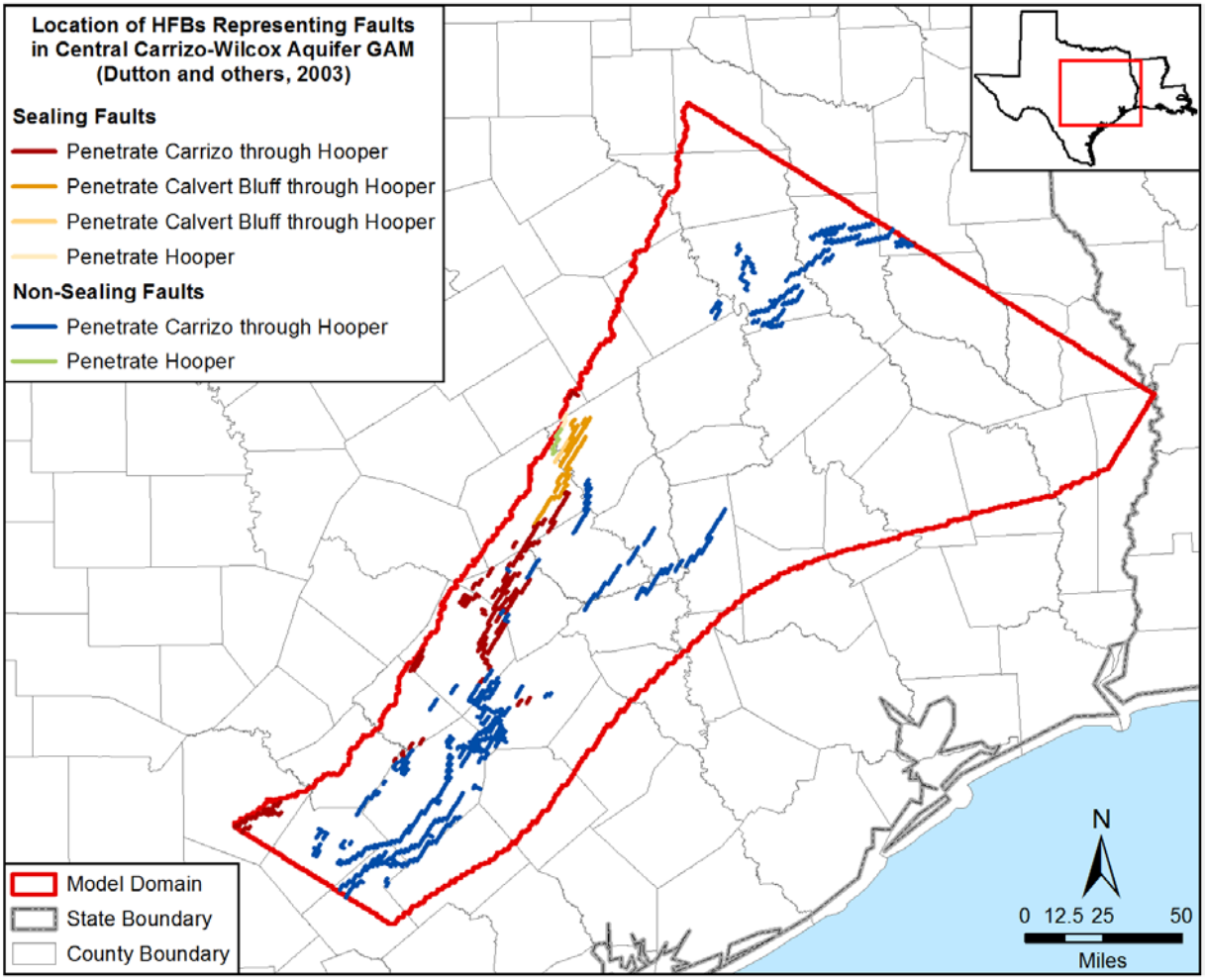

Figure 3-5. Location of horizontal flow barriers (HFBs) used to represent sealing and non-sealing faults in the central Carrizo-Wilcox Aquifer groundwater availability model (GAM).

This page is intentionally blank.

4 Methods

Several different analyses were performed to identify, characterize, and evaluate the potential impact of the Milano Fault Zone on groundwater flow. Identification of fault locations primarily involved the analysis of geophysical logs and review of the faults shown at surface outcrop on the Geologic Atlas of Texas (Barnes, 1970; 1979; 1981, Stoeser and others, 2007). To help evaluate whether faults were impacting groundwater flow, versions of the central Queen City and Sparta aquifers groundwater availability model were used to simulate regional groundwater flow and aquifer pumping tests.

4.1 Approach for Mapping Faults Associated with the Milano Fault Zone

Faults in the Milano Fault Zone were mapped using a combination of geophysical logs, existing fault traces based on seismic and outcrop data, and expert knowledge of fault structure and geometry. The fault traces shown at surface outcrop on the Geologic Atlas of Texas (Barnes, 1970, 1979, 1981) were considered to be the best indicators of probable fault locations. Using the previously mapped fault traces as a guide, we reviewed more than 700 geophysical logs in the vicinity of the Milano Fault Zone to identify fault locations and estimate fault offsets. Our evaluations of fault offsets was based primarily on picks for the top of the Cretaceous Navarro Formation and, secondarily, on the picks for the Simsboro Aquifer. The top of the Navarro Formation was used as our signature pick because the marine clays that comprise this formation provide a relatively clean and identifiable signature on geophysical logs.

4.2 Approach for Evaluating the Importance of Faults to Model Calibration, Model Validation, and Predictive Scenarios

The impact of horizontal flow barriers on groundwater flow simulated by the central Queen City and Sparta aquifers groundwater availability model was evaluated by simulating three modeling scenarios with three faults representations: the faults in the current model, no faults, and the faults developed by this study. The three modeling scenarios are the calibration period from 1975 to 2000 and the model verification period from 2000 to 2010 in the groundwater availability model, and a predictive period used to evaluate drawdown from 2010 to 2070 for Groundwater Management Area 12. The pumping distribution and the hydraulic boundary conditions for the model calibration scenario was taken from Kelly and others (2004), and the pumping distribution and hydraulic boundary conditions for the model verification and predictive scenarios were prepared by Groundwater Management Area 12.

Sensitivity of model results to the location and representation of faults with horizontal flow barriers for these three modeling scenarios was evaluated by comparing changes in predicted water levels caused solely by making changes to the horizontal flow barriers in the central Queen City and Sparta aquifers groundwater availability model. Two changes were investigated: removal of the horizontal flow barriers to represent no faults, modification in the location and properties of the horizontal flow barriers so that they represent the faults identified by this study.

4.3 Approach for Evaluating Fault Properties by the Analysis and Simulation of Aquifer Pumping Tests

Aquifer pumping test data were assembled and analyzed for evidence that a reduction in aquifer transmissivity, such as might be caused by a fault, occurs within a few miles of the pumping well. Two approaches were used to identify evidence of a fault that acts to reduce aquifer transmissivity located near a pumping well acted to reduce aquifer transmissivity. For convenience, the two approaches are called the Cooper-Jacob straight line (CJSL) (Cooper and Jacob, 1946) approach and the TTim approach.

The CJSL approach relies on the fact that the slope of a semi-log plot of time-drawdown data for a constant-rate pumping test can be used to calculate aquifer transmissivity if the pumping rate is known (Cooper and Jacob, 1946). Butler (1990), Streltsova (1988), and Young (1995) show that the CJSL method is a robust method that can be used to analyze different time periods of a time-drawdown curve to determine whether the aquifer's transmissivity field away from the pumping well is different than the aquifer's transmissivity field close to the pumping well. The application of the CJSL method involved two steps. First, a late-time transmissivity and an early-time transmissivity was calculated for approximately one hundred aquifer pumping tests. Second, the ratio of late and early transmissivity values was calculated and compared between two groups of pumping wells, with one group located near faults and the other group located away from faults.

The TTim approach used the analytical element code TTim (Bakker, 2013) to determine if the observed slope changes in the time-drawdown data from an aquifer pumping test could be reproduced by a two-dimensional aquifer model of constant transmissivity that contains the faults determined by this study. The TTim approach involved simulating the time-drawdown response for eight constant-rate aquifer pumping tests. Data for five of the aquifer pumping tests show time-drawdown plots with a steeper slope at late times than at early times. This trend was interpreted as evidence that a "sealing" fault is located near the pumping well. Data for the other three aquifer pumping tests show time-drawdown plots that do not have a steeper slope at late times than at early times. This trend was interpreted as evidence that no "sealing" fault is located near the pumping well. The application of the TTim approach focuses on whether the analytical model results could reasonable reproduce the trends observed in the data from the eight aquifer pumping tests that were simulated.

5 Analysis of Geophysical Logs to Identify Fault Zones

5.1 Geophysical Logs

Borehole geophysics involves the recording and analysis of physical and electrical measurements made in a borehole (or a well). Structural and stratigraphic interpretations made for this study relied almost solely upon the analysis of geophysical logs to understand the physical and electronic signatures of various geologic units. Within the study area, the geophysical signature of the geologic units (mainly the Carrizo Formation and Wilcox and Navarro groups) is consistent enough to allow for the discretization of the study area geology into formations and units. Once this was done, the occurrence and distribution of the geologic units provided insights into the post-depositional processes, mainly faulting, that impacted the structure within the study area.

5.1.1 Types of Borehole Geophysical Logs

Given the economic significance of the oil and gas industry, a multitude of geophysical probes have been developed to measure nearly every possible physical parameter in a borehole. In general, different logging tools are not named according to any particular system. Some are named on the basis of the parameter measured, others according to the principle by which the measurement is made, and still others on the geometric configuration of the probe. Table 5-1 summarizes basic information on the most important and widely applied logging tools in hydrogeology.

Table 5-1. General description of types of geophysical logs.

Log type	Specific Log	Borehole Conditions	Information
Nuclear	Gamma-ray Gamma-gamma (density) Neutron-neutron (porosity)	Open and cased holes with or without fluid Open holes with fluid	Lithology, density, porosity, calibration of surface geophysics
Electrical	Spontaneous potential Resistivity Focused resistivity	Open or screened holes with fluid	Lithology, salinity of groundwater, calibration of surface geophysics, location of PVC screens
Electromagnetic	Induction Nuclear magnetic resonance	Open and PVC cased holes with or without fluid	Lithology, salinity of groundwater
Acoustical	Sonic	Open holes with fluids	Lithology (porosity)
Optical	Borehole camera Optical borehole televiewer	Borehole camera Optical borehole televiewer	Borehole camera Optical borehole televiewer
Flow	Impeller flowmeter Heat pulse flowmeter	Open and cased holes with fluid	Vertical water movement in the borehole
Fluid	Water quality	Open and cased holes with fluid	Electrical conductivity, temperature, pH, oxygen, nitrate, Eh, total gas pressure

Three types of geophysical logs were used as part of this the study: resistivity, induction, and spontaneous potential. Each of these types are described in the following subsections.

5.1.2 Resistivity Log

In conventional resistivity logging, an electric current is forced between two electrodes, and the resulting electric potential (voltage) is measured between two other electrodes. Because the current path is through the geologic material surrounding the borehole, the resistance of surrounding geologic material to an induced current is computed from the resulting voltage measurement. The unit of resistivity (reciprocal of conductivity) measurement is the square ohm-meter per meter.

Dry formations will have very high resistivities because they are poor conductors of electricity. Fluid saturation of a deposit reduces its resistivity because water, oil, and gas are all electrical conductors and, if the unit has some permeability, then the induced current can flow to the receiver. In general, saturated subsurface materials with low resistivity include silts, clays, and shales. Fresh water deposits composed of sands and gravel tend to have higher resistivities because there are fewer ions in solution to carry the electrical charge. Therefore, the resistivity of a formation will vary inversely with the total dissolved solids concentrations of its pore water. One of the reasons that clays tend to have low apparent resistivities is because their interstitial waters are often highly mineralized. Sands and gravels saturated with fresh water tend to have high apparent resistivities because their surfaces are relatively inert and tend to release few minerals into solution.

Figure 5-1 illustrates how apparent resistivity can vary with differences in subsurface material and total dissolved solids concentration in groundwater. The difference in apparent resistivity between sandy and clayey deposits is considerably greater in fresh water than in very brackish water. In salt water, the difference in apparent resistivity between clay and sand is subtle. In situations that involve heterogeneous deposit types and vertical variations in water quality, analysis of the resistivity logs should be performed in concert with the analysis of other logs that provide independent information on either the characteristics of the deposits or the quality of the water saturating the deposits.

To help identify and account for the influence of the borehole fluids, several electrodes spacings may be used to obtain different depths of penetration of the resistivity tool into the surrounding geological material. The resistivity logs that were most commonly analyzed for this study consist of two downhole electrodes. When the separation of the electrodes is 16 inches or less, the configuration is called a short normal. If the two electrodes are separated by 64 inches, the configuration is called a long normal. The larger the spacing between the two downhole electrodes, the deeper the penetration of the measurement into the formation. In general, the short normal log is used for picking bed boundaries while the long normal log is used to determine the true formation resistivity.

5.1.3 Induction Logs

Induction logs provide similar information as resistivity logs. However, the induction logging tool can be used in dry boreholes, in boreholes containing nonconducting fluids, and in polyvinyl chloride-cased boreholes, whereas resistivity tools cannot.

Instead of using electrodes to generate electric current in the subsurface, a borehole induction tool uses electric coils to create magnetic fields that, in turn, induce electric currents in the geologic formation. The induced electrical eddy currents are proportional to the conductivity of the rock. An induction tool usually contains two coil systems with different coil spacings and, thus, different investigation depths. Coil systems with several transmitter and receiver coils are used to focus the electrical field to minimize the influence of the borehole itself on the recorded signal. The investigation depth depends on the conductivity of the rock and is 60 to 350 centimeters for a dual induction log.

5.1.4 Spontaneous Potential Log

Spontaneous potential logs record naturally occurring electrical potentials (voltages) that occur between the borehole and formation fluid. The spontaneous potential log primarily measures the electrochemical potential between a stationary reference at the surface and a moving electrode in the borehole.

The circuitry between the surface and the downhole electrode does not include an external source for an electric current. In greatly simplified terms, the electrochemical potential measured on a spontaneous potential log is generated by ions moving between the borehole fluid and the formation water. If there is no contrast in the ionic concentrations of the borehole fluid and the formation water (resistivity of the mud is equal to the resistivity of the formation water), there is no electrochemical potential, and therefore the spontaneous potential is zero. The downhole electrode usually has a lower (more negative) potential than the surface electrode. Spontaneous potential logs only record values relative to the borehole fluid rather than the absolute values of resistivity tools.

Figure 5-1 illustrates spontaneous potential responses that can be expected in formations containing fresh water, brackish water, and salt water when the drilling fluid is composed of fresh water. As shown in Figure 5-1, at shallow depths where there may be little difference in the concentration of ions between the drilling fluid and the aquifer, the analysis of the spontaneous potential log may be difficult because of the lack of deflections. Fortunately, the resistivity signature can usually be relied upon through this zone. However, at deeper depths where the formation waters are more mineralized than the drilling fluid, the leftward deflections (more negative values) in the spontaneous potential logs are useful for identifying differences between sandy and clayey deposits. At deeper, more brackish depths, the resistivity signature is usually small and the spontaneous potential signature is usually much more pronounced.

5.2 Characterization of Milano Fault Zone

Faults in the Milano Fault Zone were initially mapped using locations from Ayers and Lewis (1985), the Tectonic Map of Texas (Ewing and others, 1990), and the Geological Atlas of Texas

sheets (Barnes, 1970, 1979, 1981). Figures 2-5 through 2-7 show the fault locations associated with each of these studies. In the vicinity of these fault zones, evidence of faulting was primarily based on picks for the top of the Navarro Group. In the vicinity of the Milano Fault Zone, the top of the Navarro Group is approximately 2,000 feet below the top of the Simsboro Aquifer.

The Navarro Group pick offers several advantages over picks for the formations in the Carrizo-Wilcox Aquifer. One advantage is that the Navarro Group is a marine clay with interbedded sands that produces a distinct geophysical signature on both the spontaneous potential and resistivity logs when compared to the unconformably overlying Midway Group (Figure 5-2). Carrizo Formation and Wilcox Group picks are much more problematic because the Milano Fault Zone is in the updip extent of the Carrizo Formation and Wilcox Group, where flooding surfaces pinch out/transition into their terrestrial equivalent and erosional processes are most prevalent. Thus, the picks within the Wilcox Group (such as for the Simsboro and Hooper formations) can be inconsistent and irregular on any but the most local of basis, showing as much as 200 to 400 feet of variability over several miles. These picks are traditionally made on the top and base of a sand-rich section that contains fresh water (characteristically high resistivity values); but there are fresh-water sands in both the overlying Calvert Bluff Formation and the underlying Hooper Formation that amalgamate and can potentially be recognized as Simsboro. In addition, in the updip extent of the Wilcox Group, log coverage in the Navarro Group is much better than in the Wilcox Group.

Figure 5-3 shows the spatial distribution of the 650 geophysical logs for which picks on the top of the Navarro Group were made. These picks were used to create a generalized fault-free map of the top of the Navarro Group. Comparison of the Navarro Group picks with the fault-free surface, along with analysis of logs that intersect a fault and faults identified on the Geological Atlas of Texas sheets (Barnes, 1970; 1979; 1981), were used to locate and estimate fault offsets. The offsets associated with the faults are shown in Figure 5-3.

Several “fault-cut” logs are shown in Figure 5-3. A fault cut occurs when a log intersects a fault and the geophysical log is a combination of the upthrown and downthrown side of the fault. These scenarios are termed fault cuts because a section of formation has been shifted and, therefore, not represented in the geophysical log. Figure 5-4 shows a schematic of a fault-cut log. Figure 5-5 is a schematic showing digitized logs for six of the 16 fault cut wells identified. As can be seen, most of the identified fault cuts are in the Navarro Group.

Once the geometry and displacement of faults on the top of the Navarro Group were determined, the fault segments were projected up to the top of the Simsboro horizon. In the vicinity of the projected faults, picks for the Simsboro Formation were made on 470 logs to check the fault location and offset. Where possible, the picks for the Simsboro Formation were compared to picks available in the Brackish Resource Aquifer Characterization System (BRACS) database. These comparisons occurred primarily in Caldwell and Bastrop counties, and the picks were usually very close. Figure 5-6 shows the location of the fault locations in the Navarro and Simsboro formations. Because of the fuzzy and inconsistent nature of the picks for the top of the Simsboro Formation, some difference in the fault displacements relative to the top of the

Simsboro Formation are not consistent with known displacement at the top of the Navarro Group.

As a check on the final placement of the faults in the Simsboro Formation, Figure 5-7 shows the Simsboro faults from this study plotted with faults mapped by Ayers and Lewis (1985) and the Geological Atlas of Texas sheets (Barnes 1970, 1979, 1981 as digitally provided in Stoeser and others, 2007). The comparisons show very good agreement between the faults identified as part of this study and those mapped by Barnes (1970, 1979, 1981) and moderate to good agreement with the faults mapped by Ayers and Lewis (1985).

For the purpose of this study, the Milano Fault Zone was divided into four grabens and one complex. These areas are shown in Figure 5-8 and are named, from south to north, the Kovar Complex, the Paige Graben, the Tanglewood Graben, the Calvert Graben, and the South Kosse Graben. For each of these areas, a comment regarding the results of the geophysical analysis is provided along with a cross-section through the area.

5.2.1 Kovar Complex

In southern Bastrop and western Fayette counties, there is an area containing mainly southeast-down faults, which have been called the Kovar Complex (see Figure 5-8), named after the settlement of Kovar. The area is about 10 miles long and 5 miles wide; and the top of the Navarro Group lies at about 4,000 feet subsea. The log control is insufficient to reliably map the faults, but they appear to strike N50E. One fault appears to be northwest-down and bounding a graben. Fault displacements range from 100 to 500 feet. The faulting dies out to the northeast, where wells show no apparent offsets of strata. Similar faults are reported to the south into Gonzales County, as part of an en echelon segment of the peripheral graben system. Additional faults exist in western Bastrop County, but are part of the Luling Fault Zone and mostly do not affect the aquifers in the Wilcox Group.

Figure 5-9 shows the location of cross section A-A' through the Kovar Complex. Figure 5-10 shows formation tops and the relative location of faults that were determined from the interpretation of logs in and near cross section A-A'. Two main faults are represented in this section with throw being to the south (normal). As stated previously, fault throws in the Kovar Complex range from 100 to 500 feet.

Two wells appear to have intersected the same antithetic fault within the Kovar Complex:

- Well 4202100823 has 330 feet of missing section at a structural elevation of -5,416 feet below sea level.
- Well 4202100824 has 230 feet of missing section at a structural elevation of -1,770 feet below ground surface in the Calvert Bluff Formation.

5.2.2 Paige Graben

In northeastern Bastrop and western Lee counties, the Paige Graben complex (see Figure 5-8), named after the settlement of Paige, is well defined by the data and is also evident on surface geologic maps. The graben is 24 miles long and 3.7 miles wide, trending N20E. The top of Cretaceous-age sediments lies about 3,500 feet subsea in this graben. The northwestern,

southeast-down fault is well marked and very continuous, showing 690 to 700 feet of displacement at the top of the Navarro Group. The eastern, northeast-down faults are less continuous, but generally show 450 to 700 feet of displacement. The details of fault relationships here are not well determined from well control. It appears that there are internal faults within the graben and some that cross from one side to another. The faults toward the northeast end of the graben become more easterly trending (N37E). The northwest fault appears to feather out into a series of smaller faults, and the displacement steps northwest into the western boundary fault of the next graben to the north; however, well control is not adequate to map this fully.

Figure 5-11 shows the location of cross sections B-B' and C-C' that cross through the Paige Graben. Figure 5-12 shows the formation tops and the location of faults that were determined from the interpretation of logs near and in cross Section B-B'. The section shows the northwestern (southeast-down) fault within the Graben and clearly shows the more than 700 feet of throw. Further down dip on the cross section between wells 4202131558 and 4202131041, the southwestern extent of the graben system is intersected.

Figure 5-13 shows the top surfaces of formations and the location of faults that were determined from the interpretation of logs near and in cross section C-C'. This section transects both bounding graben faults between wells 4228700098 and 4228700101 in the updip (throw to the southeast) and 4228700048 and 4228731157 in the downdip, where throw is up away from the Gulf of Mexico.

Two localities within the Paige Graben have designated fault-cut wells:

East Bounding Fault in Bastrop County Locality

- Well 4202130581 has 650 feet of missing section at an elevation of -5,820 feet below sea level in the Austin Chalk.
- Well 4202100143 has 550 feet of missing section at an elevation of -4,709 feet below sea level in the Taylor Marl and shows an apparent dip of 41 degrees.
- Well 4202100144 has 700 feet of missing section at an elevation of -3,630 feet below sea level, faulting out the Midway and Navarro groups. The fault has an apparent dip of 42 degrees.

Lee County Part of the Graben

- Well 4228731293 has 750 feet of missing section at a structural elevation of -5,254 feet below sea level in the Austin Chalk.
- Well 4228700048 has 850 feet of missing section at a structural elevation of -4,600 feet below sea level in the Navarro Group.
- Well 4228700050 has 400 feet of missing section at a structural elevation of -2,000 feet below sea level in the Simsboro Formation, giving an apparent fault dip of 36 degrees.

5.2.3 Tanglewood Graben

The Tanglewood Graben is located in northern Lee, western Burleson and southeastern Milam counties (see Figure 5-8). This graben is more complicated than the Paige Graben, but abundant well control allows a fairly reliable interpretation. The main graben system is 21 miles long and 3 miles wide, trending N47E. The top of Cretaceous-age sediment lies about 3,000 feet below

sea level in this graben. The graben consists of two segments, one in northern Lee and the other along the Milam-Burleson counties border, separated by a small left-stepping displacement. The northwestern boundary faults are well defined, and typically have 700 to 750 feet of displacement. In northern Lee County, this fault appears to splinter into two faults with lesser displacement; however, well control was not adequate to make any concrete interpretations. The southeastern bounding faults are discontinuous and complicated.

In northern Lee County, the faults show around 450 to 730 feet of displacement, and to the north along the county line they are from 100 to 700 feet of displacement. An area between these two faults shows no evident faulting, but a reversal of regional dip. It is possible that there may be smaller, more distributed faults in this area. Northeastward into Milam County, the fault pattern becomes less regular. Faults of 200 to 400 feet of displacement form two or more small grabens. The northwestern bounding fault, trending N31E, is the most continuous. This fault, with 200 feet of throw at the top of Navarro Group, has a surface expression in the city of Milano. Faulting continues into eastern Milam County, but the well control is not sufficient to map it in this area. Faults in this area, if present, are either small or closely spaced.

Figure 5-14 shows the location of cross sections D-D', E-E' and F-F' that cross through the Tanglewood Graben. Figures 5-15, 5-16, and 5-17 show the formation tops and the location of faults that were determined from the interpretation of logs near and in cross sections D-D', E-E', and F-F', respectively. Based on these cross-sections and nearby geophysical logs, the following observations have been made:

South End of Lee County

- The southernmost well in the graben system, 4228730366, penetrated a fault with about 450 feet of displacement at a structural elevation of -270 feet below sea level in the Calvert Bluff Formation.
- To the northwest, well 4228700005 has 730 feet of missing section at a subsea elevation of -3,323 feet below ground surface in the Navarro Group. A fault dip of 57 degrees was calculated.
- Well 4228700013, which is oblique to fault strike, has a displacement of 750 feet at a structural elevation of -4,320 feet below ground surface in the Taylor Marl.
- A similar displacement is observed in well 4228700012 in the Austin Chalk to the northwest.

Southeastern Milam County

- The southeastern well 4233100783 has 730 feet of missing section at a structural elevation of -3,310 feet below ground surface in the Navarro Group.
- Well 4233100782 has 690 feet of missing section at a structural elevation of -4,900 feet below sea level in the Austin Chalk. The apparent dip of the fault is 44 degrees.

Northern Fringe of the Tanglewood Graben

- Well 4233100863 has 400 feet of missing section at a structural elevation of -2,670 feet below sea level in the Navarro Group.
- Well 4233132745 has 400 feet of missing section at a structural elevation of -4,700 feet below sea level in the Austin Chalk. Apparent fault dip is 45 degrees.

- Well 4233130170 has 240 feet of missing section at a structural elevation of -3,030 feet below sea level in the Taylor Group.
- Well 4233130197 shows 200 feet of missing section at a structural elevation of -348 feet below sea level in the Calvert Bluff Formation. Apparent fault dip is 60 degrees.

5.2.4 Calvert Graben

In western Robertson County is a small graben called the Calvert Graben (see Figure 5-8). Figure 5-18 shows the location of cross section G-G', which crosses through the Calvert Graben. Figure 5-19 shows the formation tops and the location of faults that were determined from the interpretation of logs near and in cross section G-G'. This graben has little expression at surface, probably because surface rocks are the Calvert Bluff Formation, which does not yield reliable mapping horizons. The graben is 15 miles long and 2.5 to 3.0 miles wide, trending N42E. The top of the Navarro Group lies at a structural elevation of -1,800 feet below sea level in this graben. The deeper eastern part of the graben is bounded by a southeast-down fault on the northwest with 480 to 500 feet of displacement. The northwest-down faults on the southeast show 150 and 820 feet of displacement, varying fairly rapidly along strike. To the south, smaller faults outline two or more grabens with 100 to 270 feet of displacement. Faulting of this magnitude exists at the northeastern end, but isn't well resolved by the log control.

5.2.5 South Kosse Area

Finally, a set of faults, called the South Kosse Graben (see Figure 5-8), is identified in northernmost Robertson, eastern Falls, and southern Limestone counties. Figure 5-18 shows the location of cross section H-H', which crosses through the South Kosse Graben. Figure 5-20 shows the formation tops and the location of faults that were determined from the interpretation of logs near and in cross section H-H'. Within the area mapped, the well control only suffices to map a few faults, but some have 600 feet of displacement. The top of Cretaceous-age sediments lies at a structural elevation of only -1,000 feet below sea level here, and the Simsboro Formation is exposed at the surface or absent by erosion. Faulting continues northwest into Falls County and north into Limestone County, where faulting becomes well organized into a graben complex at Kosse. This is the southernmost portion of the Mexia Fault Zone, which continues northward to Corsicana. The surface geology is well mapped as surficial rocks here are pre-Wilcox Group in age (mainly Midway Group).

5.3 Implication Regarding Model Update

This, and previous, studies identify faults in the central portion of the Carrizo-Wilcox Aquifer. Therefore, they should be included in the central Queen City and Sparta aquifers groundwater availability model. This study advocates representing the faults in the same manner as was done in the central Carrizo-Wilcox aquifers groundwater availability model and the central Queen City and Sparta aquifers groundwater availability model; that is, using the Horizontal Flow Barrier package developed by the United States Geological Survey for the MODFLOW family of groundwater codes. This package provides the ability to cite and parameterize faults in a manner consistent with the impact on aquifer transmissivity and groundwater flow associated with faults.

The faults identified in this study were placed on the grid for the central Queen City and Sparta aquifers groundwater availability model. In order to do this, the fault locations were adjusted and manipulated to be compatible with the numerical grid. The adjusted location of the faults in the Simsboro Formation determined by this study are shown in Figure 5-21 as a series of straight-line segments that match the boundaries of the 1-mile square grid cells in the central Queen City and Sparta aquifers groundwater availability model. Each of the fault segments are characterized by a vertical offset for the fault estimated from the interpretation of the geophysical logs. The faults are grouped into the following three categories: (1) offset greater than 500 feet; (2) offset greater than 200 feet but less than 500 feet; and (3) offset less than 200 feet.

Also shown in Figure 5-12 are the sealing faults from the central Queen City and Sparta aquifers groundwater availability model. These faults are shown as thick lines to help simplify the comparison between the two set of faults. Comparing the two set of faults indicates that the faults identified in this study cover considerably less area than the existing set of faults in the groundwater availability model. Thus, one of the implications of this study is a considerably smaller area potentially affected by faulting relative to the fault representation in the current central Queen City and Sparta aquifers groundwater availability model.

Another implication of this study is the characterization of the faults in the Milano Fault Zone. Our detailed review of geophysical logs indicates that the Milano Fault Zone consists of a series of connected grabens. This contrasts with the long, continuous faults, some of which are 100 miles in length, in the central Queen City and Sparta aquifers groundwater availability model to represent this fault zone. Our reconceptualization of the character of the faults in the Milano Fault Zone provides for “windows” and “gates” which allow groundwater to flow more freely perpendicular to the strike of the faults, flow that is not possible with the current system of faults in the groundwater availability model. In addition, estimation of offset provides a method for assigning different conductance values to the faults identified with this study based on differences in offset.

The detailed characterization from which vertical offset could be assigned to individual fault segments provides for adjusting fault conductances to improve the performance and calibration of the updated model. A possible option for assigning conductance to the faults from this study is to consider only those faults with offsets greater than 500 feet as candidates for being sealing faults. In this case, the footprint of the sealing faults is reduced by about 60 percent.

No matter how the conductances are assigned to the new network of faults based on this study, the updated model will be significantly different from the existing model because there are no faults identify in two areas where the current model has considerable faults. One area is in northern Burleson County where an over 50-mile long fault currently in the model will be removed. The other area is in Robertson County, where a single continuous fault that divides the county will be removed.

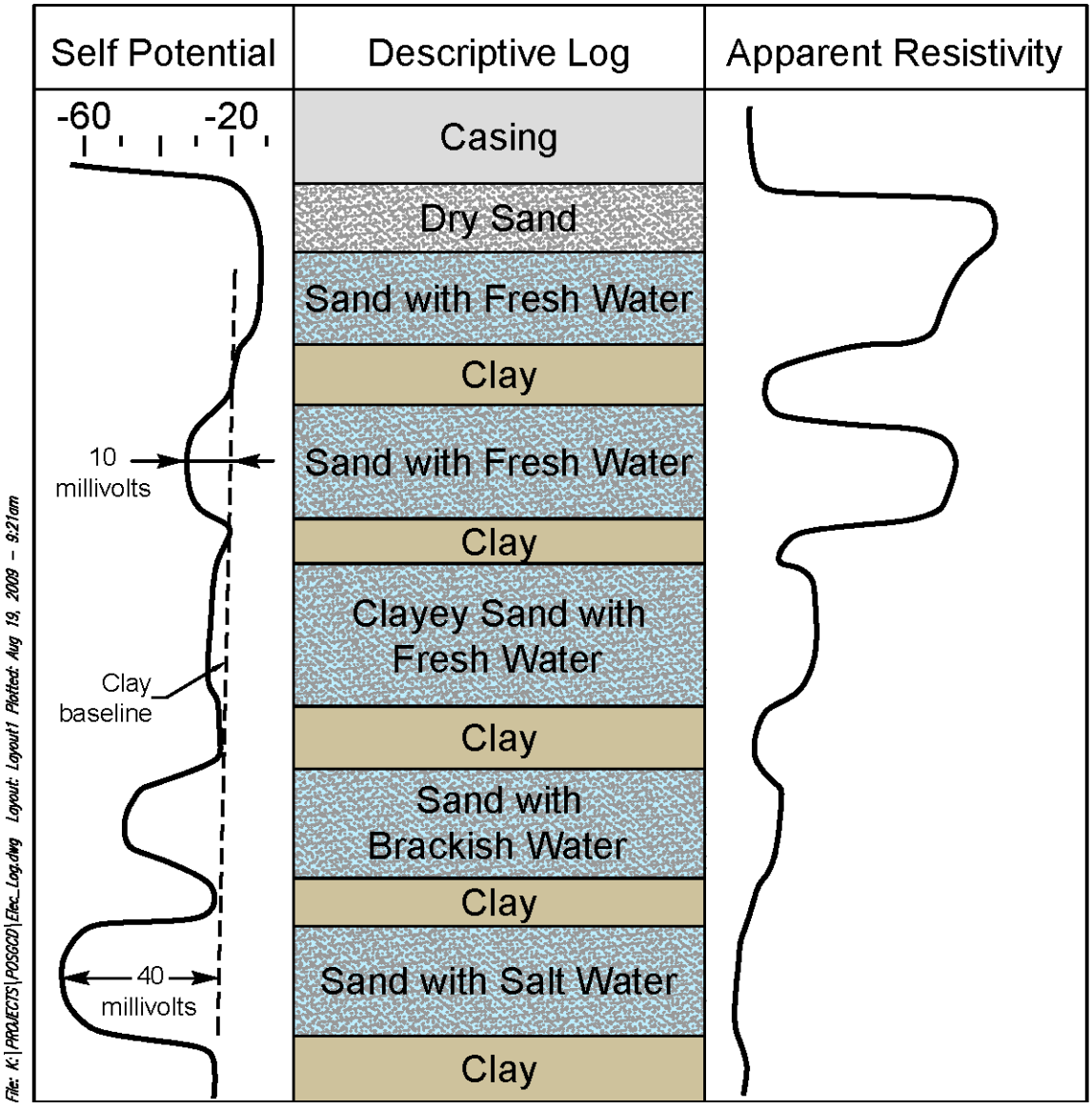

Figure 5-1. **Idealized self potential (also know as spontaneous potential) and apparent resistivity curve showing the responses corresponding to alternating sand and clay strata saturated with groundwater that increases significantly in total dissolved solids concentrations with depth (modified from Driscoll, 1986).**

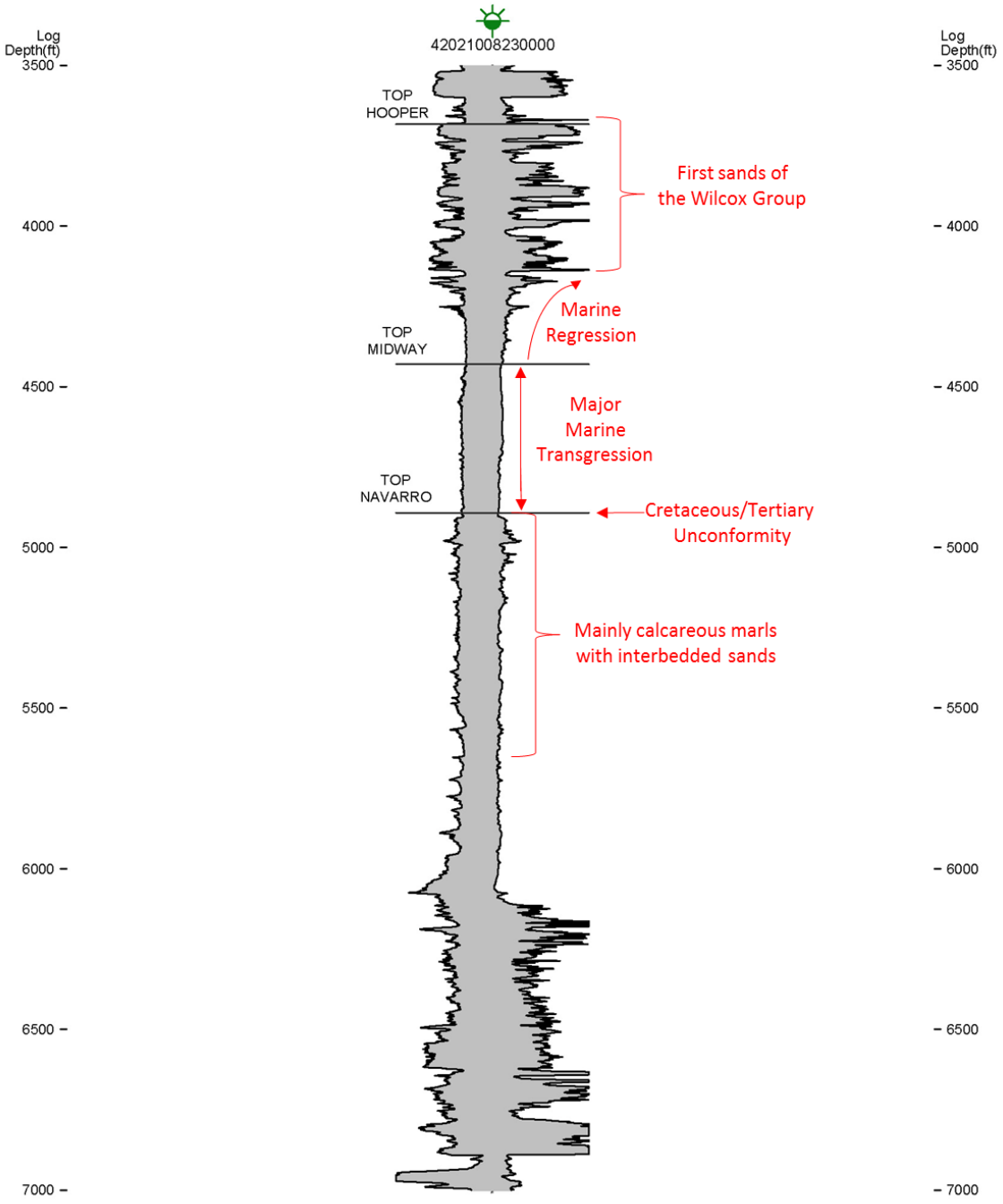

Figure 5-2. Geophysical signature of the Navarro Group on both the spontaneous potential and resistivity logs

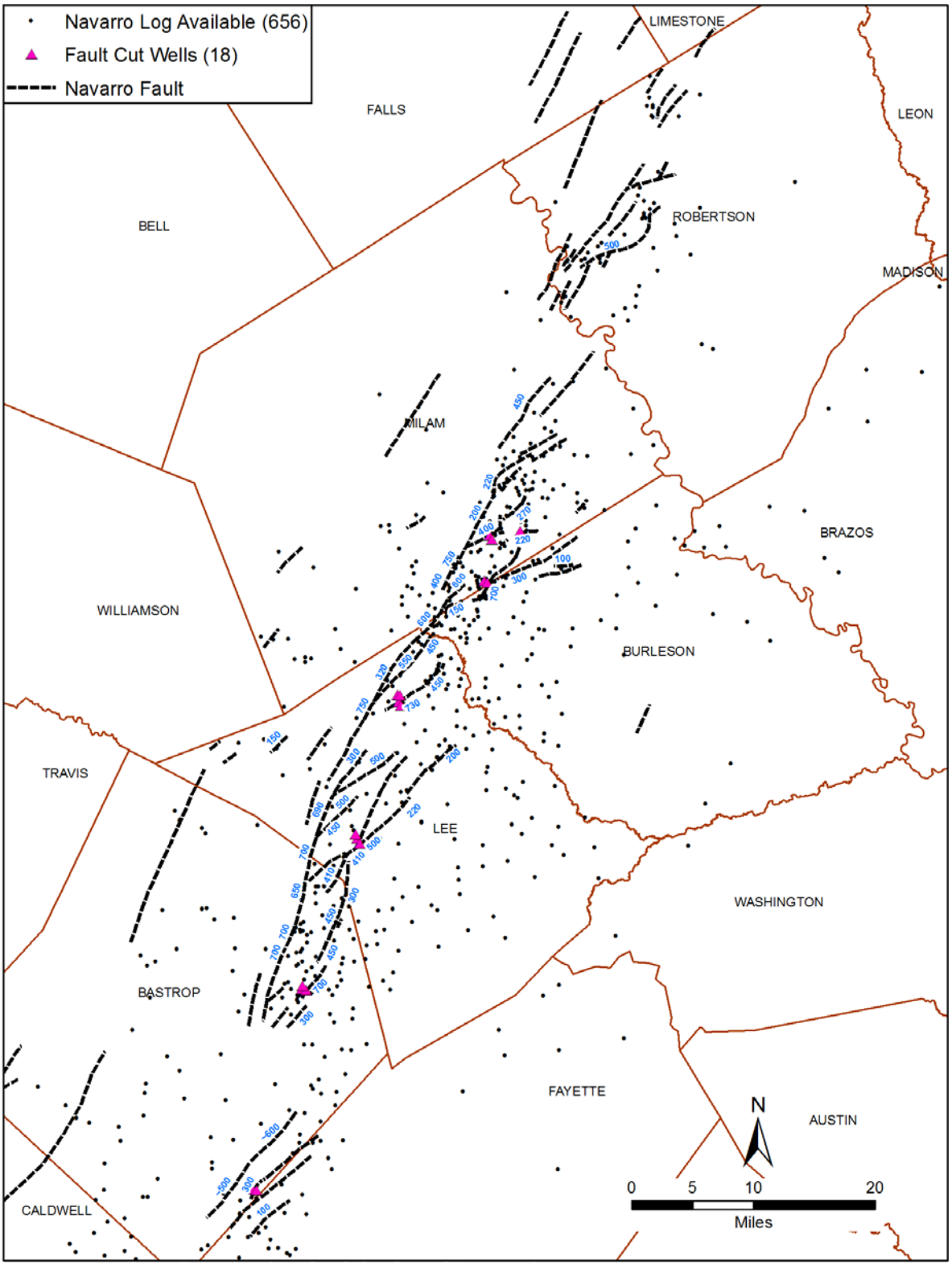

Figure 5-3. **Faults mapped onto the top of the Navarro Group and estimated fault offsets determined primary from the top of the Navarro Group picks from 650 geophysical logs with fault traces mapped on Geological Atlas of Texas sheet (Barnes 1970; 1979; 1981). Fault arrow point to the down-throw side of the fault.**

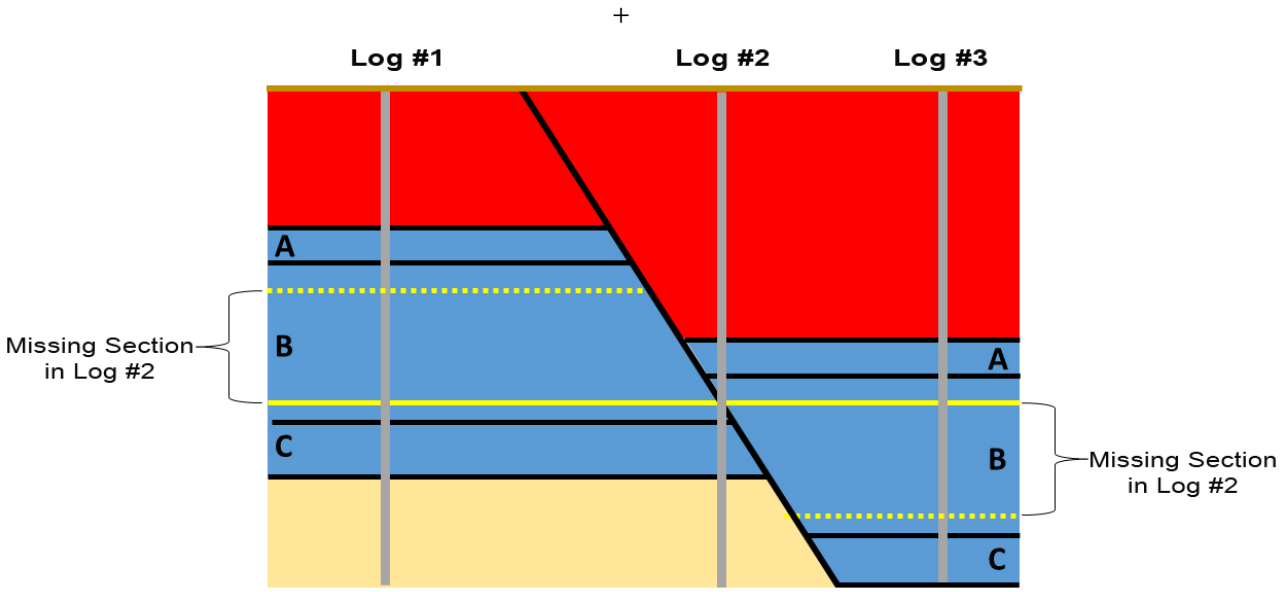

Figure 5-4. **Schematic representation of how fault-cut logs are identified. Log #1 intersects all three portions of Sections A, B and C. Log #2 intersects all of Section A, the top part of Section B on the down-thrown side and the bottom part of Section B on the up-thrown side, and all of Section C. Log #3 intersects all three portions of Sections A, B, and C. Using all three of these logs together, geologists can piece together missing sections within geologic units. The amount of missing section is referred to as a fault cut, and can be used as a quantitative way to characterize the offset associated with faults.**

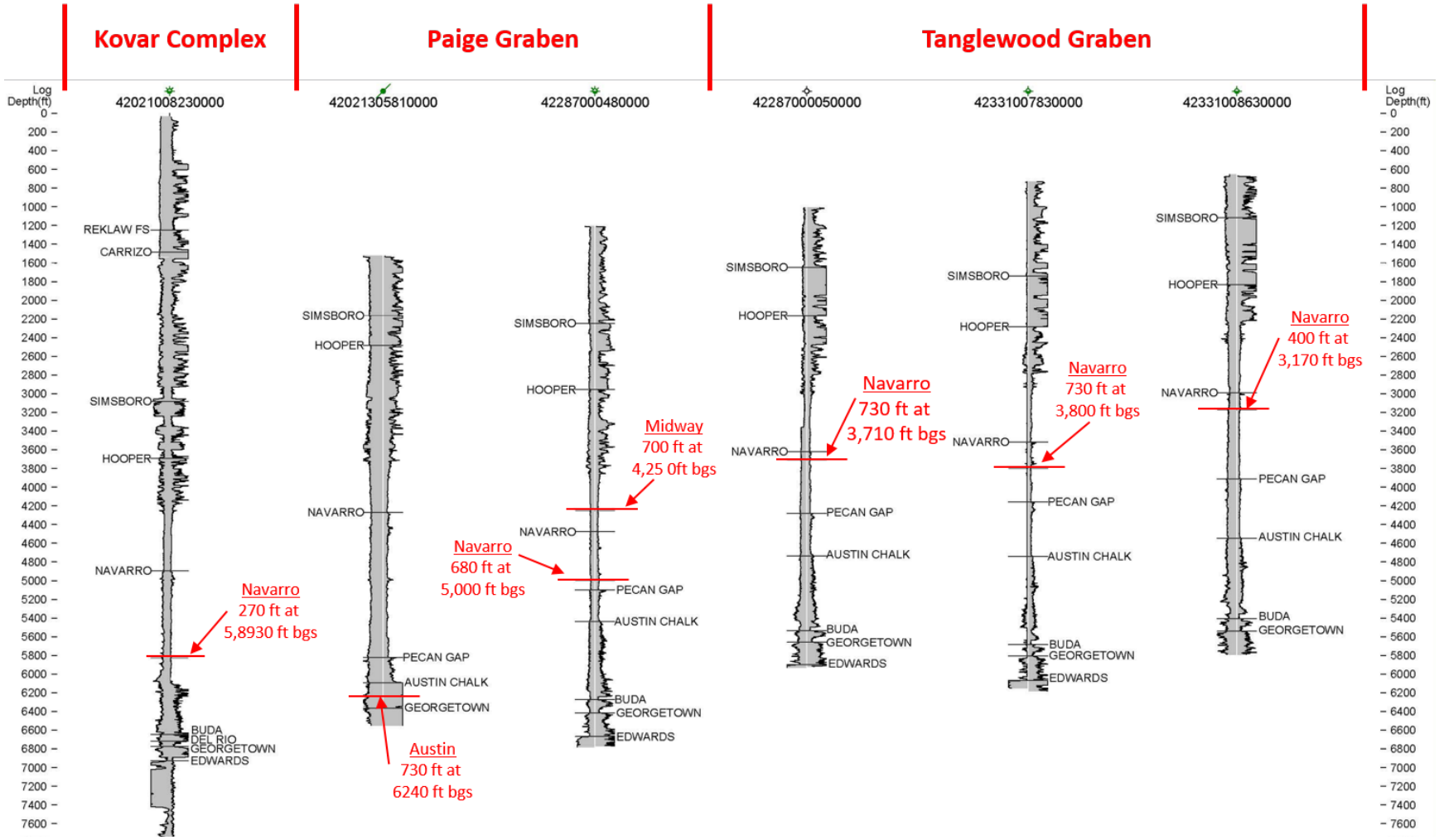

Figure 5-5. Six logs identified in Figure 5-8 that intersected one or more faults and are missing the formation intervals identified in red.

Note: ft = feet, bgs = below ground surface

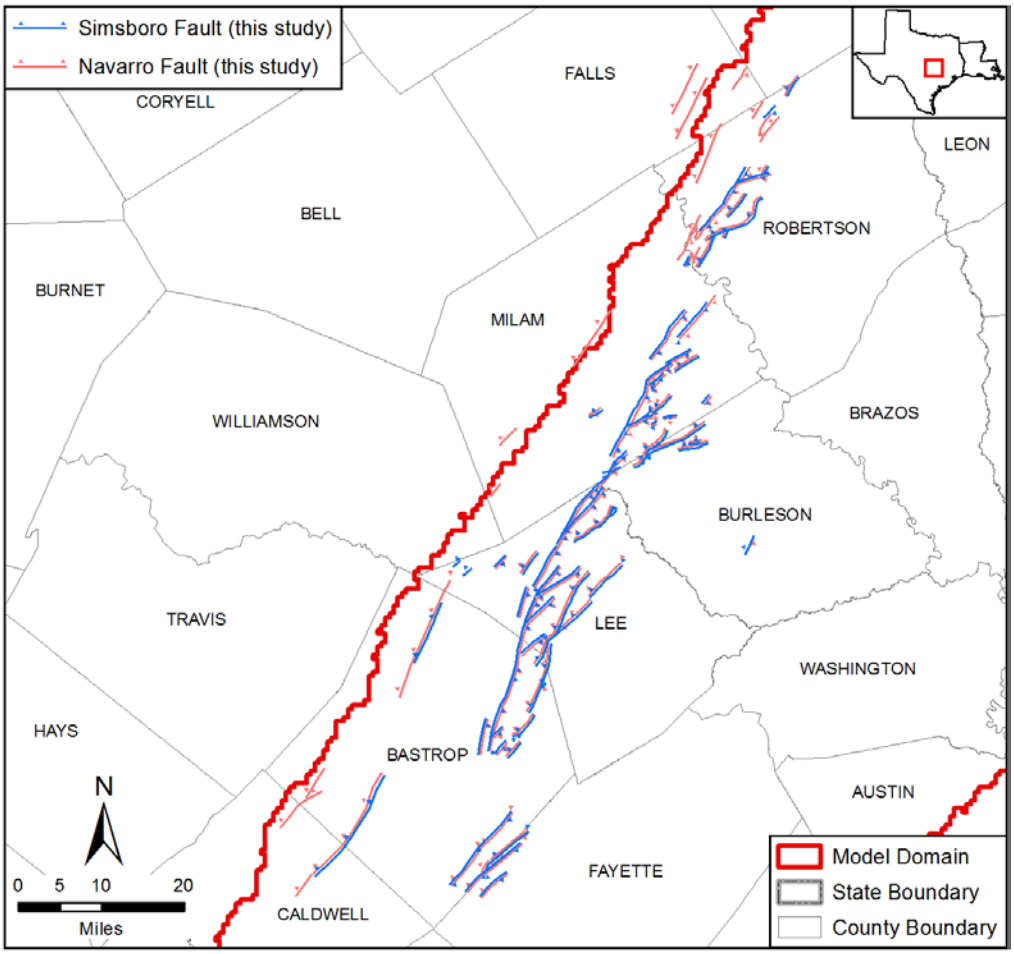

Figure 5-6. **Navarro Group and Simsboro Formation faults mapped by this study. Arrows on fault lines point to the down-thrown side of the fault.**

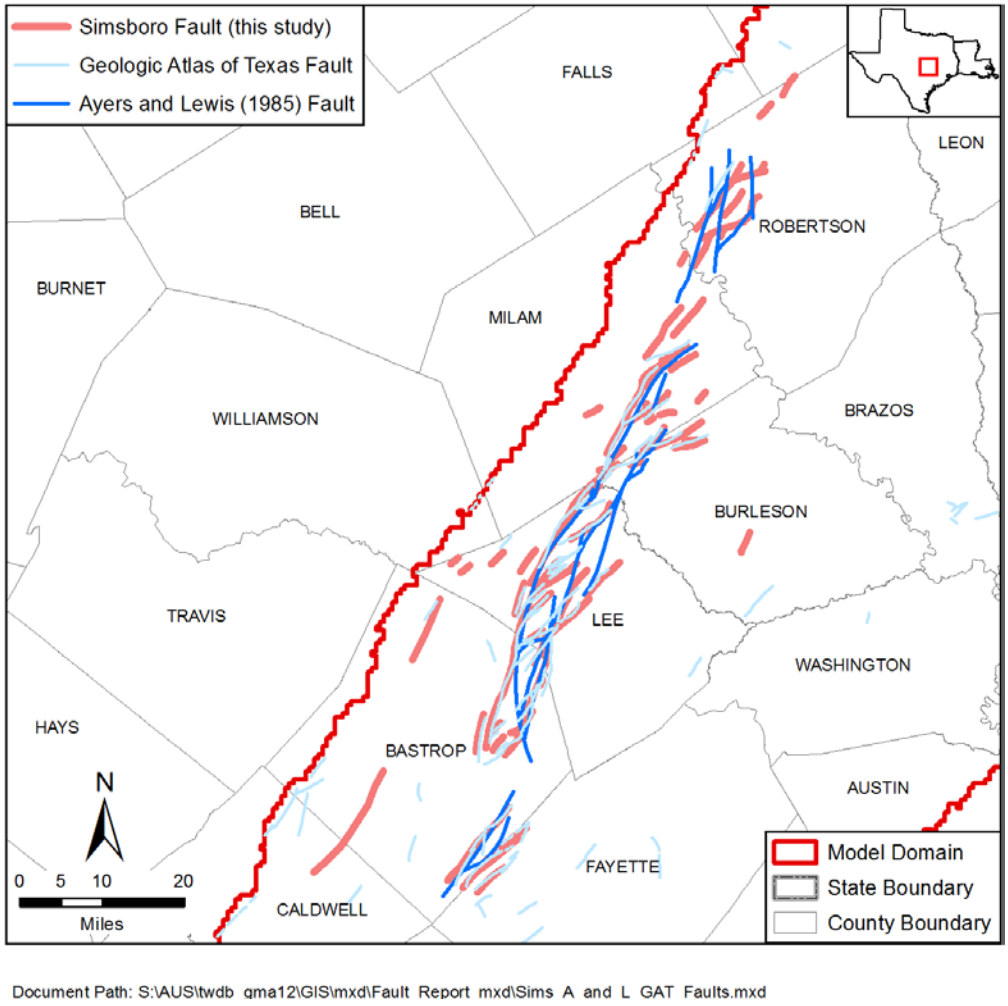

Figure 5-7. Simsboro Formation faults from this study mapped with faults from Ayers and Lewis (1985) and from the Geological Atlas of Texas sheets of Barnes (1970; 1979; 1981) as presented by Stoeser (2007).

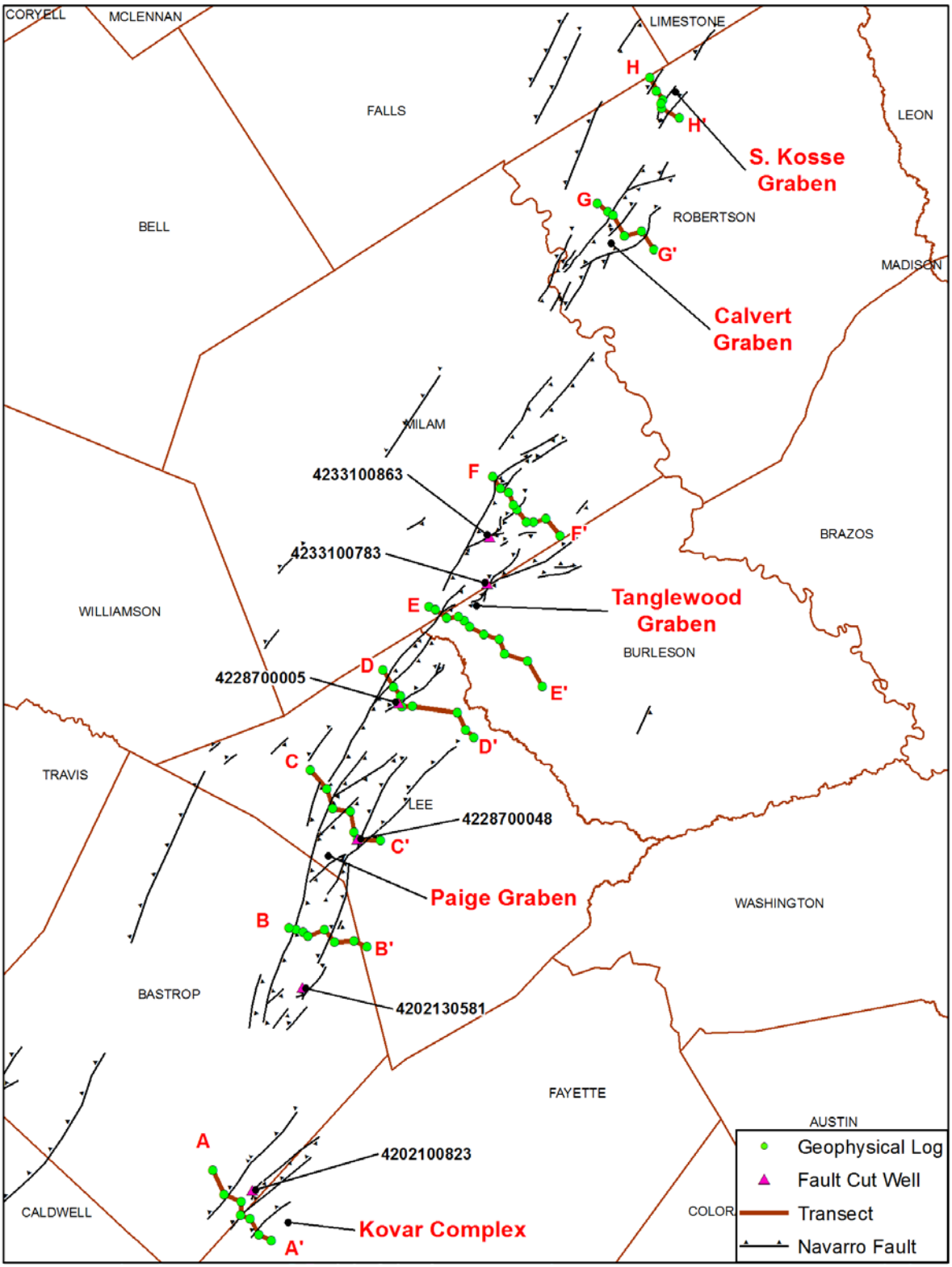

Figure 5-8. **Plan view map of Milano Fault Zone showing the five named major areas of faulting and locations of cross-sections that transect the fault zone.**

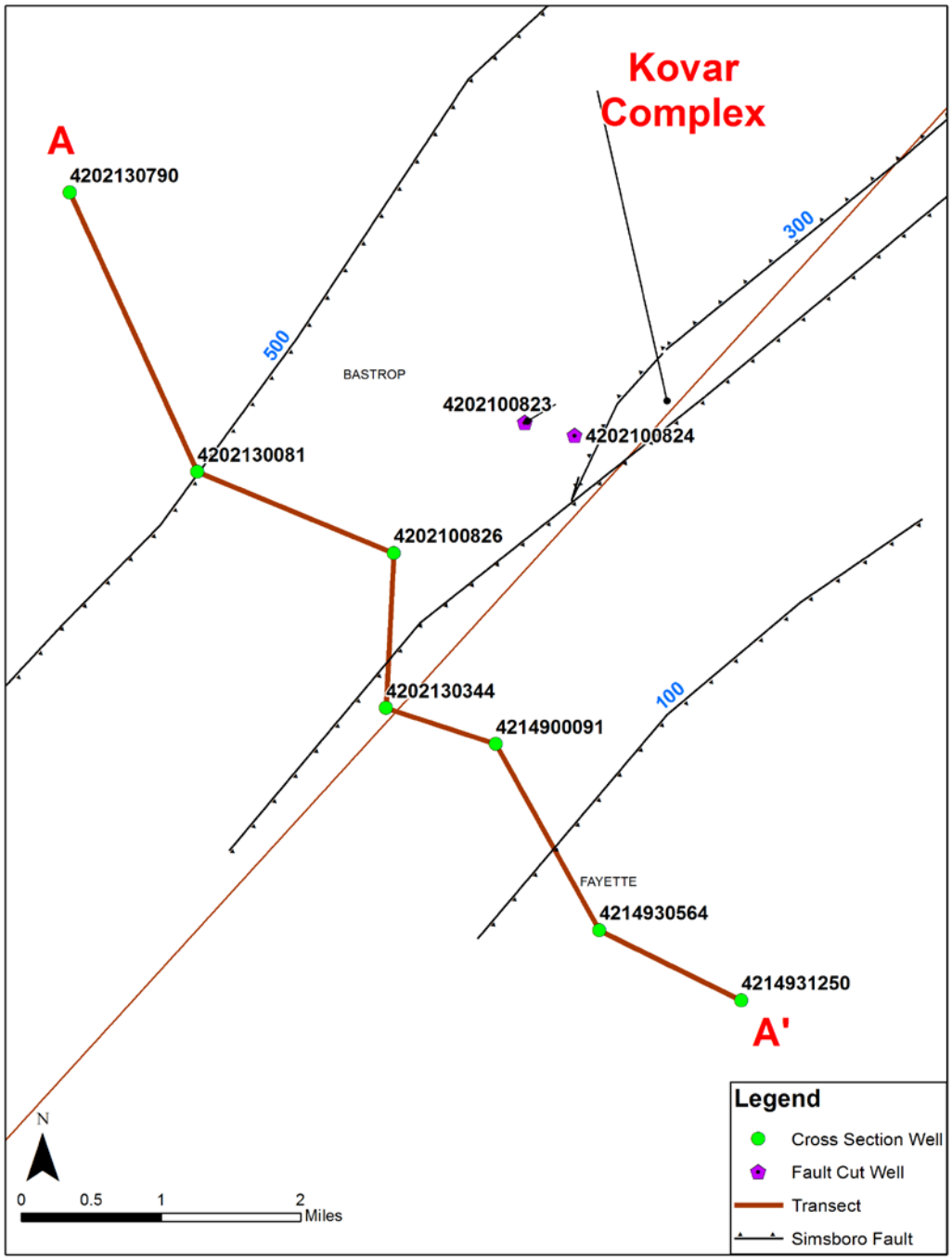

Figure 5-9. **Location of cross section A-A', which crosses through the Kovar Complex in Bastrop and Fayette counties. The American Petroleum Institute numbers of the geophysical logs comprising cross section A-A' are used to label the geophysical logs.**

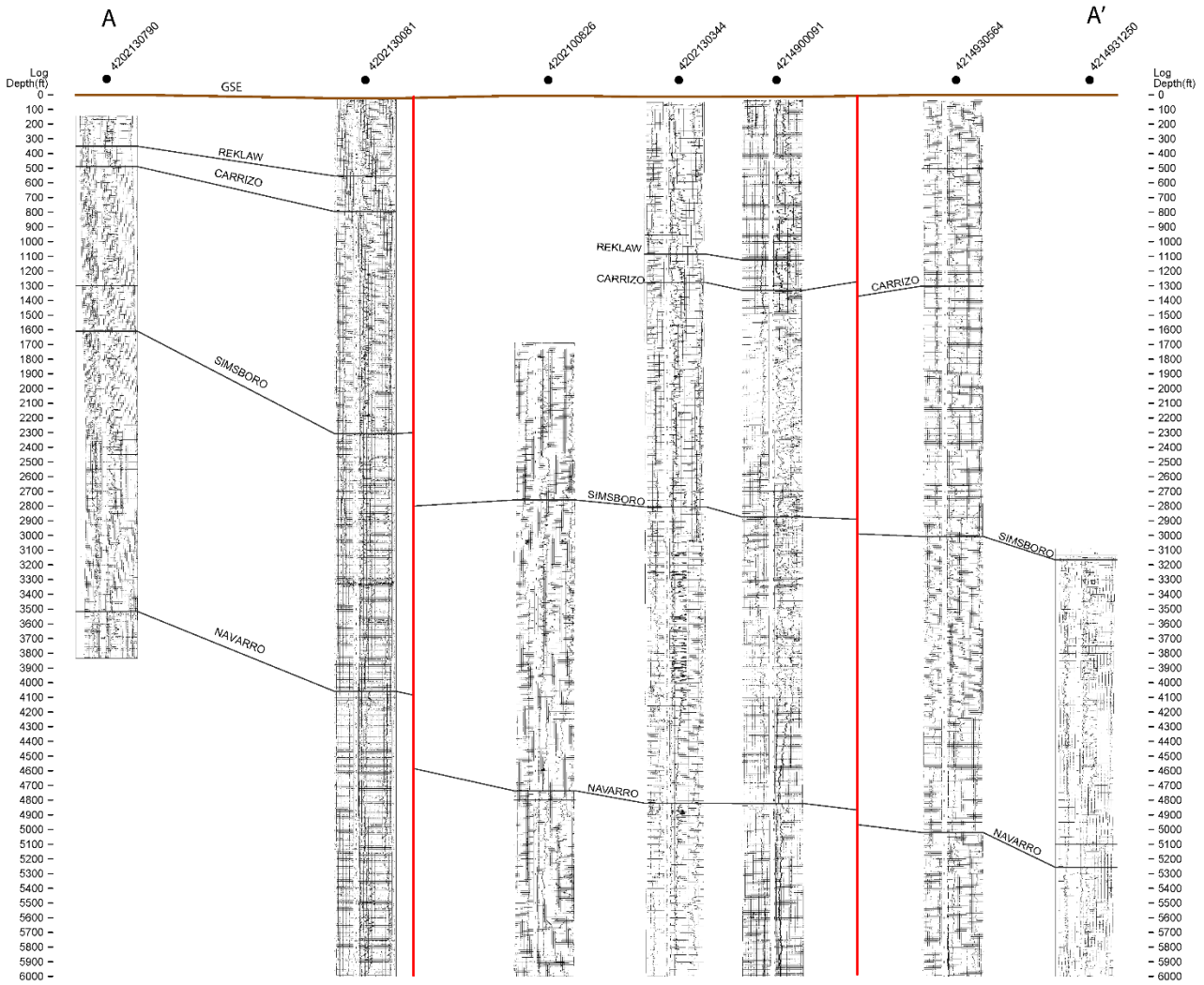

Figure 5-10. Geophysical logs associated with crossssection A-A' through the Kovar Complex showing geophysical logs with top surface of selected formations and mapped fault locations based on interpretation of geophysical logs in and near cross section A-A'.

Note: ft = feet

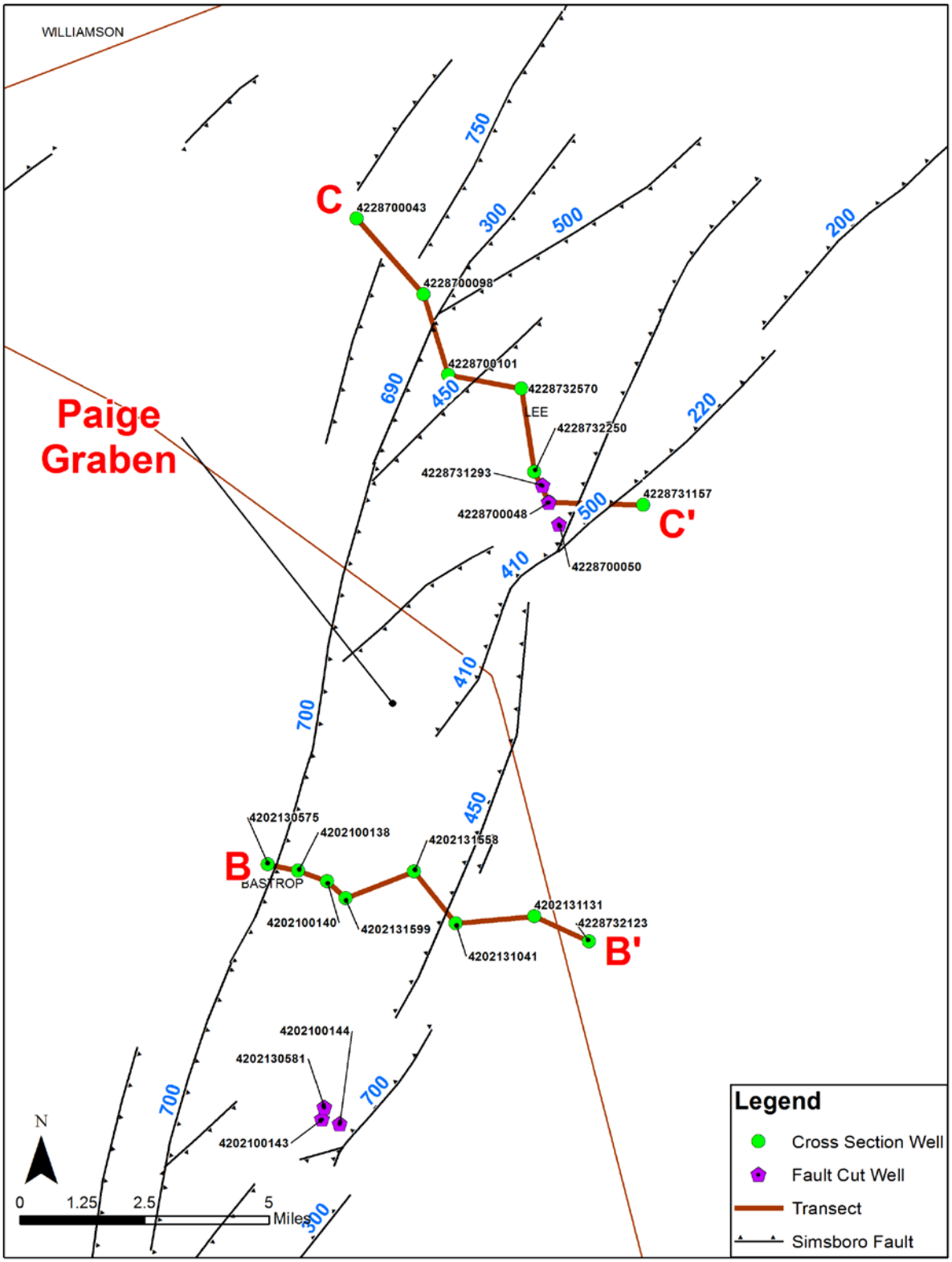

Figure 5-11. **Location of cross sections B-B' and C-C', which cross through the Paige Graben in Bastrop and Lee counties. The American Petroleum Institute numbers of the geophysical logs comprising the cross sections are used to label the geophysical logs.**

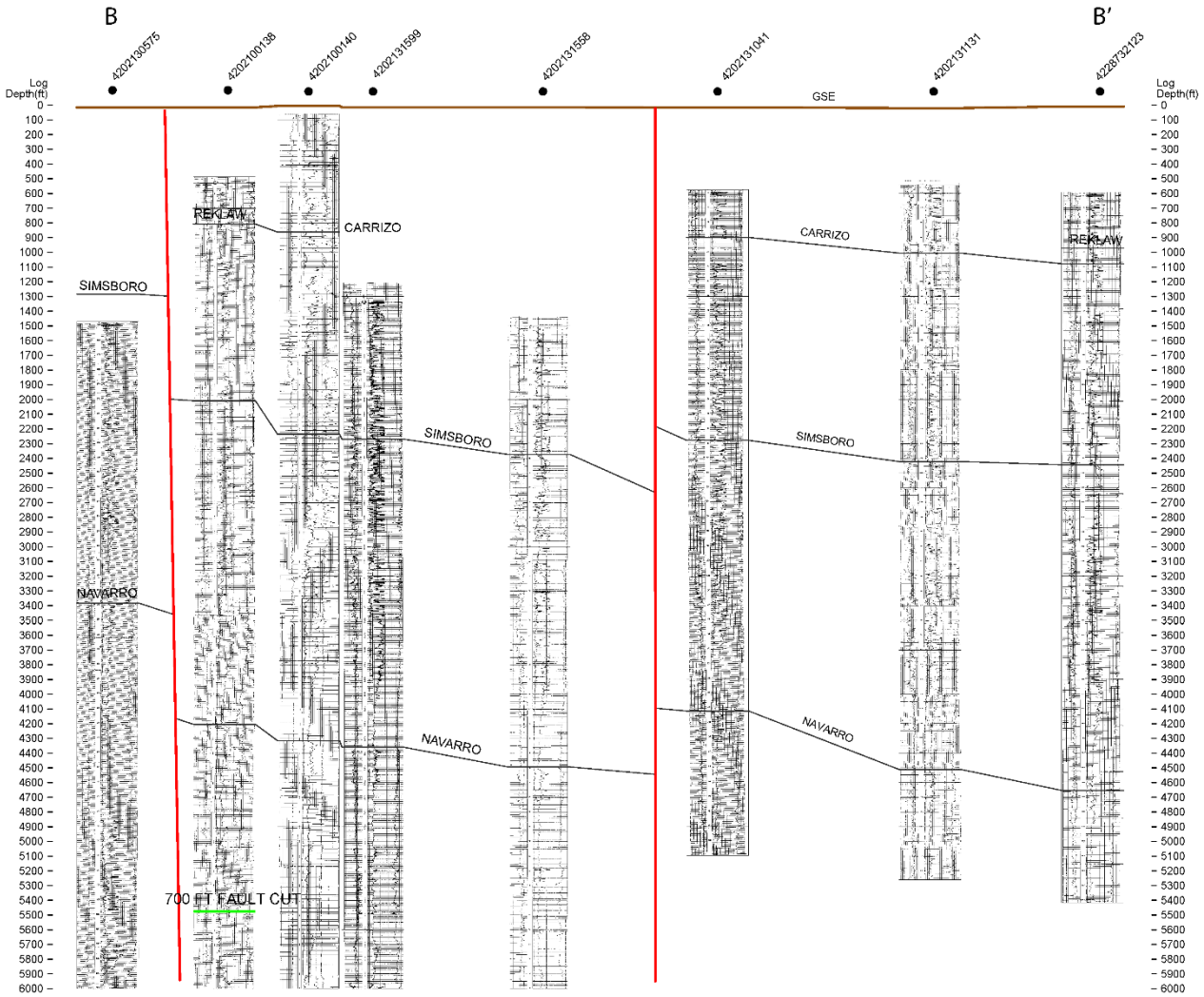

Figure 5-12. Geophysical logs associated with cross section B-B' through a southern portion of the Paige Graben showing the top surface of selected formations and mapped fault locations based on interpretation of geophysical logs in and near cross section B-B'.

Note: ft = feet

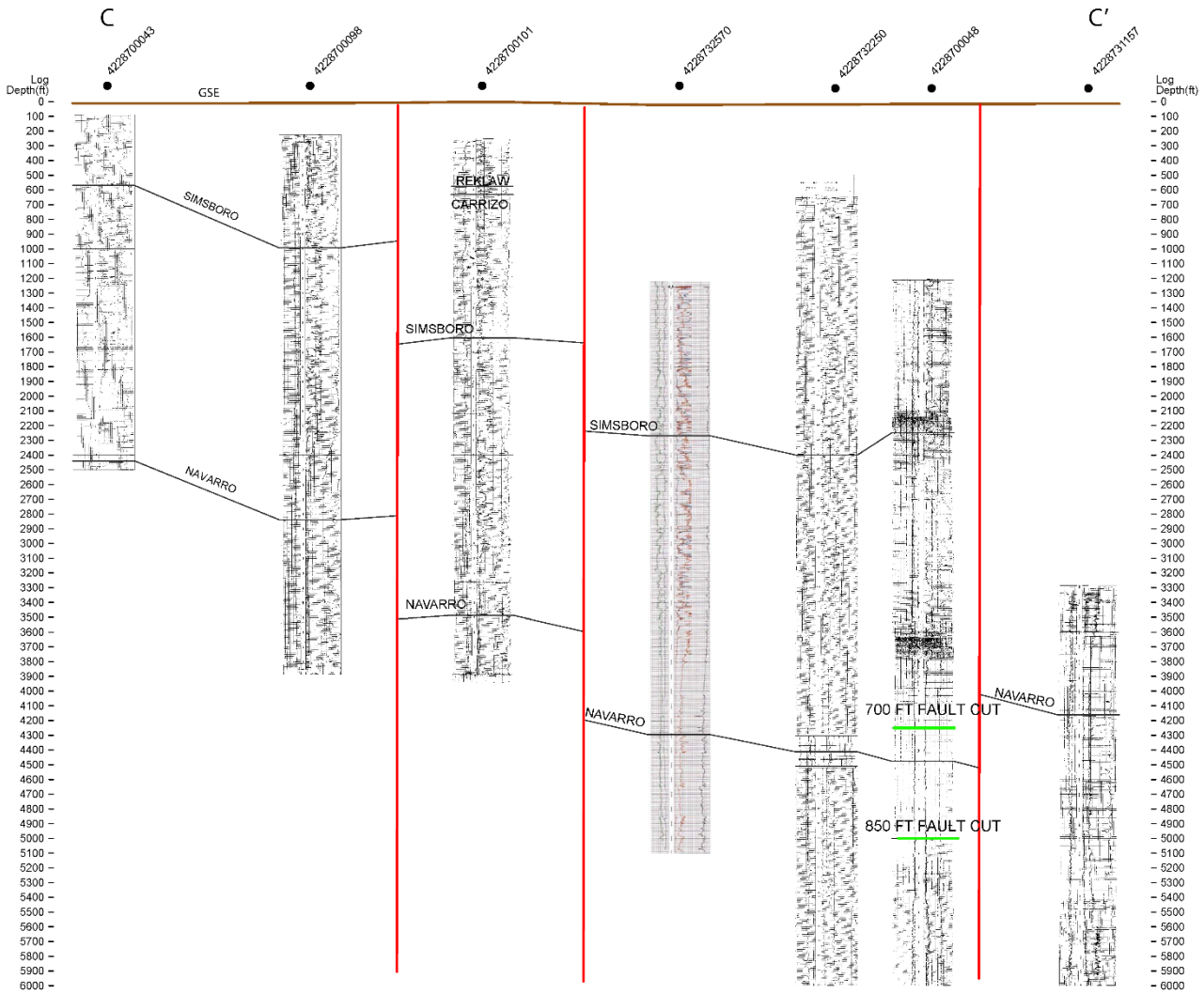

Figure 5-13. Geophysical logs associated with cross section C-C' through a northeastern portion of the Paige Graben showing the top surface of selected formations and mapped fault locations based on interpretation of geophysical logs in and near cross section C-C'.

Note: ft = feet

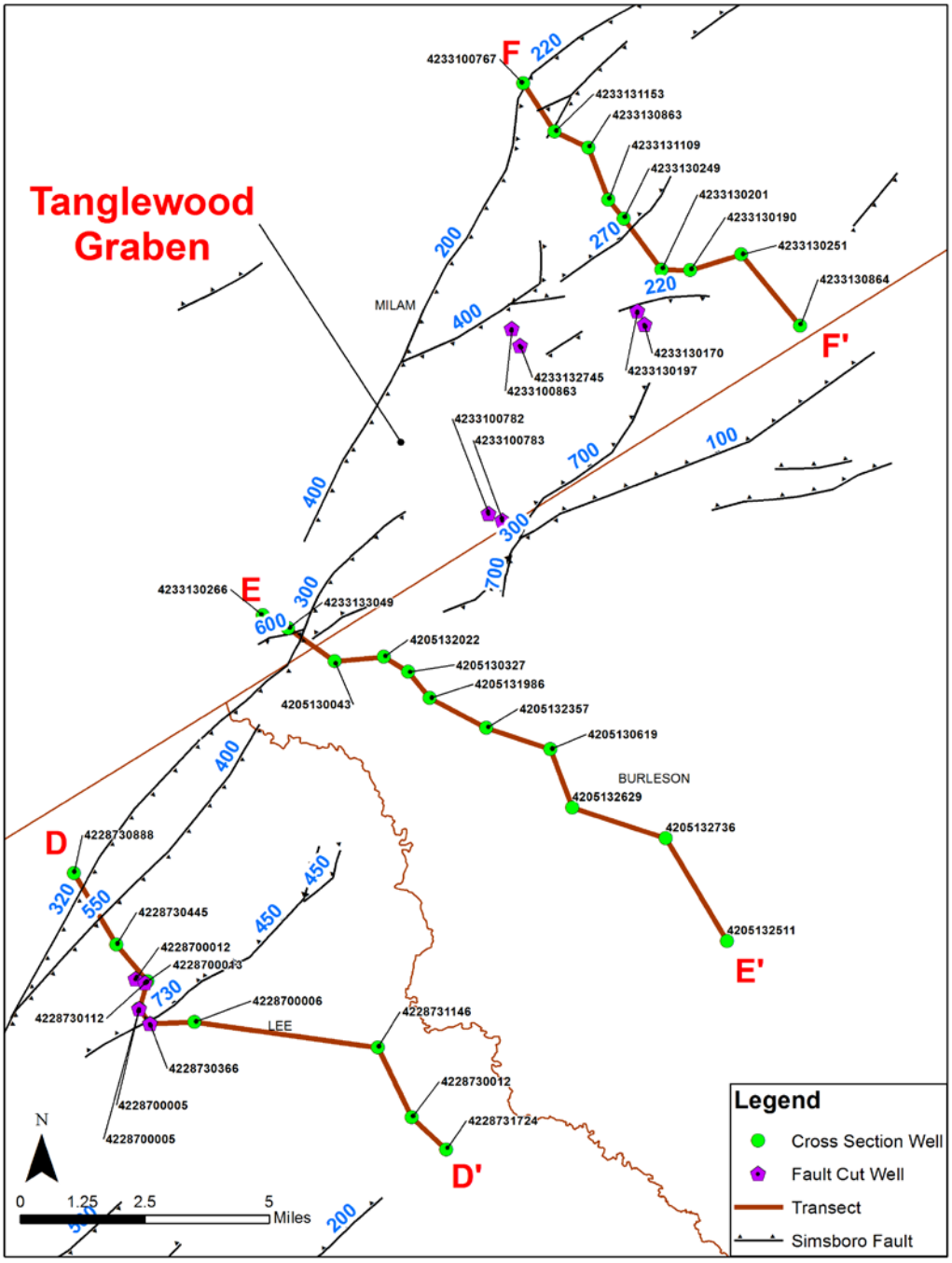

Figure 5-14. Location of cross sections D-D', E-E' and F-F', which cross through the Tanglewood Graben in Lee, Milam and Burleson counties. The American Petroleum Institute numbers of the geophysical logs comprising the cross sections are used to label the geophysical logs.

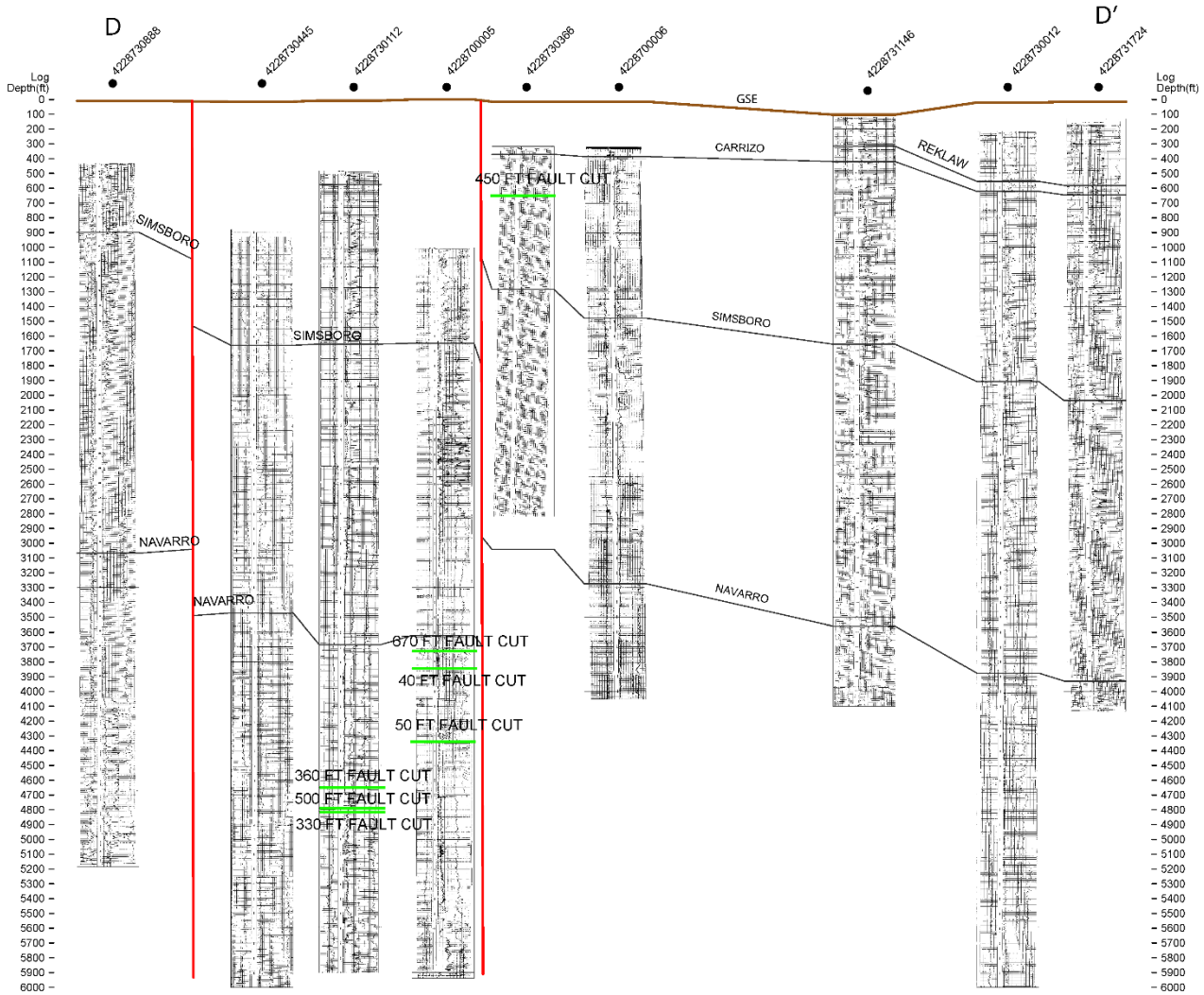

Figure 5-15. Geophysical logs associated with cross section D-D' through a southern portion of the Tanglewood Graben showing the top surface of selected formations and mapped fault locations based on interpretation of geophysical logs in and near cross section D-D'.

Note: ft = feet

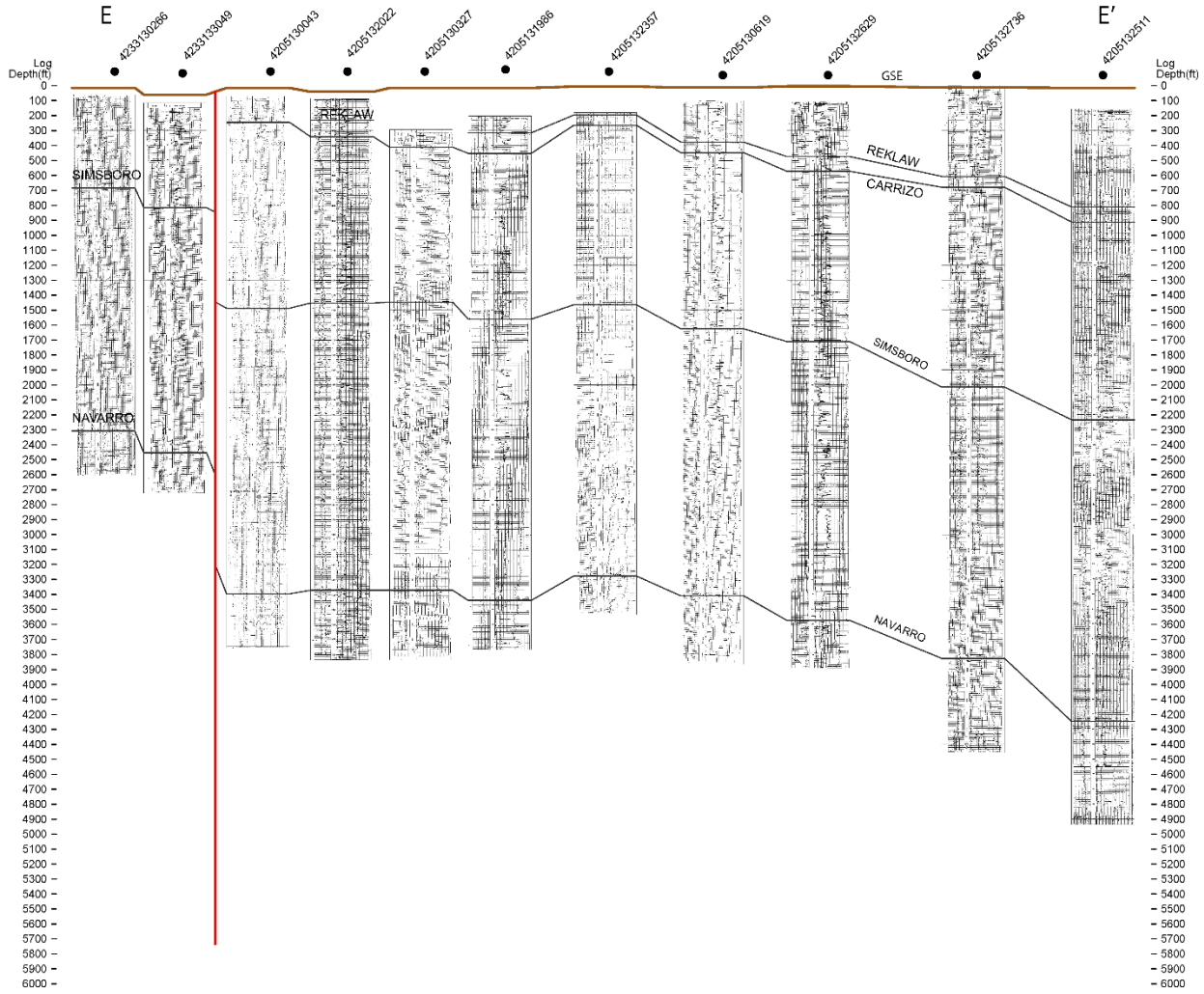

Figure 5-16. Geophysical logs associated with cross section E-E' through a middle portion of the Tanglewood Graben showing the top surface of selected formations and mapped fault locations based on interpretation of geophysical logs in and near cross section E-E'.

Note: ft = feet

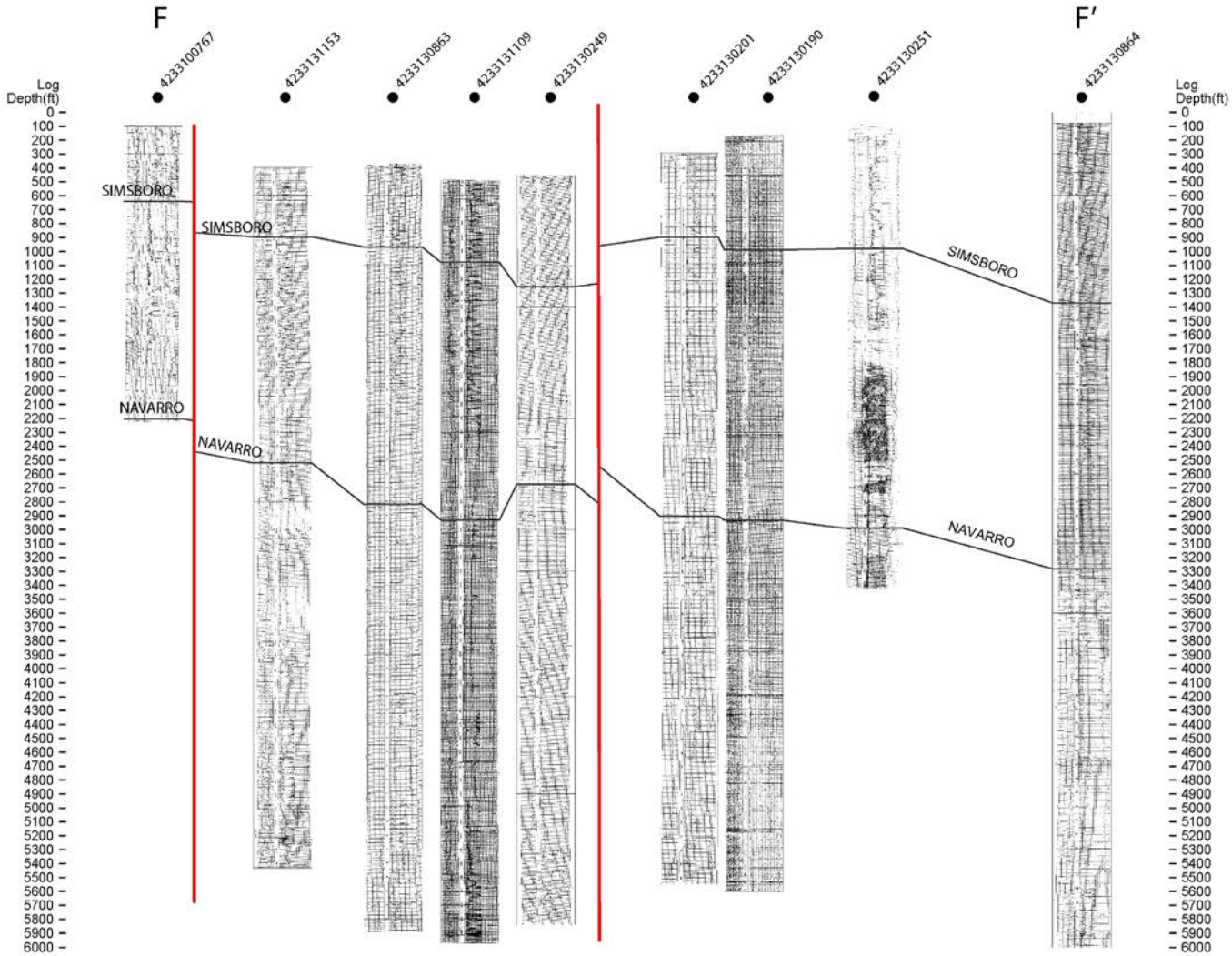

Figure 5-17. Geophysical logs associated withcross -section F-F' through a northeastern portion of the Tanglewood Graben showing the top surface of selected formations and mapped fault locations based on interpretation of geophysical logs in and near cross section F-F'.

Note: ft = feet

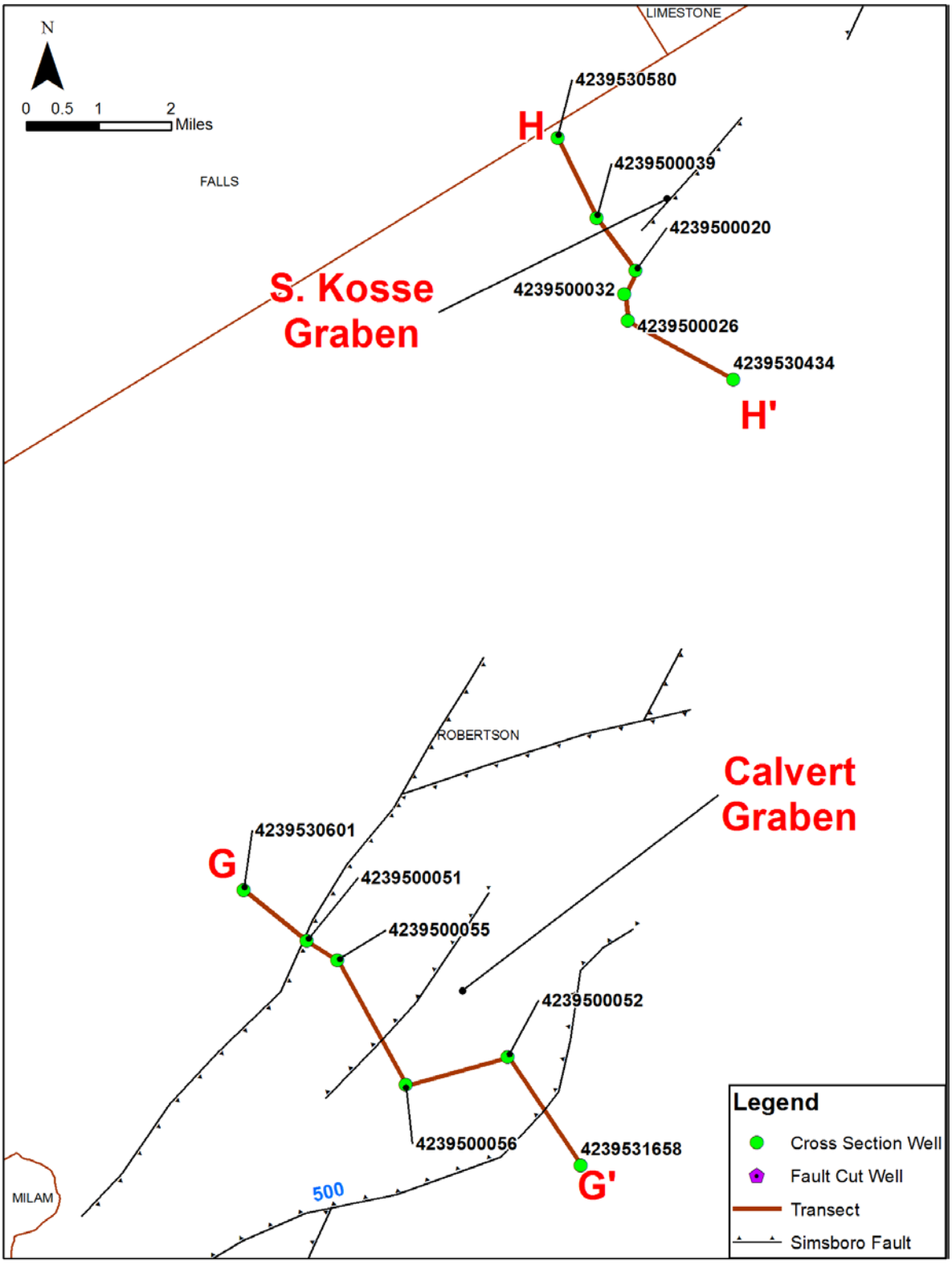

Figure 5-18. **Location of cross sections G-G', which crosses through the Calvert Graben in Robertson County and the location of cross section H-H', which crosses through the South Kosse Graben in Robertson County. The American Petroleum Institute numbers of the geophysical logs comprising the cross sections are used to label the geophysical logs.**

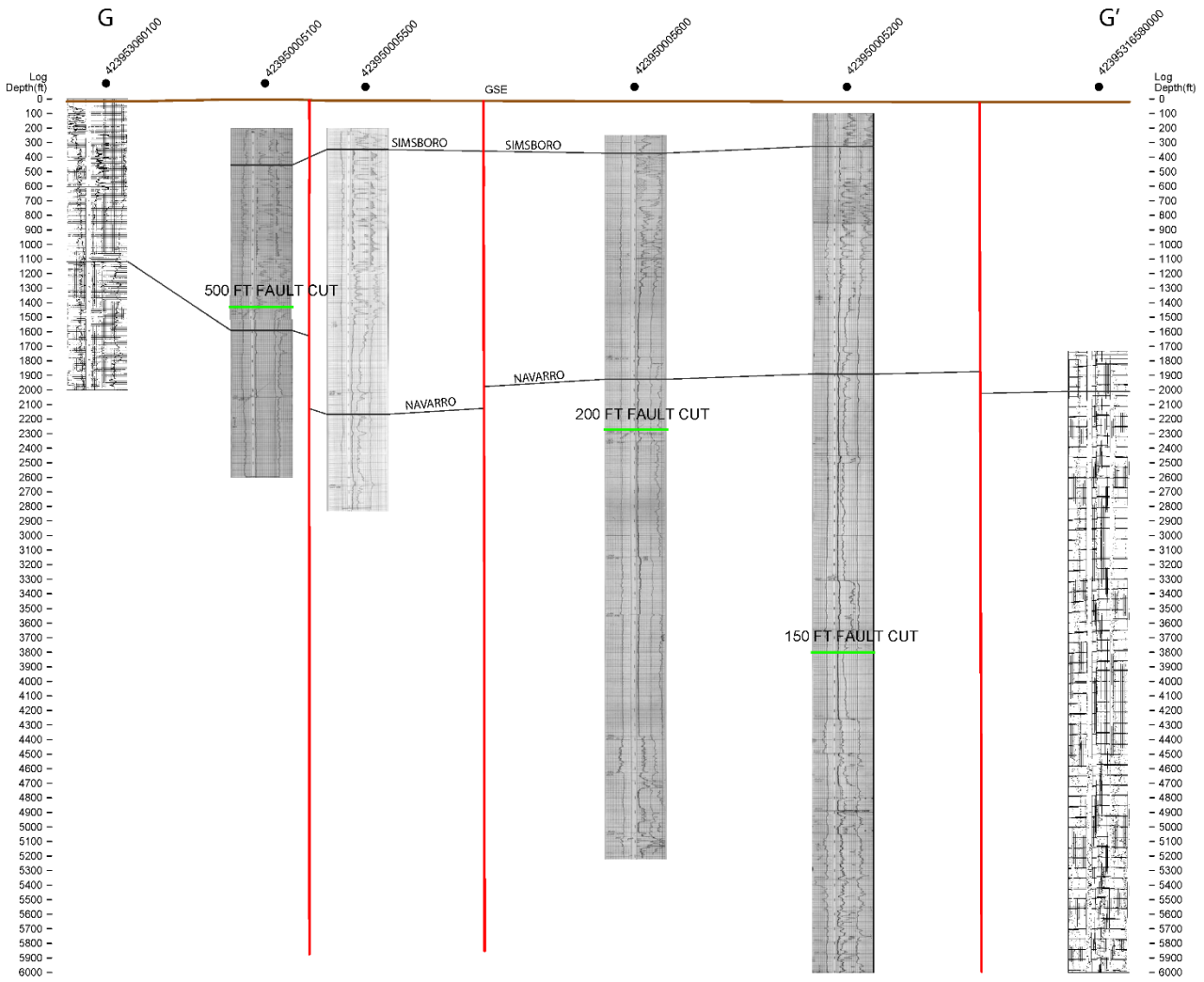

Figure 5-19. Geophysical logs associated with cross section G-G' through the Calvert Graben showing the top surface of selected formations and mapped fault locations based on interpretation of geophysical logs in and near cross section G-G'.

Note: ft = feet

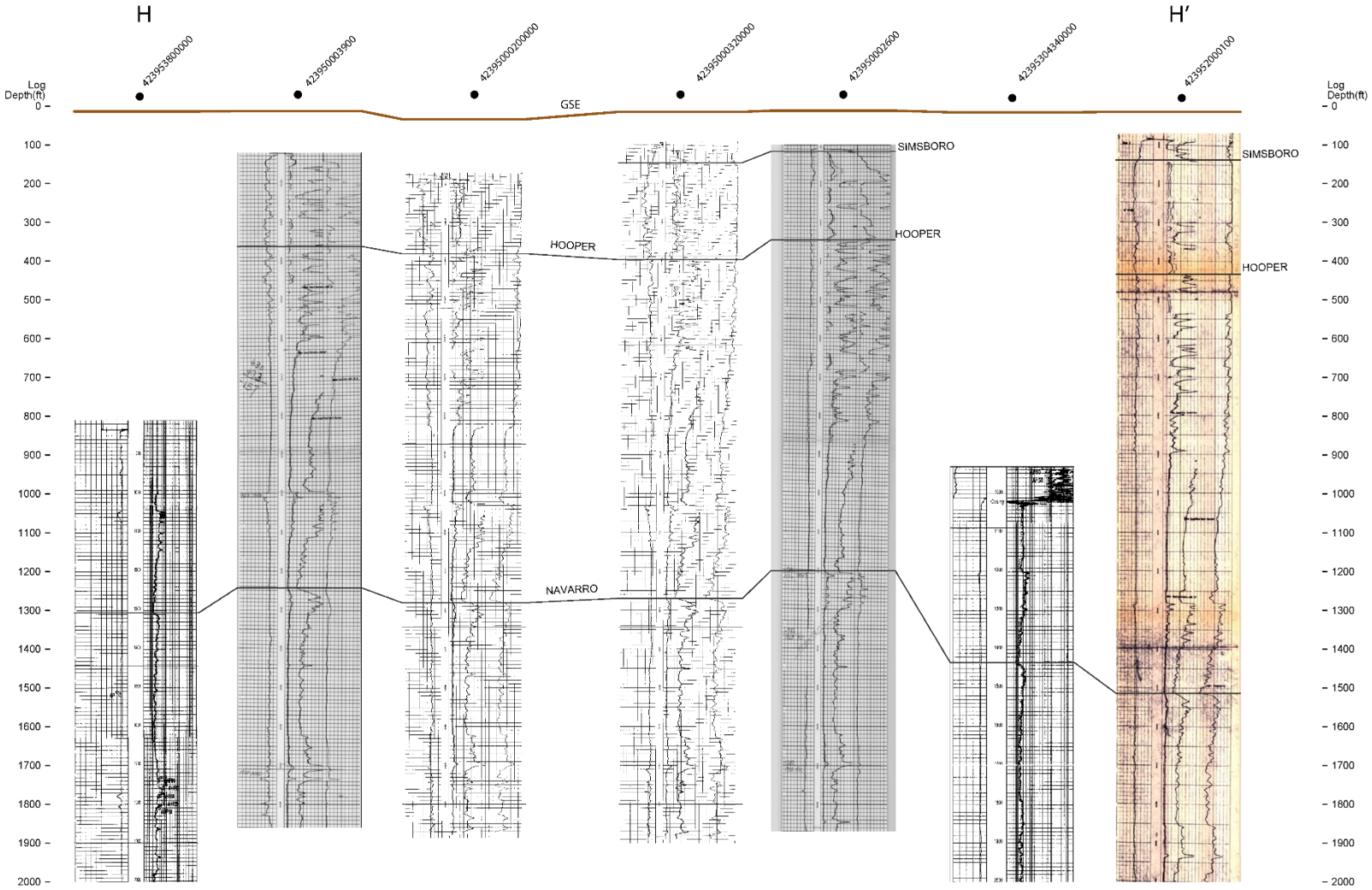

Figure 5-20. Geophysical logs associated with cross section H-H' through the South Kosse Graben showing the top surface of selected formations and mapped fault locations based on interpretation of geophysical logs in and near Cross Section H-H'.

Note: ft = feet

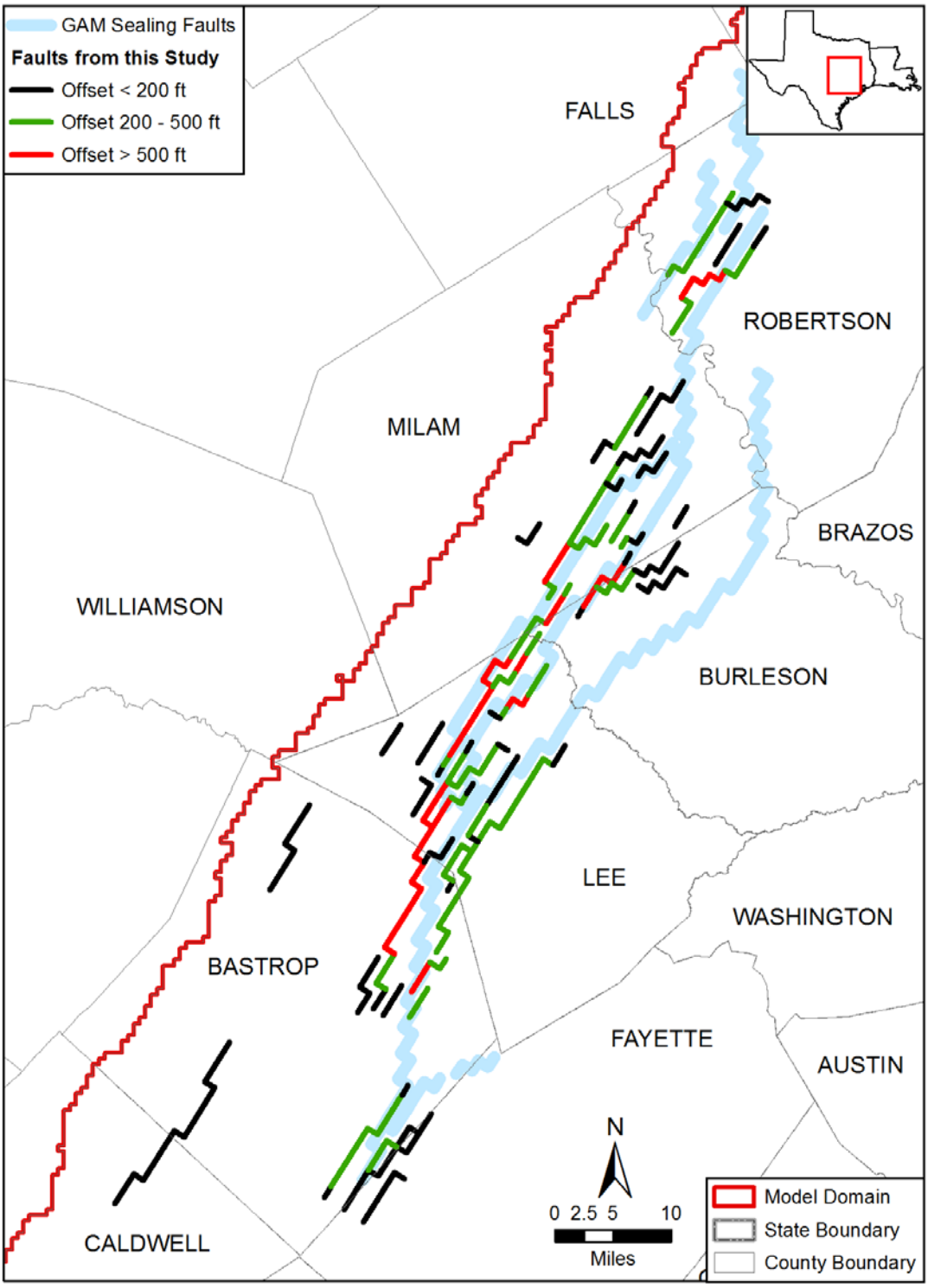

Figure 5-21. Sealing faults in the central Queen City and Sparta aquifers groundwater availability model and the Simsboro faults from this study sampled onto the groundwater availability model grid and color-coded based on the amount of offset between the Simsboro Formation updip and downdip of the fault.

Note: ft = feet

6 Sensitivity Analysis for Central Queen City and Sparta Aquifers Groundwater Availability Model

This section investigates whether the central Queen City and Sparta aquifers groundwater availability model predictions of water level change are sensitive to the changes in the properties and locations of horizontal flow barriers used to simulate the effects of faults on groundwater flow. To answer this question, three modeling scenarios were performed using the current groundwater availability model with different approaches for representing the faults. The three modeling scenarios represent the calibration period for the current groundwater availability model (1975 to 2000); the period from 2000 to 2010, which is a validation period for the existing updated groundwater availability model; and a predictive period from 2010 to 2070. The three approaches for representing the faults in the Milano Fault Zone are: 1) current groundwater availability model faults; 2) no faults; and 3) faults as they are characterized in Section 5 of this report.

6.1 Pumping Rates for the Modeling Scenario

The pumping rates for the modeling scenarios are based on a desired future condition simulation developed by Groundwater Management Area 12 called Pumping Scenario 10, or PS10. An important component of PS10 is that Groundwater Management Area 12 hydrogeological consultants made a concerted effort to accurately represent pumping in the model from 2000 to at least 2010. The primary reason for Groundwater Management Area 12 to develop PS10 was to improve the temporal and spatial distribution of pumping in the desired future condition predictive simulation using the most recent and best pumping information available.

Figure 6-1 shows the annual pumping rates in PS10 from 1975 to 2070 for the six model layers that represent aquifers in the groundwater availability model. The plot shows that, in Groundwater Management Area 12, the most heavily pumped aquifers are the Carrizo and Simsboro aquifers, both of which were being pumped at about 150,000 acre-feet per year in 2010. Because about 90 percent of the Carrizo pumping occurs away from the Milano Fault Zone, but about 90 percent of the Simsboro pumping occurs near and within the Milano Fault Zone, this study is primarily focused on pumping from the Simsboro Aquifer. The annual Simsboro pumping from 1975 to 2070 for six counties in the vicinity of the Milano Fault Zone shows that most of the Simsboro pumping occurs in Brazos and Robertson counties (Figure 6-2).

The PS10 pumping scenario is divided into three modeling scenarios based on time. The time period from 1975 to 2000 is the calibration period because the central Queen City and Sparta aquifers groundwater availability model was calibrated using measured water levels from this 25-year period. The period from 2000 to 2010 is a validation period because the predictive capability of the groundwater availability model can be validated using measured pumping rates and water levels during this period. The period from 2000 to 2070 is a predictive desired future condition period because Groundwater Management Area 12's desired future conditions are based on drawdowns over this 70-year period.

To help to interpret the drawdowns simulated by the central Queen City and Sparta aquifers groundwater availability model for PS10 from 1975 to 2070, the spatial distribution of pumping from the Simsboro is provided in Figures 6-3, 6-4, and 6-5. These three figures show the spatial distribution of pumping that has occurred in 1980, 1990, 2000, 2010 and the pumping that is expected to occur in 2050 and 2070.

6.2 Calibration Period from 1975 to 2000

The central Queen City and Sparta aquifers groundwater availability model was calibrated over the period from 1975 to 2000 (Kelley and others, 2004). For model calibration, the model's aquifer parameters, such as transmissivity and storativity, were adjusted to improve the match to historical water-level measurements. The difference between a measured and simulated water level is called the residual. For this study, the residual is defined by Equation 6-1.

$$r = h_o - h_s \qquad \text{(Equation 6-1)}$$

where:

r = residual,
h_o = observed water level, and
h_s = simulated water level.

Among the statistical metrics used to evaluate model performance with respect to water-level residuals is the root mean squared error and the mean error (Anderson and Woessner, 1992). The root mean squared error is defined as the square root of the average square of the residuals and is calculated by Equation 6-2.

$$\text{Root Mean Squared Error} = \sqrt{\frac{1}{n}\sum_{t=1}^{n}\left(h_s - h_o\right)_t^2} \qquad \text{(Equation 6-2)}$$

where:

n = number of observations.

A root mean squared error represents an estimate of the model's average error with regard to matching historical water levels. The mean error, which is described in Equation 6-3, is the average of the residuals.

$$\text{Mean Error} = \frac{1}{n}\sum_{t=1}^{n}\left(h_s - h_o\right)_t \qquad \text{(Equation 6-3)}$$

A mean error provides a general measure of the model's bias with regard to either overpredicting or underpredicting observed water levels.

The sensitivity of the central Queen City and Sparta aquifers groundwater availability model's ability to simulate historical water levels for the three assumptions regarding faults was evaluated for three sets of water-level measurement data. Each of the three data sets include two years of water-levels measurements for the winter months of November, December, January, and February. One data set contains water-level measurements for the winter months of 1979 and 1980. A second data set contains water-level measurements for the winter months of 1989 and 1990. A third data set contains water-level measurements for the winter months of 1999 and 2000.

Observed water-level data were compared to simulated water levels for three versions of the groundwater availability model. All versions were identical, except for how the groundwater availability model represented the faults. One groundwater availability model run did not alter the representation of the faults with the Horizontal Flow Barrier Package (see Section 2) from that used by Kelly and others (2004). No faults were included in a second groundwater availability model run, so it did not contain a Horizontal Flow Barrier Package (Hsieh and Freckleton, 1993). A third groundwater availability model run included the faults as defined by this study.

The faults defined in this study are described in Section 5. Figure 5-21 shows the location of this study's faults placed on the numerical grid for the central Queen City and Sparta aquifers groundwater availability model. For the purpose of this study, the conductance assigned to a fault identified by this study was based on the vertical offset associated with the fault. Faults having an offset greater than 500 feet were represented by horizontal flow barriers with a conductance of 10^{-4} day^{-1}. Faults having an offset between 200 and 500 feet were represented by horizontal flow barriers with a conductance of 10^{-3} day^{-1}. Faults having an offset of less than 200 feet were not represented in the model.

Table 6-1 provides the water-level residuals calculated between measured and simulated water levels for 1979-1980, 1989-1990 and 1999-2000. Figure 6-6a,b,c compares the different root mean squared error values by model layer and fault representation using bar charts for 1979-1980, 1989-1990, and 1999-2000, respectively. The comparisons show relatively little difference in the calculated root mean squared error values for the three fault representations for all model layers and time periods, except for layer 7 (Simsboro Aquifer) in 1999-2000 where the range is between 26 and 39 feet. Except for this one notable difference, there is a paucity of evidence based on root mean squared error values to indicate that how the faults are represented notably affects the ability of the groundwater availability model to accurately simulate historical water levels during the model calibration period.

Table 6-1. Statistical evaluation of water-level residuals (feet) for the central Queen City and Sparta aquifers groundwater availability model for three different representations of faults

Fault Type	Layer	1979 to 1980			1989 to 1990			1999 to 2000		
		Count	ME	RMSE	Count	ME	RMSE	Count	ME	RMSE
GAM Faults	1	11	-4.3	19.3	30	-9.6	21.4	47	-11.5	30.9
	2	23	-22.5	35.5	38	-10.9	27.1	38	-3.1	17.3
	3	32	10.5	34.1	54	3.3	30.1	72	10.7	35.2
	4	22	-0.5	38.1	59	-3.2	39.3	46	-13.9	34.6
	5	72	1.3	22.9	72	-7.9	29.7	79	-15.4	32.3
	6	58	-6.0	37.9	71	-11.3	32.3	106	-20.5	44.6
	7	23	-13.2	33.0	68	-7.3	29.5	84	10.9	38.8
	8	23	-10.3	31.3	38	-10.8	33.0	38	-3.6	25.6
No Faults	1	11	-4.3	19.4	30	-11.1	23.0	47	-13.4	32.9
	2	23	-22.5	35.5	38	-10.9	27.1	38	-3.2	17.5
	3	32	10.4	34.1	54	2.0	29.4	72	8.8	34.6
	4	22	-1.6	37.8	59	-5.3	39.0	46	-15.7	34.9
	5	72	1.0	22.8	72	-8.5	29.8	79	-17.0	32.6
	6	58	-6.5	37.7	71	-13.2	32.3	106	-22.6	45.4
	7	23	-16.7	30.9	68	-12.5	28.9	84	-2.6	26.2
	8	23	-11.3	31.7	38	-11.5	33.3	38	-4.5	25.7
This Study Faults	1	11	-4.3	19.4	30	-10.5	22.3	47	-12.5	31.9
	2	23	-22.5	35.5	38	-10.9	27.1	38	-3.2	17.4
	3	32	10.5	34.1	54	2.9	29.6	72	9.7	35.1
	4	22	-1.6	37.7	59	-4.5	39.0	46	-14.4	34.7
	5	72	1.1	22.7	72	-8.3	29.7	79	-16.5	32.6
	6	58	-6.4	37.7	71	-12.6	32.3	106	-21.8	45.3
	7	23	-16.0	31.0	68	-11.6	28.4	84	-1.4	26.4
	8	23	-11.2	31.6	38	-11.4	33.2	38	-4.3	25.7

Note: GAM = groundwater availability model; ME = mean error; RMSE = root mean squared error

6.3 Validation Period from 2000 to 2010

The sensitivity of the the central Queen City and Sparta aquifers groundwater availability model ability to reproduce measured water-level measurements from the winter months in 2009 and 2010 was evaluated with respect to three fault representations, Table 6-2 provides the statistical summary of water-level residuals for 2009 and 2010 and Figure 6-6d compares the root mean squared error values by model layer using a bar chart. Calculation of the statistics in Table 6-2 used the same process as that used to calculate the statistics in Table 6-1. Like that observed for the calibration period, the three different fault representations produce nearly identical root mean squared error values for the Sparta, Queen City, Calvert Bluff, and Hooper formations. But unlike the comparisons for the calibration period, the root mean squared error value of 92 feet for the Simsboro for the groundwater availability model run using the current groundwater availability model faults is much larger than the root mean squared error values for the groundwater availability model run with no faults (45 feet) and using the faults from this study (53 feet).

The simulations of the validation period reflect a trend of increasing model error in predicted Simsboro water levels over time for the groundwater availability model run with the fault representation from the central Queen City and Sparta aquifers groundwater availability model. The root mean squared error values for the Simsboro increased from 29 feet in 1990 to 39 feet in 2000, and then jumped to 92 feet in 2010. A possible explanation for the trend of increasing root mean squared error values over time in the Simsboro is that the current groundwater availability model overpredicts drawdown because the horizontal flow barriers do not allow sufficient groundwater flow through the Milano Flow Zone to pumping wells located in Brazos and Robertson counties. Figure 6-2 shows that a large increase in Simboro pumping has occurred in Brazos and Robertson counties from 1990 to 2010. Over this same time period, Figure 6-7 shows that the mean error between observed and simulated water levels in the Simsboro steadily becomes more positive over time (a positive value indicates the model is underpredict the water-level elevation). In 1980, the mean error was -14 feet, and in 2010, the mean error was 50 feet. This indicates that as Simsboro pumping in Brazos and Robertson counties downgradient of the faults has increased, the ability of the model to matched observed water levels has decreased. This lack of match between observed and simulation heads was not observed during the calibration period because of lower pumping and a paucity of observed data for use as calibration targets.

Table 6-2. Statistical evaluation of water-level residuals (feet) for 2009 and 2010 for the central Queen City and Sparta aquifers groundwater availability model for three different representations of faults.

Fault Type	Layer	2009 to 2010		
		Count	ME	RMSE
GAM Faults	1	40	-8.1	25.7
	2	51	2.2	20.8
	3	67	6.7	30.4
	4	39	-20.5	49.9
	5	128	13.1	48.2
	6	103	-19.7	50.8
	7	76	50.7	91.6
	8	51	1.7	36.6
No Faults	1	40	-10.1	27.2
	2	51	2.1	21.0
	3	67	5.1	29.9
	4	39	-22.3	50.3
	5	128	9.8	48.1
	6	103	-22.9	52.3
	7	76	17.9	45.2
	8	51	-0.9	38.8
This Study Faults	1	40	-9.3	26.4
	2	51	2.1	20.9
	3	67	5.8	30.2
	4	39	-21.3	50.2
	5	128	11.3	47.9
	6	103	-21.6	51.3
	7	76	23.4	52.9
	8	51	0.0	38.5

Note: GAM = groundwater availability model; ME = mean error; RMSE = root mean squared error

6.3.1 Simulated Simsboro Water Levels for 2010

Figures 6-8, 6-9, and 6-10 show contours of water levels in the vicinity of the Milano Fault Zone for the Simsboro for the groundwater availability model runs with the current central Queen City and Sparta aquifers groundwater availability model faults, no faults, and the faults from this study, respectively. All three figures show very similar patterns in the water-level contours in terms of the inferred direction of groundwater flow. The primary difference between the simulated values is the magnitude of the water-level elevations. Across most of the Milano Fault Zone, including Bastrop, Fayette, Lee, Milam and Burleson counties, the difference in the water levels is between 30 and 50 feet. In these areas, it would be difficult to evaluate the water levels residuals to conclusively determine which of the three groundwater availability model runs provides the best representation of the Milano Fault Zone in the groundwater availability model. Among the problems associated with trying to evaluate the merits of different faults conceptualizations is the uncertainty in the model predictive capability, the uncertainty and error in representing actual pumping, the limited locations of the monitoring locations, and the error and uncertainty associated with obtaining representative water-levels measurements for a well that is partially screened in a model layer and may have been recently pumped before the sampling event.

A comparison of the water levels in Figures 6-8, 6-9, and 6-10 shows that in northwest Brazos County and west and northwest Roberstson County, the differences in predicted water levels between the various fault representations are greater than 100 feet. This area also correponds to the two regions of highest pumping in the Simsboro in 2010 (see Figure 6-4b) and the location of the largest 2010 water-level residuals for the simulation with the central Queen City and Sparta aquifers groundwater availability model faults simulation shown Figure 6-11.

6.3.2 Hydrographs for Wells in Northwest Robertson and Northwest Brazos County

Figure 6-12 shows 2010 water-level residuals for wells in central and western Robertson County and northwest Brazos County, and identifies several of the the wells with residuals greater than 50 feet. These wells are grouped into three areas. Area 1 is in Brazos County and encompasses the well fields for the Cities of Byran and College Station. Area 2 includes wells in Robertson County that are about 10 miles east of the Calvert Graben (see Figure 5-8). Area 3 includes wells in western Robertson County downdip of the Calvert Graben. Figures 6-13 through 6-15 show hydrographs for wells in the three areas, respectively. Each hydrograph includes measured water levels through 2014 and simulated water levels for the well based on simulations with the three aforementioned fault representations.

For wells in these three areas, there is a significant difference in the simulated water levels between the groundwater availability model simulation with the current groundwater availability model faults and the groundwater availability model simulation without faults. At the selected well locations, the groundwater availability model simulation with the current groundwater availability model faults over predicts drawdowns between 60 and 150 feet by 2010. For the majority of the wells, the water levels simulated by groundwater availability model run without faults match the historical water levels significantly better than do the water levels from the groundwater availability model simulation with the current groundwater availability model

faults. For two of the wells (wells 3961501 [Figure 6-14] and 591209 [Figure 6-13]), where water levels have been measured for more than 30 years, the simulated water levels from the groundwater availability model run with no faults provide a good match with measured water levels. Over this 30-year period, the water level in well 591209 declined about 225 feet and the water level in well 3961501 declined about 110 feet. For both wells, the groundwater availability model simulation without faults produces a root mean squared error value that is less than 10 percent of the water-level decline, while the groundwater availability model simulation with the current groundwater availability model faults produces a root mean squared error value that averages 40 percent of the of the water-level decline. This comparison is a strong line of evidence that there may be too much restriction of groundwater flow throught the Milano Fault Zone with the fault representation in the current Queen City and Sparta aquifers groundwater availability model.

Between 2010 and 2014, the measured water levels in all the selected wells are significantly better matched by the water levels simulated with the groundwater availability model run without faults than those simulated with the groundwater availability model run using the current groundwater availability model faults. To illustrate this point, root mean squared error values were calculated using water-level data from 2010 to 2014 for seven of the nine wells in Areas 1 and 2. The root mean squared error for the water levels simulated by the groundwater availability model run without faults is 25 feet, but the root mean squared error for the water levels simulated by the groundwater availability model run with the current groundwater availability model faults is 97 feet. This comparison is also a strong line of evidence that the current groundwater availability model faults may be restricting too much groundwater flow through the Milano Fault Zone.

At this point in our investigation, we have not determined how to assign properties to the faults identified by this study. However, a groundwater availability model run with the faults using reasonable hydraulic parameters based strictly on fault offset provides reasonable drawdown predictions. Visual comparison of the hydrographs in Figures 6-13 through 6-15 shows that, for our initial assumptions for assigning conductance to faults, the simulated water levels are reasonable and do not result in the large over prediction of drawdowns found with the current groundwater availability model faults.

6.4 Prediction Period from 2000 to 2070

Several of Groundwater Management Area 12's desired future condition simulations are based on the drawdowns predicted by the central Queen City and Sparta aquifers groundwater availability model from 2000 and 2070. For this reason, the focus of the sensitivity of the groundwater availability model results to fault representation for the prediction period compares drawdowns instead of water levels. Table 6-3 provides the average drawdowns calculated from predicted drawdowns for the groundwater availability model simulations using the fault representation in the central Queen City and Sparta aquifers groundwater availability model, no faults, and the faults from this study.

The largest average drawdown occurs for the groundwater availability model run using the current groundwater availability model faults and the smallest average drawdown occurs for the

groundwater availability model run with no faults. The largest drawdowns are for the Simsboro Aquifer, followed by the Hooper Aquifer and then the Calvert Bluff Aquifer. The primary cause of drawdown in the Hooper and Calvert Bluff aquifers is pumping in the Simsboro Aquifer. The largest drawdowns in the Simsboro, Hooper, and Calvert Bluff aquifers all occur in Burleson County and are 423, 273, and 192 feet, respectively.

Figures 6-16, 6-17, and 6-18 show contours of simulated average drawdown for 2000 to 2070 using PS10 for the Simsboro and Carrizo aquifers for groundwater availability model runs with the current groundwater availability model faults, no faults, and the faults from this study, respectively. The impacts of the faults on simulated drawdowns is most evident for the Simsboro, with differences greater than 250 feet occurring across individual faults in northwest Burleson County and northwest Roberson County. A review of Simsboro pumping in 2070 (see Figure 6-5) shows that, at both locations, large pumping occurs immediately down dip of a fault line in the current groundwater availability model.

From the perspective of managing groundwater resources, a relevant question is the sensitivity of average drawdown values to how faults are represented in the groundwater availability model. This question is partially addressed by evaluating the differences in average drawdowns between the groundwater availability model runs with the different fault representations. This calculation was done for the six counties with drawdown most sensitive to the faults (Bastrop, Brazos, Burleson, Lee, Milam, and Robertson counties). Figure 6-19 shows the difference between the average drawdowns calculated for the groundwater availability model run with current groundwater availability model faults and the groundwater availability model run with no faults. The results indicate that, whether or not the faults are included in the groundwater availability model simulation, has an impact of 20 feet or less on the average drawdowns calculated for the Sparta, Queen City and Carrizo aquifers for all six counties and for all aquifers in both Milam and Bastrop counties. However, whether or not the faults are included in the groundwater availability model simulations can have a notable impact on the average drawdowns calculated for the Hooper, Simsboro, and Calvert Bluff aquifers in Brazos, Burleson, and Robertson counties. For instance, the difference is greater than 100 feet for the Simsboro aquifer in Brazos and Burleson counties and more than 85 feet for the Simsboro in Robertson and Lee counties.

The drawdown differences shown in Figure 6-19 are for the assumption that the faults are not influencing groundwater flow near the Milano Fault Zone; that is, it compares the difference between the drawdown for the current groundwater availability model faults and no faults. Another assumption that merits consideration is that faults do affect groundwater flow, but to a lesser degree than presumed by the current groundwater availability model faults and more akin to a degree provided by the faults identified in this study. Figure 6-20 illustrates the difference between the average drawdowns calculated for groundwater availability model runs with the current groundwater availability model faults and groundwater availability model runs with the faults from this study. These differences are similar to the comparison without faults for the Sparta, Queen City, and Carrizo aquifers but are generally slightly lower for the Hooper, Simsboro, and Calvert Bluff aquifers. For instance, for all six counties, the difference in the average drawdown is less than 65 feet for the Hooper and Calvert Bluff aquifers and less than 110 feet for the Simsboro Aquifer.

Besides average drawdown, another potential concern with managing groundwater is maximum drawdown predicted for a county as a result of groundwater pumping. Table 6-4 provides the maximum drawdowns calculated from predicted drawdowns for the groundwater availability model simulations using the fault representation in the central Queen City and Sparta aquifers groundwater availability model no faults, and the faults from this study. The largest maximum drawdown occurs for groundwater availability model runs using the current groundwater availability model faults and the least drawdown occurs with groundwater availability model runs using no faults. The largest maximum drawdowns are for the Simsboro Aquifer, followed by the Hooper Aquifer and then the Calvert Bluff Aquifer. The largest maximum drawdown in the Simsboro, Hooper, and Calvert Bluff aquifers are 686 feet in Burleson County, 307 feet in Bastrop County, and 203 feet in Burleson County, respectively.

Figures 6-21 and 6-22 show the sensitivity of simulated maximum drawdown to how the faults are represented in the groundwater availability model. Figure 6-21 illustrates the difference between the maximum drawdowns for the groundwater availability model run with current groundwater availability model faults and the groundwater availability model run with no faults. The results show that this difference is more than 100 feet in the Simsboro Aquifer in Bastrop, Brazos, Lee, Milam, and Robertson counties and is 265 feet in Burleson County. Figure 6-22 shows the difference between the maximum drawdown for the groundwater availability model run with the current groundwater availability model faults and the groundwater availability model run with the faults from this study. These differences are similar for the Sparta, Queen City, and Carrizo aquifers but are slightly lower for the Hooper, Simsboro, and Calvert Bluff aquifers. For instance, the difference in the maximum drawdown between the two groundwater availability model runs is less than 70 feet for the Hooper and Calvert Bluff aquifers and less than 250 feet for the Simsboro Aquifer.

Table 6-3. Average Drawdown(ft) from 2000 to 2070 for select counties for groundwater availability model simulations using three different representation of faults.

County	Fault Type	Sparta	Queen City	Carrizo	Calvert Bluff	Simsboro	Hooper
Bastrop	GAM Faults	-9	16	74	81	175	154
	This Study Faults	-9	15	72	72	160	140
	No Faults	-10	15	72	68	155	136
Brazos	GAM Faults	19	22	81	178	360	248
	This Study Faults	17	20	66	135	271	187
	No Faults	17	19	63	124	250	171
Burleson	GAM Faults	29	34	76	192	423	273
	This Study Faults	25	28	64	146	315	208
	No Faults	25	27	62	132	287	189
Lee	GAM Faults	10	16	64	142	350	225
	This Study Faults	7	13	56	112	283	183
	No Faults	7	12	55	101	262	169
Milam	GAM Faults	n/a	-5	27	66	179	129
	This Study Faults	n/a	-5	36	58	188	119
	No Faults	n/a	-5	38	55	182	114
Robertson	GAM Faults	-9	-4	36	85	250	181
	This Study Faults	-10	-6	30	65	177	134
	No Faults	-10	-6	28	60	160	123

Note: GAM = groundwater availability model

Table 6-4. Maximum drawdown from 2000 to 2070 for select counties for groundwater availability model simulations using three different representation of faults.

County	Fault Type	Sparta	Queen City	Carrizo	Calvert Bluff	Simsboro	Hooper
Bastrop	GAM Faults - No Faults	10	14	6	18	107	23
	This Study Faults - No Faults	2	2	3	5	29	7
Brazos	GAM Faults - No Faults	2	6	18	60	126	83
	This Study Faults - No Faults	0	1	3	12	24	17
Burleson	GAM Faults - No Faults	5	9	21	63	265	86
	This Study Faults - No Faults	1	2	1	13	34	20
Lee	GAM Faults - No Faults	5	7	15	62	176	82
	This Study Faults - No Faults	1	2	5	14	34	20
Milam	GAM Faults - No Faults	n/a	1	-13	56	139	83
	This Study Faults - No Faults	n/a	0	-8	12	18	19
Robertson	GAM Faults - No Faults	2	5	13	61	125	83
	This Study Faults - No Faults	0	1	2	12	24	17

Note: GAM = groundwater availability model

6.5 Implication Regarding Model Update

The comparison of the water level residuals from the three sets of groundwater availability model runs for the three fault representations strongly indicates that the additional fault segments that were added to the Simsboro Aquifer as part of the development of the central Queen City and Sparta aquifers groundwater availability model (see Section 2) could be one of the primary causes of the high water-level residuals that are calculated in Areas 1 to 3 shown in Figure 6-12. These additional faults include the continuous segments of sealing faults across Burleson County and into Brazos County. The implication to the model update is that large continuous sections of sealing faults will not be incorporated into the model unless there are field data that support such a representation.

The match to measured water levels is significantly better with the groundwater availability model runs using the faults from this study than those with the groundwater availability model runs using the faults in the Queen City and Sparta aquifers groundwater availability model. The favorable comparison suggests that our initial estimate of conductances for the faults is reasonable and could be a starting assumption for the model update.

The groundwater availability model simulations performed related to both the model validation and the predictive PS10 scenario demonstrate that the large amount of current and planned pumping in Robertson and Brazos counties elevates the area to one of high importance with regard to collecting reliable water level data. For most of the hydrographs shown for wells in Area 1, the measured water level has fluctuated 50 feet or more over periods of a few weeks. To better understand how to properly assign a confidence limit to the average water-level value, TWDB or INTERA should discuss the protocol that the Brazos Valley Groundwater Conservation District uses for monitoring water levels.

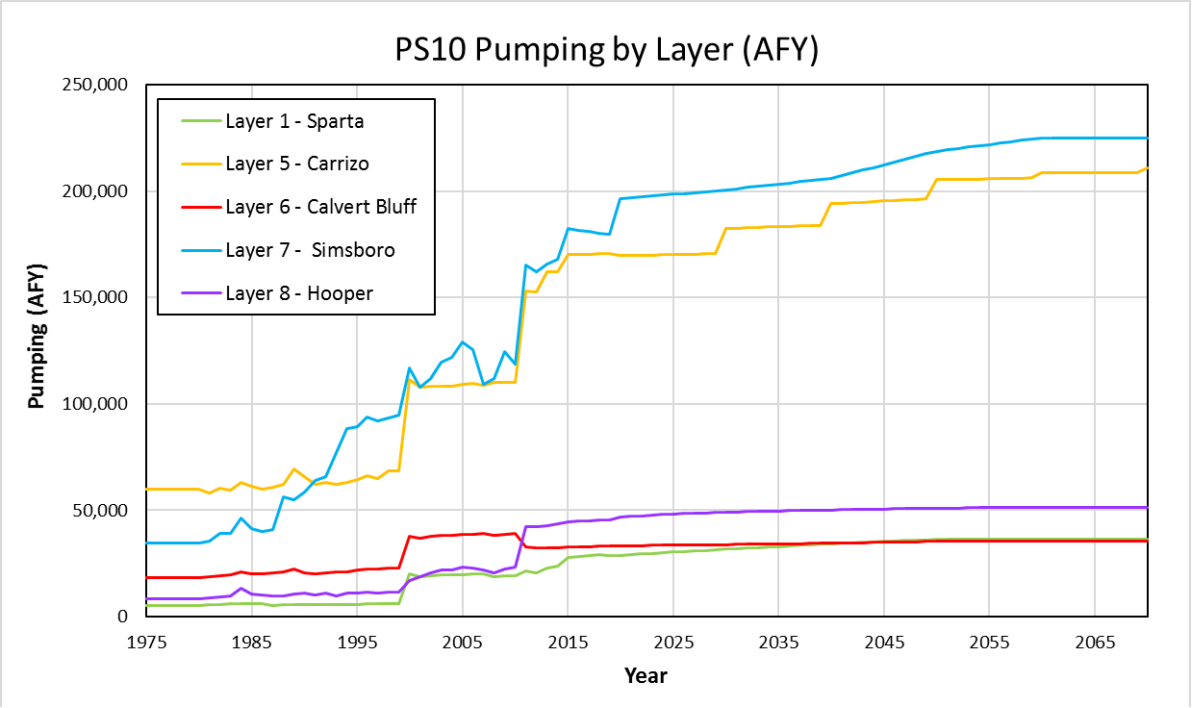

Figure 6-1. Pumping by aquifer in the central portion of the Queen City, Sparta, and Carrizo-Wilcox aquifers for pumping scenario 10.

Note: AFY = acre-feet per year

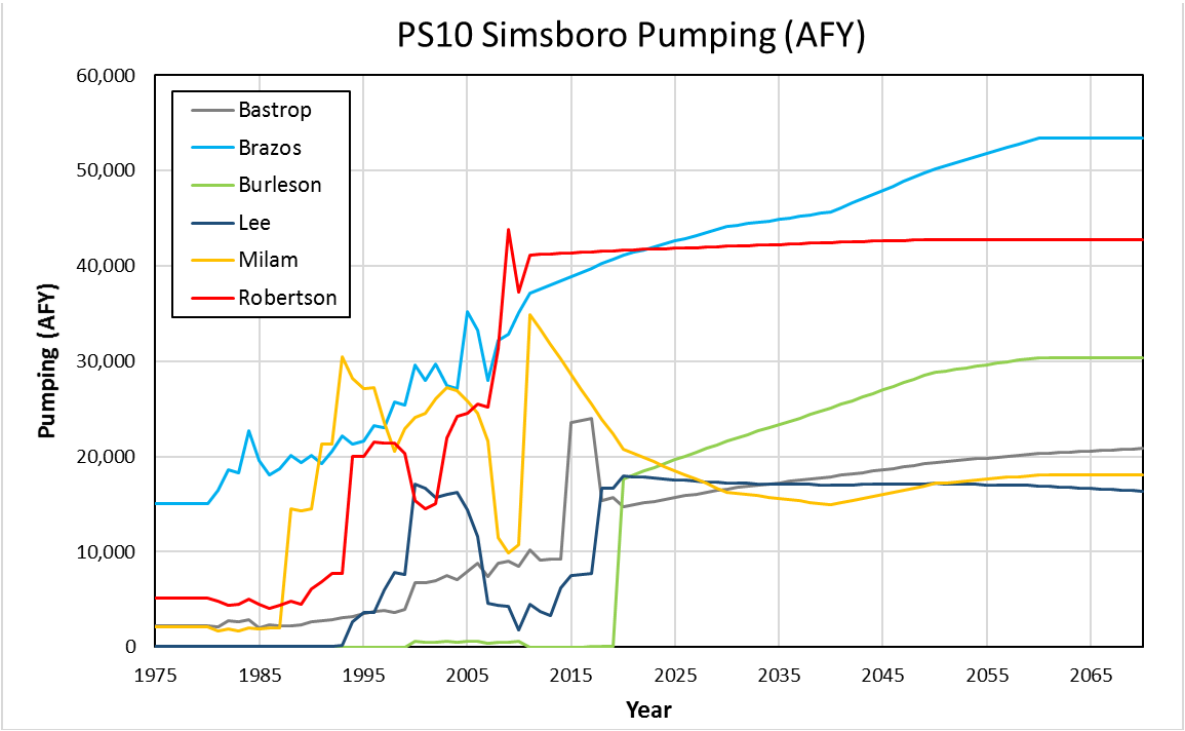

Figure 6-2. Simsboro pumping for select counties in the central portion of the Carrizo-Wilcox Aquifer for pumping scenario 10.

Note: AFY = acre-feet per year

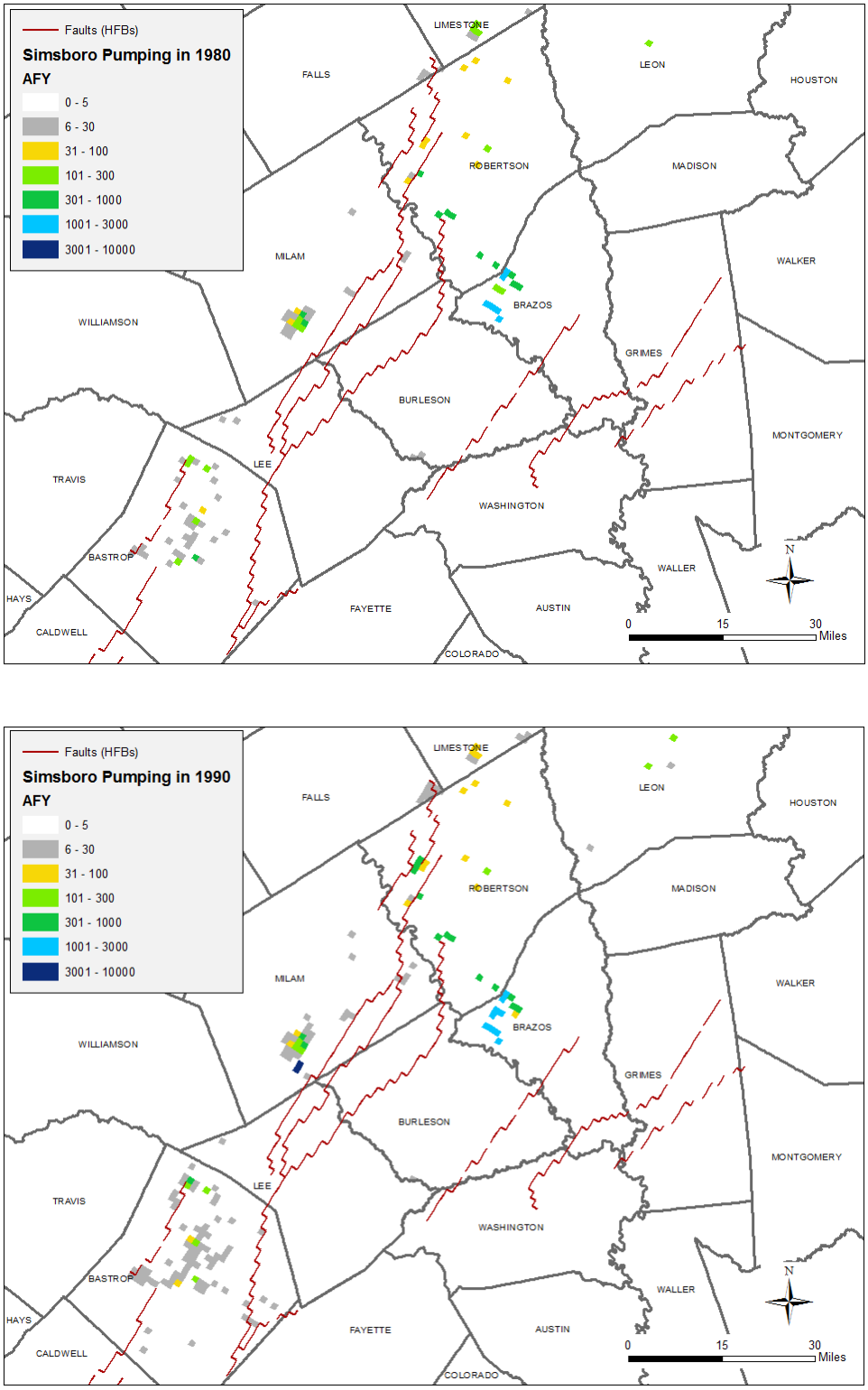

Figure 6-3. Spatial distribution of pumping in the Simsboro in (a) 1980 and (b) 1990 for pumping scenario 10.

Note: HFB = horizontal flow barrier; AFY = acre-feet per year

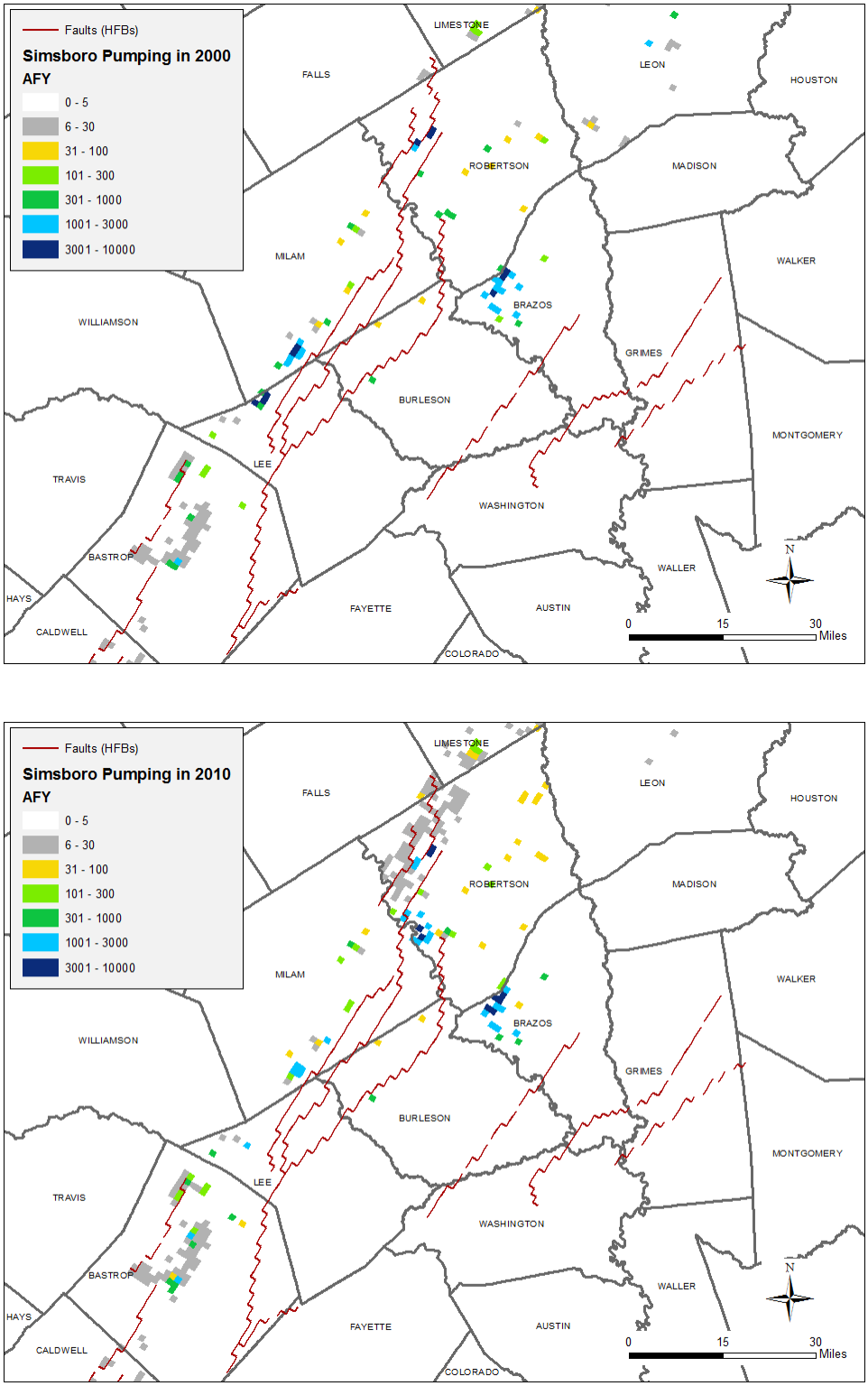

Figure 6-4. Spatial distribution of pumping in the Simsboro in (a) 2000 and (b) 2010 for pumping scenario 10.

Note: HFB = horizontal flow barrier; AFY = acre-feet per year

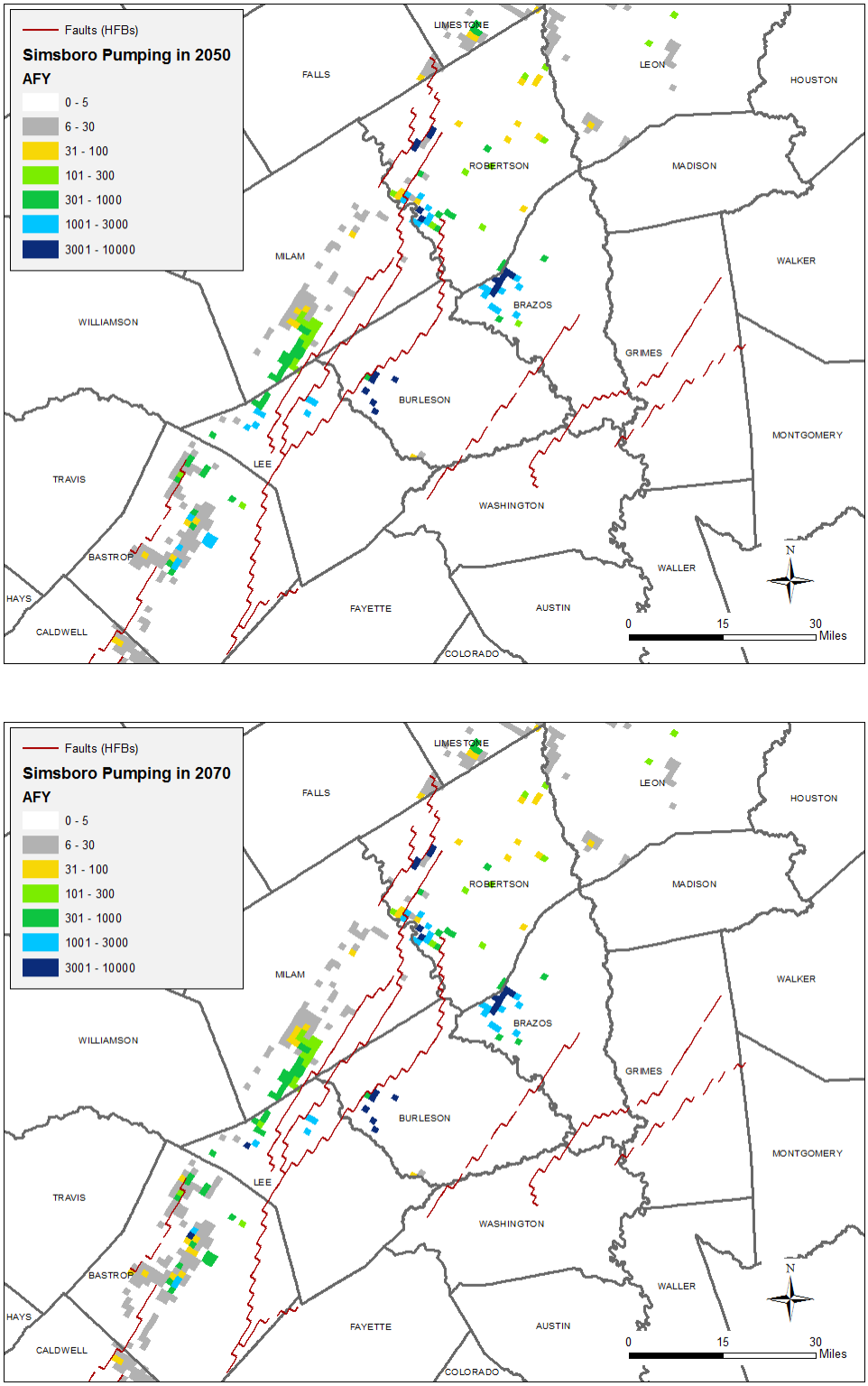

Figure 6-5. Spatial distribution of pumping in the Simsboro in (a) 2050 and (b) 2070 for pumping scenario 10.

Note: HFB = horizontal flow barrier; AFY = acre-feet per year

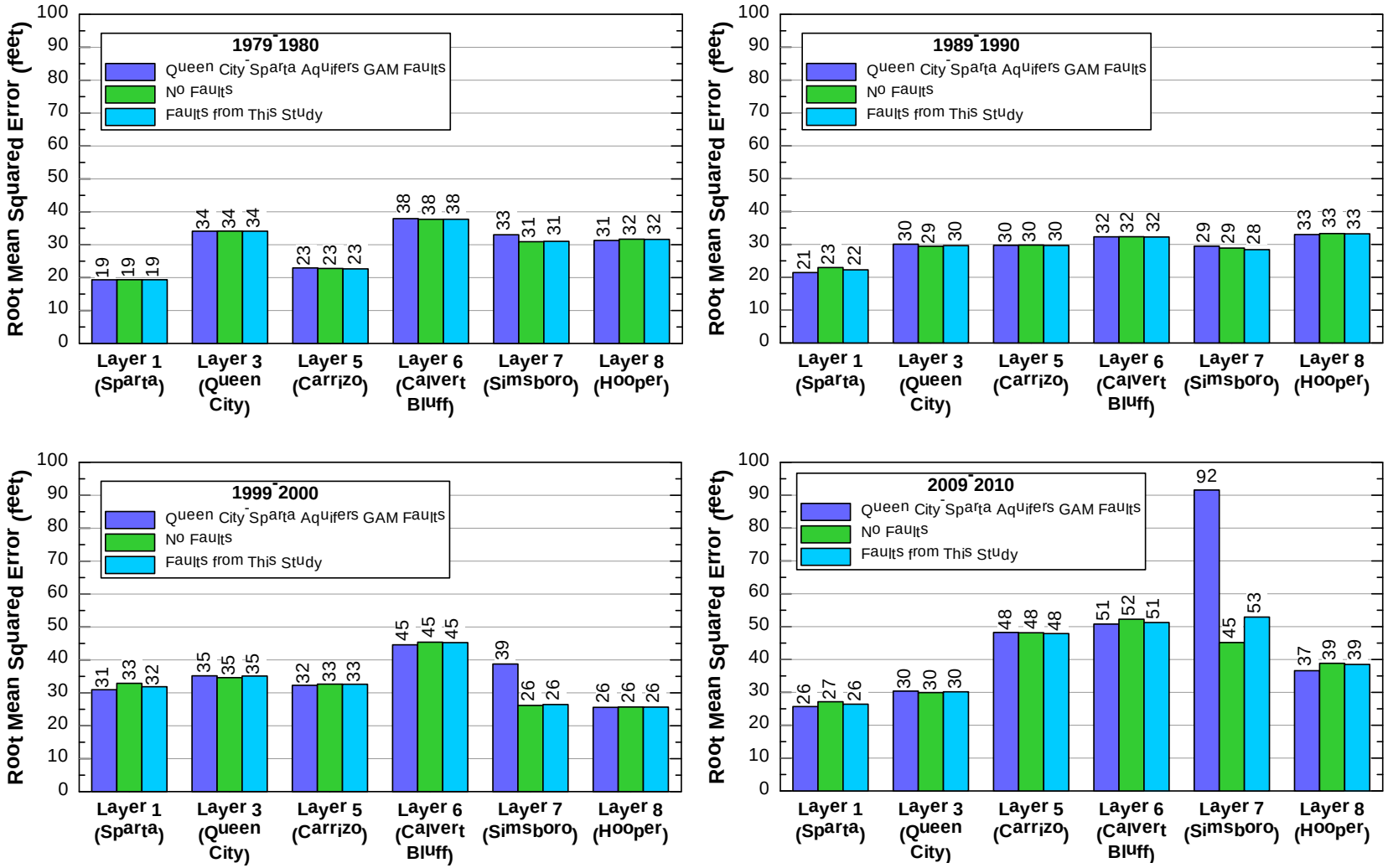

Figure 6-6. **Comparison of the root mean squared error for groundwater availability model (GAM) runs with the faults from the central Queen City-Sparta aquifers GAM, no faults, and the faults from this study for the years (a) 1979-1980, (b) 1989-1990, (c) 1999-2000, and (d) 2009-2010.**

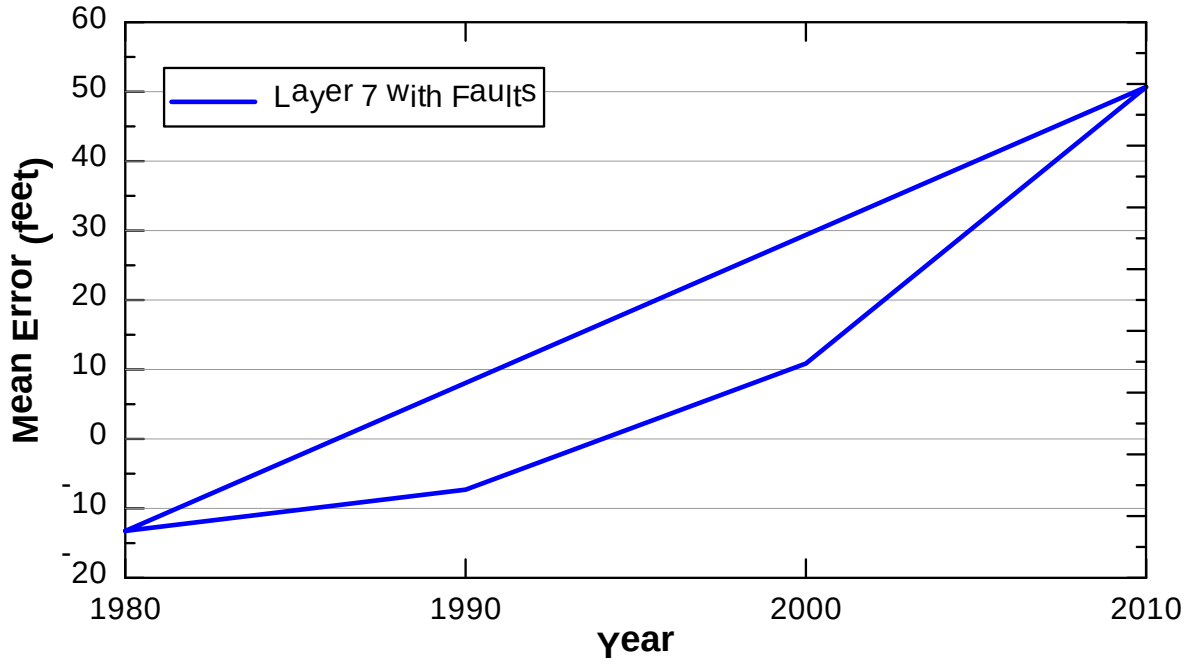

Figure 6-7. **Comparison of the mean error for groundwater availability model (GAM) runs with and without the faults in the central Queen City-Sparta aquifers GAM for (a) model layers 1, 3, and 5, (2) model layers 6 and 8, and (c) model layer 7.**

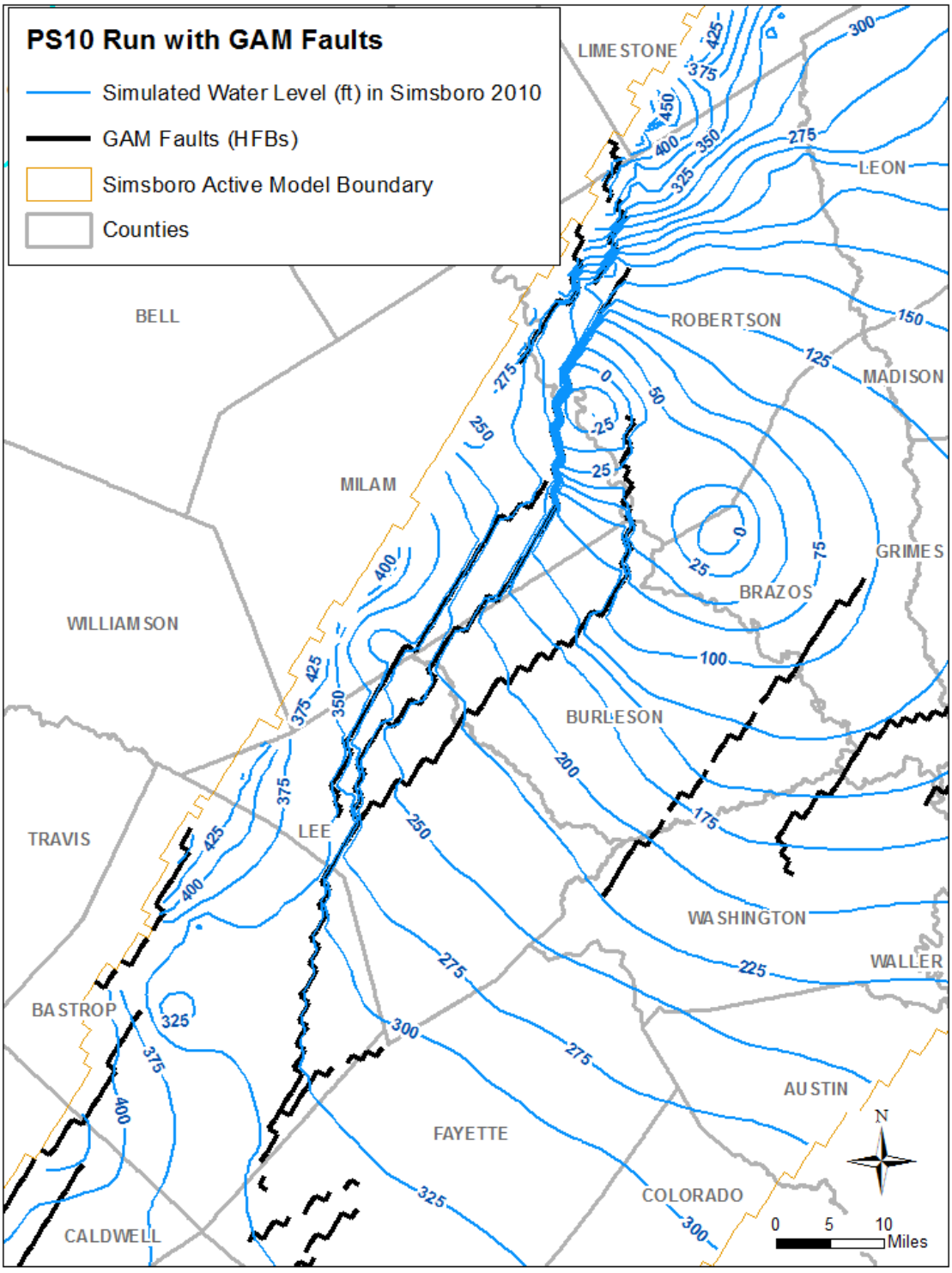

Figure 6-8. Predicted 2010 drawdown in the Simsboro for a groundwater availability model (GAM) run with the faults from the central Queen City-Sparta aquifers GAM faults.

Note: ft = feet; HFB = horizontal flow barrier

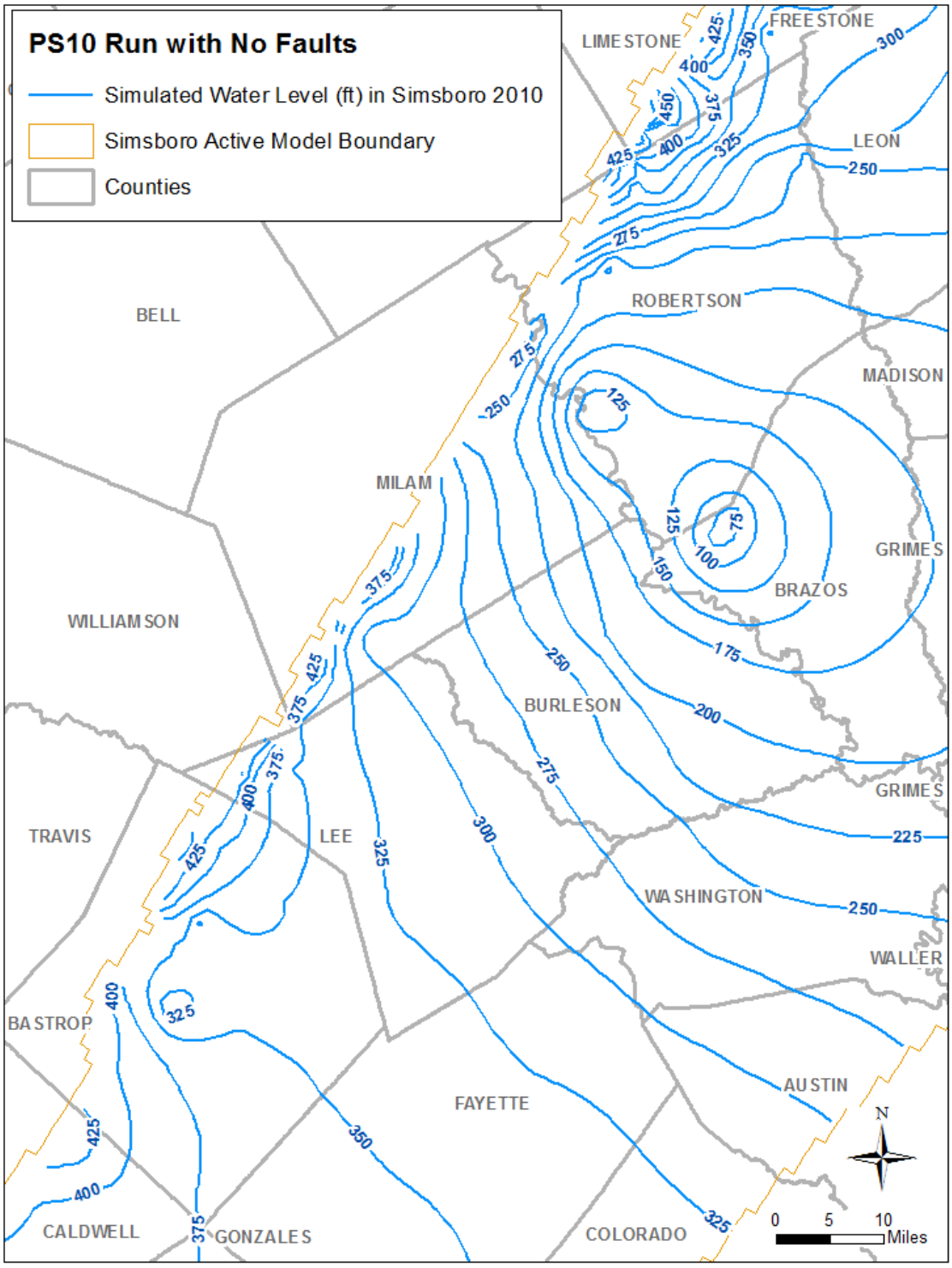

Figure 6-9. Predicted 2010 drawdown in the Simsboro for a groundwater availability model run with no faults.

Note: ft = feet

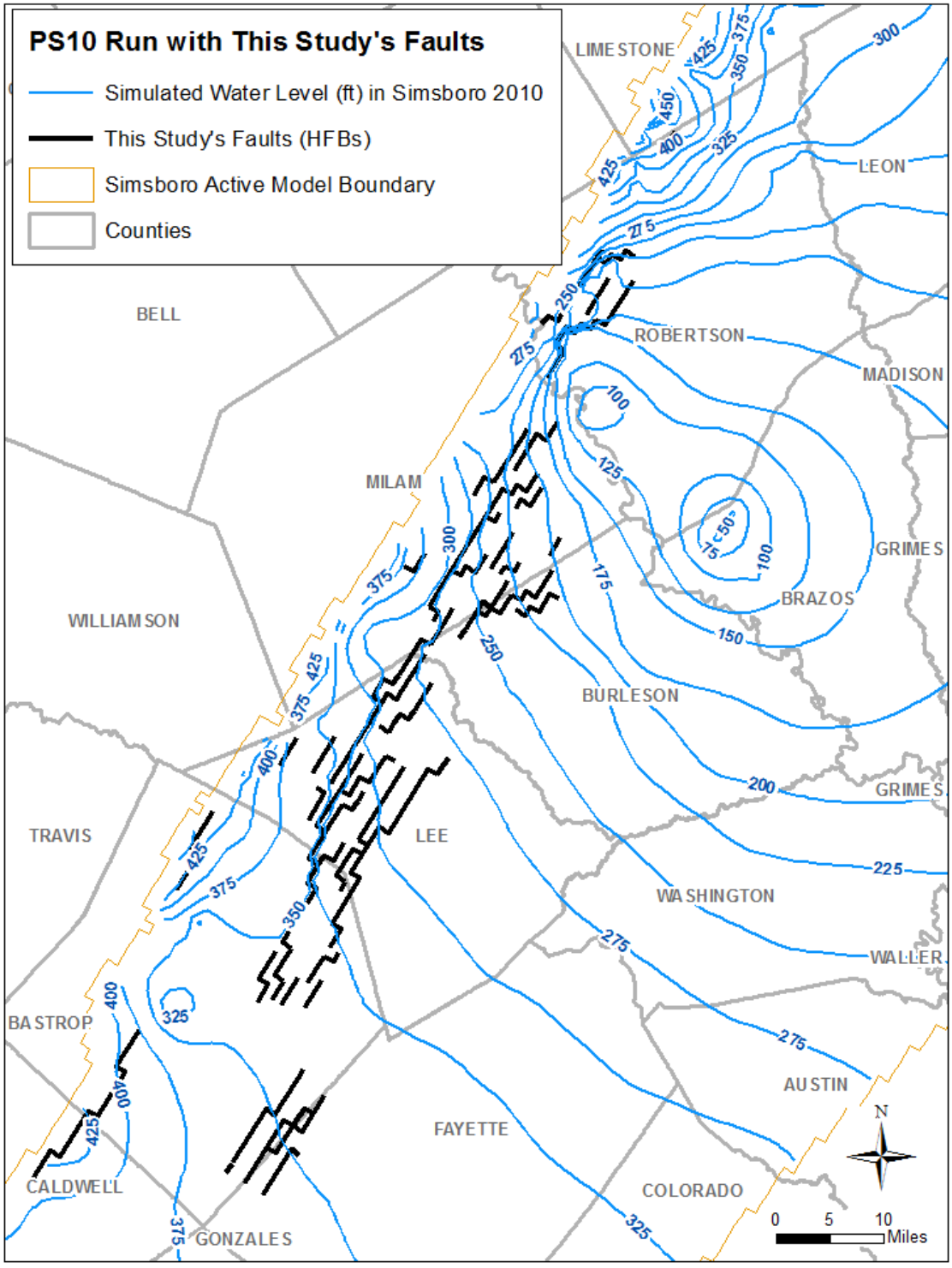

Figure 6-10. Predicted 2010 drawdown in the Simsboro for a groundwater availability model run with the faults from this study.

Note: ft = feet; HFB = horizontal flow barrier

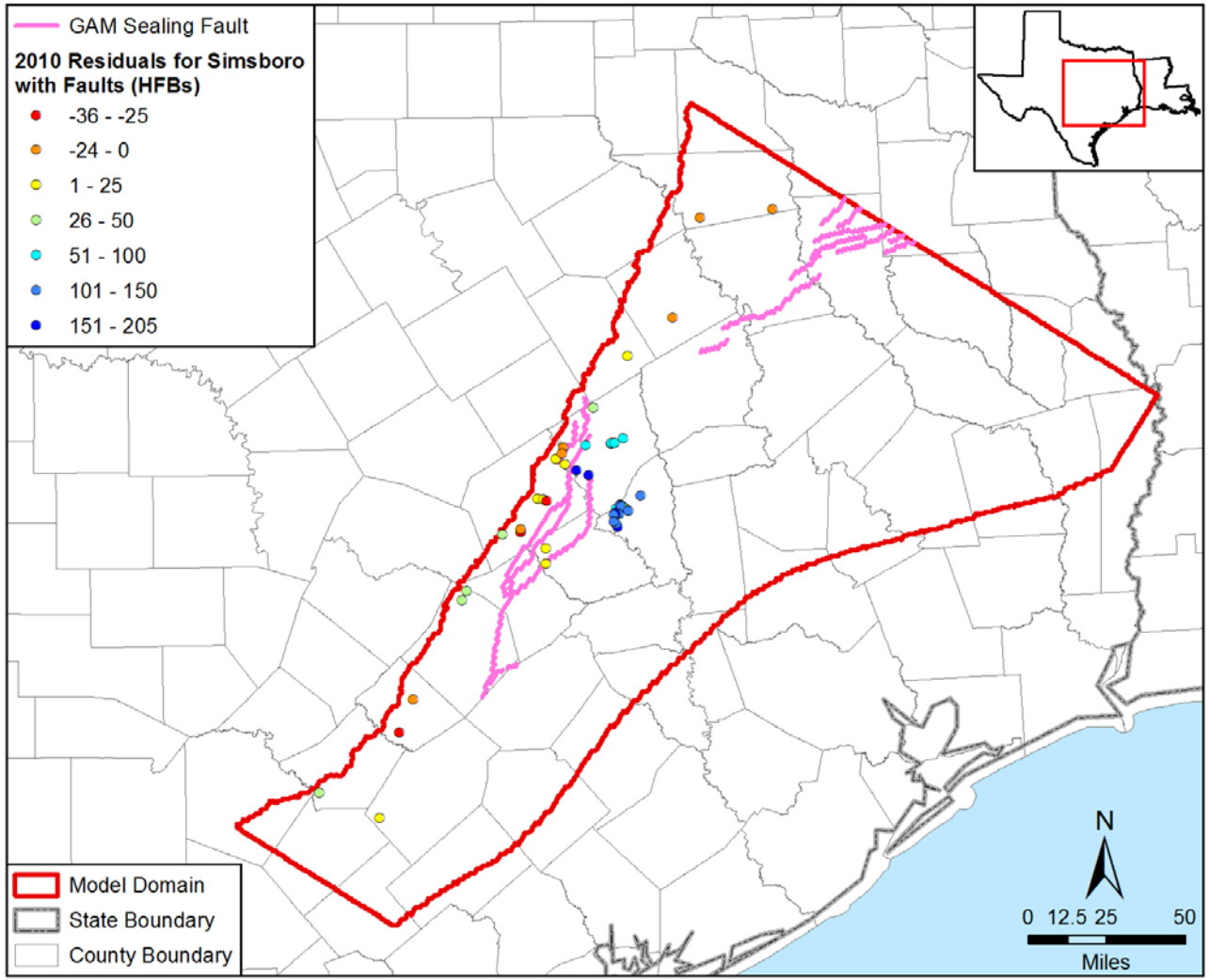

Figure 6-11. 2010 head residuals in the Simsboro across the model domain for groundwater availability model (GAM) run that includes the faults from the central Queen City-Sparta GAM.

Note: HFB = horizontal flow barrier

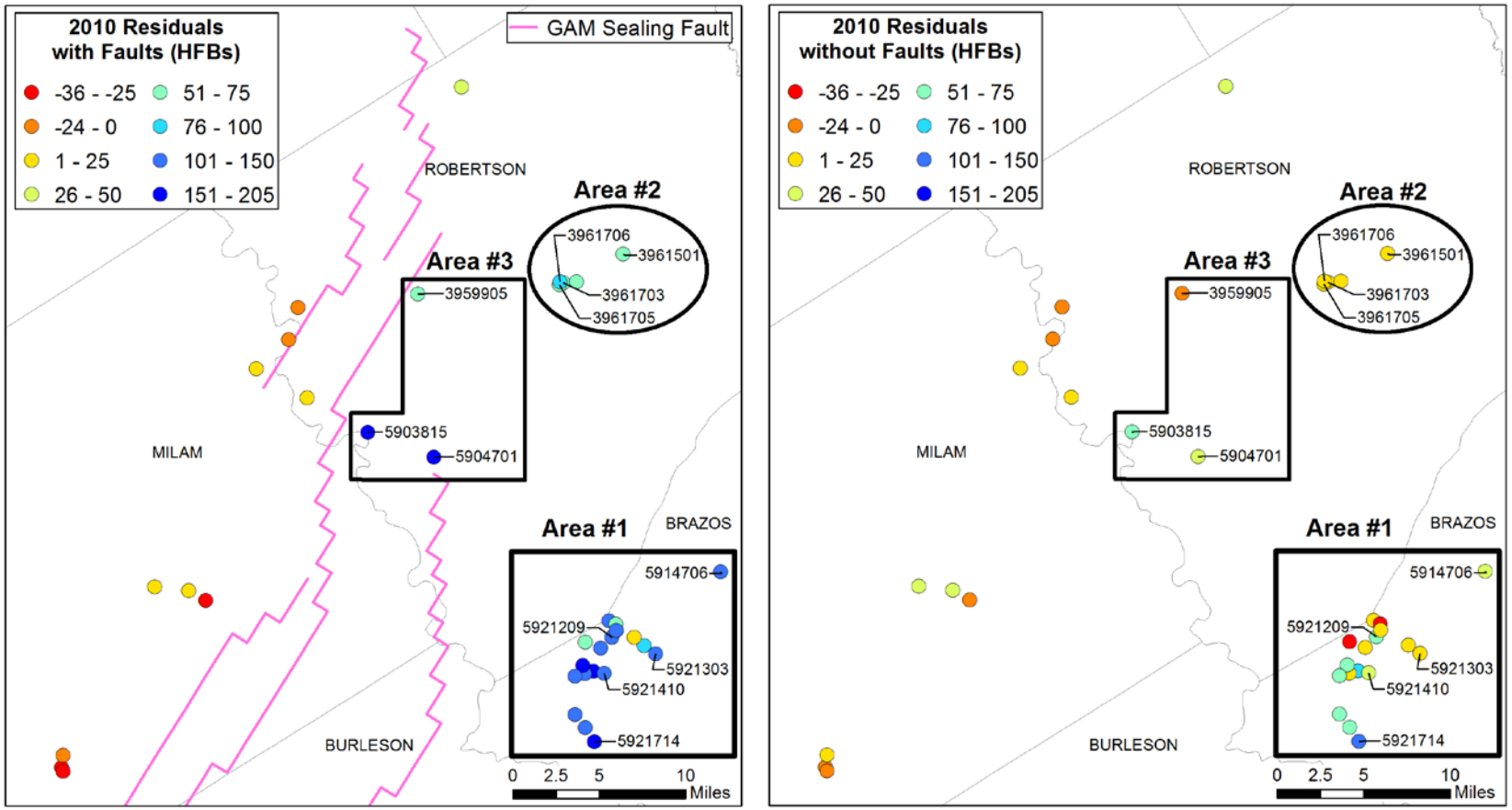

Figure 6-12. 2010 head residuals in the Simsboro in select counties for groundwater availability model (GAM) runs with (a) the faults from the central Queen City-Sparta GAM and (b) no faults.

Note: HFB = horizontal flow barrier

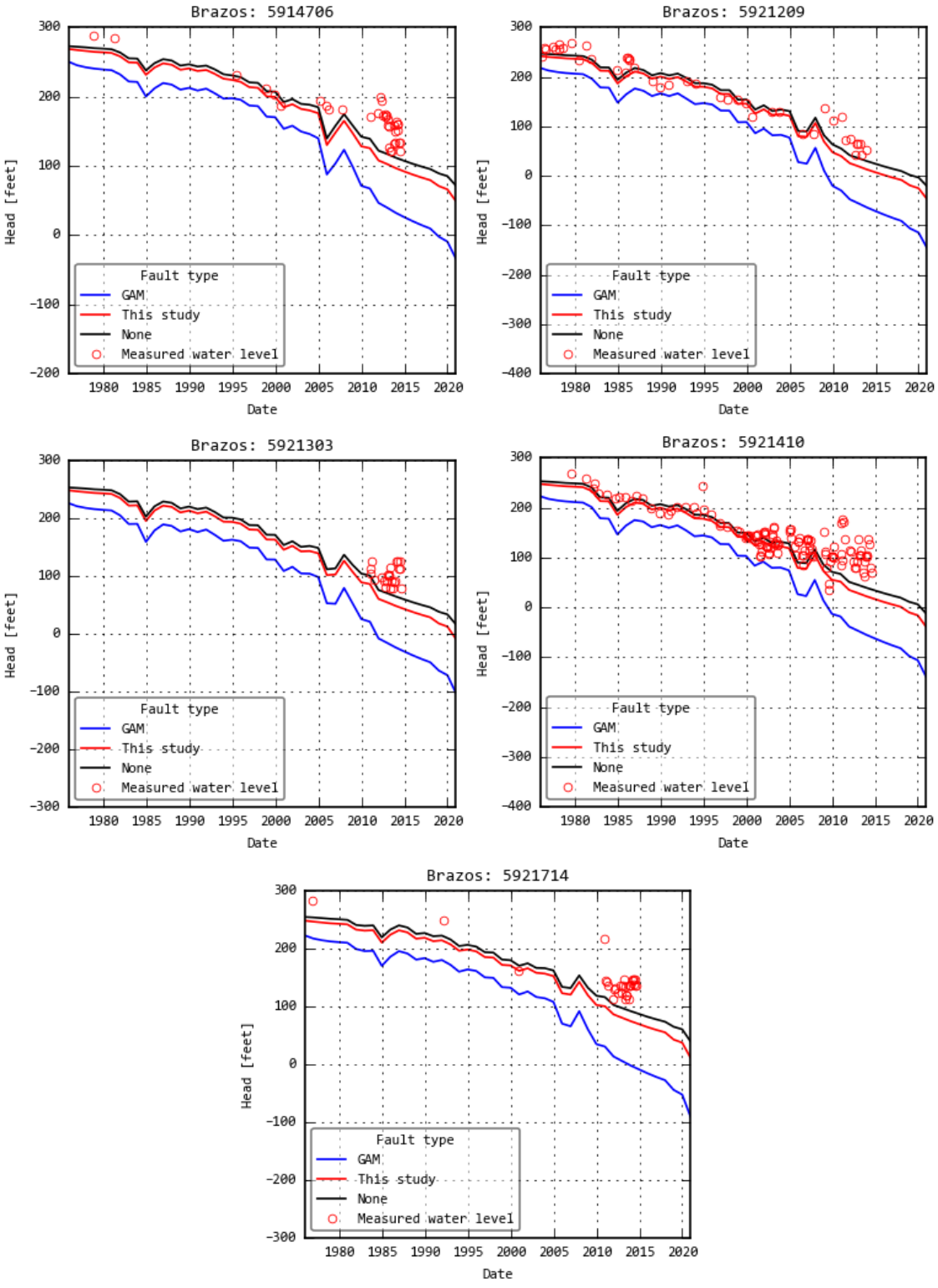

Figure 6-13. Hydrographs showing observed data and model results for groundwater availability model (GAM) runs with the faults in the central Queen City-Sparta GAM, the faults from this study, and no faults for select wells in Area #1 shown on Figure 6-12.

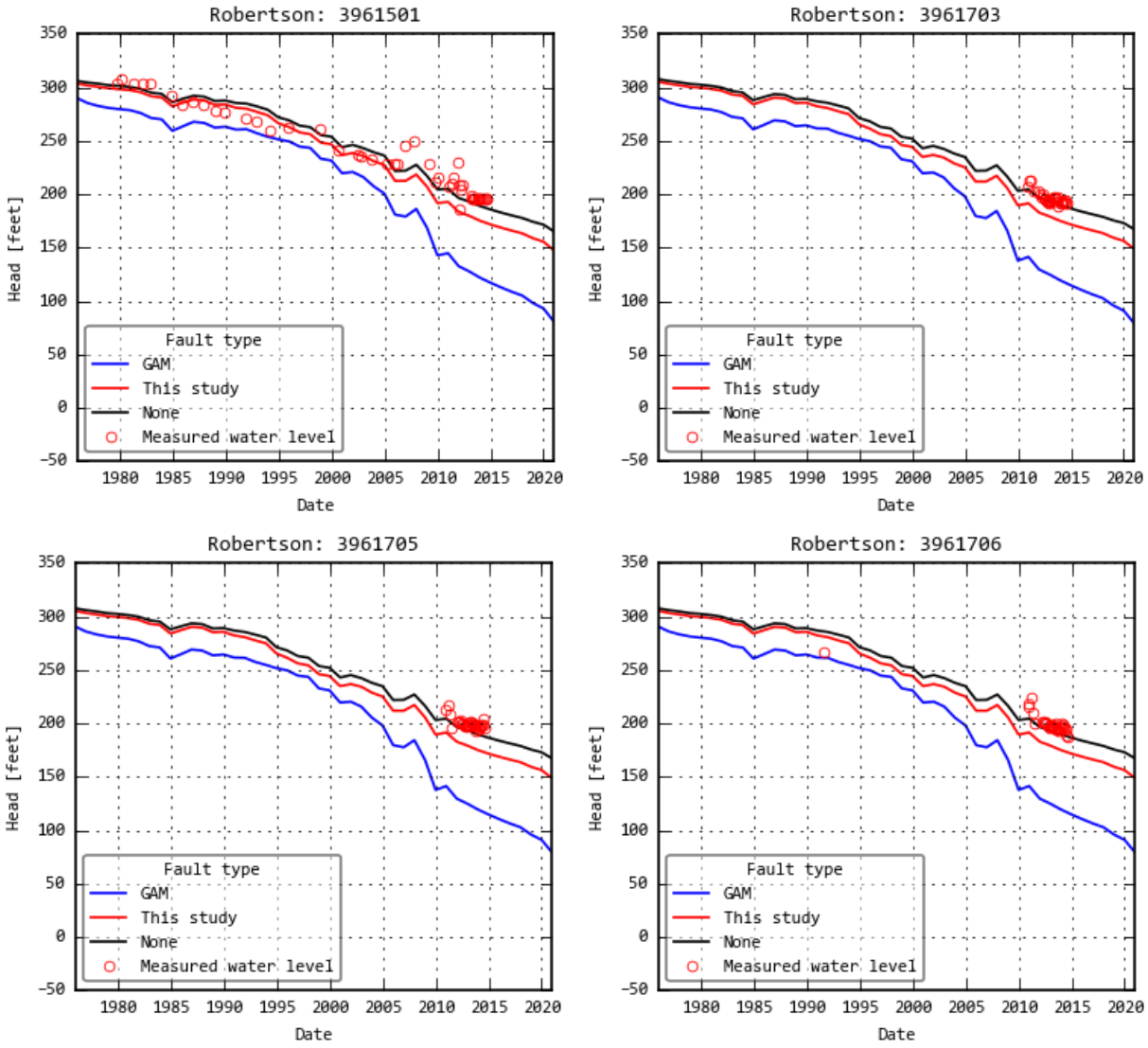

Figure 6-14. **Hydrographs showing observed data and model results for groundwater availability model (GAM) runs with the faults in the central Queen City-Sparta GAM, the faults from this study, and no faults for select wells in Area #2 shown on Figure 6-12.**

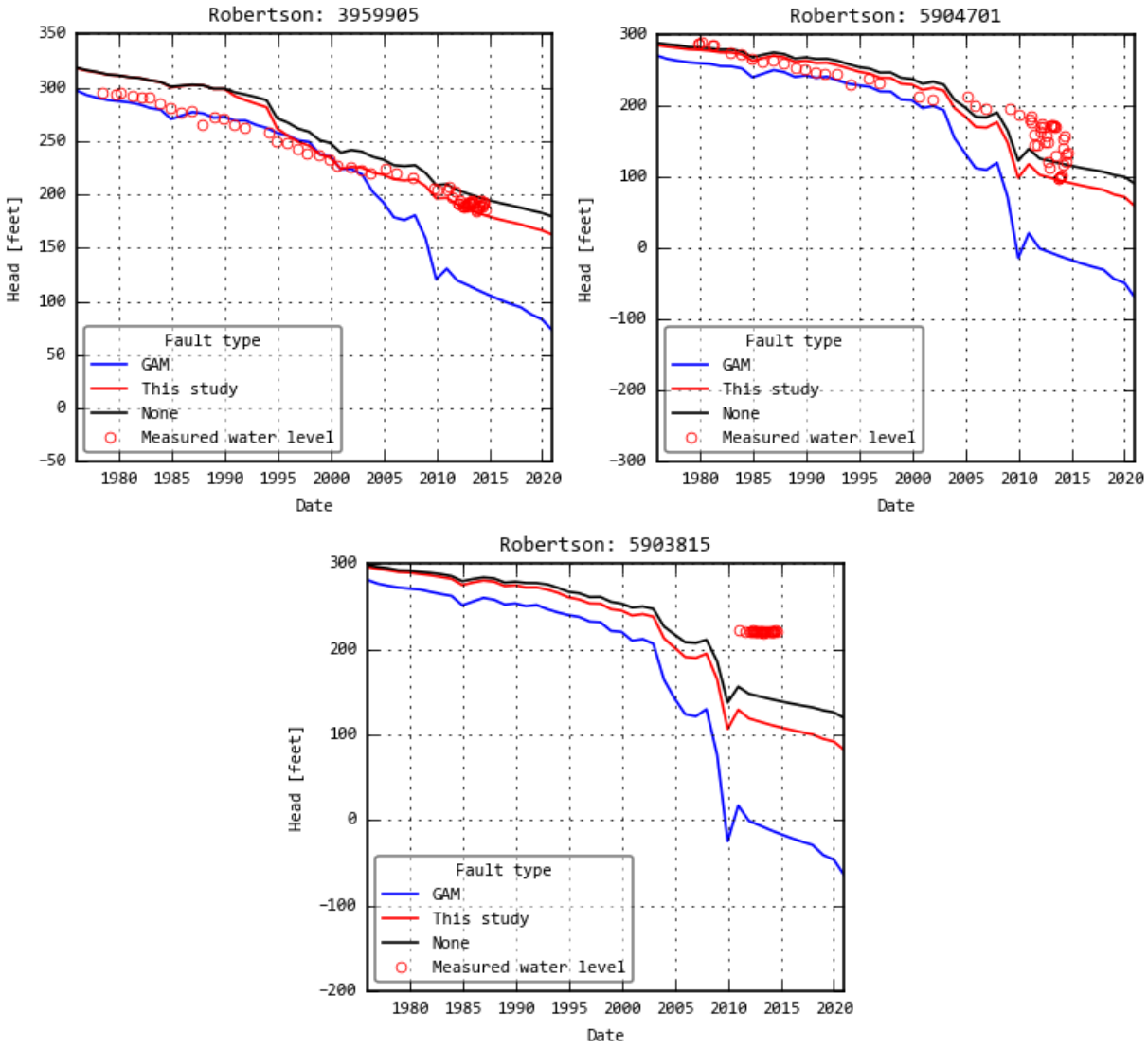

Figure 6-15. **Hydrographs showing observed data and model results for groundwater availability model (GAM) runs with the faults in the central Queen City-Sparta GAM, the faults from this study, and no faults for select wells in Area #3 shown on Figure 6-12.**

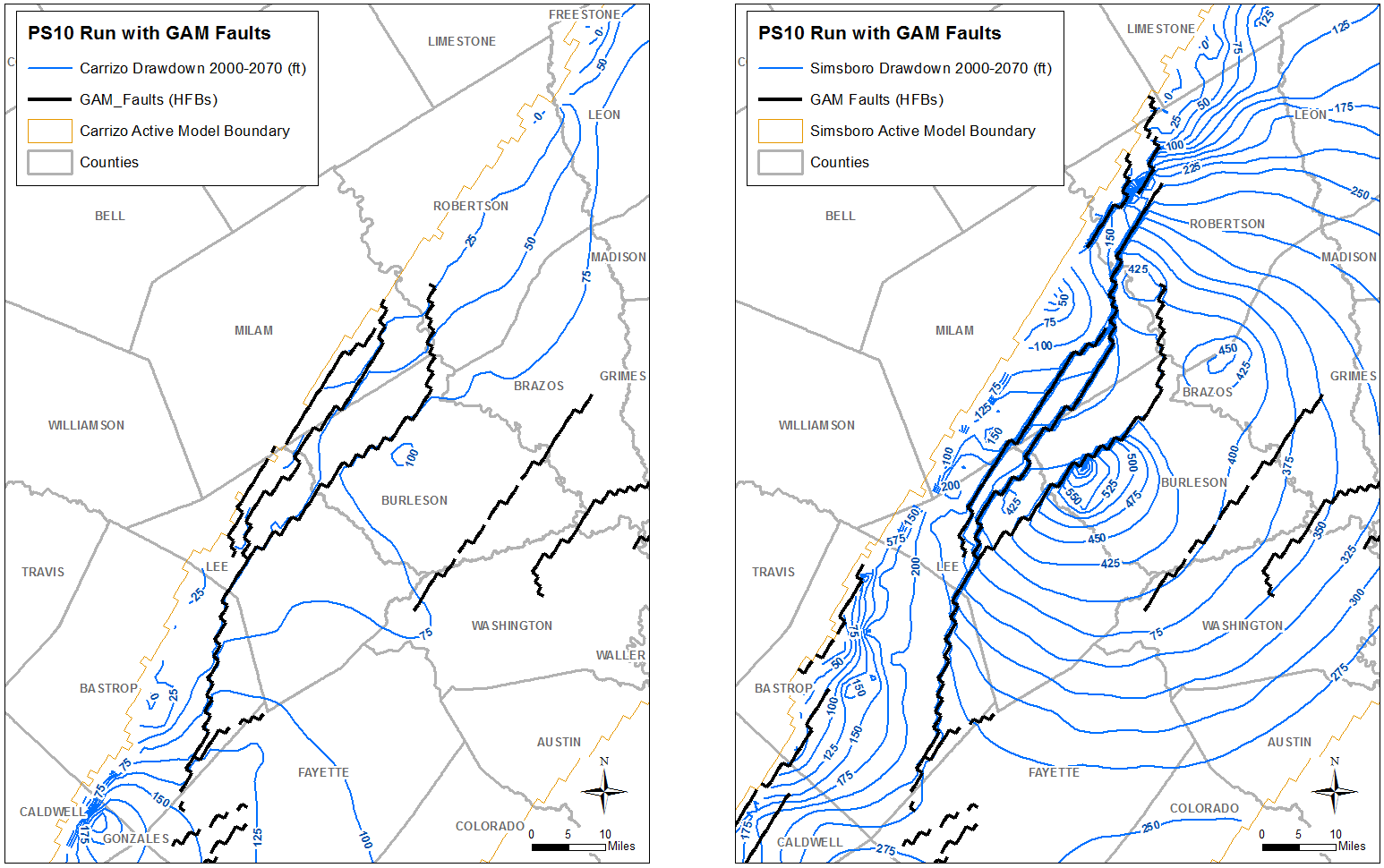

Figure 6-16. Predicted drawdown in the (a) Carrizo and (b) Simsboro for a groundwater availability model (GAM) run with the faults from the central Queen City-Sparta GAM faults.

Note: ft = feet; HFB = horizontal flow barrier

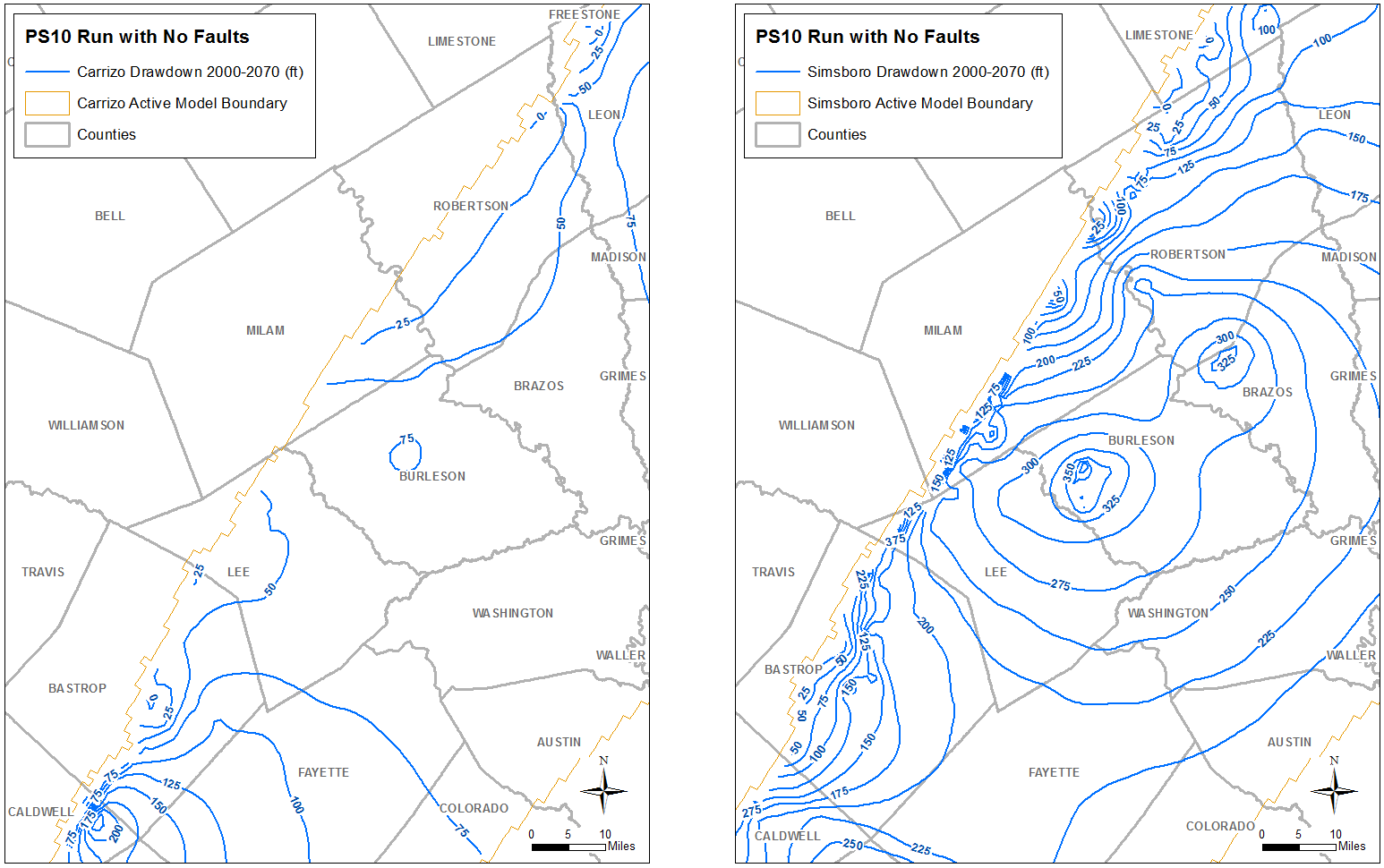

Figure 6-17. Predicted drawdown in the (a) Carrizo and (b) Simsboro for a groundwater availability model run with no faults.

Note: ft = feet

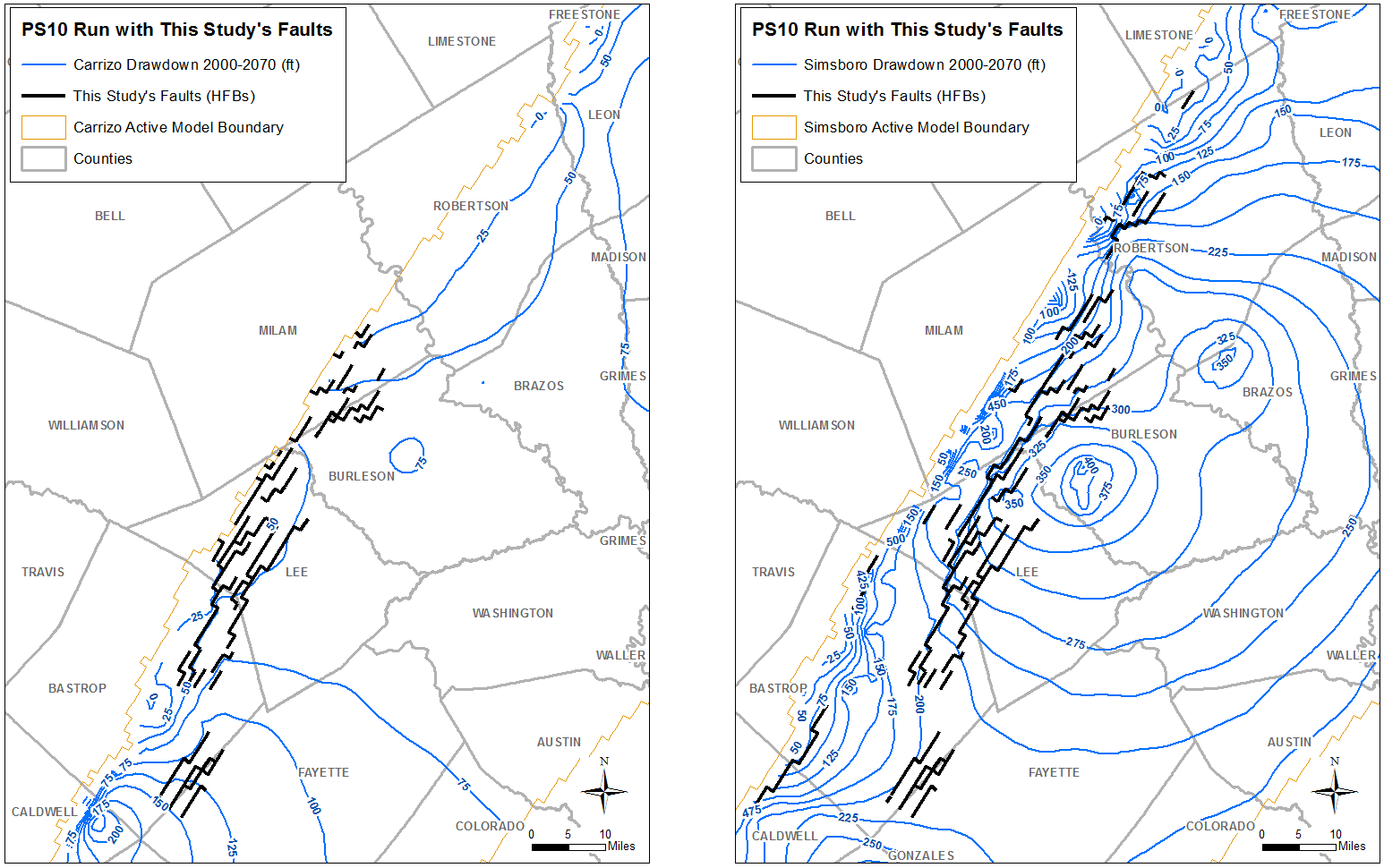

Figure 6-18. Predicted drawdown in the (a) Carrizo and (b) Simsboro for a groundwater availability model run with the faults from this study.

Note: ft = feet; HFB = horizontal flow barrier

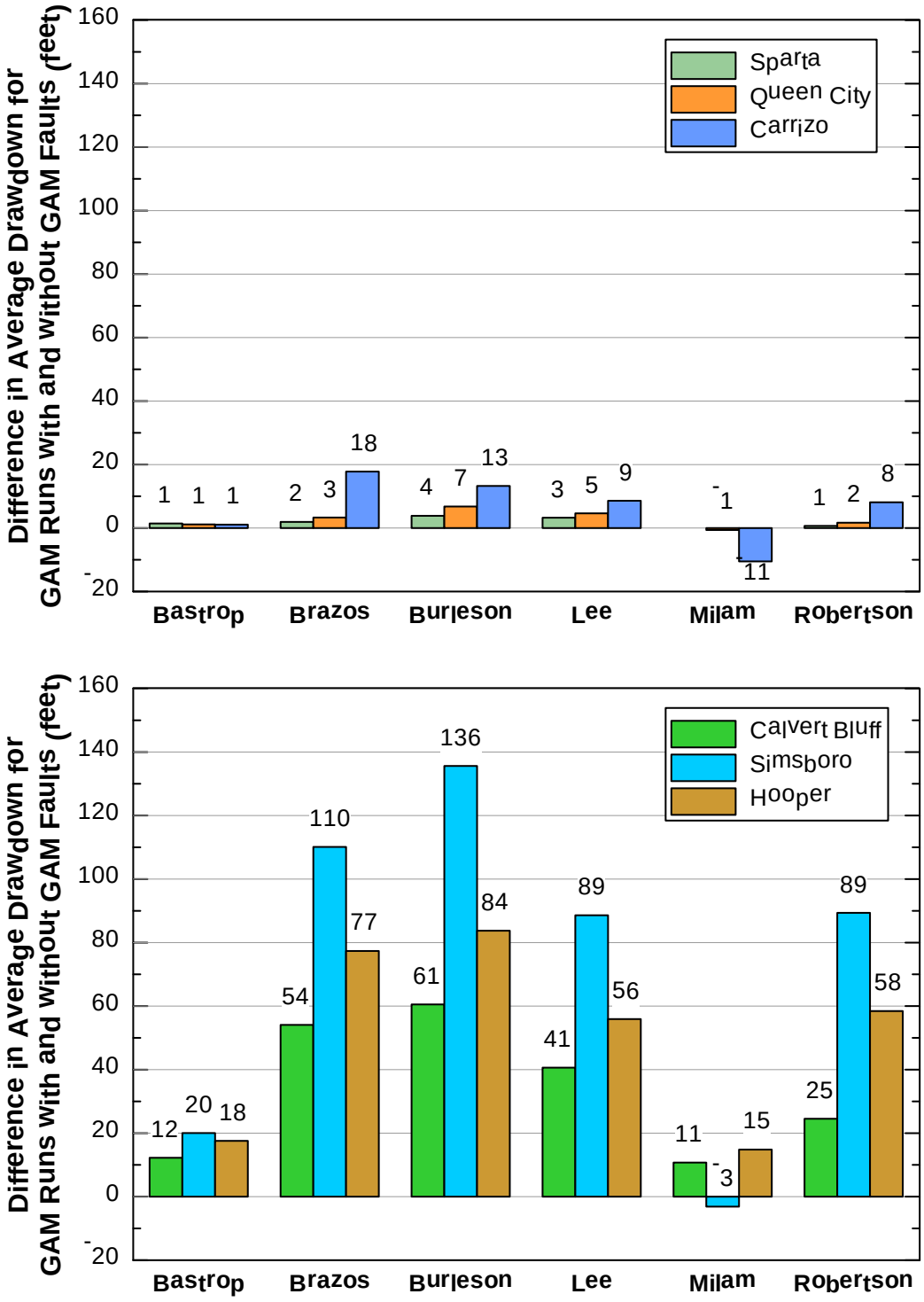

Figure 6-19. **The difference in the average drawdown between groundwater availability model (GAM) runs with and without the faults from the central Queen City-Sparta GAM for (a) the Sparta, Queen City, and Carrizo and (b) the Calvert Bluff, Simsboro, and Hooper.**

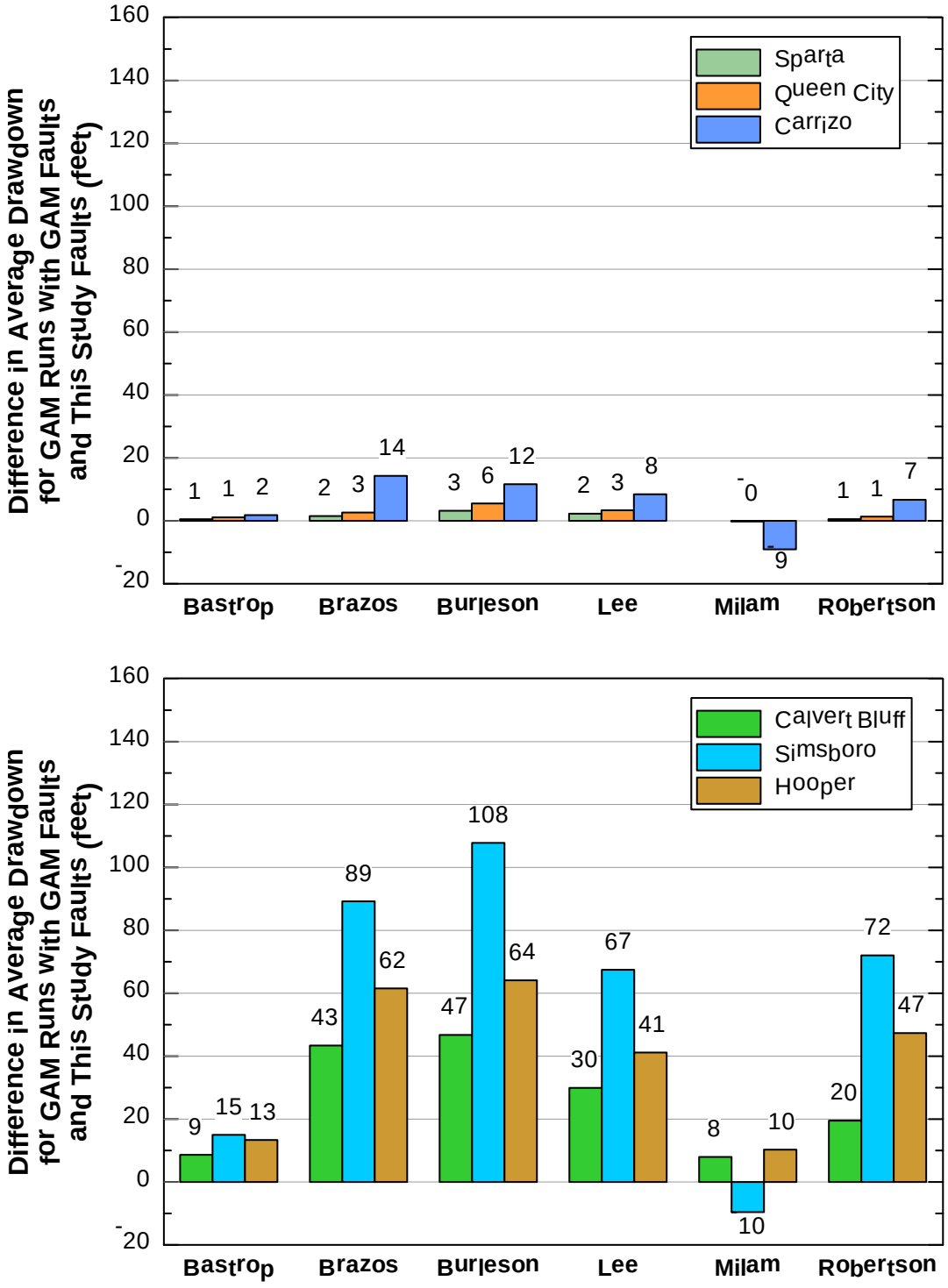

Figure 6-20. **The difference in the average drawdown between groundwater availability model (GAM) runs with the GAM faults and the faults from this study for (a) the Sparta, Queen City, and Carrizo and (b) the Calvert Bluff, Simsboro, and Hooper.**

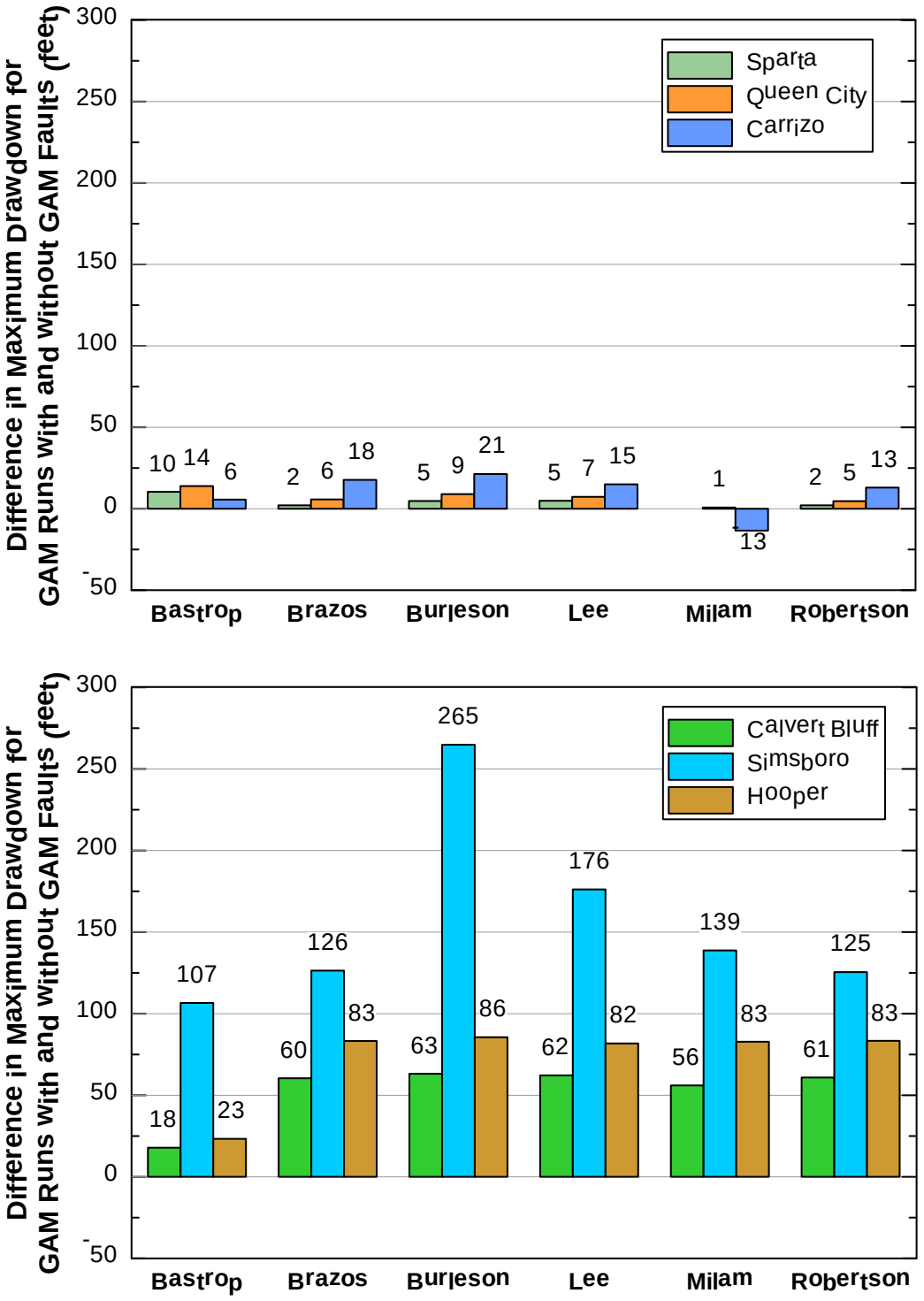

Figure 6-21. **The difference in the maximum drawdown between groundwater availability model (GAM) runs with and without the faults from the central Queen City-Sparta GAM for (a) the Sparta, Queen City, and Carrizo and (b) the Calvert Bluff, Simsboro, and Hooper.**

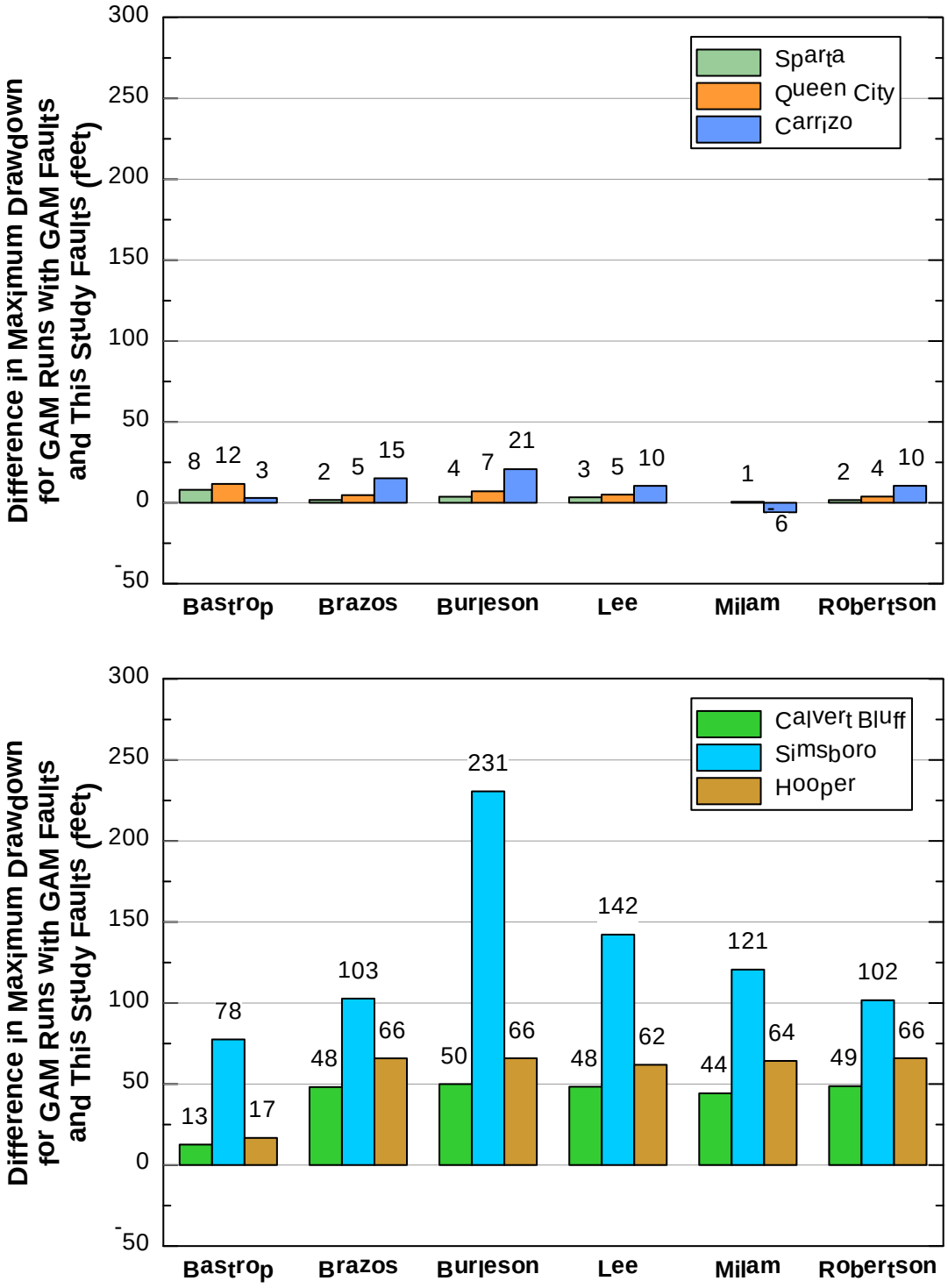

Figure 6-22. **The difference in the maximum drawdown between groundwater availability model (GAM) runs with the GAM faults and the faults from this study for (a) the Sparta, Queen City, and Carrizo and (b) the Calvert Bluff, Simsboro, and Hooper.**

This page is intentionally blank.

7 Aquifer Pumping Tests

7.1 Analysis of Aquifer Tests to Detect Changes in Aquifer Transmissivity

Dutton and others (2003) and Kelley and others (2004) simulated the Milano Fault Zone using the Horizontal Flow Barrier Package (Hsieh and Freckleton, 1993) in a MODFLOW (Harbaugh and McDonald, 1996) groundwater model. This package conceptualizes faults as a vertical sheet of low horizontal conductance that reduces the effective transmissivity of the aquifer that it intersects. Based on this simple conceptualization, the effects of a fault on groundwater flow should be detectable from the analysis of aquifer pumping test data if the test is conducted sufficiently close to the fault, is of sufficient duration, and is analyzed by the Cooper-Jacob straight-line method (Cooper and Jacob, 1946) or an equivalent method that relies on a slope or derivative of the time-drawdown data.

7.1.1 Cooper-Jacob Straight-Line Solution for Calculating Transmissivity

A standard approach for interpreting constant-rate drawdown tests to determine aquifer transmissivity is the Cooper-Jacob approximation to the Theis nonequilibrium well equation (Cooper and Jacob, 1946). After well bore storage effects have dissipated based on the calculated threshold times provided by Papadopoulos and Cooper (1967), the Cooper-Jacob analysis is applied. This analysis method involves fitting a logarithmic model to the elapsed-time/drawdown data for the test, selecting drawdown points one log cycle apart, and applying the equation:

$$T = \frac{35.3Q}{\Delta s} \qquad \text{(Equation 7-1)}$$

Where

T = Transmissivity in square feet per day
Q = Flow in gallons per minute
Δs = Change in drawdown in feet over one log cycle

Figure 7-1 shows an example application of the Cooper-Jacob Straight-Line (CJSL) method for the first 1,500 minutes of an aquifer pumping test performed in the northern Trinity Aquifer. In this example, a transmissivity value of 1,300 square feet per day is calculated based on a pumping rate of 715 gallons per minute and a Δs of 19.5 feet. As explained by Butler (1991), a powerful feature of the CJSL analysis method is that, because it uses the slope of the time-drawdown data and not the absolute value of drawdown for calculating transmissivity, it can be used to estimate changes in the transmissivity field with distance from the pumping well. In his discussion of the CJSL, Butler (1991) explains that the slope of the time-drawdown data is determined by the aquifer material that the "ring-of-influence" passes through over time. After the "ring-of-influence" passes through and beyond a region of the aquifer, that aquifer region no longer affects the slope of the time-drawdown curve.

Butler (1990) defines the "ring-of-influence" as that portion of the aquifer that contributes 95 percent of the flow to the pumping well. For a uniform and infinite aquifer, the inner and outer radii for the "ring-of-influence" is provided by Equations 7-2 and 7-3.

$$r_{inner} = \sqrt{(.1)T_t/S} \quad \text{(Equation 7-2)}$$

$$r_{outer} = \sqrt{(14.8)T_t/S} \quad \text{(Equation 7-3)}$$

Where

T = Transmissivity, L^2/T
S = Storativity, dimensionless
t = duration of pumpage, T

To demonstrate the application of the CJSL method to identify and characterize transmissivity changes in a non-uniform aquifer, aquifer pumping test data were numerically generated using the analytical element model TTim (Bakker, 2013) for the two aquifer conditions shown in Figure 7-2 and then analyzed using the CJSL method. TTim (Bakker, 2013) is a three-dimensional analytical element model capable of simulating groundwater flow through a multi-layer aquifer system that can contain simple inhomogeneities that can be approximated using cylinders and planes.

Aquifer with a Radial Discontinuity in its Transmissivity Field

Aquifer Description: Figure 7-2a is a plan view schematic of a 400-foot thick aquifer with a uniform hydraulic conductivity of 2.5 feet per day that contains a circular disk of media with a uniform hydraulic conductivity of 25 feet per day. Both the circular disk and the aquifer have the same storage properties. A well is located in the middle of the circular disk.

Generation of Aquifer Pumping Test Data: The analytical element program TTim was used to generate time-drawdown data for the well pumping at a rate of 1,500 gallons per minute for 100 days for three different radii of the circular disks, 1, 2, and 3 miles. For a specific storage values of 1.0 E-6 and of 1.0 E-7 $feet^{-1}$, TTim generated the time-drawdown data shown in Figure 7-3a and 7-3b, respectively. The data were generated using an exponentially-increasing time interval so that approximately 30 drawdown values were generated per log cycle.

Analysis of the Time-Drawdown Data to Calculate Transmissivity: At every data point in the plot of time-drawdown, slope of the semi-log time-drawdown curve is calculated by a linear regression using five data points. Using the calculated value of the semi-log slope and a pumping rate of 1,500 gallons per minute, a transmissivity value is generated by applying the CJSL method. Figures 7-4a and 7-4b show a plot of calculated transmissivity values as a function of time.

Notable Features of the Calculated Transmissivity Values: The results in Figure 7-4 show that, at early times, the CJSL transmissivity equals the transmissivity of the disk, which is 10,000 square feet per day and, at late times, the CJSL transmissivity equals the transmissivity of the aquifer, which is 1,000 square feet per day. In between the early and late times, the CJSL transmissivity is decreasing with time from 10,000 to 1,000 square feet per day. With regard to the "ring-of-influence" concept described by Butler (1990), the "ring-of-influence" is totally within the circular disk with a transmissivity of 10,000 square feet per day at early times and, at late times, the "ring-of-influence" has exited the circular disk and is totally within the main aquifer with a transmissivity of 1,000 square feet per day. During the transition from early to late times, the "ring-of-influence" resides in both the circular disk and the main aquifer. Per Equations 7-2

and 7-3, the start and end time for the transition period is a function of the specific storage. The smaller the specific storage value, the faster the "ring-of-influence" moves outward from the well and through the circular disk.

Aquifer with a 10-mile Long Linear fault

Aquifer Description: Figure 7-2b is a plan view schematic of a 400-foot thick aquifer that contains a vertical fault that fully penetrates the aquifer, is 10 miles long, and is located 1 mile from a pumping well. The aquifer has a uniform specific storage and a uniform hydraulic conductivity of 25 feet per day.

Generation of Aquifer Pumping Test Data: The program TTim was used to generate time-drawdown data for a well pumping at a rate of 1,500 gallons per minute for 100 days for four different conductance values for the fault, 0.01, 0.001, 0.0001, and 0.00001 day^{-1}. For specific storage values of 1.0 E-6 and 1.0 E-7 $feet^{-1}$, TTim generated the time-drawdown curves shown in Figure 7-5a and 7-5b, respectively. The data were generated based on an exponential scale, so that approximately 30 drawdown values are generated per log cycle.

Analysis of the Time-Drawdown Data to Calculate Transmissivity: At every data point, a semi-log slope is calculated by a linear regression of five data points. Using the value of the semi-log slope and a pumping rate of 1,500 gallons per minute, a transmissivity value is generated by applying the CJSL method. Figure 7-6a and 7-6b show a plot of calculated transmissivity over time.

Notable Features of the Calculated Transmissivity Values: The results in Figure 7-6 show that the CJSL transmissivity equals the transmissivity of the aquifer at early times, which is 10,000 square feet per day; the CJSL transmissivity decreases and then increases at intermediate times when the "ring-of-influence" moves through the portion of the aquifer with the fault, and the CJSL transmissivity returns to the transmissivity of the aquifer once the "ring-of-influence" moves beyond the fault in late time. The smaller the specific storage value, the faster the "ring-of-influence" moves outward from the well and through the fault.

7.2 Evaluation of Aquifer Tests in the Vicinity of the Milano Fault Zone

If fault zones represent areas of low transmissivity, then their impact on groundwater flow should be evident in the semi-log slope of the time-drawdown plot for a pumping well located near a fault. In this section, aquifer test data for wells located close to and away from the Milano Fault Zone were evaluated to determine whether or not there are lines of evidence to support representing some or all of the faults as regions of low transmissivity.

7.2.1 Location of Aquifer Tests

Aquifer pumping test data were obtained from the Texas Commission on Environmental Quality and from hydrogeologic consulting reports. The data from the Texas Commission on Environmental Quality were assembled with the help of commission staff in the Public Water Supply Supervision program. The Public Water Supply Supervision program maintains a set of paper records to manage information regarding the location, construction, borelog lithology, and data from a 36-hour aquifer test for each public supply well. INTERA obtained the paper

records for public water supply wells with aquifer test data of sufficient quality to be analyzed by the CJSL method to calculate transmissivity. R.W. Harden and Associates, Inc. assembled data from consulting reports. R.W. Harden and Associates, Inc. is well qualified for this task because they were involved with the initial development of public water supply wells in northwest Brazos County in the late 1950s and with the initial dewatering of the Simsboro Aquifer to help mine lignite from the Calvert Bluff Formation in Lee, Milam, and Robertson counties.

Our review of the aquifer pumping test data from these two sources produced a data set of 113 wells. Figure 7-7 shows the location of the wells along with the faults from this study mapped in Section 2. The wells are labeled using a unique identification number assigned by INTERA for this project. Identification numbers that contain the letter "P" indicate the source of the pumping test data is the Texas Commission on Environmental Quality paper files. Identification numbers that contain the letter "C" indicate the source of the pumping test data is from a consulting report. The wells were assigned to an aquifer by intersecting their well screen to the top and bottom of the surfaces that define the aquifers in the Central Queen City and Sparta aquifers groundwater availability model (Kelley and others, 2004). Wells were associated with the aquifer in which most of their well screen intersected. Appendix A provides the following information for each well: identification number, longitude, latitude, county, well and test data source, well depth, depth to the top of the uppermost screen, depth to the bottom of the lowermost screen, length of screen from the top of the uppermost screen to the base of the lowermost screen, screen length open to the aquifer, and model layer in which the majority of the screen is located. Table 7-1 lists the number of wells assigned to the different aquifers in the Central Queen City and Sparta aquifers groundwater availability model.

Table 7-1. Distribution of aquifer pumping test among aquifers.

Layer	Number Wells
Sparta	12
Queen City	4
Carrizo	10
Calvert Bluff	26
Simsboro	33
Hooper	28
Total	113

The semi-log time-drawdown data for each test were analyzed using the CJSL method. In all cases, the slope of the semilog plot of the time-drawdown data was calculated using software to best fit a straight-line through the time period of interest. In instances where there are at least four data points in the time-drawdown curve that indicate a change in slope of more than 10 percent, a second slope, and transmissivity, were calculated. The transmissivity based on the semi-log slope calculated at early time is called the early transmissivity, T_{early}, and the transmissivity based on the semi-log slope calculated at late time is called the late transmissivity,

T_{late}. One of the limitations placed when calculating T_{late} was ending the second time period at 2 days. Therefore, if an aquifer pumping test lasted longer than 2 days, the end time for the second slope was set to 2 days in the analysis of T_{late}.

Appendix B contains the CJSL analysis for the 113 aquifer pumping tests. The graphical format of the CJSL analysis for the plots in Appendix B is as follows. For each aquifer pumping test, the CJSL analysis shows the T_{early} drawdown data with red circles and a red line shows the best fit straight-line to the drawdown data for the T_{early} period. Blue circles and a blue best fit straight line denotes the drawdown data for the T_{late} period, if T_{late} data was available. In some cases, the aquifer test lasted long than 2 days and these drawdown values are denoted with black circles to indicate that they occur after the T_{late} analysis period. Summary statistics are displayed in the lower right corner of the plot within a red rectangle for the T_{early} data and within a blue rectangle for the T_{late} data. The summary statistics include the slope of the CJSL analysis; the coefficient of determination, R^2, that quantifies the quality of the slope estimated from the drawdown data; the estimated transmissivity; and the flow rate at the well during the aquifer pumping test.

For each aquifer pumping test, the value of T_{late} divided by $T_{early,}$ or T_{late}/T_{early}, was calculated. For tests with a single slope and one interpreted transmissivity, the T_{late}/T_{early} value is 1, indicating no change in aquifer transmissivity with distance from the well during the 2-day analysis period. For tests with two slopes, the value of T_{late}/T_{early} is considered a potentially useful indicator of whether or not the aquifer transmissivity changes with distance from the well. If the analysis for well tests located near faults yield a T_{late} value lower than the T_{early} value, that provides a line of evidence that the faults were affecting groundwater flow.

Figures 7-8 through 7-11 show the CJSL analysis for select wells located in the Milano Fault Zone in Robertson, Milam, Lee, and Bastrop counties, respectively, that produce lower values for T_{late} than for T_{early} and, thereby, provide a line of evidence that faults are affecting groundwater in these areas. In these figures, the faults from this study and from the groundwater availability model are mapped. In the vicinity of all of the wells with a calculated T_{late} lower than T_{early}, the faults in the groundwater availability model are located close to the faults identified with this study.

In northwestern Burleson County, the groundwater availability model includes a sealing fault that was not identified with this study. In that region, there are no aquifer tests with data suggesting a nearby low transmissivity zone associated with a sealing fault. Figure 7-12 shows the data for three pumping tests located close to the groundwater availability model fault in this region. The data from these tests do not provide evidence that a region of low transmissivity associated with the sealing fault in the groundwater availability model exists near the wells.

To evaluate a possible spatial pattern in the observed aquifer test responses and to help verify the location of faults and their impact on groundwater flow, the wells were assigned to one of the four categories listed in Table 7-2 based on its value for T_{late}/T_{early}. For wells with only one slope, this value was set to 1. Otherwise, the value was calculated using the transmissivity values determined by the CJSL analysis (see plots in Appendix B). Figure 7-13 shows aquifer test data that represent each of the four categories.

Table 7-2. Transmissivity categories used to classify wells based on the results of the CJSL analysis.

Transmissivity Category	Criteria for Grouping Based on the Ratio of T_{late}/T_{early}
No change in Transmissivity	> 0.85 and < 1.15
Small decrease in Transmissivity	>0.65 and < 0.85
Large decrease in Transmissivity	<0.65
Increase in Transmissivity	> 1.15

Figures 7-14 and 7-15 show the well locations color coded based on their value of $T_{late}/T_{early.}$ All the wells used for the analysis are screened in the Carrizo-Wilcox Aquifer. Based on visual inspection, it appears that the result from the aquifer test is much more likely to have a T_{late} value that is significantly less than the T_{early} value when the well it is located within and near the Milano Fault Zone than if the well is located outside of the fault zone. To test the validity of this observation, a statistical analysis of the pattern of T_{late}/T_{early} in Figures 7-14 and 7-15 was performed. The analysis used geographic information system software to determine each wells proximity to faults to evaluate whether low values of T_{late}/T_{early} are more likely to occur close to the faults. This analysis was conducted for the faults identified in this study and the faults in the Queen City and Sparta aquifers Groundwater Availability Model. Figure 7-16 contains histograms showing the number of wells by transmissivity categories as a function of distance from the faults.

The key information in Figure 7-16 is distilled in Table 7-3. This table shows that, the closer a well is located to a fault identified by this study, the more likely the data from the aquifer test conducted in the well indicates a region of low transmissivity located near the well. For the 16 wells located within 4 miles of a fault from this study with an offset of 500 feet or more, 63 percent have a T_{late} that is lower than the T_{early}. For the 58 wells located more than 8 miles from a fault from this study with an offset of 500 feet or more, only 5 percent have a T_{late} that is lower than T_{early}. These results clearly demonstrate that the faults from this study with at least 500 feet of offset are affecting groundwater flow. Similarly, compelling statistics also support the same claim for faults from this study that have an offset greater than 200 feet. For the 20 wells that are located within 4 miles of a fault from this study with an offset of 200 feet or more, 55 percent have a T_{late} that is lower than $T_{early.}$ For the 48 wells located more than 8 miles from a fault with an offset of 200 feet or more, only 4 percent have aquifer tests with a T_{late} that is lower than T_{early}. Table 7-3 also shows that the percentage of wells with a T_{late} lower than T_{early} is less when the groundwater availability model faults are considered relative to the faults from this study. For example, the 33 percent of the wells located within 4 miles of a groundwater availability model faults have aquifer test results that indicate a low transmissivity zone while this percentage is 55 percent for the faults from this study with an offset of greater than 200 feet.

Table 7-3. Percentage of aquifer pumping tests that indicate that a region of low transmissivity is located close to the well as a function of the distance between the well and the closest fault.

Fault Type	Fault Offset (feet)	Distance from Closest Fault (miles)	Total Number of Wells	Percentage of Wells with T_{late}/T_{early} Ratio < 0.65	Percentage of Wells with T_{late}/T_{early} Ratio < 0.85
This Study Faults	> 500	2	10	50%	70%
	> 200		17	35%	53%
GAM Faults			23	26%	39%
This Study Faults	> 500	4	16	38%	63%
	> 200		20	30%	55%
GAM Faults			30	20%	33%
This Study Faults	> 500	6	24	29%	50%
	> 200		34	21%	38%
GAM Faults			38	24%	39%
This Study Faults	> 500	> 8	58	3%	5%
	> 200		48	2%	4%
GAM Faults			47	6%	9%

7.3 Modeling of Aquifer Tests in the Vicinity of the Milano Fault Zone

Groundwater modeling of field data from aquifer pumping tests provides a method to investigate whether or not observed changes in the slope of the semi-log plots of time-drawdown (see Appendix B) were likely caused by a fault. This can be done by modeling the aquifer pumping tests with and without the fault. If the "no fault" simulation produces time-drawdown data that do not exhibit the slope change observed in the field data but the "fault" simulation does, then the modeling results demonstrate that the fault is responsible for the slope change observed in the field data.

Two options were used to simulate the aquifer pumping tests. For one option, the central Queen City and Sparta aquifers groundwater availability model was updated from MODFLOW 96 (Harbaugh and McDonald, 1996) to MODFLOW-USG (Panday and others, 2013, 2015) and the MODFLOW-USG version was used to simulate the test. For the other option, the analytical element code TTim (Bakker, 2013) was to use to simulate the test.

7.3.1 MODFLOW USG Application

The current central Queen City and Sparta aquifers groundwater availability model has two issues that prevent its easy use for simulating aquifer pumping tests. The first issue is that the model does not converge to a steady-state solution with no pumping in the model. The second issue is that its grid cells are too large to accurately simulate the local scale of an aquifer pumping test and are not easily refined. Both issues were rectified by converting the central Queen City and Sparta aquifers groundwater availability model from a MODFLOW-96

(Harbaugh and McDonald, 1996) to MODFLOW-USG (Panday and others, 2013, 2015). Appendix C documents the conversion process.

The analysis in Figure 7-17, which shows the ratios of model layer thickness to well screen length and groundwater availability model to measured transmissivity for wells with a T_{late}/T_{early} that is less than 0.6, was performed to identify a suitable aquifer pumping test to simulate using the central Queen City and Sparta aquifers groundwater availability model. The goal of the analysis was to find a well with an aquifer pumping test for which the well screen interval was the same length as the thickness of the model layer assigned to the well and where the transmissivity interpreted from the test data was the same as the model transmissivity for the grid cell that contained the well. Using these two criteria, we selected aquifer pumping test AT-95P as the prime candidate for our numerical analysis.

AT-95P consisted of pumping the Simsboro Aquifer for about 1 day at a constant rate of 300 gallons per minute. The CJSL analysis of the time-drawdown data produced a T_{early} of 10,121 square feet per day and a T_{late} of 5,076 square feet per day, giving a T_{late}/T_{early} value of 0.5. Figure 7-9 shows the location of the pumping well relative to the current groundwater availability model faults and this study's faults. The well is located approximately 1 mile from the closest groundwater availability model fault and the closest fault from this study.

The MODFLOW-USG simulation was performed in two steps. First, the 1-mile x 1-mile grid cell intersected by the well was refined into numerous grid cells that were 1/16-mile x 1/16-miles and, second, the entire model grid was solved for a steady and stable water table. The time-drawdown data from the MODFLOW-USG simulations for the "faults" and "without-faults" scenarios are shown in Figures 17-18a and 17-18b. The simulated results for the "without-faults" scenario has a straight-line and a constant transmits of about 12,500 square feet per day. The simulated results for the "faults" scenario has a curved response, indicative of a transmissivity change over time, and a T_{late}/T_{early} value of 0.6. These results provide additional evidence that faults are the principal reason for the low T_{late}/T_{early} value of 0.5 for aquifer pumping test AT-95C.

Among the concerns with using the central Queen City and Sparta aquifers groundwater availability model is that, besides under predicting water levels at the well for test AT-95P, there may be spatial trends in the model parameters that do not reflect reality. To check against the later, the analytical code TTim (Bakker, 2013) was used to simulate AT-95P. Figures 7-19a and 17-19b show the generated time-drawdown data and Table 7-4 provides the transmissivity values calculated for those data using the CJSL method. Both the graphs and the calculated transmissivity values are in-line with the analyses of the drawdown data generated using MODFLOW-USG. For these TTim simulations, the aquifer parameters were assigned based on those assigned to the grid cell containing the well in the central Queen City and Sparta aquifers groundwater availability model. The grid cell has a thickness of 682 feet, a hydraulic conductivity of 22 feet per day, and a specific storage of 1.73E-07 $feet^{-1}$.

Table 7-4. Compilation of T_{late}/T_{early} values determined from CJSL analysis of measured and modeled time-drawdown data for AT-95C.

Source of Time-Drawdown Data	Fault Location	Pumping Test Transmissivity Used	With Faults			No Faults
			T_{early} (ft^2/day)	T_{late} (ft^2/day)	T_{late}/T_{early}	T_{early} (ft^2/day)
Aquifer Test	-	-	10,100	5,070	0.50	-
MODFLOW-USG Simulation	GAM	No	11,700	7,040	0.60	12,500
TTim Simulation	GAM	No	14,090	6,620	0.47	15,200
TTim Simulation	GAM	Yes	8,050	3,220	0.4	10,100
TTim Simulation	This Study	Yes	9,260	5,530	0.60	10,000

Note: GAM = groundwater availability model; ft^2/day = square feet per day

Because of the favorable results from CJLS analysis of the TTim simulated data (see Figure 17-19), two additional sets of drawdown data were generated using TTim. For these simulations, the well screen length, rather than the model layer thickness, was used for the aquifer thickness and the calculated T_{early} for test AT-95C, rather than the model value, was used for the transmits. Figures 17-20a and 17-20b show TTim results with and without the faults as time-drawdown graphs for simulations using the faults in the current groundwater availability model and Figures 17-21a and 17-21b show the time-drawdown graphs for the simulations using the faults from this study. These figures also provide the transmissivity values interpreted from the CJSL analysis of these TTim generated data. Table 7-4 summarizes the interpreted values for T_{late} and T_{early} for both sets of simulated data. The compilation of low values of T_{late}/T_{early} in Table 7-4 demonstrates that the faults near AT-93C are the primary mechanism for the changing slope in the semi-log plot of time-drawdown.

7.3.2 TTim Applications

TTim was also used to generate simulated drawdown data for aquifer pumping tests AT-73P, AT-76C, AT-112C, AT-105P, AT-43C, and AT-42C. The semi-log plots of the observed time-drawdown data for these tests, along with the interpreted CJSL transmissivity values, can be found in Appendix B. The simulated TTim time-drawdown data and the transmissivity values from CJSL analyses of those data for these six tests are shown in Figures 7-22 through 7-27. For each test, simulated drawdown data were generated using TTim for the conditions of no faults, the faults in the current groundwater availability model, and this study's faults. Parameterization of the analytical model was the same for all tests, with the except of the well location and properties of the nearby faults. All sealing faults from the groundwater availability model are assigned a conductance of $1E^{-4}$ day^{-1}. The faults from this study have two values of conductance based on offset. Faults with offset greater than 500 feet were also assigned a conductance of $1E^{-4}$ day^{-1}, and faults with offsets between 200 and 500 feet were assigned a conductance of $1E^{-3}$ day^{-1}. The number of interpreted transmissivity values shown in Figures 7-22 through 7-27

for the simulations with faults is a function of the number of slopes in the drawdown data generated by TTim.

This analysis was primarily performed to provide additional evidence supporting the assertion that faults are the primary cause of the observed slope decrease in the semi-log plots of time-drawdown data for aquifer pumping tests performed near known faults. Table 7-5 compares the T_{late}/T_{early} values interpreted from the observed and TTim-simulated drawdown data for the six aquifer tests. This comparison indicates that the three T_{late}/T_{early} values are consistent for test AT-73P, the value from the simulated data with groundwater availability model faults better matches the value from the observe data for test AT-76C, and the values from the simulated data with this study's faults best match the values from the observe data for the remaining four tests. Specific implications from these results are the likelihood of a fault near test AT-105P consistent with that determined from this study but missing from the groundwater availability model and the strong indication that the groundwater availability fault near tests AT-43C and AT-42C, an area where no faults were identified by this study, does not impact groundwater flow in the area and, likely, is not present or is not a sealing fault.

Table 7-5. Comparison of T_{late}/T_{early} values from CJSL analysis of measured and modeled time-drawdown for six aquifer pumping tests.

Aquifer Test ID	From Interpretation of Observed Data	From Interpretation of TTim Simulated Data	
	T_{late}/T_{early}	This Study Faults	GAM Faults
		T_{late}/T_{early}	T_{late}/T_{early}
AT-73P	0.72	0.73	0.71
AT-76C	0.59	0.86	0.64
AT-112C	0.82	0.76	0.97
AT-105P	0.50	0.68	0.99
AT-43C	1.00	1.00	0.52
AT-42C	1.00	0.91	0.65

Note: ID = identification; GAM = groundwater availability model

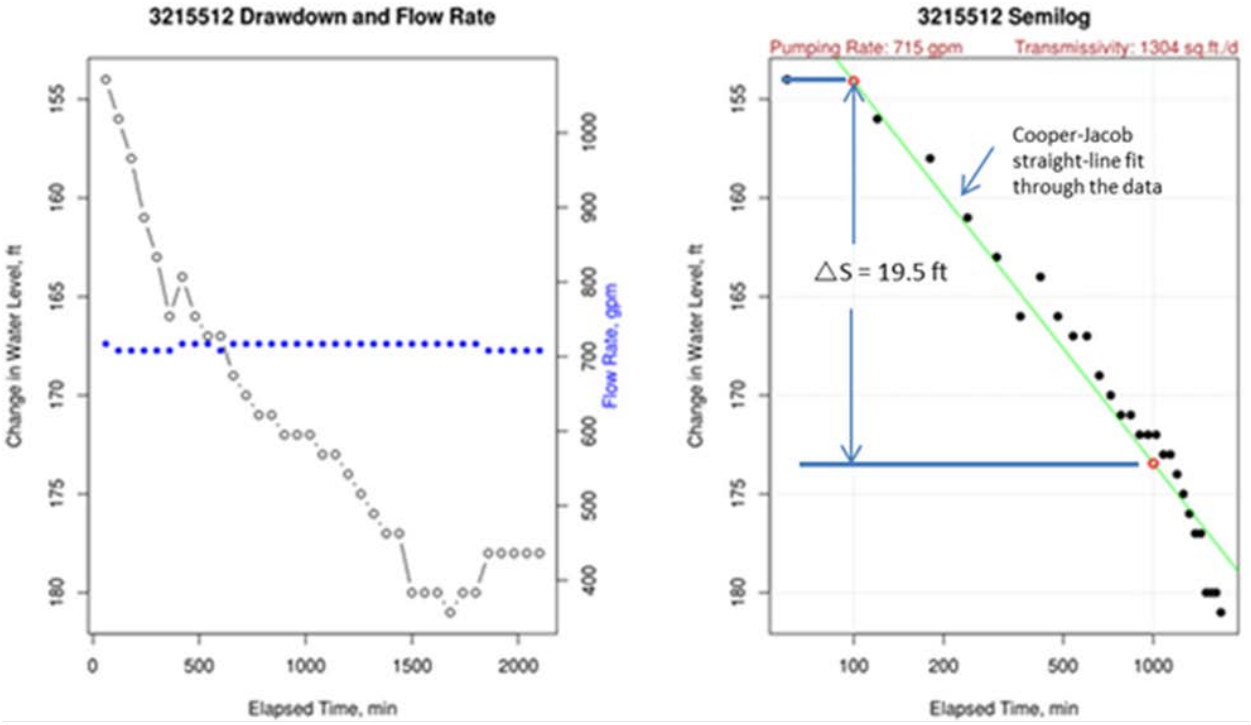

Figure 7-1. Example application of the CJSL method to calculate aquifer transmissivity (modified from Kelley and others, 2014).

Note: CSJL = Cooper-Jacob straight line; ft= feet; gpm = gallons per minute; min = minutes; sq. ft/d = square feet per day; Δs = Change in drawdown in feet over one log cycle

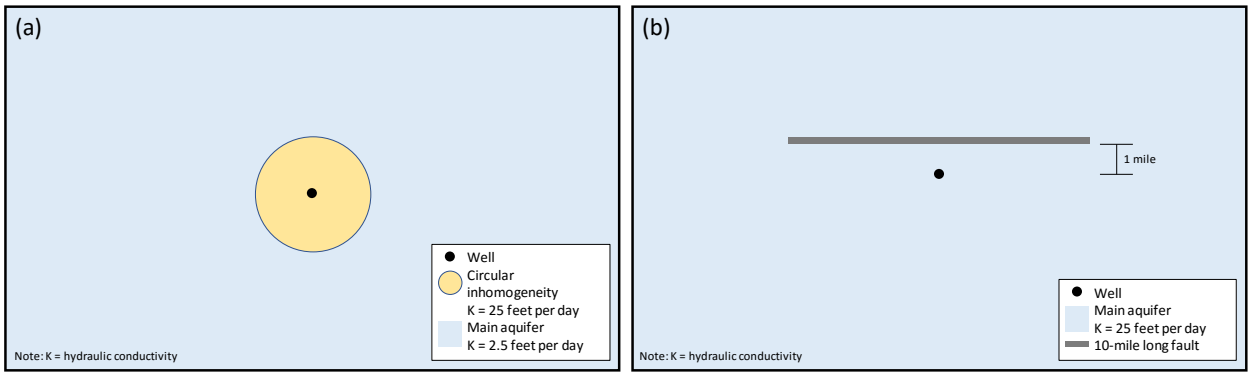

Figure 7-2. Plan view of two hypothetical aquifers used to demonstrate the application of the CJSL method for estimating changes in transmissivity with radial distance from a well for (a) a uniform and infinite aquifer containing a circular inhomogeneity centered on the well, and (b) a uniform and infinite aquifer with a 10-mile long fault located 1 mile from the well.

Note: CSJL = Cooper-Jacob straight line; K = hydraulic conductivity

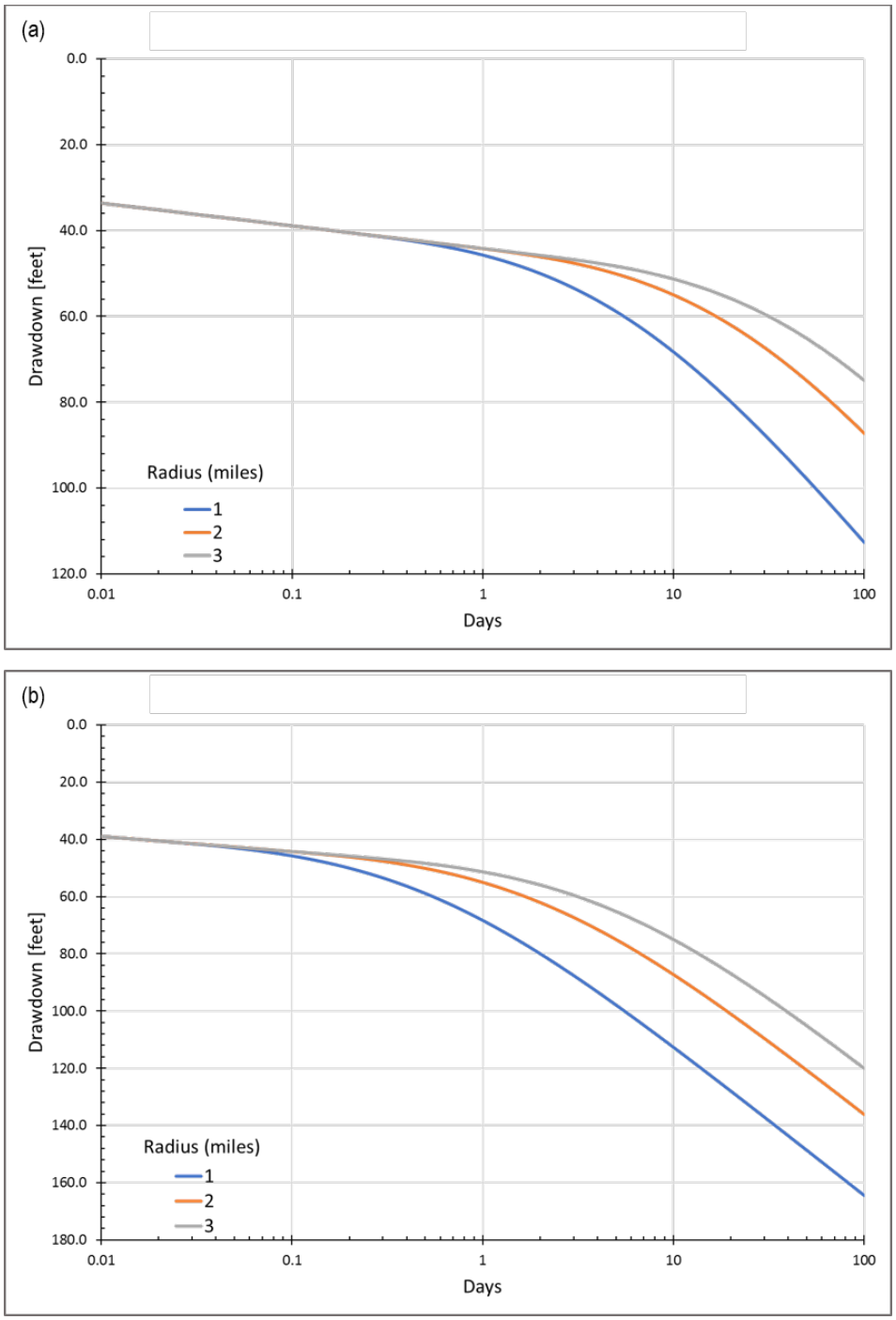

Figure 7-3. **Time-drawdown data produced by the analytical element code TTim for the well in the hypothetical aquifer shown in Figure 7-2a for a specific storage of (a) 1E-6 feet-1 and (b) E-7 feet-1.**

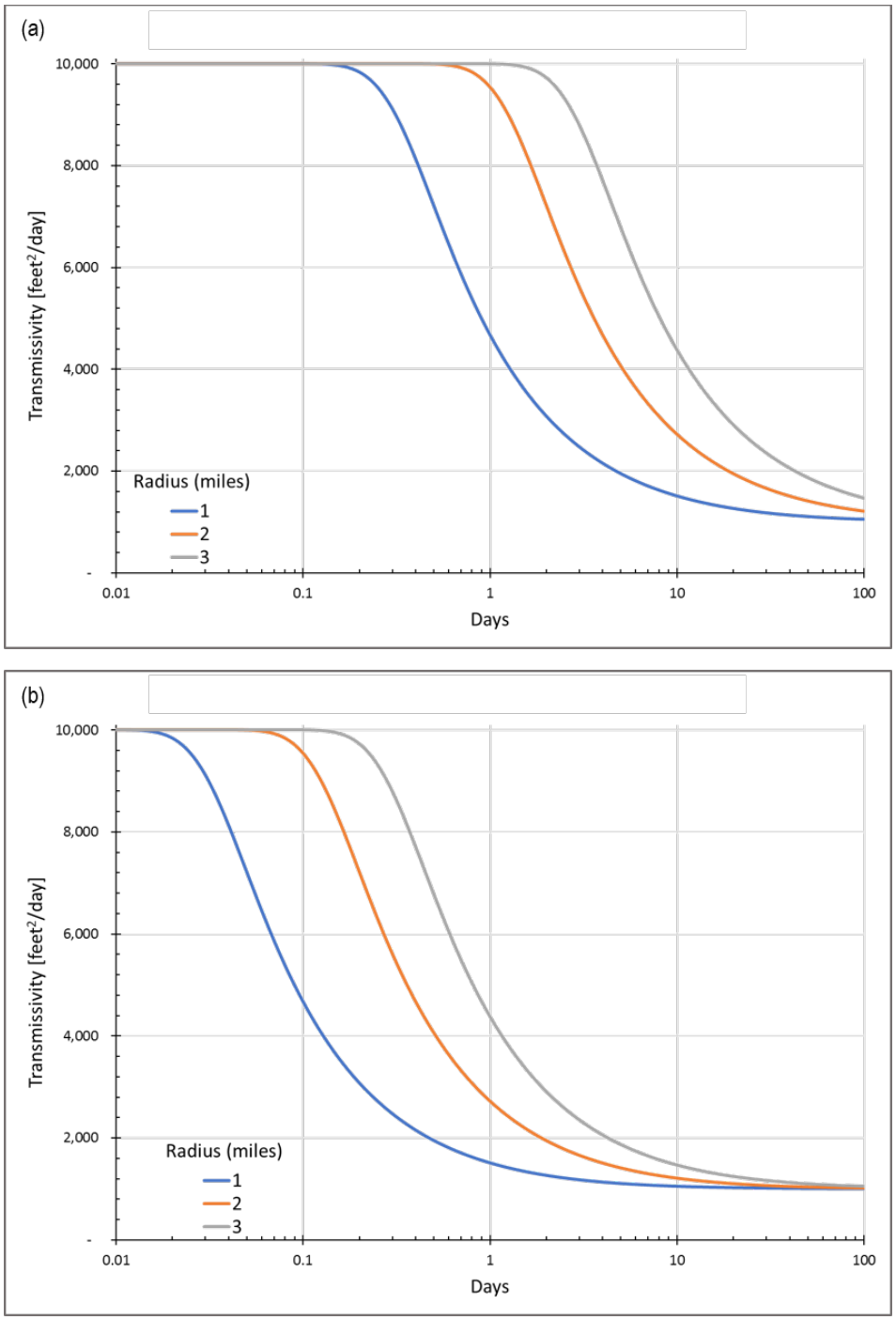

Figure 7-4. **Aquifer transmissivity values calculated over time by applying the CJSL method to (a) the time-drawdown data in Figure 7-3a and a pumping rate of 1,500 gallons per minute and (b) the time-drawdown data in Figure 7-3b and a pumping rate of 1,500 gallons per minute.**

Note: CSJL = Cooper-Jacob straight line

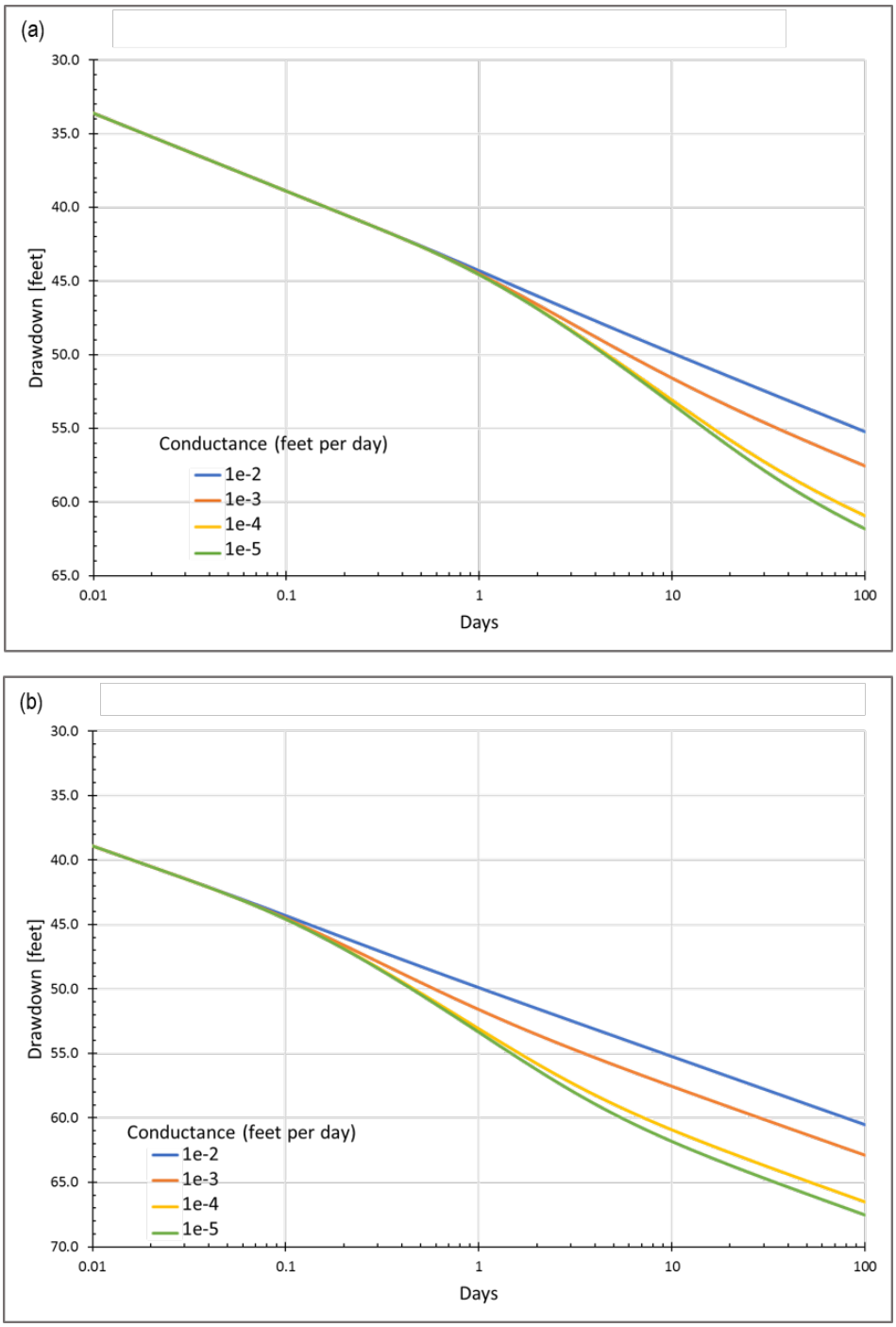

Figure 7-5. **Time-drawdown data produced by the analytical element code TTim for the well in the hypothetical aquifer shown in Figure 7-2b for a specific storage of (a) 1E-6 feet-1 and (b) Ss=1E-7 feet-1.**

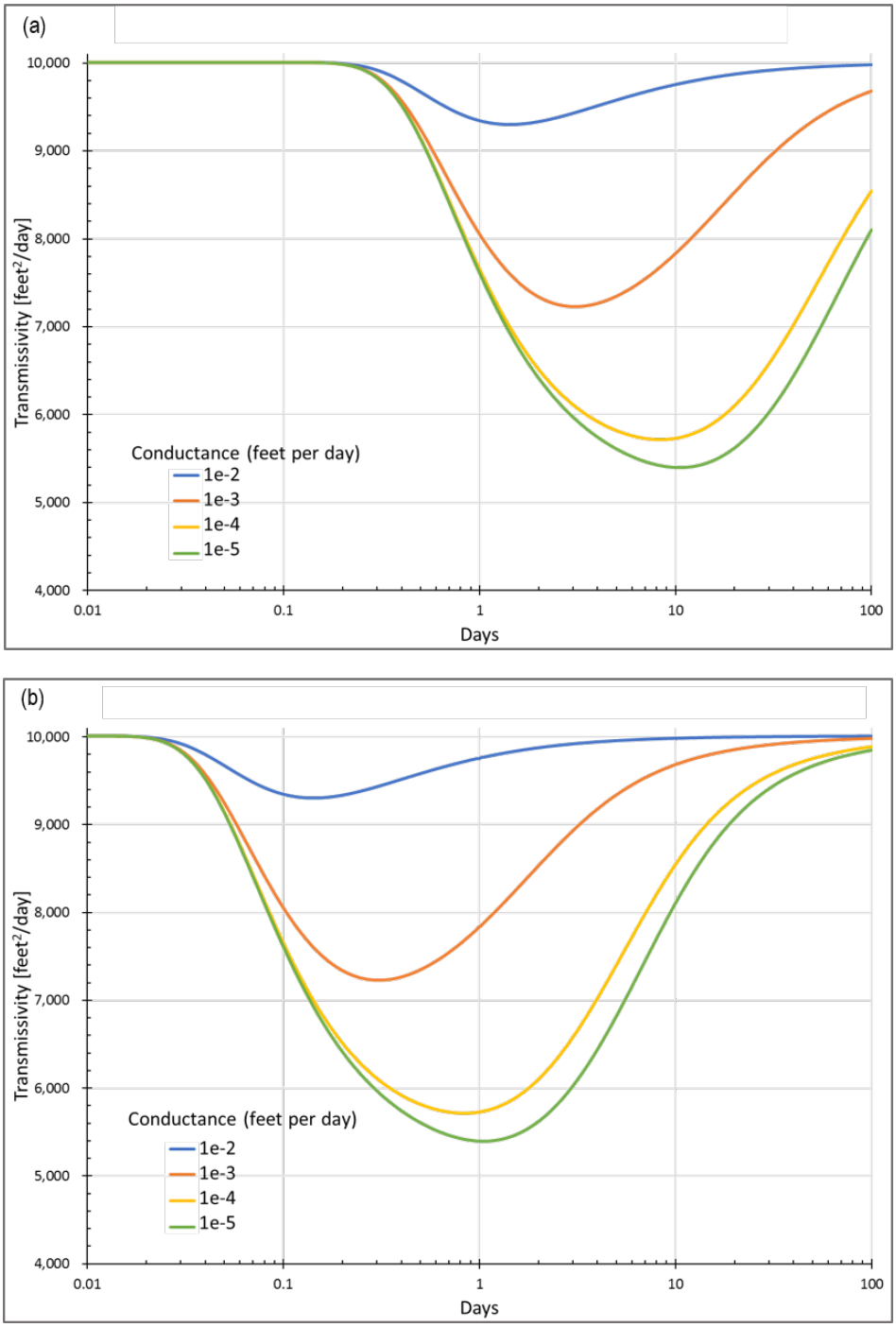

Figure 7-6. **Aquifer transmissivity values calculated over time by applying the CJSL method to (a) the time-drawdown data in Figure 7-5a and a pumping rate of 1,500 gallons per minute, and (b) the time-drawdown data in Figure 7-5b and a pumping rate of 1,500 gallons per minute.**

Note: CSJL = Cooper-Jacob straight line

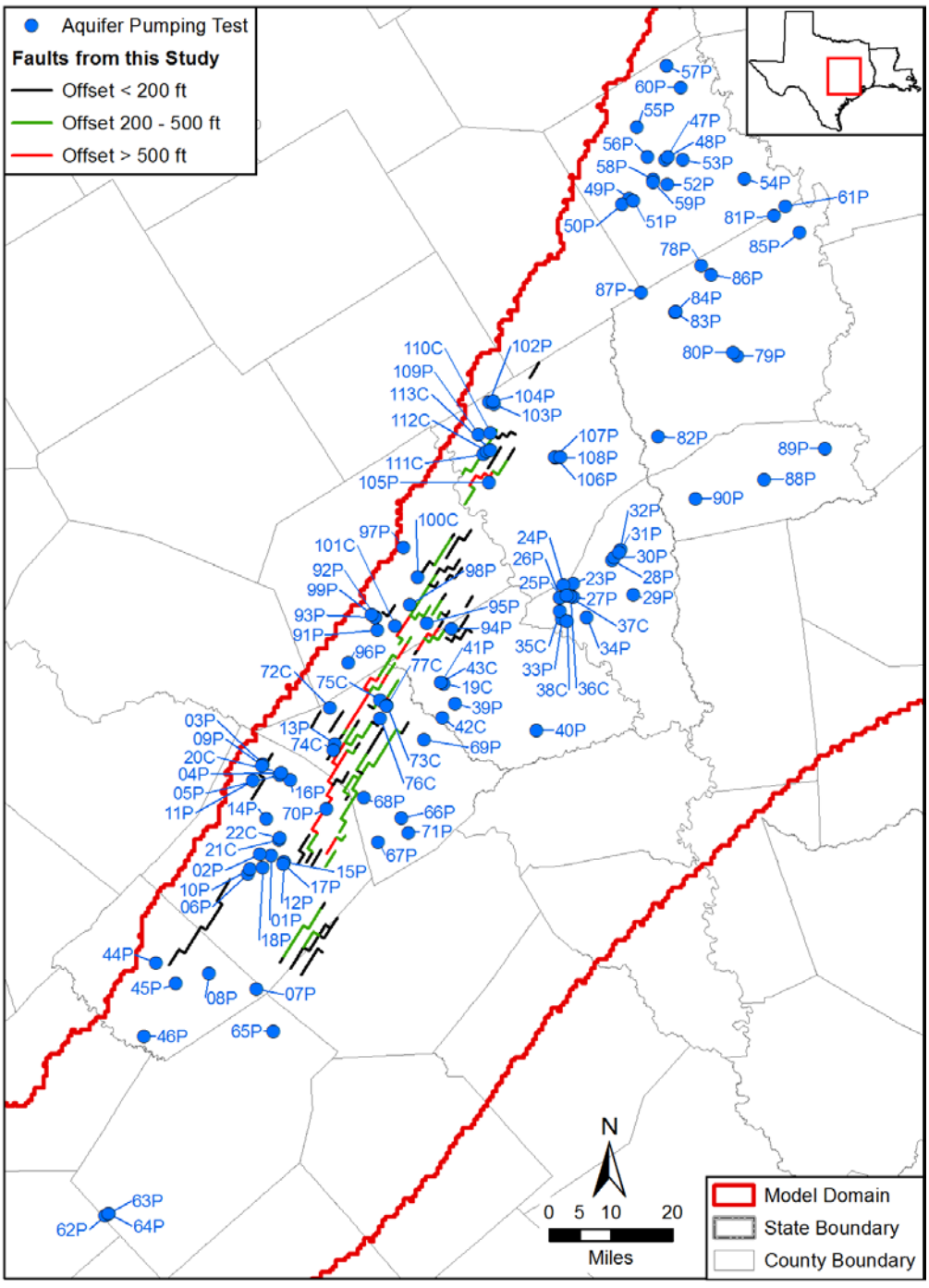

Figure 7-7. Location of wells with aquifer pumping test data and the faults identified by this study mapped to the numerical grid of the Central Queen City and Sparta aquifers groundwater availability model.

Note: ft = feet

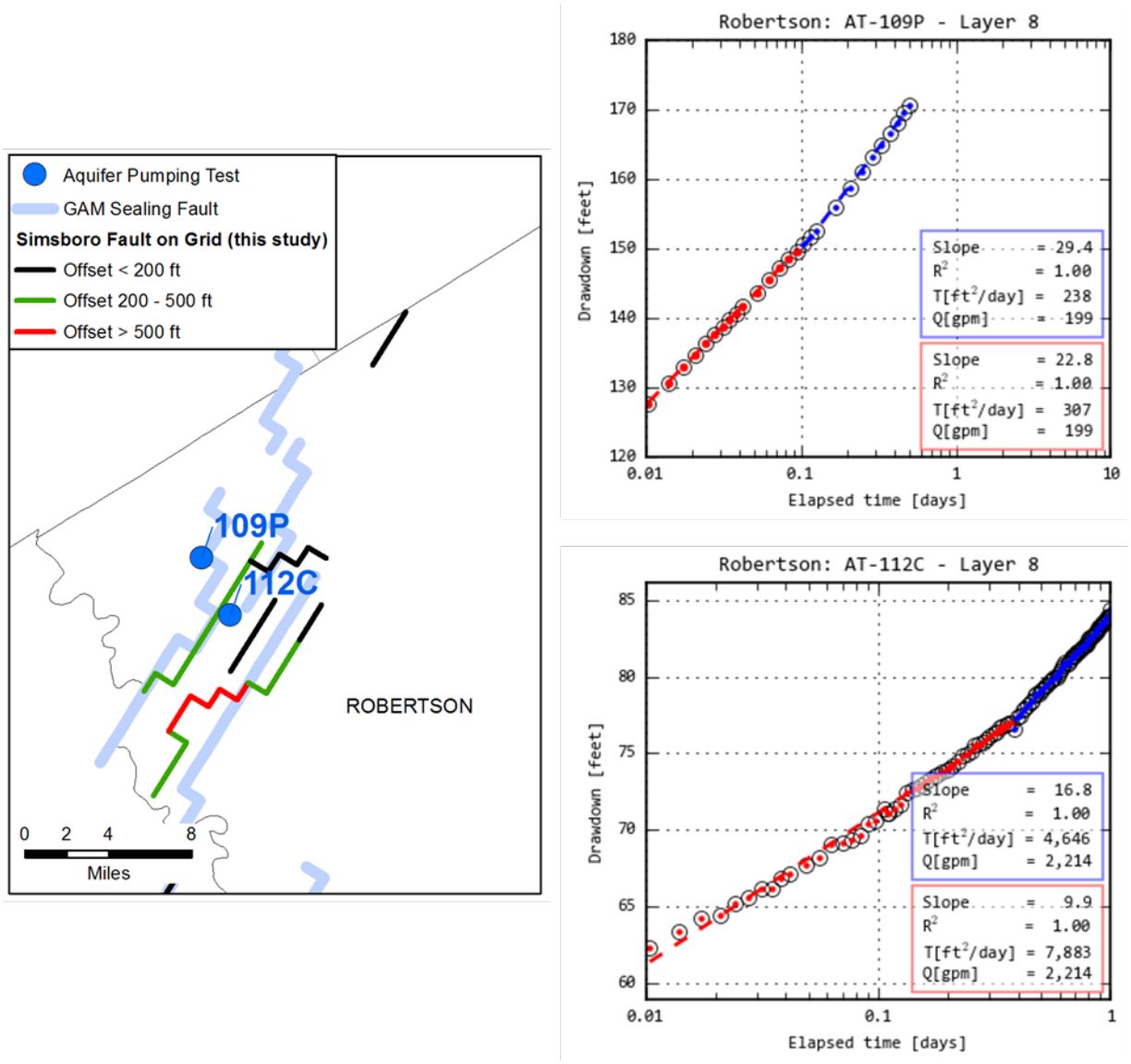

Figure 7-8. Location of aquifer pumping tests performed near faults in Robertson County that produced a CJSL-calculated T_{late} that is less than the CJSL-calculated T_{early} and thereby provides a line of evidence that faults could be affecting groundwater flow.

Note: ft = feet, GAM = groundwater availability model; CSJL = Cooper-Jacob straight line; ft^2/day = square feet per day; gpm = gallons per minute; Q = flow rate of the aquifer test; T = transmissivity; R^2 = coefficient of determination

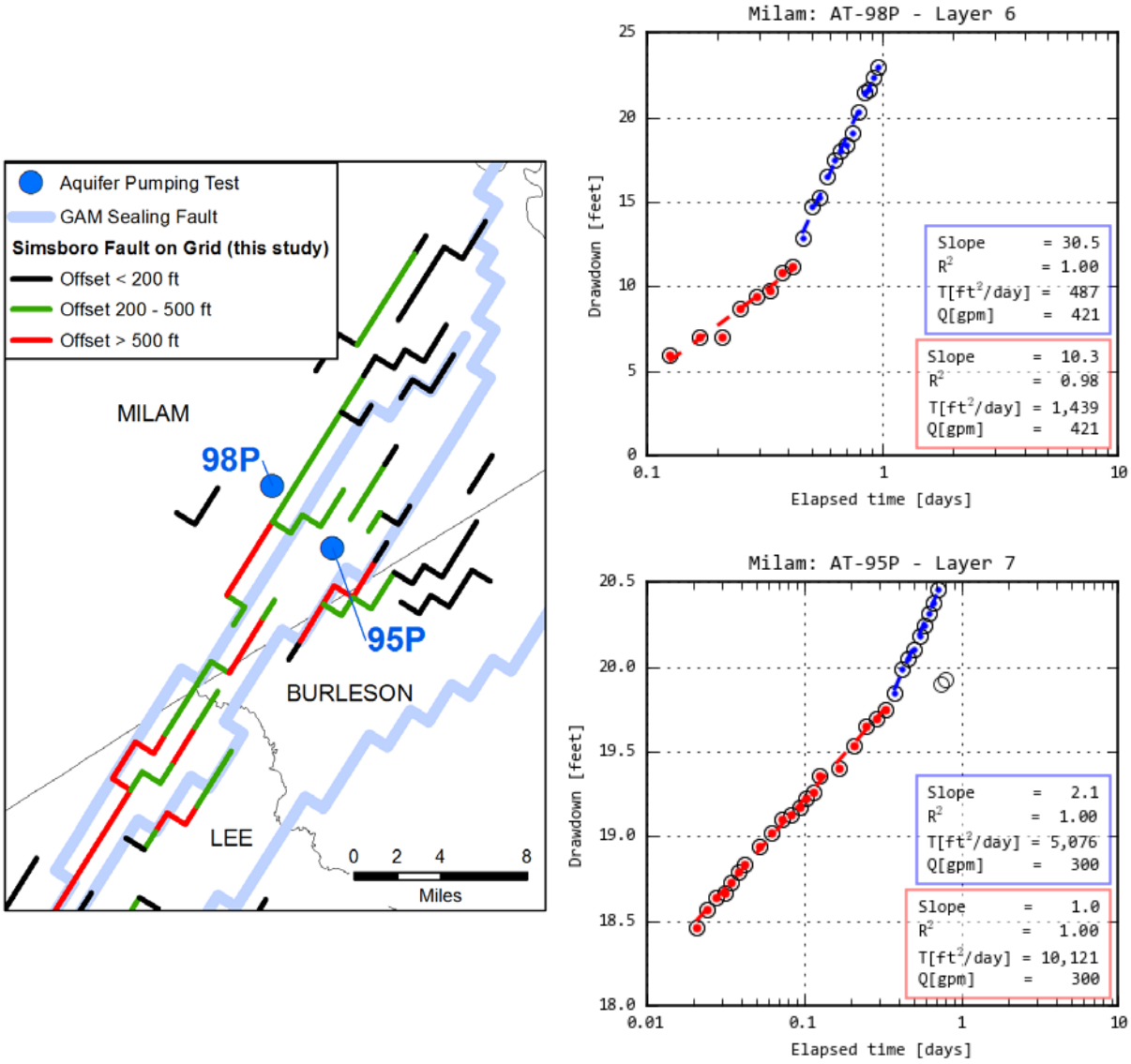

Figure 7-9. Location of aquifer pumping tests performed near faults in Milam County that produced a CJSL-calculated T_{late} that is less than the CJSL-calculated T_{early} and thereby provides a line of evidence that faults could be affecting groundwater flow.

Note: ft = feet, GAM = groundwater availability model; CSJL = Cooper-Jacob straight line; ft^2/day = square feet per day; gpm = gallons per minute; Q = flow rate of the aquifer test; T = transmissivity; R^2 = coefficient of determination

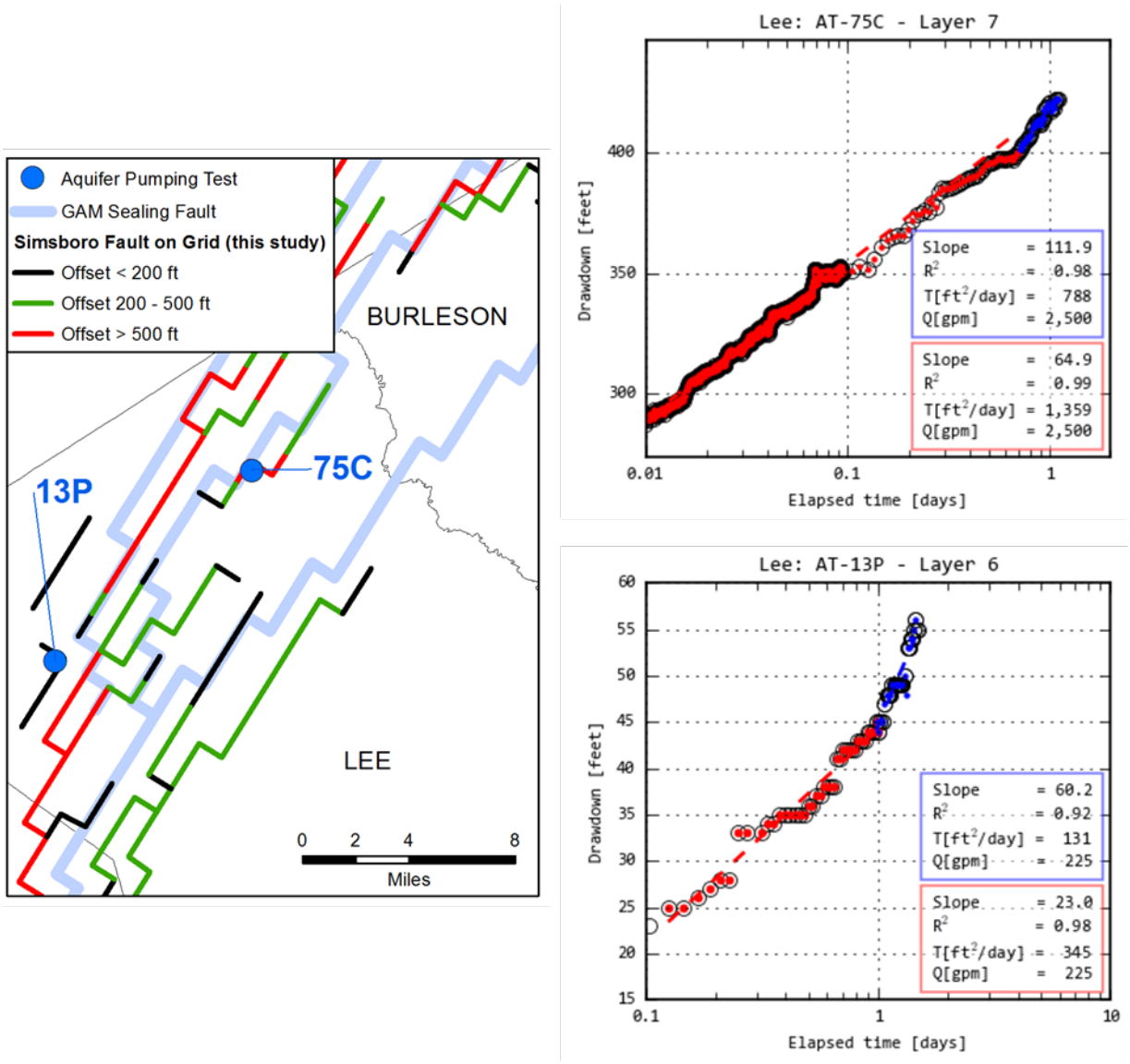

Figure 7-10. Location of aquifer pumping tests performed near faults in Lee County that produced a CJSL-calculated T_{late} that is less than the CJSL-calculated T_{early} and thereby provides a line of evidence that faults could be affecting groundwater flow.

Note: ft = feet, GAM = groundwater availability model; CSJL = Cooper-Jacob straight line; ft^2/day = square feet per day; gpm = gallons per minute; Q = flow rate of the aquifer test; T = transmissivity; R^2 = coefficient of determination

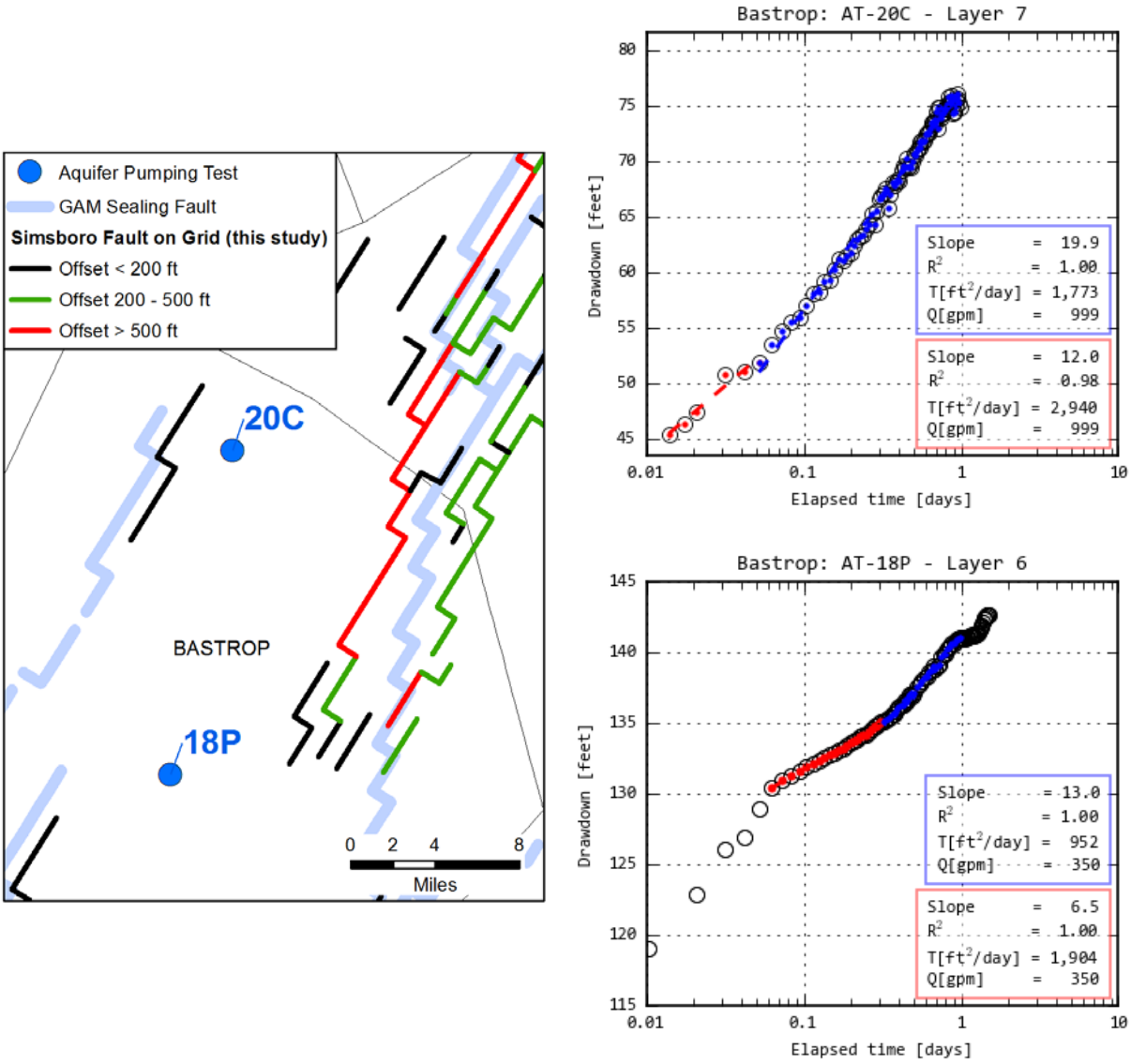

Figure 7-11. Location of aquifer pumping tests performed near faults in Bastrop County that produced a CJSL-calculated T_{late} that is less than the CJSL-calculated T_{early} and thereby provides a line of evidence that faults could be affecting groundwater flow.

Note: ft = feet, GAM = groundwater availability model; CSJL = Cooper-Jacob straight line; ft^2/day = square feet per day; gpm = gallons per minute; Q = flow rate of the aquifer test; T = transmissivity; R^2 = coefficient of determination

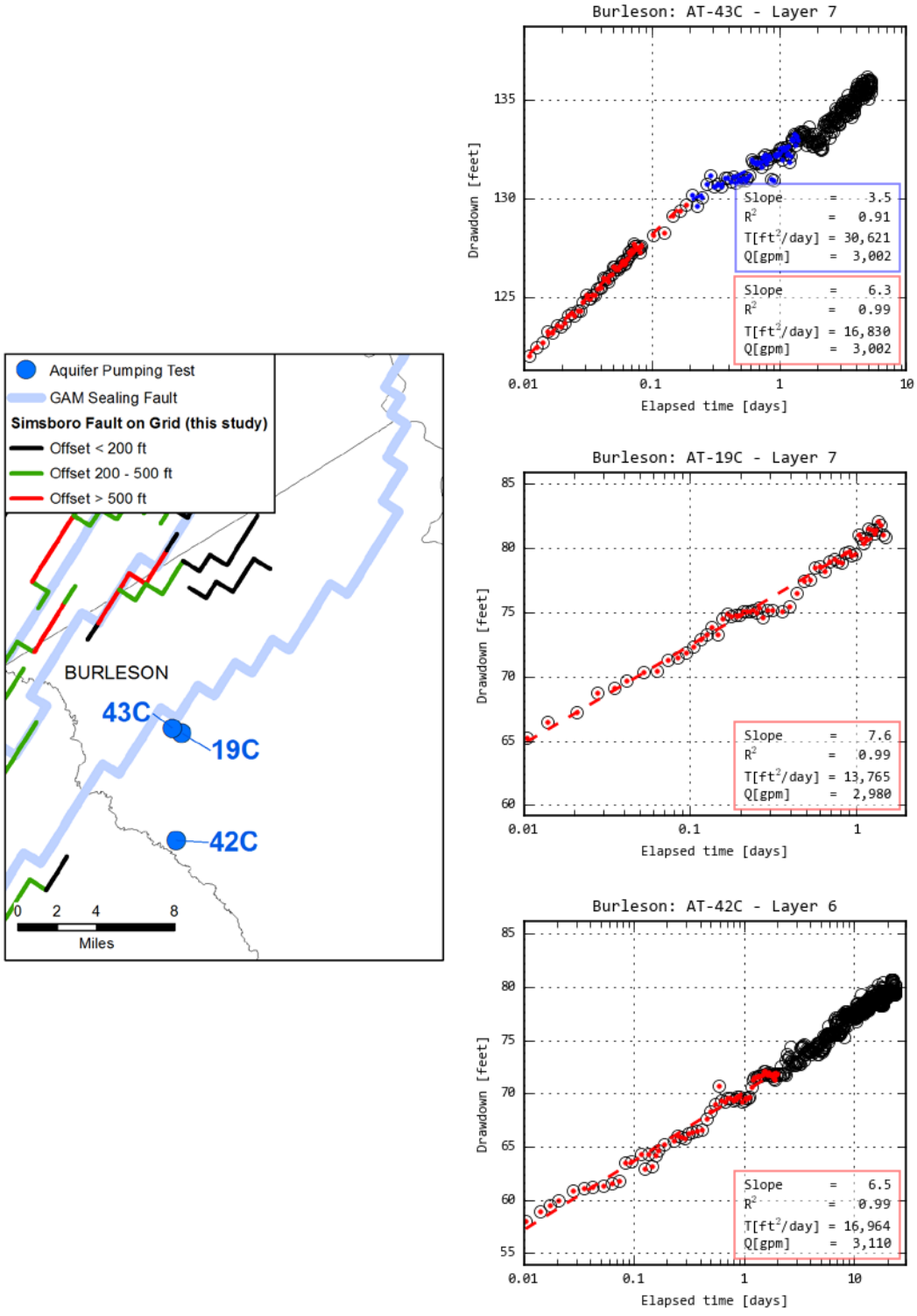

Figure 7-12. Location of aquifer pumping tests performed near faults in Burleson County that produced a CJSL-calculated T_{late} that is equal to or greater than the CJSL-calculated T_{early} and thereby provides little evidence that faults could be affecting groundwater flow.

Note: ft = feet, GAM = groundwater availability model; CSJL = Cooper-Jacob straight line; ft^2/day = square feet per day; gpm = gallons per minute; Q = flow rate of the aquifer test; T = transmissivity; R^2 = coefficient of determination

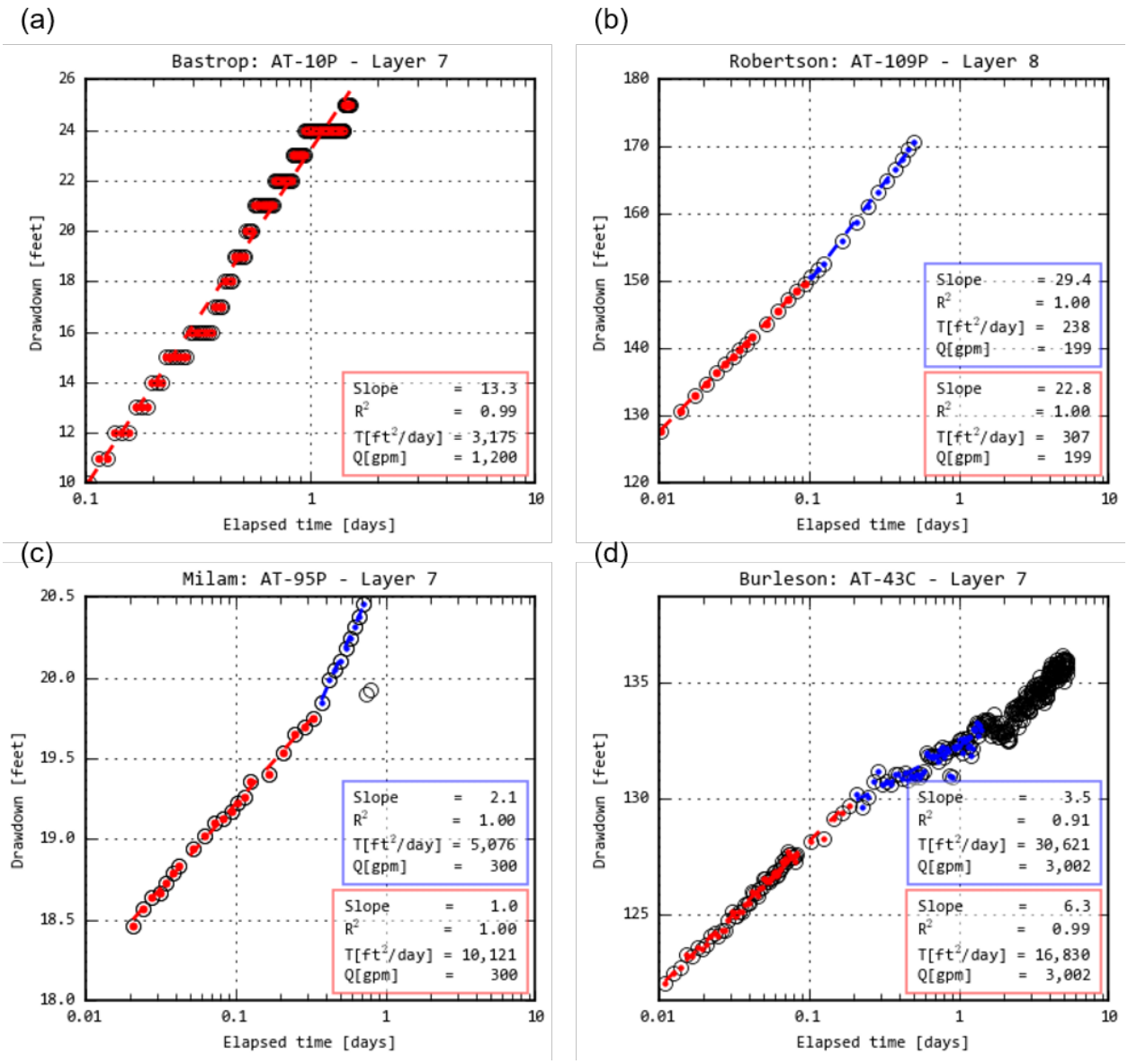

Figure 7-13. Four example applications of the CJSL method to calculate transmissivity (a) aquifer test classified as "no change" in calculated transmissivity value over time, (b) aquifer test classified as "small decrease" in calculated transmissivity values over time, (c) aquifer test classified as "large decrease" in calculated transmissivity values over time, and (d) aquifer test classified as "increase" in calculated transmissivity values over time.

Note: ft = feet; CSJL = Cooper-Jacob straight line; ft^2/day = square feet per day; gpm = gallons per minute; Q = flow rate of the aquifer test; T = transmissivity; R^2 = coefficient of determination

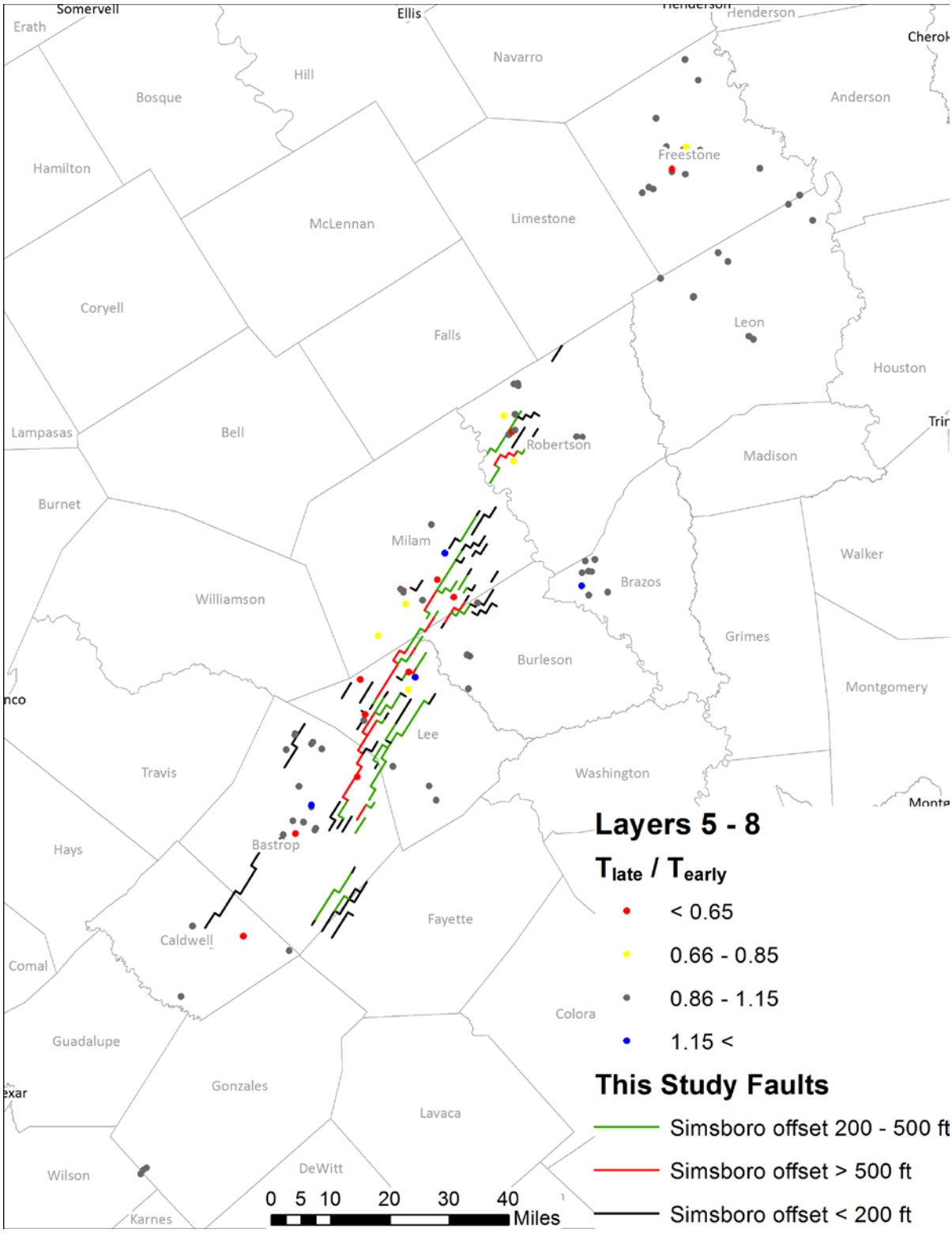

Figure 7-14. Spatial distribution of transmissivity categories for wells based on the ratio of T_{early}/T_{late} relative to the faults identified in this study.

Note: ft = feet

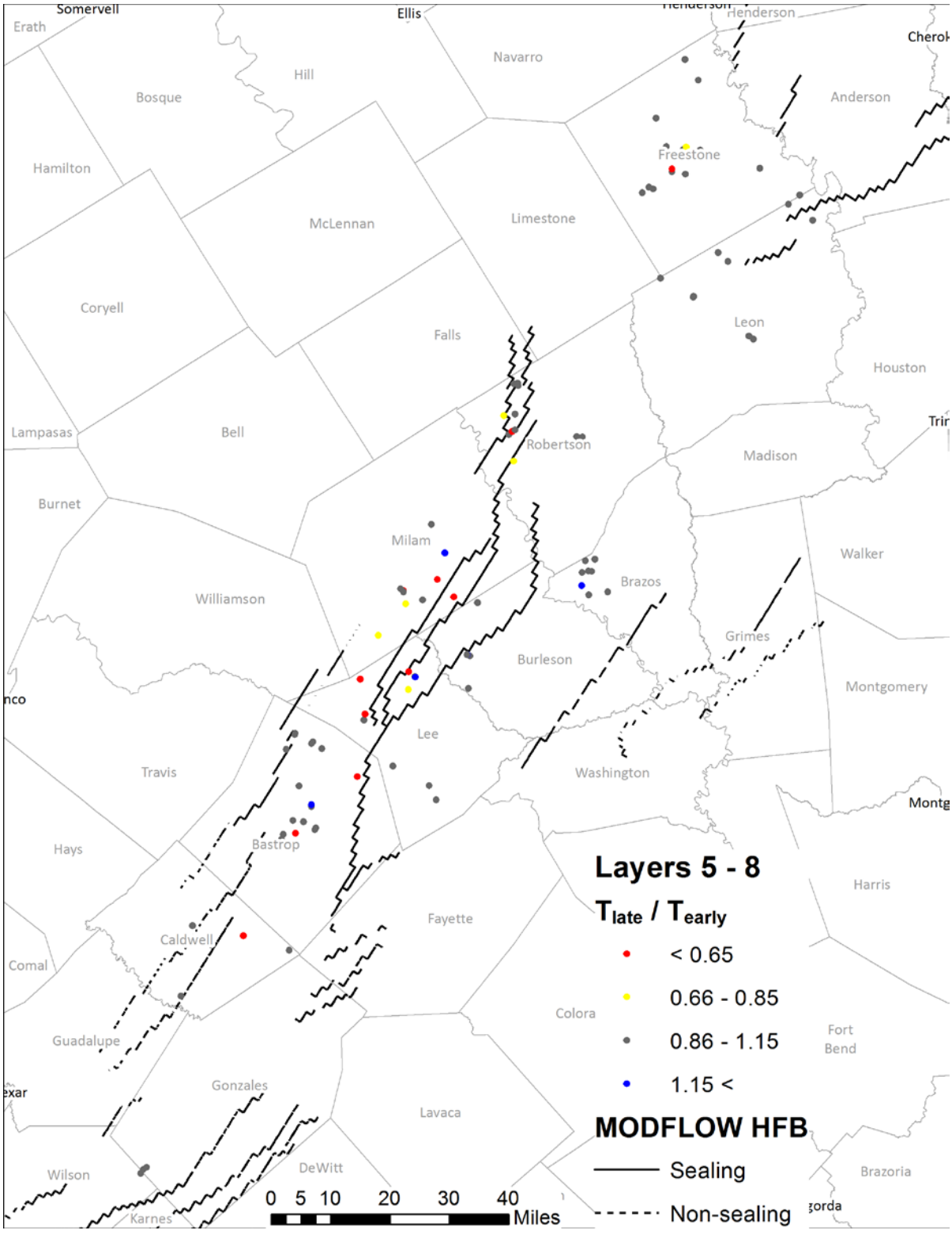

Figure 7-15. Spatial distribution of transmissivity categories for wells based on the ratio of T_{early}/T_{late} relative to the faults in the Central Queen City and Sparta aquifers Groundwater Availability Model.

Note: HFB = horizontal flow barrier

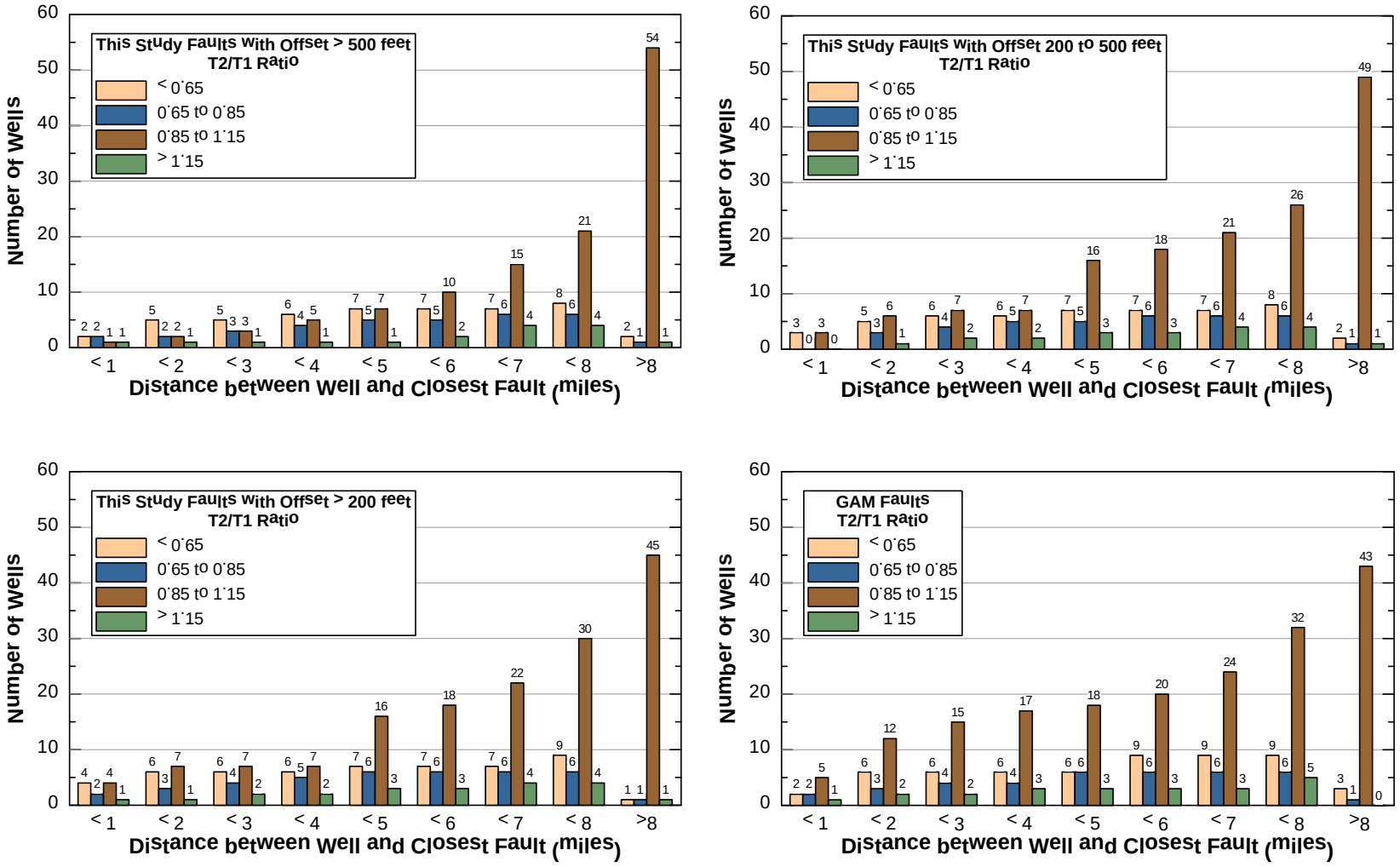

Figure 7-16. Distribution of wells by transmissivity category as a function of distance from the faults identified in this study and the faults in the Queen City and Sparta aquifers groundwater availability model.

Note: T1 = T_{early}; T2 = T_{late}

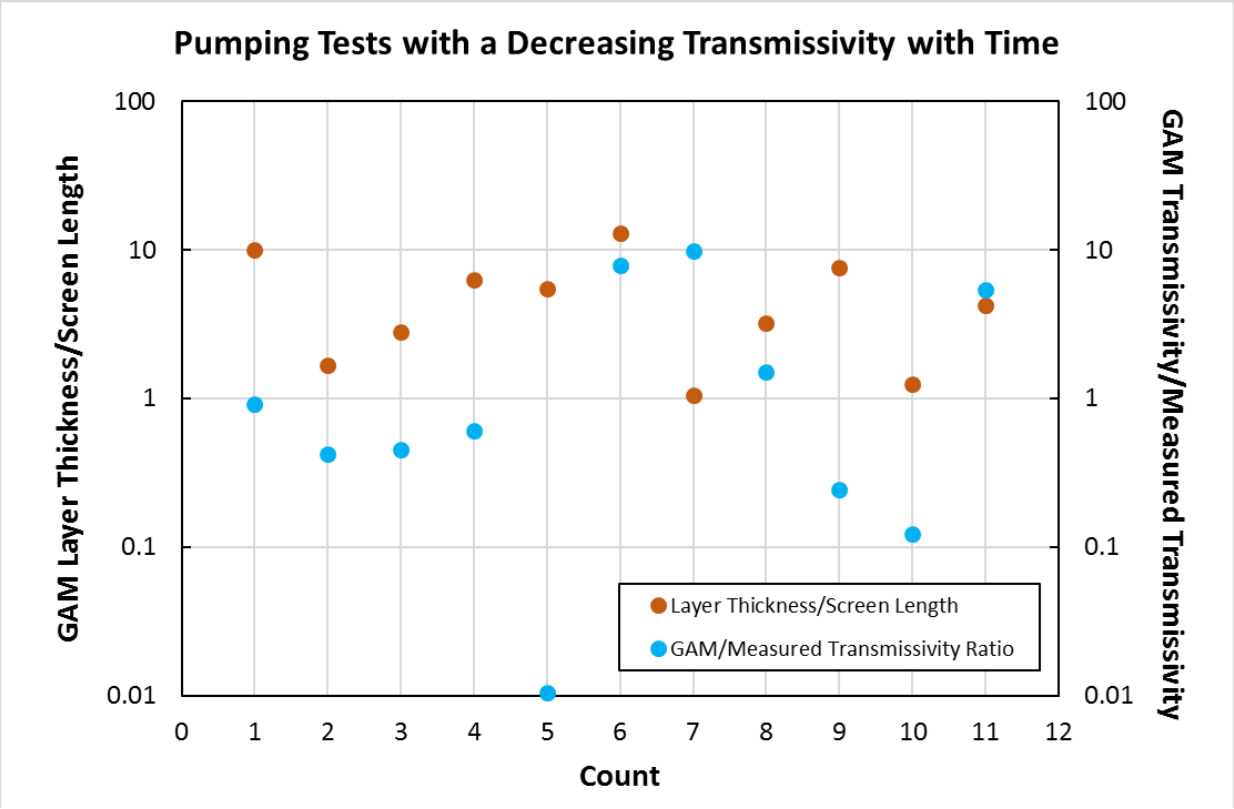

Figure 7-17. **Ratios of layer thicknesses to well screen length and groundwater availability model to measured transmissivities for aquifer pumping test wells that have field data that produce a T_{late}/T_{early} that is less than 0.6.**

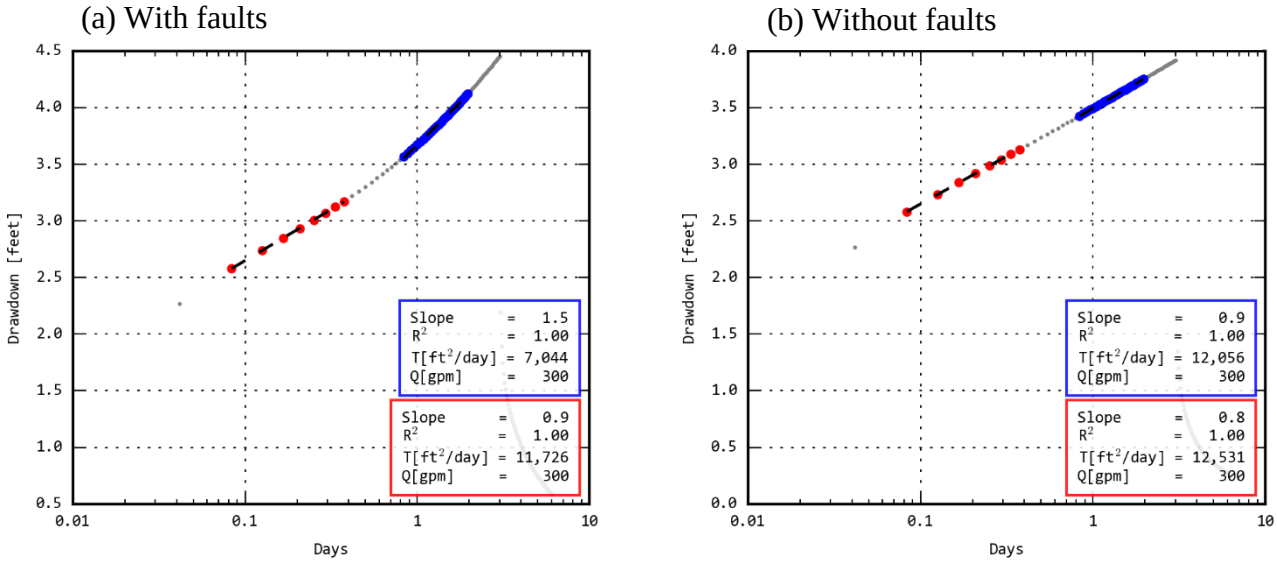

Figure 7-18. **Numerical simulation of time-dradown data for aquifer pumping test AT-95P using MODFLOW-USG and a refined grid spacing of 1/16 mile at the well and CJSL analysis of the data.**

Note: ft^2/day = square feet per day, gpm = gallons per minute

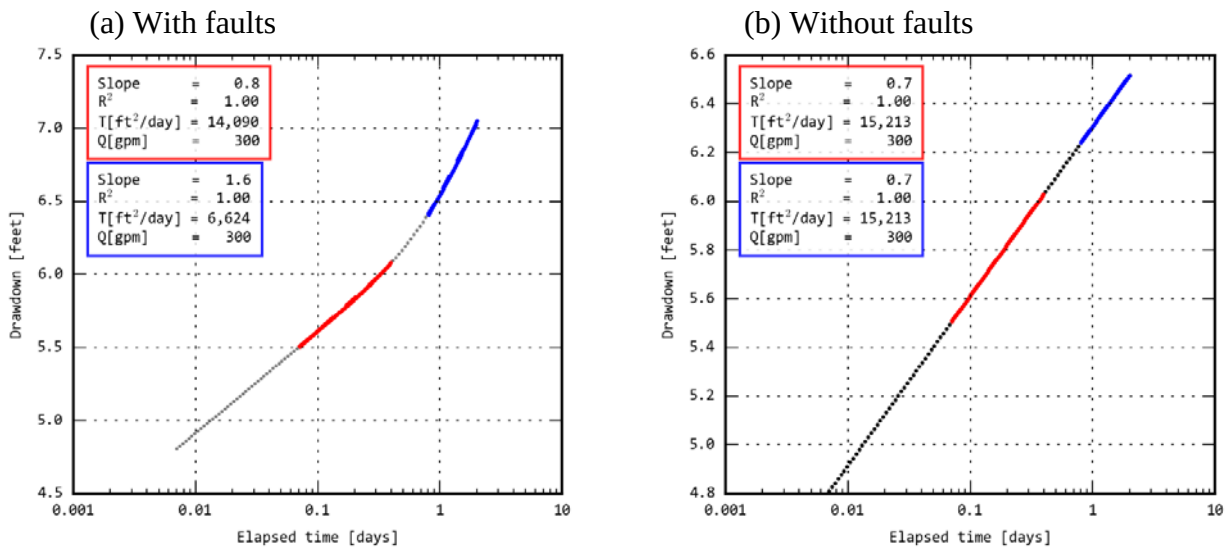

Figure 7-19. TTim- simulated time-dradown data for aquifer pumping test AT-95P using aquifer and fault hydraulic propertes from the central Queen City and Sparta aquifers groundwater availability model and CJSL analysis of the data.

Note: ft^2/day = square feet per day, gpm = gallons per minute

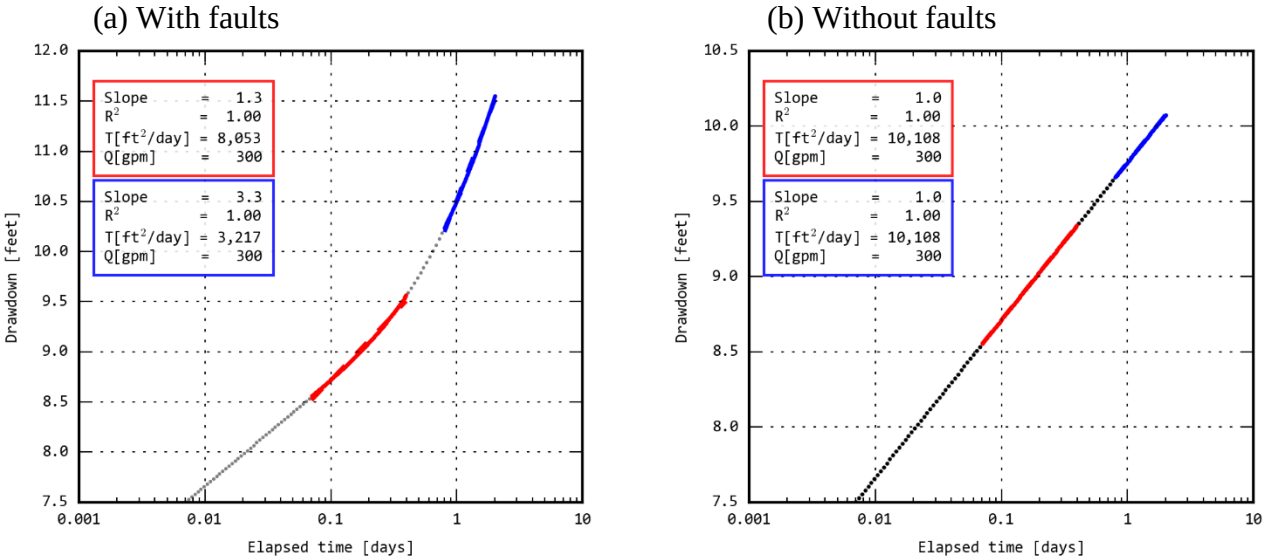

Figure 7-20. TTim-simulated time-dradown data for aquifer pumping test AT-95P using screen length and transmissivity from the aquifer test, storage parameters from the groundwater availability model, and the faults from the central Queen City and Sparta aquifers groundwater availability model and CJSL analysis of the data.

Note: ft^2/day = square feet per day, gpm = gallons per minute

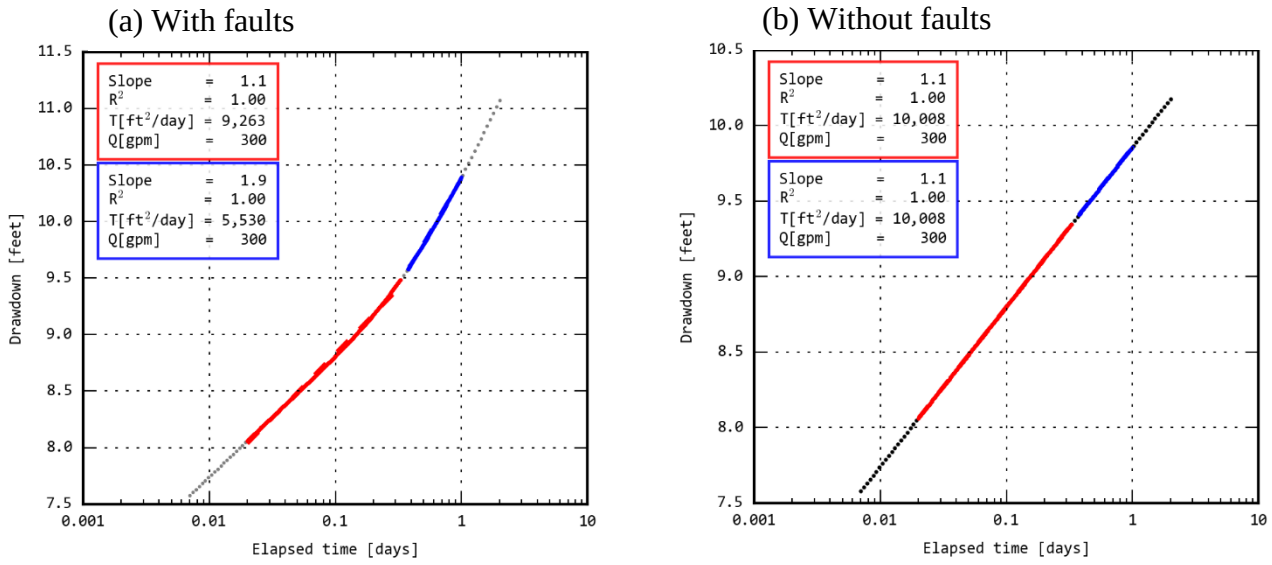

Figure 7-21. TTim-simulated time-dradown data for aquifer pumping test AT-95P using screen length and transmissivity from the aquifer test, storage parameters from the groundwater availability model, and this study faults and CJSL analysis of the data.

Note: ft^2/day = square feet per day, gpm = gallons per minute

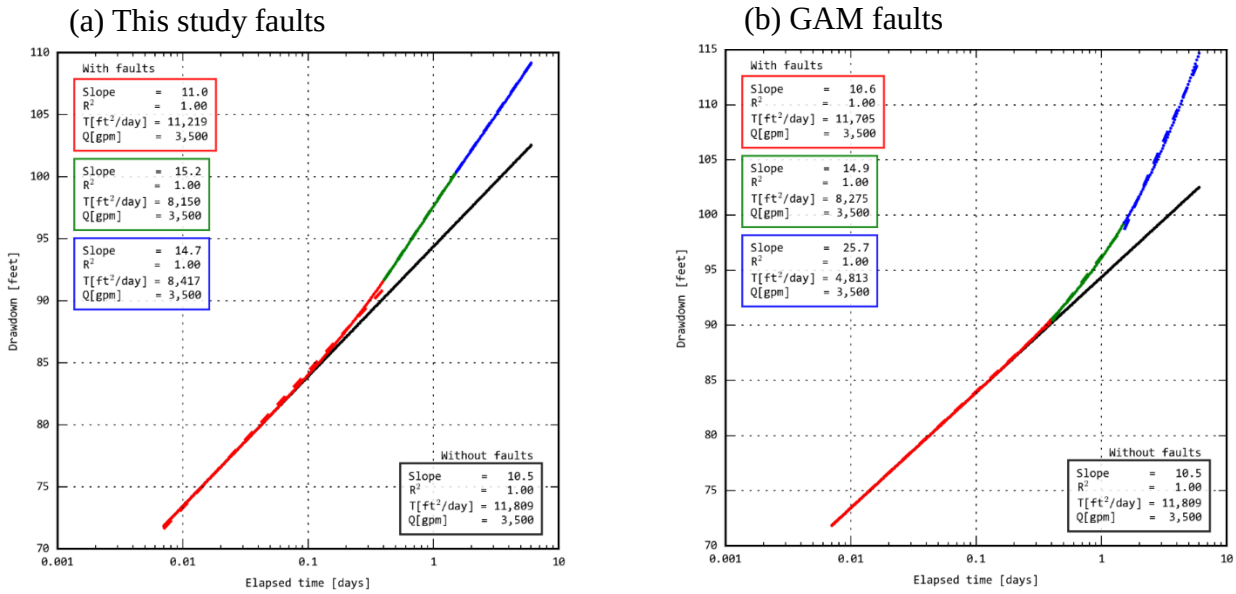

Figure 7-22. TTim-simulated time-dradown data for aquifer pumping test AT-71P using screen length and transmissivity from the aquifer test, storage parameters from the groundwater availability model, and this study faults and CJSL analysis of the data.

Note: GAM = groundwater availability model; ft^2/day = square feet per day, gpm = gallons per minute

(a) This study faults

(b) GAM faults

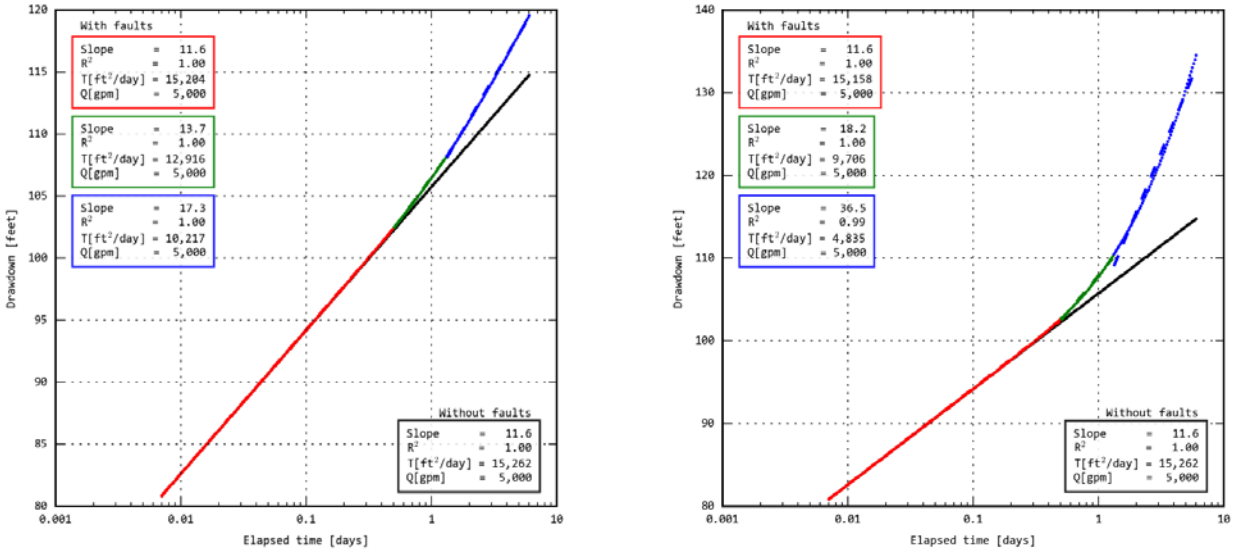

Figure 7-23. TTim-simulated time-dradown data for aquifer pumping test AT-76C using screen length and transmissivity from the aquifer test, storage parameters from the groundwater availability model, and this study faults and CJSL analysis of the data.

Note: GAM = groundwater availability model; ft^2/day = square feet per day, gpm = gallons per minute

(a) This study faults

(b) GAM faults

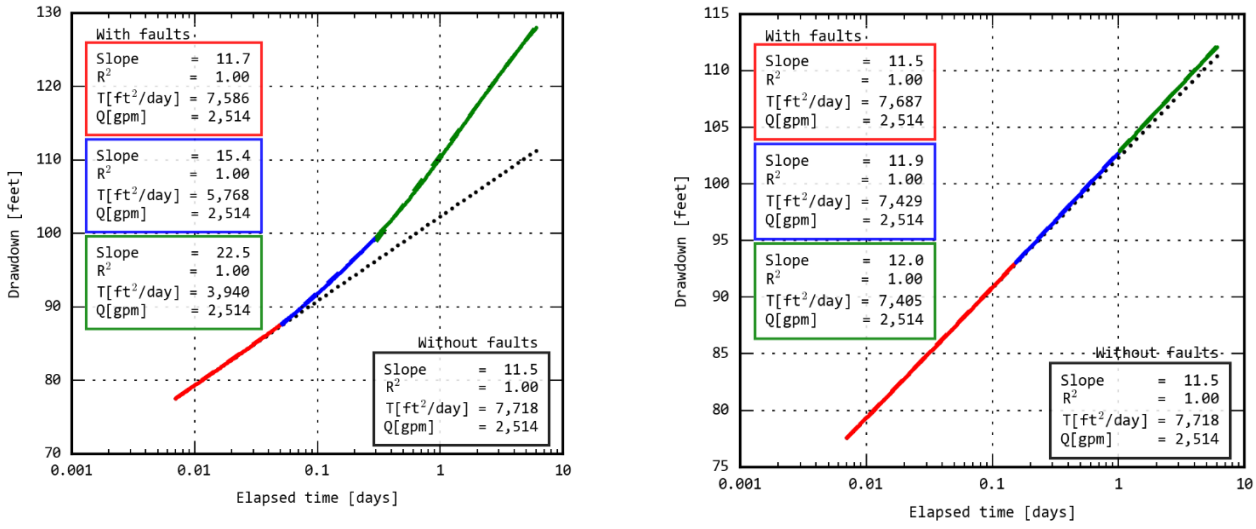

Figure 7-24. TTim-simulated time-dradown data for aquifer pumping test AT-112C using screen length and transmissivity from the aquifer test, storage parameters from the groundwater availability model, and this study faults and CJSL analysis of the data.

Note: GAM = groundwater availability model; ft^2/day = square feet per day, gpm = gallons per minute

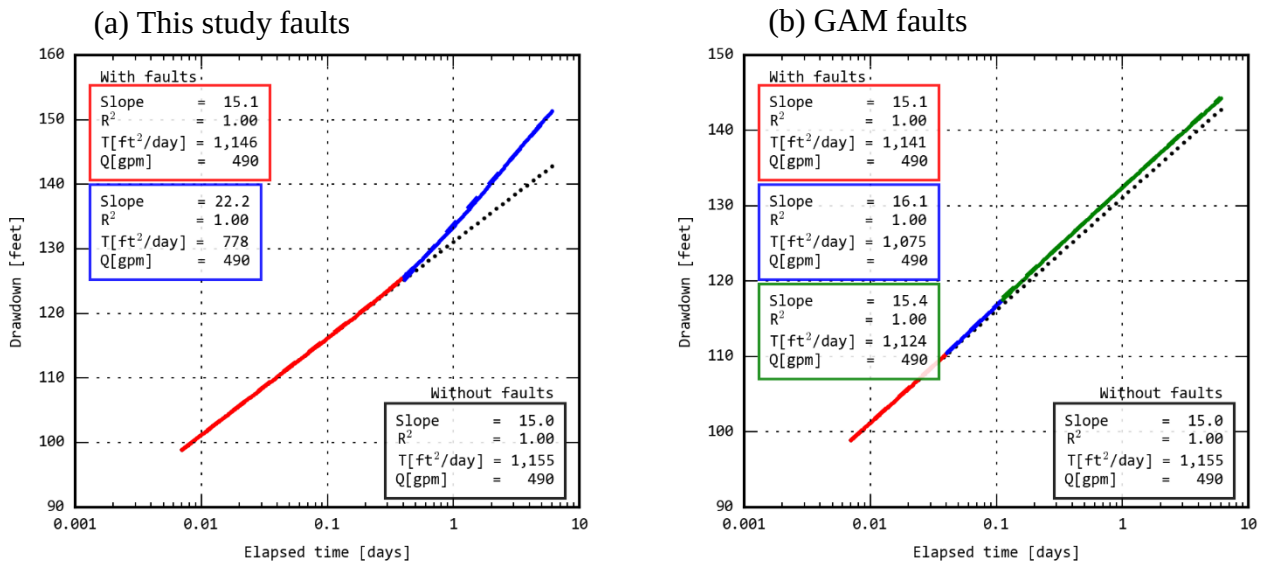

Figure 7-25. TTim-simulated time-dradown data for aquifer pumping test AT-105P using screen length and transmissivity from the aquifer test, storage parameters from the groundwater availability model, and this study faults and CJSL analysis of the data.

Note: GAM = groundwater availability model; ft^2/day = square feet per day, gpm = gallons per minute

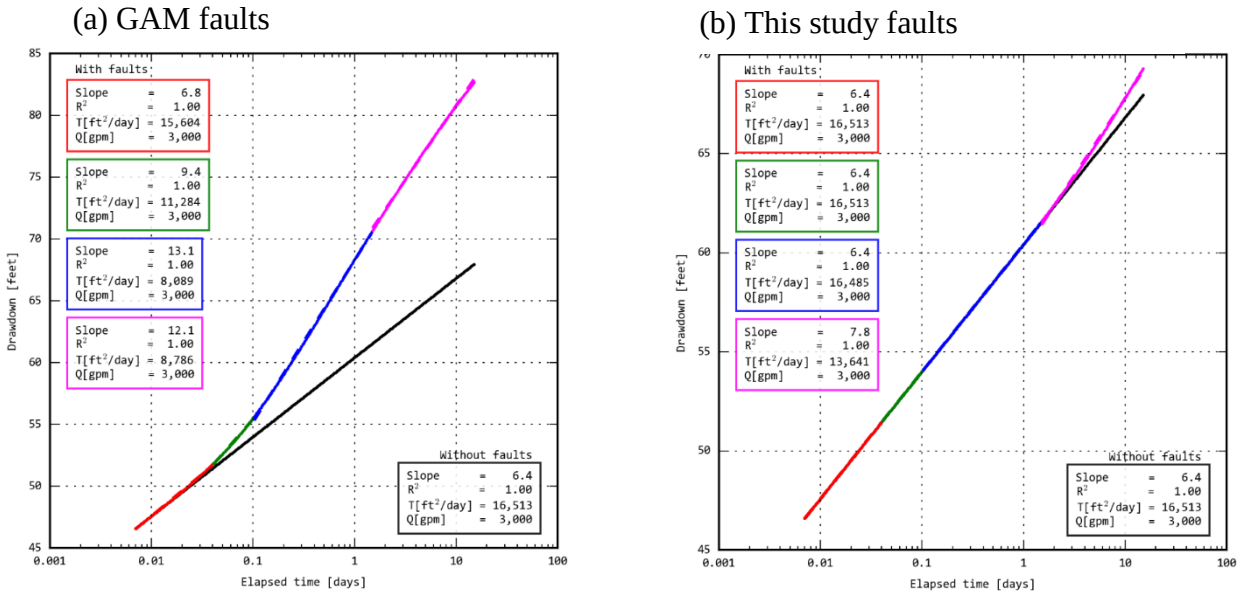

Figure 7-26. TTim-simulated time-dradown data for aquifer pumping test AT-43C using screen length and transmissivity from the aquifer test, storage parameters from the groundwater availability model, and this study faults and CJSL analysis of the data.

Note: GAM = groundwater availability model; ft^2/day = square feet per day, gpm = gallons per minute

(a) GAM faults

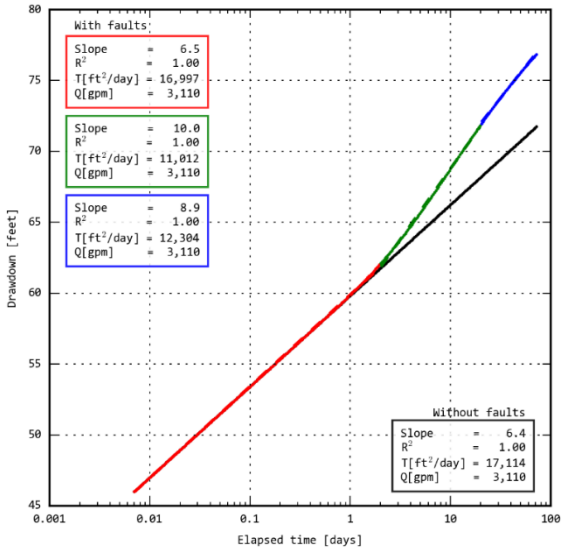

(b) This study faults

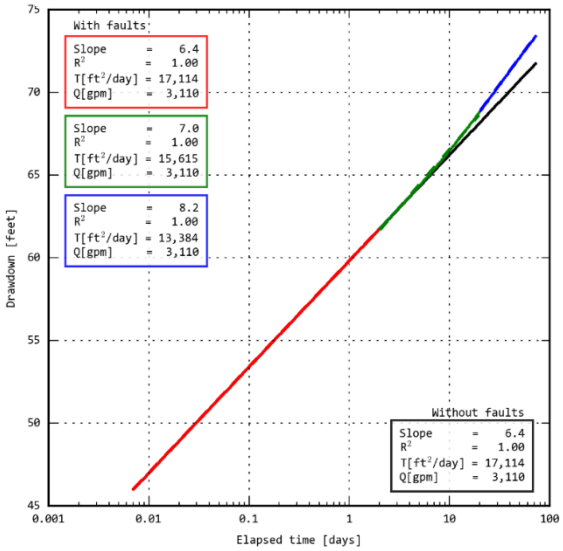

Figure 7-27. TTim-simulated time-dradown data for aquifer pumping test AT-42C using screen length and transmissivity from the aquifer test, storage parameters from the groundwater availability model, and this study faults and CJSL analysis of the data.

Note: GAM = groundwater availability model; ft^2/day = square feet per day, gpm = gallons per minute

This page is intentionally blank.

8 Summary and Recommendations

This study consists of several mini investigations conducted to characterize faults in the Milano Fault Zone and their effect on groundwater flow, and to investigate the sensitivity of water levels simulated using the central Queen City and Sparta aquifers groundwater availability model to the conceptualization of faults in the Milano Fault Zone. The first study involved a geological investigation of the Milano Fault Zone to develop a method for mapping faults associated with the fault zone. That investigation relied on several sources of information. The top surface of the Navarro Group was picked based on interpretation of approximately 650 geophysical logs. Those picks, evaluated in conjunction with faults mapped at ground surface by Barnes (1970; 1979; 1981), were used to develop a network of faults in the Milano Fault Zone. Fault offsets were estimated through analysis of logs that intersect a fault and faults identified by Barnes (1970; 1979; 1981). The faults determined from this study were mapped to the numerical grid of the central Queen City and Sparta aquifers groundwater availability model and fault segments were assigned offsets of greater than 500 feet, between 200 and 500 feet, and less than 200 feet.

An important aspect of the geological investigation was deconstruction of the Milano Fault Zone into four grabens and one complex. These are named, from south to north, the Kovar Complex, the Paige Graben, the Tanglewood Graben, the Calvert Graben, and the South Kosse Graben. A cross-section showing the stratigraphic picks is provided for each of the four grabens and the complex. The fault footprint resulting from this study is considerably smaller in Burleson and Robertson counties than the footprint of faults in the current groundwater availability model.

The smaller footprint of faults from this study occurs in part because this study represents the Milano Fault Zone as series of connected grabens instead of representing the Milano Fault Zone as several long continuous faults, some of which are 100 miles in length in the current groundwater availability model. This reconceptualization provides for “windows” and “gates” in the fault zone that allow groundwater to flow more freely perpendicular to the strike of the faults than does the conceptualization of faults in the current groundwater availability model. In addition to the “gates” and “windows” in the Milano Fault Zone where no faults exist, the assessment indicates different vertical offsets, which can be used to assign different conductance values to the faults. More groundwater flow is likely to occur in areas where fault offset is less and less likely to occur in areas where fault offset is greater.

Characterization of vertical offsets for individual fault segments also provides for adjusting the conductances of the faults to improve the performance and calibration of the updated model. A possible option for assigning conductance to the faults from this study would be to consider only those faults with offsets greater than 500 feet as potential sealing faults. In this case, the footprint of the sealing faults is reduced by about 60 percent relative to that in the current groundwater availability model. Regardless of how the conductances are assigned to the new network of faults, the updated model will differ significantly from the existing groundwater availability model in two areas. In northern Burleson County, the over 50-mile long fault segment in the current groundwater availability model will be removed because the geologic investigation conducted for this study does not support the presence of a fault in this area. Likewise, evidence of the single continuous fault that divides Robertson County currently in the

groundwater availability model was not seen in our investigation, and this fault will also be removed from the updated model.

In addition to the geological study, a second study investigated whether water-level changes predicted by the central Queen City and Sparta aquifers groundwater availability model are sensitive to changes in the properties and locations of faults, represented in the model using horizontal flow barriers. Simulations of groundwater flow were performed using three versions of the groundwater availability model. All three versions were identical except for the representation of faults in the groundwater availability model. One version did not alter the representation of the faults from that used by Kelly and others (2004) and, therefore, used the Horizontal Flow Barrier package in the current Queen City and Sparta aquifers groundwater availability model. No faults were included in a second version of the groundwater availability model, so it did not contain a Horizontal Flow Barrier Package. A third groundwater availability model run included the faults as defined by this study, which were also represented using the Horizontal Flow Barrier package. Several different types of simulations were performed using the three models, with the model results indicating that the simulated water levels can be very sensitive to how the faults are represented numerically.

The three groundwater availability model versions were used to simulate historical water levels from 1975 to 2010 and to predict drawdown that would occur from 2010 to 2070 using a pumping scenario developed by Groundwater Management Area 12 called Pumping Scenario 10 (or PS10). For the purpose of this study, the conductance assigned to a fault identified by this study was based on the vertical offset associated with the fault. Faults having an offset greater than 500 feet were represented by horizontal flow barriers with a conductance of 10^{-4} day^{-1}. Faults having an offset between 200 and 500 feet were represented by horizontal flow barriers with a conductance of 10^{-3} day^{-1}. Faults having an offset of less than 200 feet were not included in the groundwater availability model.

The most critical aspect associated with simulating historical water levels centered on nine wells located in areas of high pumping in northwest Robertson and Brazos counties. For these wells, the model with the fault representation from the current groundwater availability model over predicts drawdowns between 60 and 150 feet by 2010. However, such large over predictions in drawdown are not simulated by the groundwater availability model without faults or by the model with the faults from this study. The root mean squared error for 150 measured water levels simulated by the groundwater availability model runs using the current groundwater availability model faults, no faults, and the faults from this study is 97, 25, and 37, respectively.

This model evaluation using the three different fault conceptualizations indicates that the set of faults in the current groundwater availability model either have conductances that are too low and/or are too contiguous. In addition, the evaluation indicates that the additional fault segments added in the Simsboro Aquifer as part of the development of the central Queen City and Sparta aquifers groundwater availability model could be one of the primary causes of the high water-level residuals calculated for wells in northwest Brazos and Robertson counties.

Application of the three versions of the groundwater availability model to predict water-level changes from 2010 to 2070 show that the average drawdown calculated across a county is very

sensitive to whether or not the model includes faults. For a pumping scenario developed by Groundwater Management Area 12, called PS10, the difference in the predicted average drawdown from 2010 to 2070 between model scenarios with and without the current faults in the groundwater availability model is greater than 100 feet for the Simsboro Aquifer in Brazos and Burleson counties and more than 85 feet for the Simsboro Aquifer in Robertson and Lee counties. This difference is much greater considering the maximum drawdown rather than the average drawdown. The difference in maximum predicted drawdown in the Simsboro Aquifer is 265 feet in Burleson County and more than 100 feet in Bastrop, Brazos, Lee, Milam, and Robertson counties.

Because of the large sensitivity of simulated water levels to faults in the central Queen City and Sparta aquifers groundwater availability model for the PS10 scenario, aquifer pumping test data were assembled and analyzed to evaluate whether the observed responses provide sufficient evidence to support representation of the Milano Fault Zone in the groundwater availability model. Based on the simple conceptualization that faults can be represented as units of low conductance in an aquifer, the effects of a fault on groundwater flow should be detectable from the analysis of aquifer pumping test data if the test is conducted sufficiently close to the fault, is of sufficient duration, and is analyzed by the Cooper-Jacob straight-line (CJSL) method or an equivalent method that relies on a slope or derivative of the time-drawdown data.

Aquifer pumping test data were obtained from the Texas Commission on Environmental Quality and from hydrogeologic consulting reports. Our review of the data from these two sources produced a data set of 113 tests, of which 97 involved pumping of the Carrizo, Simsboro, or Hooper aquifers. The CJSL method was used to analyzed the semi-log slope of the time-drawdown plot to determine if the transmissivity of the aquifer changed with distance from the pumping well. The transmissivity based on the semi-log slope calculated at early time is called the early transmissivity, T_{early}, and the transmissivity based on the semi-log slope calculated at late time is called the late transmissivity, T_{late}. For tests with two slopes, the value of T_{late}/T_{early} is considered a potentially useful indicator of whether the aquifer transmissivity changes with distance from the well. If the analysis for tests in a well located near faults yields a T_{late} value lower than the T_{early} value, that provides a line of evidence that the faults were affecting groundwater flow.

A statistical analysis of the aquifer test interpretations demonstrated that the closer a well is located to one of the faults identified by this study, the more likely the aquifer test data indicate a region of low transmissivity located near the well. For the 16 wells located within 4 miles of a fault from this study with an offset of 500 feet or more, 63 percent have a T_{late} that is lower than the T_{early}. For the 58 wells located more than 8 miles from a fault identified by this study with an offset of 500 feet or more, only 5 percent have a T_{late} that is lower than T_{early}. These results clearly demonstrate that the faults from this study with 500 feet of offset are affecting groundwater flow.

Modeling of the drawdown for aquifer tests demonstrated that the conductance assigned to this study's faults based on vertical offset are justified and reasonable. Based on limited evaluations, fault conductance values of 10^{-4} and 10^{-3} day^{-1} produce simulated time-drawdown plots that are

consistent and in good agreement with field results when appropriate consideration is given to the uncertainty in the modeling input parameters.

Based on the findings from our study, the conceptualization of the Milano Fault Zone in the current central Queen City and Sparta aquifers groundwater availability model is not consistent with geologic and hydrogeologic conditions in the fault zone. In the current groundwater availability model, faults are typically represented as long and continuous lines of sealing faults that extend across multiple counties. Our geological work does not support this conceptualization, nor do the results from our analysis and modeling of the aquifer pumping tests. In addition, modeling conducted to evaluate the sensitivity of simulated historical water levels to three fault conceptualizations indicates that such a representation (long, continuous sealing faults) leads to large over predictions in drawdowns in northwest Brazos and Robertson counties, where large pumping is occurring down dip of the Milano Fault Zone. As a result, this study recommends that the conceptualization of the Milano Fault Zone in the current central Queen City and Sparta aquifers groundwater availability model be abandoned and not included in the update of the model. Evidence does exist to support incorporating faults at some level of representation in the updated groundwater availability model. The new fault conceptualization should be commensurate with the lines of evidence that faults are necessary for constructing an updated central Queen City and Sparta aquifers groundwater availability model that will serve the needs of the TWDB, Groundwater Management Area 12, the member districts of Groundwater Management Area 12, and the public good. In addition, this study recommends continuation of the work begun here so that the faults identified in this study can be incorporated into the update of the central Queen City and Sparta aquifers groundwater availability model. Thus far, this study's set of faults and associated fault properties has already provided modeling results superior to that of the current groundwater availability model with respect to both groundwater at a regional scale, such as calibration to historical water levels, and at a local scale, such as reproducing the effects of geological faults on plots of time-drawdown for aquifer pumping tests.

9 Limitations

A model can be defined as a representation of reality that attempts to explain the behavior of some aspect of reality, but is always less complex than the real system it represents (Domenico, 1972). As a result, limitations are intrinsic to models. Model limitations can be grouped into several categories, including: (1) key limitations in the data supporting a model, (2) key assumptions used to construct the model, and (3) limitations regarding model applicability. The limitations of this study are discussed in the following paragraphs consistent with these categories.

9.1 Key Limitation of Supporting Data

The key supporting data for this study primarily include geophysical measurements and aquifer pumping tests. The limitations associated with each data source are discussed below.

Geophysical Measurements: Our investigation regarding the mapping of faults relied on interpreting geophysical logs to infer locations and offsets associated with faults. Our ability to maintain good quality control on our picks is directly correlated to the quality and quantity of logs. Across the Milano Fault Zone, both the quality and quantity of logs varied and, in some areas, the coverage was moderate to poor. In areas of poor log coverage, we used the best available data and our professional judgement. To that point, we anticipate and hope that future researchers will have access to data and information not available to us so they would be able to improve and refine our picks. One type of data that would have been highly advantageous for this project is seismic measurements. Seismic measurements delineate reflections and refractions of compressional or shear waves off subsurface layers with differing densities and wave velocities. Seismic measurements provide a very powerful and complementary set of data that would enhance the ability to detect and characterize faults, but it was not pursued because of the costs associated with obtaining such data.

Aquifer Pumping Tests: The most important aspect of faults with respect to this study is how they affect groundwater flow. One ideal option for delineating and characterizing faults is to have monitoring wells located close to and on opposite sides of a presumed fault during an aquifer pumping test. Despite considerable efforts to locate such situations, we did not have access to multiwell pumping tests that include monitoring point that straddle the identified faults. Such tests would help to conclusively illustrate the presence of faults and their effect on groundwater flow. We hope that future researchers will perform the type of multiwell test in several areas along the Milano Fault Zone to help with both delineating faults and provide datasets that can be used to develop and validate groundwater models.

9.2 Limits for Key Assumptions

The key limitations for this study are simplifying the representation of faults as vertical lines of uniform conductance and simplifying the flow system in the Milano Flow Zone as consisting of stacked layers of aquifers with uniform properties.

Model Layering: Across the Milano Fault Zone, the subsurface deposits are complex and not necessarily well represented by model grid cells with homogenous properties across the entire

formation and for one square mile. Therefore, one must realize that our attempts to model the effects of faults on groundwater flow at the scale of a few miles is very much a scoping exercise that could be significantly enhance but bring in real-world spatial variability reflected in the geophysical logs.

Fault Location and Representation: Our representation of faults as a single line characterized by a few feet of thickness and a conductance estimated from a vertical offset across the fault is a gross simplification of the complexity associated with how groundwater moves through a fault zone. Consequently, we need to remain aware that our generalization may not work equally well across the entire Milano Fault Zone, and specific adjustments of our fault model will likely be required during recalibration of the updated central Queen City and Sparta aquifers groundwater availability model.

9.3 Limits for Model Applicability

With respect to geological faulting, of most importance is method for representing faults in the groundwater availability model, which is through use of the Horizontal Flow Barrier package (Hsieh and Freckleton, 1993). The limitations of using of this package are described below.

Horizontal Spacing: The Horizontal Flow Barrier package requires that faults be mapped to the locations of the boundaries shared by grid cells. For the case of the central Queen City and Sparta aquifers groundwater availability model, the boundaries are spaced 1 mile apart. As a result, the remapping of the actual fault lines onto these boundaries of the grid cells introduces error in their location that could be as great as a 0.5 mile. Therefore, the more localized and smaller scale a groundwater flow problem is, the more likely the shifts from their actual mapped locations to their grid cell location will be of concern.

Fault Conductance: The most important aspect associated with using a horizontal flow barrier to represent a fault is the conductance assigned to the fault. The conductance is a measurement of the resistivity the fault causes along a groundwater flow path. The ability to estimate a conductance is highly dependent on localized aquifer conditions. In this report, we assigned conductances to fault based on general concepts and profession judgement. There has not been a proper study yet into whether our conductance values are appropriate for many of the areas of Milano Fault Zone not evaluated in this report. Consequently, we believe that the applicability of our estimates is appropriate for preliminary-level analysis.

10 References

Anderson, M.P., and Woessner, W.W., 1992, Applied groundwater modeling: Simulation of flow and advective transport: Academic Press, Inc., San Diego, 381 p.

Ayers, W.B., Jr., and Lewis, A.H., 1985, The Wilcox Group and Carrizo Sand (Paleogene) in East-Central Texas: depositional systems and deep-basin lignite: The University of Texas at Austin, Bureau of Economic Geology, Geologic Folio No. 1, 19 p., 30 plates.

Bakker, M., 2013, Semi-analytic modeling of transient multi-layer flow with TTim. Hydrogeology Journal 21: 935-943

Barnes, V.E., 1970, Waco sheet: Bureau of Economic Geology, Geologic Atlas of Texas, scale 1:250,000.

Barnes, V.E., 1979, Seguin sheet: Bureau of Economic Geology, Geologic Atlas of Texas, scale 1:250,000.

Barnes, V.E., 1981, Austin sheet: Bureau of Economic Geology, Geologic Atlas of Texas, scale 1:250,000.

Bureau of Economic Geology (BEG), 2003, Report of Investigations No. 268: Salt-Related Fault Families and Fault Welds in the Northern Gulf of Mexico, University of Texas at Austin.

Butler, J. J., 1990. The Role of Pumping Tests in Site Characterization: Some Theoretical Considerations, Ground Water, May-June, Vol 28 (3), pg 394-402

Cooper, H.H., and Jacob, C.E., 1946, A Generalized Graphical Method for Evaluating Formation Constants and Summarizing Well-Field History: Tansactons of the American Geophysical Union, 217, p. 626-634.

Deeds, N., Kelley, V., Fryar, D., Jones, T., Whellan, A. J., and Dean, K. E., 2003, Groundwater availability model for the Southern Carrizo-Wilcox Aquifer, Contract Rept. prepared for the Texas Water Development Board, variably paginated., 452.

Domenico, P.A., and Schwartz, F.W., 1990, Physical and chemical hydrogeology: New York, NY, John Wiley & Sons, Inc., 824 p.

Driscoll, F.G., 1986, Groundwater and Wells: St. Paul, MN, Johnson Filtration Systems, Inc., 1079 p.

Dutton, A.R., Harden, R.W., Nicot, J.P., and O'Rourke, D., 2003, Groundwater Availability Model for the Central Part of the Carrizo-Wilcox Aquifer in Texas: The University of Texas at Austin, Bureau of Economic Geology, prepared for the Texas Water Development Board, 295 p

Environmental Simulations, Inc., 2011, Guide to using Groundwater Vistas. Reinholds, PA.

Ewing, T.E., 1990, Tectonic map of Texas: The University of Texas at Austin, Bureau of Economic Geology, scale 1:750:000.

Ewing, T.E., 1991, Structural framework: *in* Salvador, A., ed., The geology of North America: the Gulf of Mexico basin, vol. J: Boulder, Colorado, Geological Society of America, p. 31-52.

Ewing, T.E., Budnik, R.T., Ames, J.T., Ridner, D.M, and Dillon, R.L., 1990, Tectonic map of Texas: University of Texas at Austin, Bureau of Economic Geology.

Ewing, T.E., 2016, Texas through Time: Lone Star Geology, Landscapes and Resources, University of Texas at Austin.

Fenske, J.P., Leake, S.A., and Prudic, D.E., 1996, Documentation of a computer program (RESI) to simulate leakage from reservoires uing the Modular finite-Difference Ground-Water flow Model (MODFLOW): United States Geological Survey, Open-File Report 96-364.

Fryar, D., Senger, R., Deeds, N., Pickens, J., Whallon, A., and Dean, K., 2003, Groundwater Availability Model for the Northern Carrizo-Wilcox Aquifer: Prepared for the Texas Water Development Board, 529 p.

Galloway, W.E., 1982, Depositional architecture of Cenozoic Gulf Coastal Plain fluvial systems: The University of Texas at Austin, Bureau of Economic Geology Geological Circular 82-5, 29 p.

Galloway, W.E., Ganey-Curry, P.E., Li, X., and Buffler, R.T., 2000, Cenozoic depositional history of the Gulf of Mexico basin: American Association of Petroleum Geologists Bulletin, vol. 84, p. 1743–1774.

Guevara, E.H., and Garcia, R., 1972, Depositional systems and oil-gas reservoirs in the Queen City Formation (Eocene), Texas: Gulf Coast Association of Geological Societies Transactions, Volume 22.

Halbouty, M.T., 1979, Salt domes—Gulf region, United States and Mexico, 2nd edition: Houston, Texas, Gulf Publishing, 561 p.

Harbaugh, A.W., and M.G. McDonald, 1996. User's Documentation for MODFLOW-96, an Update to the U.S. Geological Survey Modular Finite-Difference Ground-Water Flow Model. U.S. Geological Survey, Open-File Report 96-485, 56 p.

Hsieh, P.A., and Freckleton, J.R., 1993, Documentation of a Computer Program to Simulate Horizontal-Flow Barriers Using the U.S. Geological Survey Modular Three-Dimensional Finite-Difference Ground-Water Flow Model: U.S. Geological Survey, Open-File Report 92-477, 32 p.

Jackson, M.P.A., 1982, Fault tectonics of the East Texas Basin: The University of Texas at Austin, Bureau of Economic Geology Geological Circular 84-2, 31 p.

Jackson, M.P.A., and S.J. Seni, 1984. Atlas of Salt Domes in the East Texas Basin. The University of Texas at Austin, Bureau of Economic Geology, Report of Investigations No. 140, 102 p.

Jackson and others, 2003

Kelley, V.A., Deeds, N.E., Fryar, D.G., and Nicot, J-P, 2004, Groundwater Availability Models for the Queen City and Sparta Aquifers: prepared for the Texas Water Development Board.

Kelley, V.A., Ewing, J.E., Jones, T.L., Young, S.C., Deeds, N.E., Hamlin, S, 2014, Updated Groundwater Availability Model of the Northern Trinity and Woodbine Aquifers. Prepared for North Texas GCD, Northern Trinity GCD, Prairielands GCD, and Upper Trinity GCD, Final Report: Prepared by INTERA, Austin, TX.

Panday, Sorab, Langevin, C.D., Niswonger, R.G., Ibaraki, Motomu, and Hughes, J.D., 2013, MODFLOW-USG version 1: An unstructured grid version of MODFLOW for simulating groundwater flow and tightly coupled processes using a control volume finite-difference formulation: U.S. Geological Survey Techniques and Methods, book 6, chap. A45, 66 p.

Panday, Sorab, Langevin, C.D., Niswonger, R.G., Ibaraki, Motomu, and Hughes, J.D., 2015, MODFLOW-USG version 1.3.00: An unstructured grid version of MODFLOW for simulating groundwater flow and tightly coupled processes using a control volume finite-difference formulation: U.S. Geological Survey Software Release, 01 December 2015, http://dx.doi.org/10.5066/F7R20ZFJ

Papadopoulos, I.S., and Cooper. H.H., 1976, Drawdown in Well of Large Diameter: Water Resources Research, Vol 3, No. 1., pp 241-244.

Prudic, D.E., 1988. Documentation of a Computer Program to Simulate Stream-Aquifer Relations Using a Modular, Finite-Difference, Ground-Water Flow Model. U.S. Geological Survey, Open-File Report 88-729.

RW Harden & Associates, Inc., 2001, Response to Section 12.139A Groundwater Control Plan, Alcoa Sandow Mine Permit 1E Mine Permit Revision No. 1, prepared for Alcoa Inc., Rockdale, Texas.

RW Harden & Associates, Inc., 1976, Records for Texas A&M University Well A-7, prepared for Riewe & Wischmeyer, Inc.

RW Harden & Associates, Inc., 1979a, Results of Testing Texas A&M University Well 7, prepared for Riewe & Wischmeyer, Inc., The City of College Station, Texas.

RW Harden & Associates, Inc., 1979b, Results of Testing – City of College Station Simsboro Well 1, prepared for Riewe & Wischmeyer, Inc., The City of College Station, Texas.

RW Harden & Associates, Inc., 1979c, Results of Testing – City of College Station Simsboro Well 2, prepared for Riewe & Wischmeyer, Inc., The City of College Station, Texas.

RW Harden & Associates, Inc., 1980, North Rockdale Production Well Test Results, prepared for Shell Oil Company Houston, Texas.

RW Harden & Associates, Inc., 1982, Results of Testing – City of College Station Simsboro Well 3, prepared for Riewe & Wischmeyer, Inc., The City of College Station, Texas.

RW Harden & Associates, Inc., 1982, South Milam Production Well B-35 Test Results Appendices, prepared for Shell Oil Company Houston, Texas.

RW Harden & Associates, Inc., 1984, North Camp Swift Project – Preliminary Ground-Water Testing, prepared for Shell Mining Company Houston, Texas.

RW Harden & Associates, Inc., 1987, Groundwater Investigation for Calvert Lignite Mine, Robertson County, Texas Volume 2, prepared for Phillips Coal Company, Richardson, Texas.

RW Harden & Associates, Inc., 1991, Groundwater Information Section 779.128 Permit No. 27B Permit Renewal/Revision Application Calvert Mine Robertson County, Texas prepared for Walnut Creek Mining Company.

RW Harden & Associates, Inc., 2001, Response to Section 12.139A Groundwater Control Plan, Alcoa Sandow Mine Permit 1E Mine Permit Revision No. 1, prepared for Alcoa Inc., Rockdale, Texas.

RW Harden & Associates, Inc., 2007, Availability of Groundwater Carrizo-Wilcox Aquifer - 130 Project, prepared for Blue Water Systems L.P.

RW Harden & Associates, Inc., 2016a, TCEQ PW-2 Interim Approval Submittal, submitted on behalf of 130 Regional Water Supply Corporation.

RW Harden & Associates, Inc., 2016b, Vista Ridge Regional Supply Project Hydrogeologic Report, prepared for Central Texas Regional Water Supply Corporation

Stoeser, D.B., Green, G.N., Morath, L.C., Heran, W.D., Wilson, A.B., Moore, D.W., and Van Gosen, B.S., 2007, Preliminary integrated geologic map databases for the United States: Central States: Montana, Wyoming, Colorado, New Mexico, North Dakota, South Dakota, Nebraska, Kansas, Oklahoma, Texas, Iowa, Missouri, Arkansas, and Louisiana, Version 1.2: United States Geological Society, Open-File Report 2005-1351, websites https://pubs.usgs.gov/of/2005/1351/ (report) and https://mrdata.usgs.gov/geology/state/state.php?state=TX (digital data).

Streltsova, T. D., 1988. Well Testing in Heterogeneous Formations, An Exxon Monograph, John Wiley and Sons, New York, New York

Thornhill Group, Inc., 2009, Data and Analyses Derived from Drilling and Testing Programs to Verify Production and Water Quality in the Simsboro Aquifer, Prepared for EndOp, LP, Elgin, Texas.

Thornhill Group, Inc., 2014a, Letter Report, prepared for Lower Colorado River Authority

Thornhill Group, Inc., 2014b, Simsboro Production Well No. 5 – LPGCD Well No: 5933412 – Draft Well Completion Report, Prepared for Forestar USA, Austin, Texas.

Thornhill Group, Inc., 2014c, Simsboro Production Well No. 7 – LPGCD Well No: 5933123 – Draft Well Completion Report, Prepared for Forestar USA, Austin, Texas.

Thornhill Group, Inc., 2014d, Simsboro Production Well No. 8 – LPGCD Well No: 5933413 – Draft Well Completion Report, Prepared for Forestar USA, Austin, Texas.

Thornhill Group, Inc., 2014e, Hydrogeologic Evaluation of Well Completion and Testing Results Simsboro Production Well No. 1 and Well No. 2 — Lee County, Texas, Prepared for Heart of Texas Suppliers, LP, Houston, Texas.

United States Geological Survey, 2017a, USGS FAQs – What is a fault and what are the different types?: United States Geological Survey website https://www2.usgs.gov/faq/categories/9838/3312.

United States Geological Survey, 2017b, MODFLOW-USG: An unstructured grid version of MODFLOW for simulating groundwater flow and tightly coupled processes using a control volume finite-difference formulation: United States Geological Survey website https://water.usgs.gov/ogw/mfusg/.Young S. C., 1995, Characterization of High-K Pathways by Borehole Flowmeter and Tracer Tests. Ground Water, 33:2, 311–318.

Young, S.C., Ewing, T. Hamlin, S., Baker, E., and Lupton, D., 2012, Updating the Hydrogeologic Framework for the Northern Portion of the Gulf Coast Aquifer, Unnumbered Report: Texas Water Development Board.

This page is intentionally blank.

11 Appendix A

Table 11-1. Well identification, coordinates, and county, and source of well and test data for the aquifer pumping test.

Test ID	Well ID	Decimal Latitude	Decimal Longitude	County	Well and Test Data Source
AT-01P	G0110001K	30.10938	-97.296099	Bastrop	TCEQ Well Records
AT-02P	G0110001L	30.11325	-97.325608	Bastrop	TCEQ Well Records
AT-03P	G0110002E	30.32533	-97.312691	Bastrop	TCEQ Well Records
AT-04P	G0110002F	30.3036	-97.263443	Bastrop	TCEQ Well Records
AT-05P	G0110002H	30.29941	-97.267693	Bastrop	TCEQ Well Records
AT-06P	G0110013AA	30.06691	-97.359189	Bastrop	TCEQ Well Records
AT-09P	G0110013AD	30.32167	-97.3137	Bastrop	TCEQ Well Records
AT-10P	G0110013E	30.07962	-97.353586	Bastrop	TCEQ Well Records
AT-11P	G0110013H	30.2868	-97.339706	Bastrop	TCEQ Well Records
AT-12P	G0110013M	30.09319	-97.260639	Bastrop	TCEQ Well Records
AT-14P	G0110013S	30.19687	-97.306008	Bastrop	TCEQ Well Records
AT-15P	G0110013W	30.09307	-97.260658	Bastrop	TCEQ Well Records
AT-16P	G0110014A	30.2866	-97.238319	Bastrop	TCEQ Well Records
AT-17P	G0110020C	30.08884	-97.264158	Bastrop	TCEQ Well Records
AT-18P	G0110020E	30.08226	-97.318531	Bastrop	TCEQ Well Records
AT-20C	Shell Mining Co. Well 1	30.30362	-97.26346	Bastrop	RW Harden & Associates (1984)
AT-21C	LCRA Lake Bastrop Well SB-1	30.14583	-97.2725	Bastrop	Thornhill Group (2014a)
AT-22C	LCRA Lake Bastrop Well SB-3	30.15111	-97.271944	Bastrop	Thornhill Group (2014a)
AT-70P	G1440005N	30.21589	-97.14151	Bastrop	TCEQ Well Records
AT-23P	G0210001L	30.73011	-96.451287	Brazos	TCEQ Well Records
AT-24P	G0210001N	30.72679	-96.477639	Brazos	TCEQ Well Records
AT-25P	G0210002E	30.69863	-96.48863	Brazos	TCEQ Well Records
AT-26P	G0210002G	30.69849	-96.488646	Brazos	TCEQ Well Records
AT-27P	G0210002H	30.6988	-96.451515	Brazos	TCEQ Well Records
AT-28P	G0210005B	30.78203	-96.343492	Brazos	TCEQ Well Records
AT-29P	G0210005C	30.69936	-96.286906	Brazos	TCEQ Well Records
AT-30P	G0210005D	30.78926	-96.336036	Brazos	TCEQ Well Records
AT-31P	G0210005E	30.80634	-96.317621	Brazos	TCEQ Well Records
AT-32P	G0210005F	30.80017	-96.322433	Brazos	TCEQ Well Records
AT-33P	G0210017I	30.64714	-96.485519	Brazos	TCEQ Well Records
AT-34P	G0210065B	30.64962	-96.416858	Brazos	TCEQ Well Records
AT-35C	Texas A&M Well 7	30.66639	-96.490031	Brazos	RW Harden & Associates (1979a)

Test ID	Well ID	Decimal Latitude	Decimal Longitude	County	Well and Test Data Source
AT-36C	City of College Station Well 1	30.70047	-96.460799	Brazos	RW Harden & Associates (1979b)
AT-37C	City of College Station Well 2	30.70186	-96.470243	Brazos	RW Harden & Associates (1979c)
AT-38C	Texas A&M Riverside Campus	30.64326	-96.471631	Brazos	RW Harden & Associates (1976)
AT-19C	Blue Water Well PW-2	30.5032	-96.8128	Burleson	RW Harden & Associates (2016a)
AT-39P	G0260014E	30.45641	-96.783528	Burleson	TCEQ Well Records
AT-40P	G0260015C	30.38686	-96.564394	Burleson	TCEQ Well Records
AT-41P	G0260050A	30.50679	-96.820706	Burleson	TCEQ Well Records
AT-42C	Blue Water Well PW-13	30.42394	-96.82004	Burleson	RW Harden & Associates (2016b)
AT-43C	Western Burleson County	30.5069	-96.820591	Burleson	RW Harden & Associates (2007)
AT-94P	G1660009C	30.63225	-96.787734	Burleson	TCEQ Well Records
AT-07P	G0110013AB	29.79633	-97.344722	Caldwell	TCEQ Well Records
AT-08P	G0110013AC	29.83499	-97.472744	Caldwell	TCEQ Well Records
AT-44P	G0280001D	29.86217	-97.615274	Caldwell	TCEQ Well Records
AT-45P	G0280001K	29.81273	-97.562775	Caldwell	TCEQ Well Records
AT-46P	G0280002C	29.69023	-97.651384	Caldwell	TCEQ Well Records
AT-47P	G0810001A	31.72199	-96.160092	Freestone	TCEQ Well Records
AT-48P	G0810001B	31.72822	-96.151913	Freestone	TCEQ Well Records
AT-49P	G0810002B	31.63268	-96.261856	Freestone	TCEQ Well Records
AT-50P	G0810002C	31.62006	-96.281919	Freestone	TCEQ Well Records
AT-51P	G0810002D	31.62777	-96.250494	Freestone	TCEQ Well Records
AT-52P	G0810005L	31.66208	-96.156806	Freestone	TCEQ Well Records
AT-53P	G0810010C	31.7195	-96.110928	Freestone	TCEQ Well Records
AT-54P	G0810013G	31.66938	-95.941631	Freestone	TCEQ Well Records
AT-55P	G0810016A	31.80071	-96.234939	Freestone	TCEQ Well Records
AT-56P	G0810029B	31.72994	-96.207511	Freestone	TCEQ Well Records
AT-57P	G0810034C	31.94158	-96.146413	Freestone	TCEQ Well Records
AT-58P	G0810037A	31.67537	-96.194486	Freestone	TCEQ Well Records
AT-59P	G0810037B	31.66825	-96.194443	Freestone	TCEQ Well Records
AT-60P	G0810039A	31.8898	-96.109886	Freestone	TCEQ Well Records
AT-61P	G0810041A	31.60079	-95.831333	Freestone	TCEQ Well Records
AT-62P	G0890002D	29.26865	-97.767159	Gonzales	TCEQ Well Records
AT-63P	G0890002E	29.27371	-97.757658	Gonzales	TCEQ Well Records
AT-64P	G0890002F	29.27371	-97.757658	Gonzales	TCEQ Well Records
AT-65P	G0890003E	29.69434	-97.301247	Gonzales	TCEQ Well Records
AT-13P	G0110013P	30.36819	-97.114858	Lee	TCEQ Well Records
AT-66P	G1440001G	30.18918	-96.938842	Lee	TCEQ Well Records

Test ID	Well ID	Decimal Latitude	Decimal Longitude	County	Well and Test Data Source
AT-67P	G1440005A	30.13543	-97.004799	Lee	TCEQ Well Records
AT-68P	G1440005B	30.24015	-97.039625	Lee	TCEQ Well Records
AT-69P	G1440005C	30.37324	-96.871094	Lee	TCEQ Well Records
AT-71P	G1440005P	30.15415	-96.920151	Lee	TCEQ Well Records
AT-72C	Sandow Mine Well H(9)-2	30.45417	-97.125875	Lee	RW Harden & Associates (2001)
AT-73C	Forestar Well 5	30.45656	-96.970519	Lee	Thornhill Group (2014b)
AT-74C	End Op Well TW-3	30.35448	-97.117803	Lee	Thornhill Group (2009)
AT-75C	Forestar Well 7	30.46895	-96.987747	Lee	Thornhill Group (2014c)
AT-76C	Forestar Well 8	30.42558	-96.990111	Lee	Thornhill Group (2014d)
AT-77C	Sustainable Water Resources	30.45613	-96.970431	Lee	Thornhill Group (2014e)
AT-78P	G1450001D	31.46827	-96.07061	Leon	TCEQ Well Records
AT-79P	G1450002D	31.25347	-95.979423	Leon	TCEQ Well Records
AT-80P	G1450002E	31.26109	-95.991532	Leon	TCEQ Well Records
AT-81P	G1450003D	31.57973	-95.863592	Leon	TCEQ Well Records
AT-82P	G1450006W	31.06927	-96.204544	Leon	TCEQ Well Records
AT-83P	G1450007B	31.36145	-96.146181	Leon	TCEQ Well Records
AT-84P	G1450007D	31.36321	-96.145237	Leon	TCEQ Well Records
AT-85P	G1450010B	31.53806	-95.796389	Leon	TCEQ Well Records
AT-86P	G1450015D	31.44545	-96.043294	Leon	TCEQ Well Records
AT-87P	G1450024B	31.40988	-96.237498	Leon	TCEQ Well Records
AT-88P	G1570001C	30.95988	-95.917947	Madison	TCEQ Well Records
AT-89P	G1570003B	31.02652	-95.748547	Madison	TCEQ Well Records
AT-90P	G1570004C	30.92056	-96.108833	Madison	TCEQ Well Records
AT-100C	Shell Milam Mine Well CF-83	30.75629	-96.876059	Milam	RW Harden & Associates (1980)
AT-101C	Shell Milam Mine Well B-35	30.64328	-96.942688	Milam	RW Harden & Associates (1982)
AT-91P	G1660002G	30.63481	-96.991083	Milam	TCEQ Well Records
AT-92P	G1660002I	30.66643	-96.995957	Milam	TCEQ Well Records
AT-93P	G1660002J	30.6636	-96.995856	Milam	TCEQ Well Records
AT-95P	G1660009E	30.64825	-96.854706	Milam	TCEQ Well Records
AT-96P	G1660012E	30.55944	-97.071114	Milam	TCEQ Well Records
AT-97P	G1660014A	30.82729	-96.912202	Milam	TCEQ Well Records
AT-98P	G1660015A	30.69131	-96.899704	Milam	TCEQ Well Records
AT-99P	G1660015H	30.67154	-97.003972	Milam	TCEQ Well Records
AT-102P	G1980001C	31.16324	-96.665914	Robertson	TCEQ Well Records
AT-103P	G1980001D	31.15884	-96.652911	Robertson	TCEQ Well Records
AT-104P	G1980001E	31.16547	-96.655222	Robertson	TCEQ Well Records
AT-105P	G1980002C	30.975	-96.673439	Robertson	TCEQ Well Records

Test ID	Well ID	Decimal Latitude	Decimal Longitude	County	Well and Test Data Source
AT-106P	G1980003A	31.02818	-96.487642	Robertson	TCEQ Well Records
AT-107P	G1980003C	31.02993	-96.491278	Robertson	TCEQ Well Records
AT-108P	G1980003D	31.02879	-96.474809	Robertson	TCEQ Well Records
AT-109P	G1980022B	31.08776	-96.697267	Robertson	TCEQ Well Records
AT-110C	Harden11-G-PTW-S	31.0899	-96.665016	Robertson	RW Harden & Associates (1987)
AT-111C	Texas New Mexico Power Co Production Well 1	31.04071	-96.685185	Robertson	RW Harden & Associates (1991)
AT-112C	Texas New Mexico Power Co Production Well 2	31.0479	-96.675284	Robertson	RW Harden & Associates (1991)
AT-113C	Texas New Mexico Power Co Production Well 3	31.05137	-96.666594	Robertson	RW Harden & Associates (1991)

Table 11-2. Completion data for aquifer pumping test wells.

Test ID	Well TD (ft)	Depth to Top of Uppermost Screen (ft)	Depth to Bottom of Lowermost Screen (ft)	Length from Top of Uppermost Screen to Bottom of Lowermost Screen (ft)	Length of Screen Open to the Aquifer (ft)	Primary Model Layer
AT-01P	650	288	630	342	240	8
AT-02P	55	39	45	6	6	8
AT-03P	598	102	578	476	220	7
AT-04P	461	315	450	135	135	8
AT-05P	782	400	760	360	242	5
AT-06P	602	435	592	157	96	6
AT-09P	670	420	650	230	150	8
AT-10P	615	441	600	159	118	6
AT-11P	725	627	700	73	73	6
AT-12P	716	626	711	85	85	8
AT-14P	660	490	650	160	160	6
AT-15P	718	611	708	97	97	6
AT-16P	610	500	600	100	100	7
AT-17P	1020	940	1004	64	64	8
AT-18P	524	455	510	55	55	7
AT-20C	461	315	450	135	131	7
AT-21C	1393	810	1266	456	334	6
AT-22C	1346	754	1270	516	394	6
AT-70P	1190	836	1168	332	298	6
AT-23P	2867	2402	2852	450	375	7
AT-24P	2770	2328	2750	422	375	6
AT-25P	2884	2364	2864	500	466	1
AT-26P	1360	1120	1340	220	168	1
AT-27P	540	446	520	74	74	1
AT-28P	760	510	750	240	130	1
AT-29P	1008	805	1008	203	173	1
AT-30P	780	530	754	224	160	1
AT-31P	780	499	767	268	170	1
AT-32P	800	585	770	185	115	6
AT-33P	505	485	505	20	20	3
AT-34P	3363	2168	2505	337	337	1
AT-35C	3018	2491	3012	521	436	8
AT-36C	2973	2530	2960	430	430	7
AT-37C	2975	2520	2910	390	390	7

Test ID	Well TD (ft)	Depth to Top of Uppermost Screen (ft)	Depth to Bottom of Lowermost Screen (ft)	Length from Top of Uppermost Screen to Bottom of Lowermost Screen (ft)	Length of Screen Open to the Aquifer (ft)	Primary Model Layer
AT-38C	3010	2742	2990	248	203	7
AT-19C	2420	2000	2400	400		7
AT-39P	814	740	800	60	60	7
AT-40P	1656	1512	1570	58	58	8
AT-41P	2241	1830	2241	411	411	6
AT-42C	2688	2290	2668	378	378	6
AT-43C	2240	1930	2260	330	278	6
AT-94P	1680	1490	1620	130	100	7
AT-07P	1060	710	1050	340	245	8
AT-08P	550	378	538	160	160	7
AT-44P	302	180	290	110	110	6
AT-45P	365	135	357	222	110	5
AT-46P	325	190	430	240	145	5
AT-47P	726	495	716	221	136	8
AT-48P	764	420	740	320	173	8
AT-49P	680	451	670	219	130	8
AT-50P	650	415	625	210	107	8
AT-51P	740	390	720	330	196	7
AT-52P	715	650	710	60	60	6
AT-53P	560	515	555	40	40	8
AT-54P	685	530	684	154	154	8
AT-55P	290	204	285	81	60	8
AT-56P	535	490	530	40	40	8
AT-57P	340	220	340	120	120	8
AT-58P	736	540	726	186	98	8
AT-59P	600	506	572	66	48	5
AT-60P	290	245	285	40	40	3
AT-61P	363	274	354	80	80	5
AT-62P	1580	1368	1560	192	192	5
AT-63P	1850	1380	1840	460	440	1
AT-64P	1830	1340	1760	420	420	5
AT-65P	866	426	856	430	162	3
AT-13P	500	419	484	65	65	6
AT-66P	1996	1745	1996	251	251	5
AT-67P	1442	1060	1190	130	100	5

Test ID	Well TD (ft)	Depth to Top of Uppermost Screen (ft)	Depth to Bottom of Lowermost Screen (ft)	Length from Top of Uppermost Screen to Bottom of Lowermost Screen (ft)	Length of Screen Open to the Aquifer (ft)	Primary Model Layer
AT-68P	897	855	897	42	42	5
AT-69P	640	544	640	96	96	3
AT-71P	2226	2061	2205	144	144	6
AT-72C	448	238	438	200	200	7
AT-73C	2125	1515	2105	590	402	7
AT-74C	1620	1060	1590	530	300	7
AT-75C	2236	1676	2216	540	374	7
AT-76C	2304	1660	2284	624	ng	7
AT-77C	2145	1515	2105	590	402	7
AT-78P	970	851	953	102	102	6
AT-79P	1033	932	1022	90	90	6
AT-80P	1274	1121	1253	132	90	3
AT-81P	810	765	807	42	42	6
AT-82P	500	420	500	80	80	6
AT-83P	700	545	660	115	70	5
AT-84P	1273	1110	1265	155	104	6
AT-85P	410	345	405	60	60	7
AT-86P	710	650	700	50	50	1
AT-87P	780	620	760	140	140	1
AT-88P	1225	1060	1210	150	140	1
AT-89P	840	750	830	80	80	7
AT-90P	665	612	660	48	39	7
AT-100C	530	322	515	193	193	7
AT-101C	388	280	386	106	106	7
AT-91P	455	241	341	100	100	8
AT-92P	356	226	346	120	120	6
AT-93P	380	238	370	132	132	7
AT-95P	1715	1462	1715	253	253	8
AT-96P	374	258	364	106	106	6
AT-97P	400	385	486	101	101	8
AT-98P	721	540	720	180	120	8
AT-99P	485	190	483	293	173	8
AT-102P	495	399	485	86	71	8
AT-103P	527	345	517	172	112	7
AT-104P	490	424	486	62	62	7

Test ID	Well TD (ft)	Depth to Top of Uppermost Screen (ft)	Depth to Bottom of Lowermost Screen (ft)	Length from Top of Uppermost Screen to Bottom of Lowermost Screen (ft)	Length of Screen Open to the Aquifer (ft)	Primary Model Layer
AT-105P	738	633	738	105	105	7
AT-106P	1217	1058	1212	154	136	7
AT-107P	1234	1093	1214	121	107	8
AT-108P	1440	1142	1420	278	278	7
AT-109P	472	436	466	30	30	6
AT-110C	272	120	264	144	130	8
AT-111C	999	614	984	370	260	8
AT-112C	1077	580	1062	482	396	7
AT-113C	1076	582	1061	479	335	7

12 Appendix B

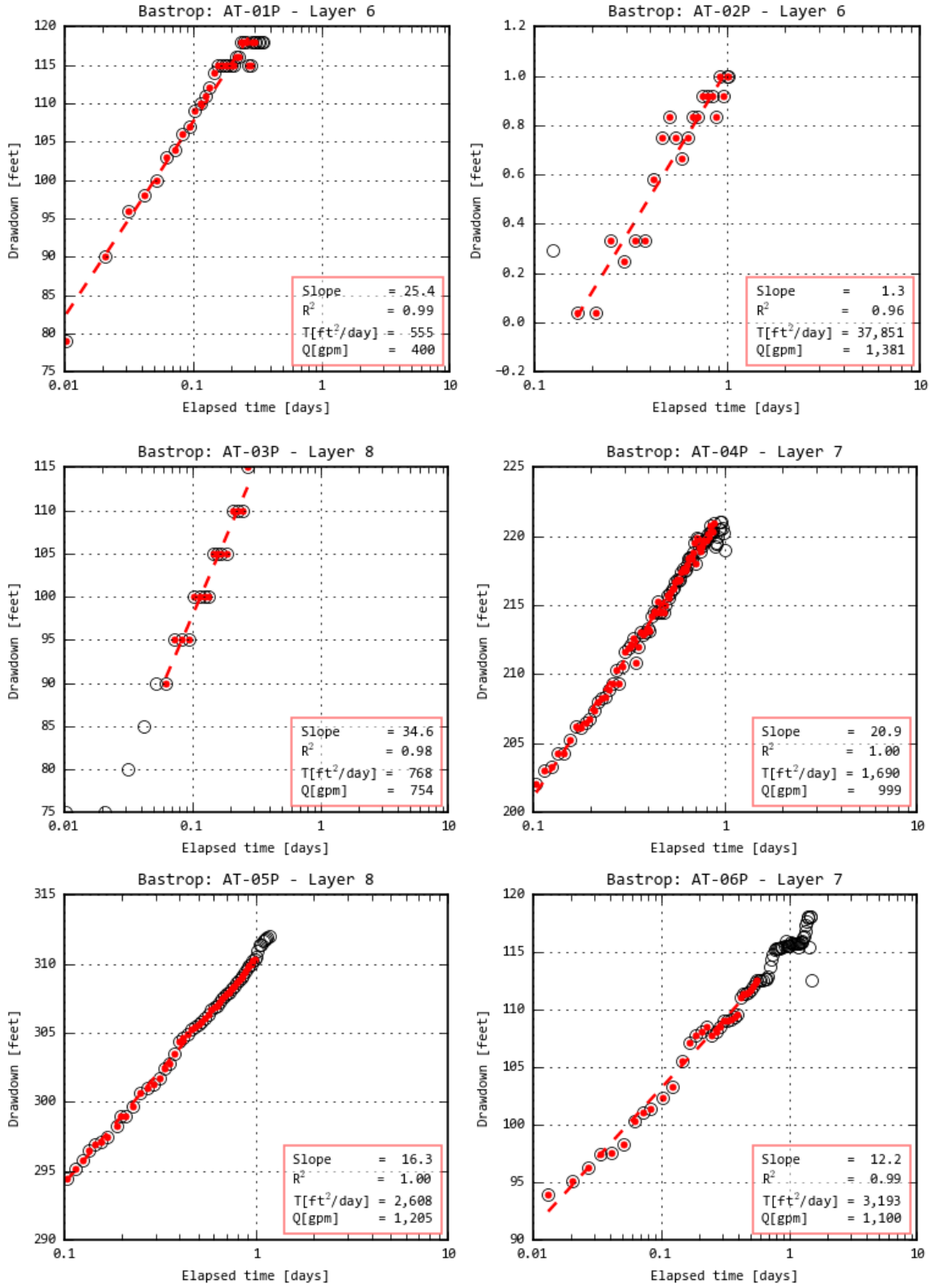

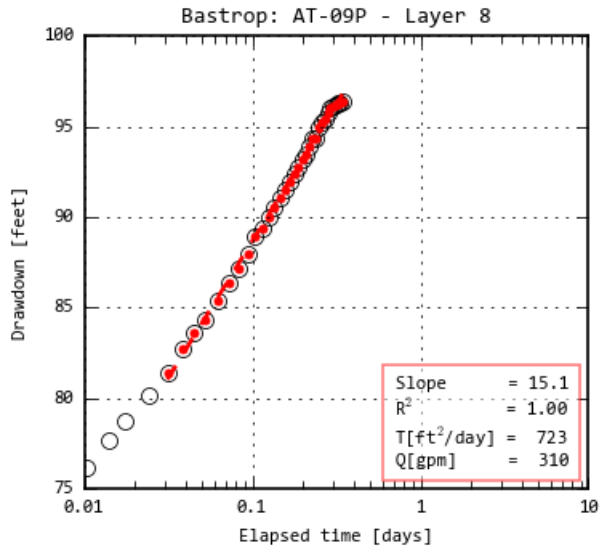
Bastrop: AT-09P - Layer 8
Drawdown [feet]
Elapsed time [days]
Slope = 15.1
R² = 1.00
T[ft²/day] = 723
Q[gpm] = 310

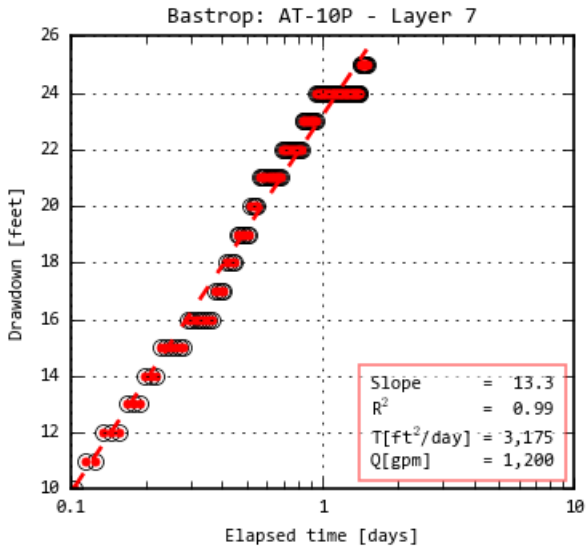
Bastrop: AT-10P - Layer 7
Drawdown [feet]
Elapsed time [days]
Slope = 13.3
R² = 0.99
T[ft²/day] = 3,175
Q[gpm] = 1,200

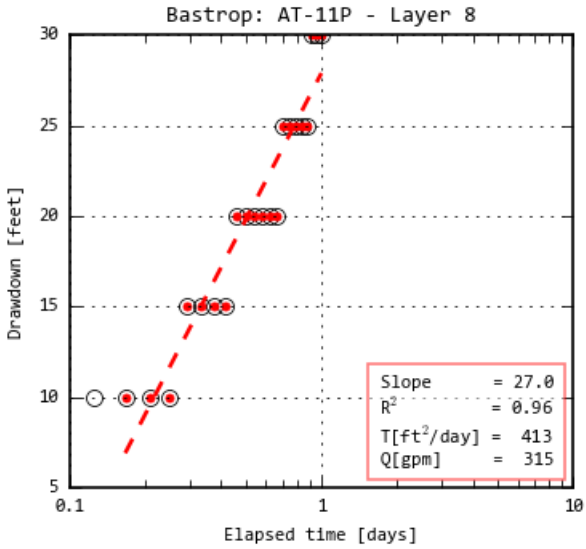
Bastrop: AT-11P - Layer 8
Drawdown [feet]
Elapsed time [days]
Slope = 27.0
R² = 0.96
T[ft²/day] = 413
Q[gpm] = 315

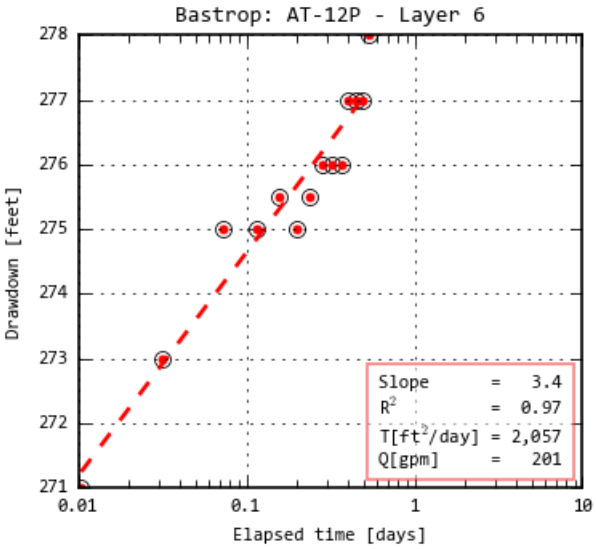
Bastrop: AT-12P - Layer 6
Drawdown [feet]
Elapsed time [days]
Slope = 3.4
R² = 0.97
T[ft²/day] = 2,057
Q[gpm] = 201

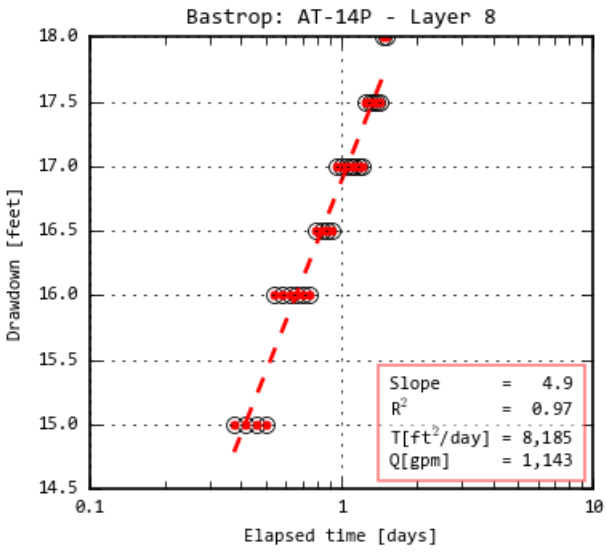
Bastrop: AT-14P - Layer 8
Drawdown [feet]
Elapsed time [days]
Slope = 4.9
R² = 0.97
T[ft²/day] = 8,185
Q[gpm] = 1,143

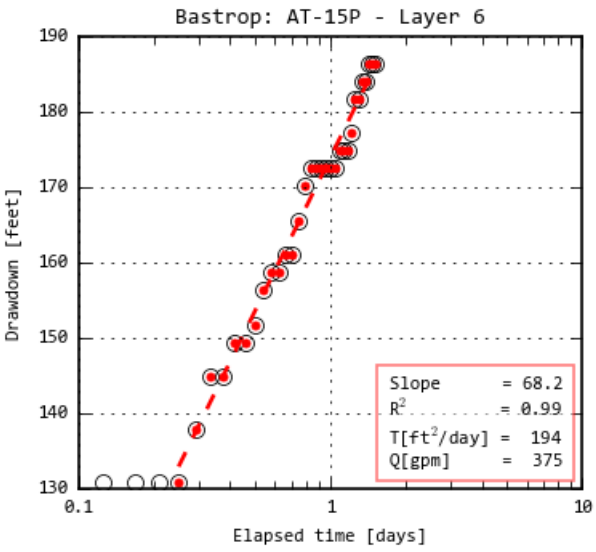
Bastrop: AT-15P - Layer 6
Drawdown [feet]
Elapsed time [days]
Slope = 68.2
R² = 0.99
T[ft²/day] = 194
Q[gpm] = 375

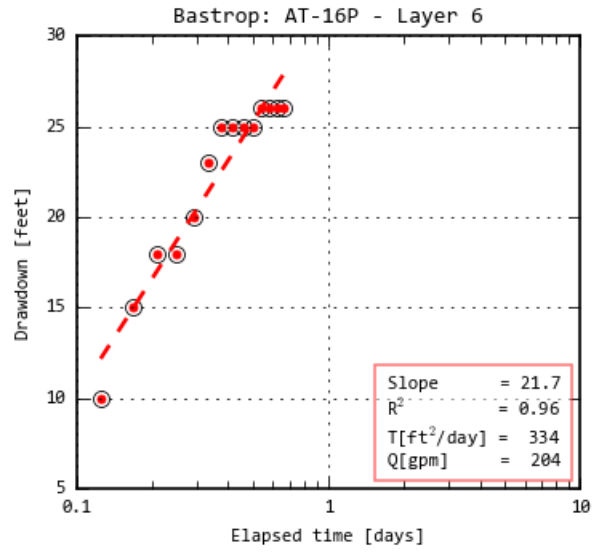
Bastrop: AT-16P - Layer 6
Drawdown [feet]
Elapsed time [days]
Slope = 21.7
R² = 0.96
T[ft²/day] = 334
Q[gpm] = 204

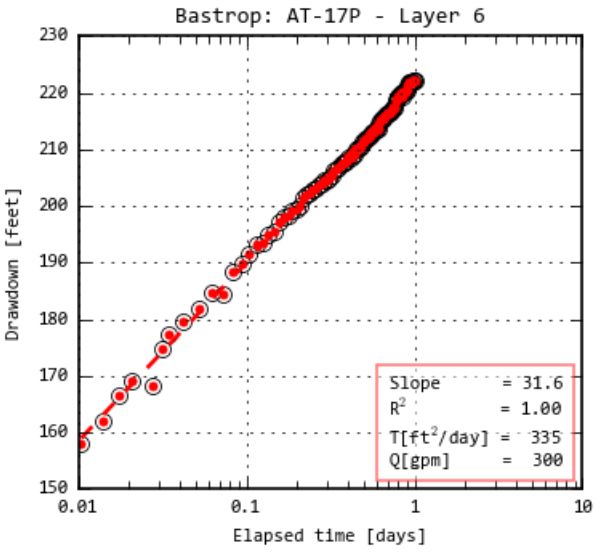
Bastrop: AT-17P - Layer 6
Drawdown [feet]
Elapsed time [days]
Slope = 31.6
R² = 1.00
T[ft²/day] = 335
Q[gpm] = 300

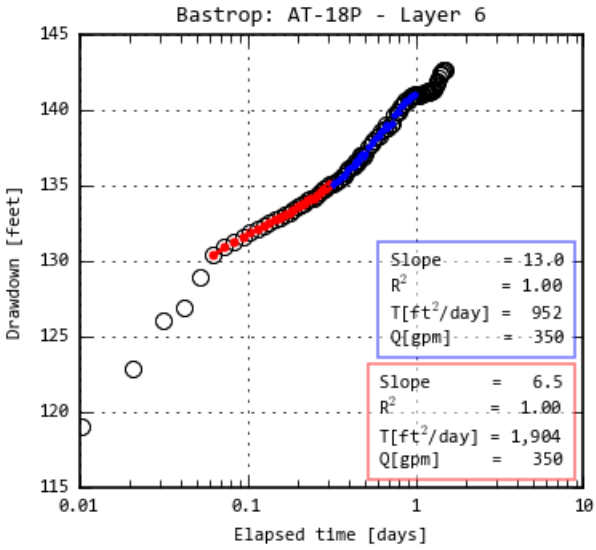
Bastrop: AT-18P - Layer 6
Drawdown [feet]
Elapsed time [days]
Slope = 13.0
R² = 1.00
T[ft²/day] = 952
Q[gpm] = 350
Slope = 6.5
R² = 1.00
T[ft²/day] = 1,904
Q[gpm] = 350

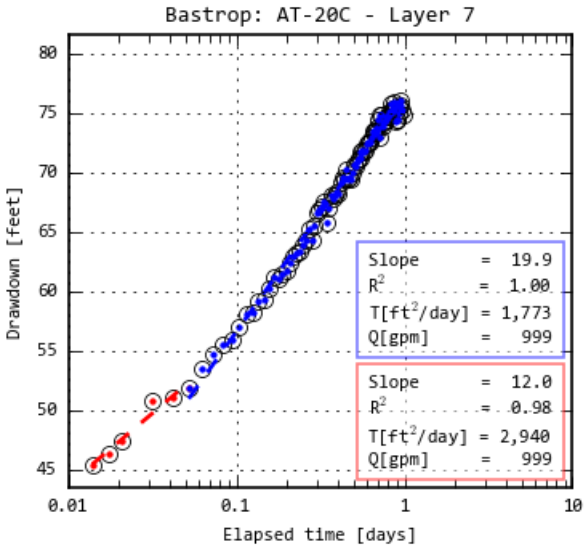
Bastrop: AT-20C - Layer 7
Drawdown [feet]
Elapsed time [days]
Slope = 19.9
R² = 1.00
T[ft²/day] = 1,773
Q[gpm] = 999
Slope = 12.0
R² = 0.98
T[ft²/day] = 2,940
Q[gpm] = 999

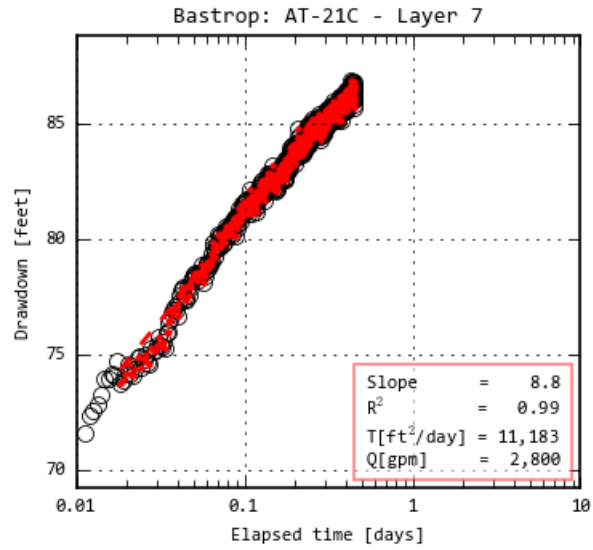
Bastrop: AT-21C - Layer 7
Drawdown [feet]
Elapsed time [days]
Slope = 8.8
R² = 0.99
T[ft²/day] = 11,183
Q[gpm] = 2,800

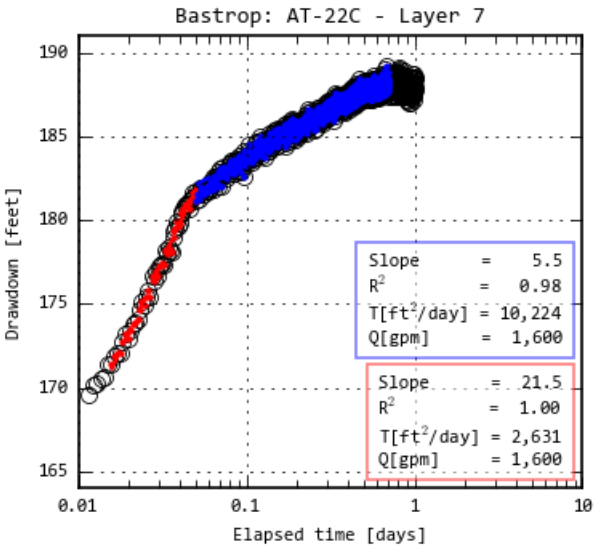
Bastrop: AT-22C - Layer 7
Drawdown [feet]
Elapsed time [days]
Slope = 5.5
R² = 0.98
T[ft²/day] = 10,224
Q[gpm] = 1,600
Slope = 21.5
R² = 1.00
T[ft²/day] = 2,631
Q[gpm] = 1,600

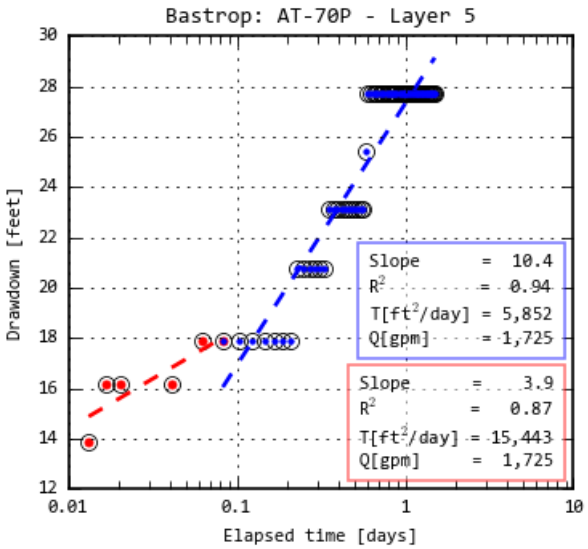
Bastrop: AT-70P - Layer 5
Drawdown [feet]
Elapsed time [days]
30
28
26
24
22
20
18
16
14
12
0.01
0.1
1
10
Slope = 10.4
R² = 0.94
T[ft²/day] = 5,852
Q[gpm] = 1,725
Slope = 3.9
R² = 0.87
T[ft²/day] = 15,443
Q[gpm] = 1,725

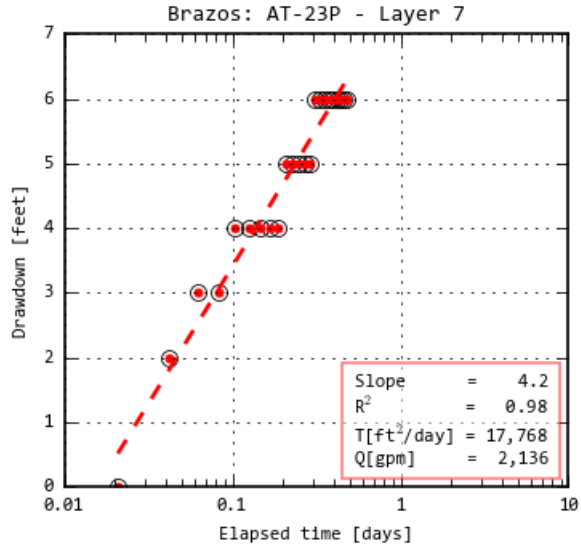
Brazos: AT-23P - Layer 7
Drawdown [feet]
Elapsed time [days]
Slope = 4.2
R² = 0.98
T[ft²/day] = 17,768
Q[gpm] = 2,136

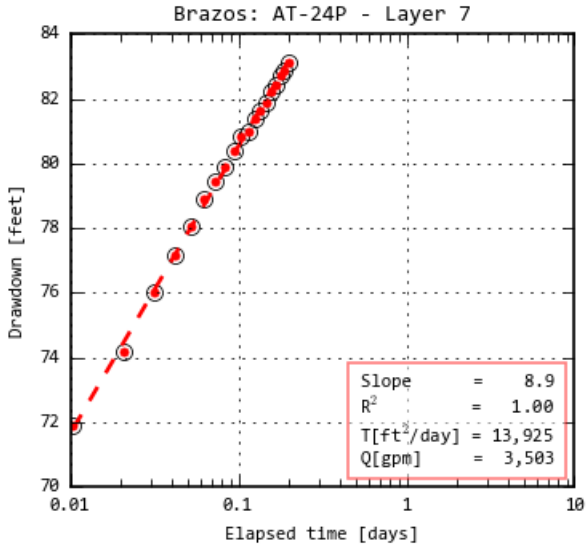
Brazos: AT-24P - Layer 7
Drawdown [feet]
Elapsed time [days]
Slope = 8.9
R² = 1.00
T[ft²/day] = 13,925
Q[gpm] = 3,503

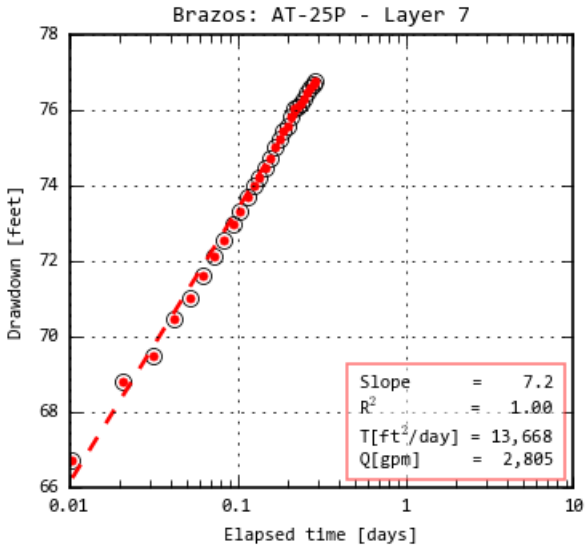
Brazos: AT-25P - Layer 7
Drawdown [feet]
Elapsed time [days]
Slope = 7.2
R² = 1.00
T[ft²/day] = 13,668
Q[gpm] = 2,805

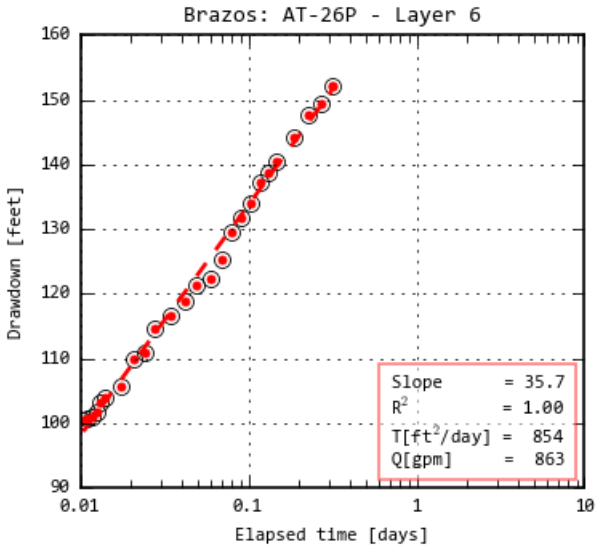
Brazos: AT-26P - Layer 6
Drawdown [feet]
Elapsed time [days]
Slope = 35.7
R² = 1.00
T[ft²/day] = 854
Q[gpm] = 863

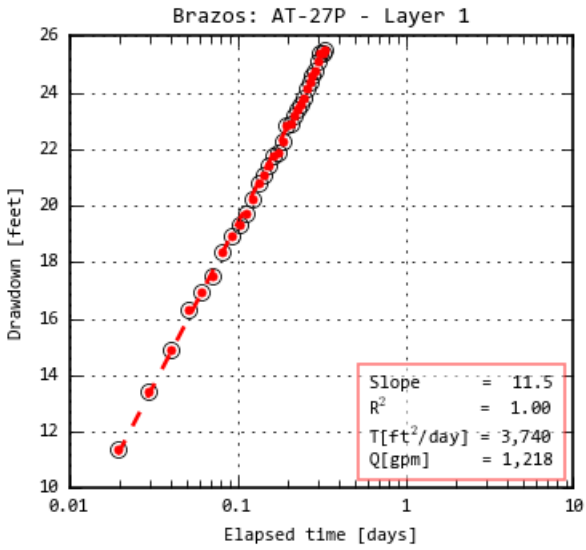
Brazos: AT-27P - Layer 1
Drawdown [feet]
Elapsed time [days]
Slope = 11.5
R² = 1.00
T[ft²/day] = 3,740
Q[gpm] = 1,218

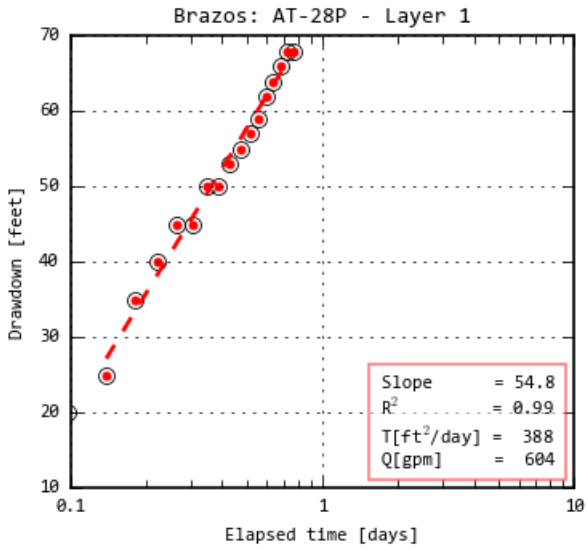
Brazos: AT-28P - Layer 1
Drawdown [feet]
Elapsed time [days]
Slope = 54.8
R² = 0.99
T[ft²/day] = 388
Q[gpm] = 604

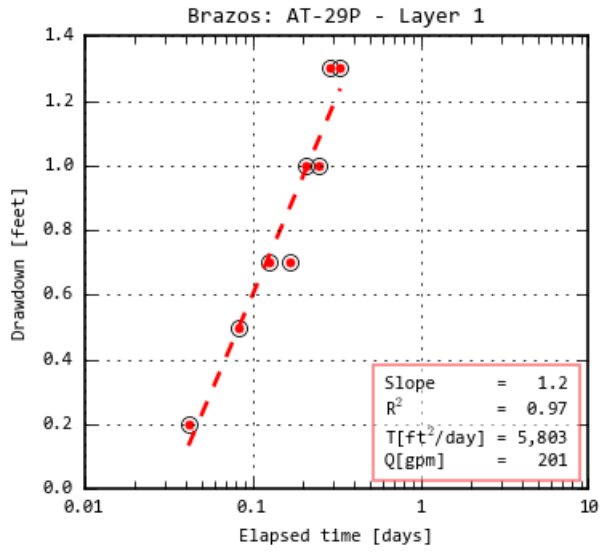
Brazos: AT-29P - Layer 1
Drawdown [feet]
Elapsed time [days]
Slope = 1.2
R² = 0.97
T[ft²/day] = 5,803
Q[gpm] = 201

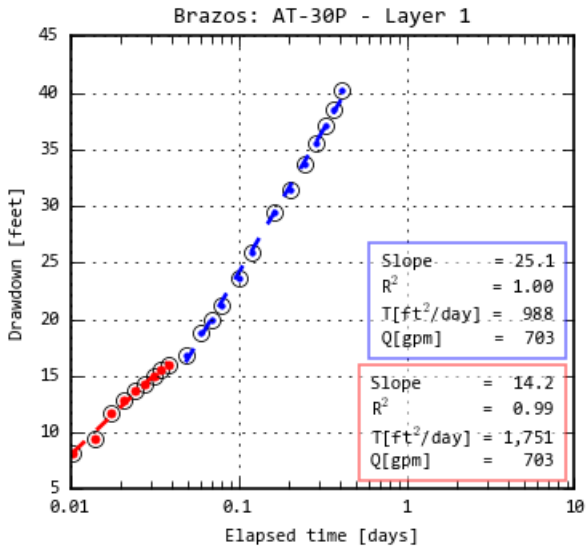
Brazos: AT-30P - Layer 1
Drawdown [feet]
Elapsed time [days]
Slope = 25.1
R² = 1.00
T[ft²/day] = 988
Q[gpm] = 703
Slope = 14.2
R² = 0.99
T[ft²/day] = 1,751
Q[gpm] = 703

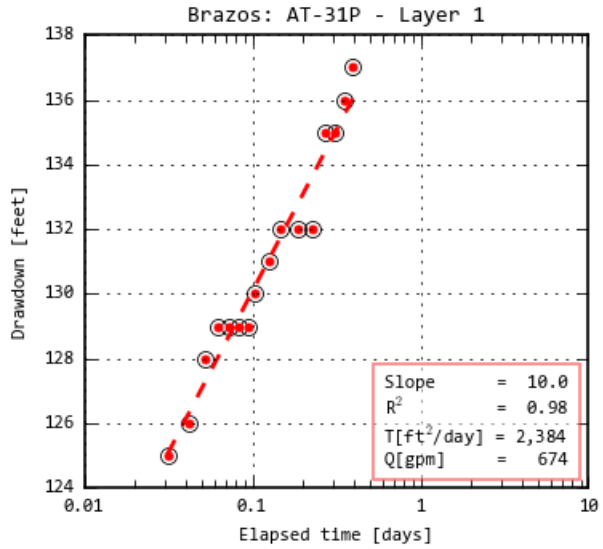
Brazos: AT-31P - Layer 1
Drawdown [feet]
Elapsed time [days]
Slope = 10.0
R² = 0.98
T[ft²/day] = 2,384
Q[gpm] = 674

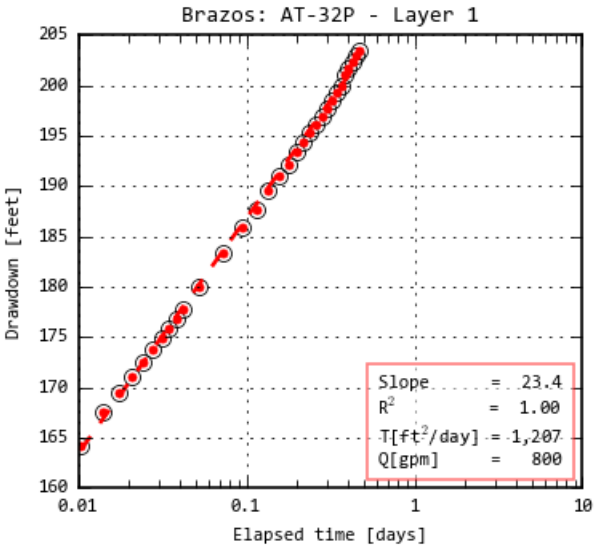
Brazos: AT-32P - Layer 1
Drawdown [feet]
Elapsed time [days]
Slope = 23.4
R² = 1.00
T[ft²/day] = 1,207
Q[gpm] = 800

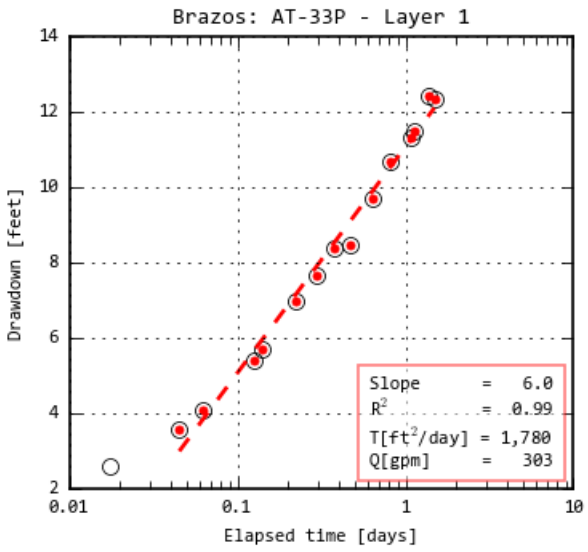
Brazos: AT-33P - Layer 1
Drawdown [feet]
Elapsed time [days]
Slope = 6.0
R² = 0.99
T[ft²/day] = 1,780
Q[gpm] = 303

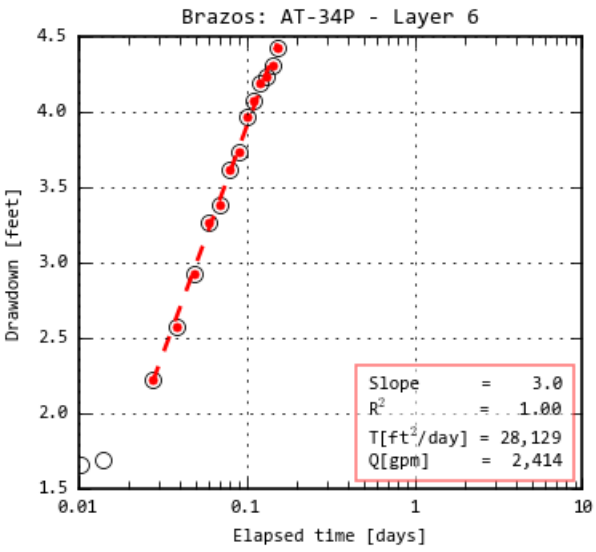
Brazos: AT-34P - Layer 6
Drawdown [feet]
Elapsed time [days]
Slope = 3.0
R² = 1.00
T[ft²/day] = 28,129
Q[gpm] = 2,414

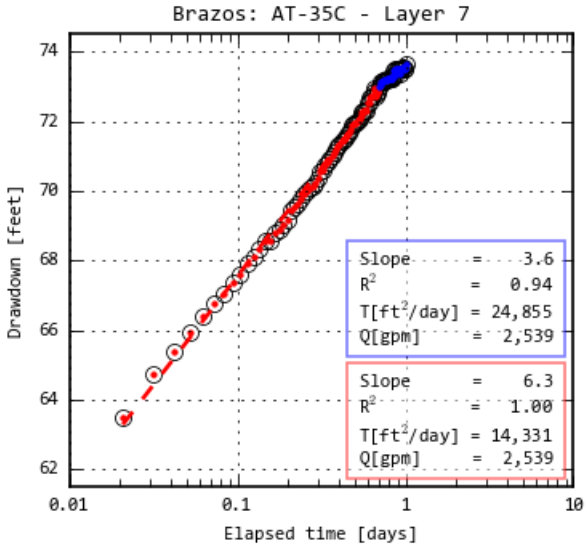
Brazos: AT-35C - Layer 7
Drawdown [feet]
Elapsed time [days]
Slope = 3.6
R² = 0.94
T[ft²/day] = 24,855
Q[gpm] = 2,539
Slope = 6.3
R² = 1.00
T[ft²/day] = 14,331
Q[gpm] = 2,539

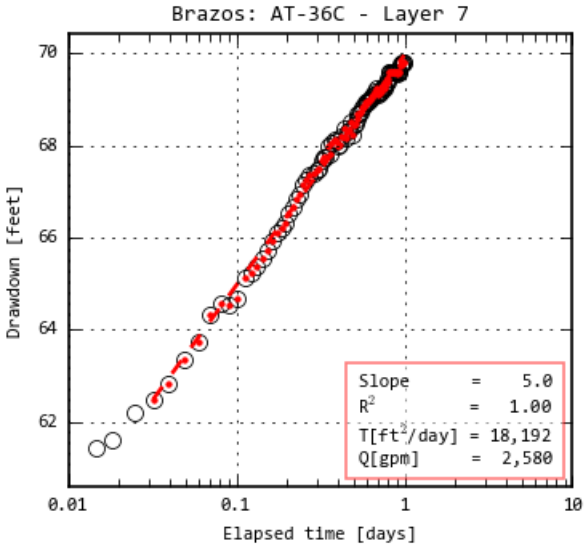
Brazos: AT-36C - Layer 7
Drawdown [feet]
Elapsed time [days]
Slope = 5.0
R² = 1.00
T[ft²/day] = 18,192
Q[gpm] = 2,580

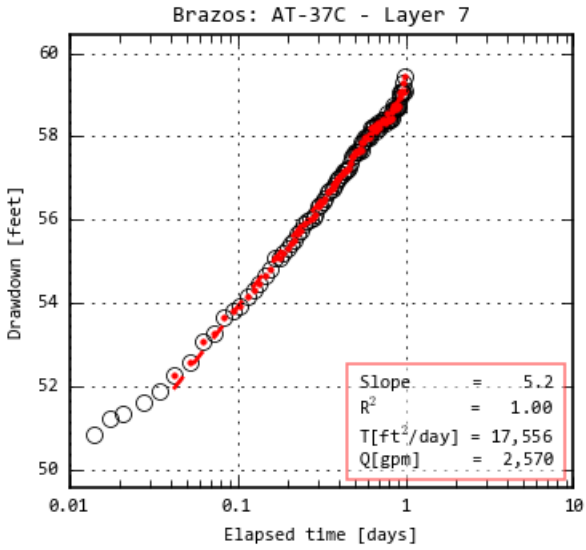
Brazos: AT-37C - Layer 7
Drawdown [feet]
Elapsed time [days]
Slope = 5.2
R² = 1.00
T[ft²/day] = 17,556
Q[gpm] = 2,570

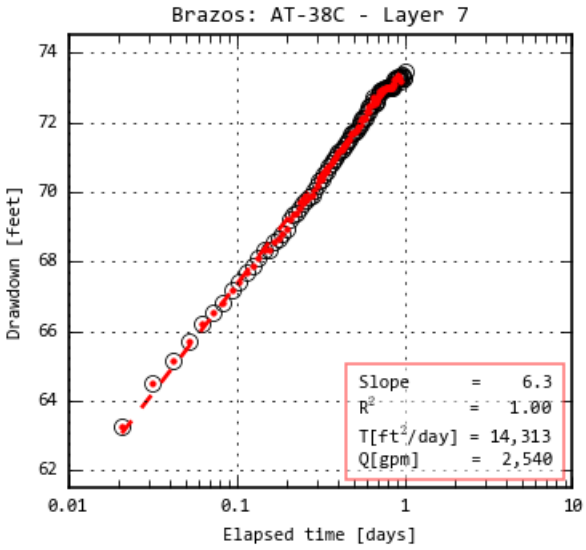
Brazos: AT-38C - Layer 7
Drawdown [feet]
Elapsed time [days]
Slope = 6.3
R² = 1.00
T[ft²/day] = 14,313
Q[gpm] = 2,540

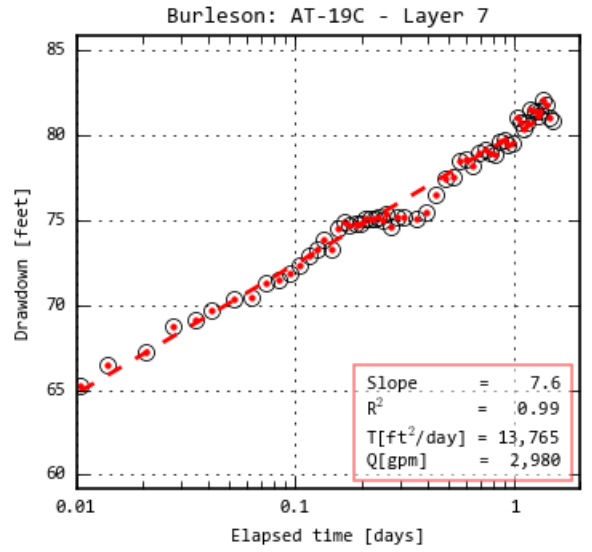
Burleson: AT-19C - Layer 7
Drawdown [feet]
Elapsed time [days]
Slope = 7.6
R² = 0.99
T[ft²/day] = 13,765
Q[gpm] = 2,980

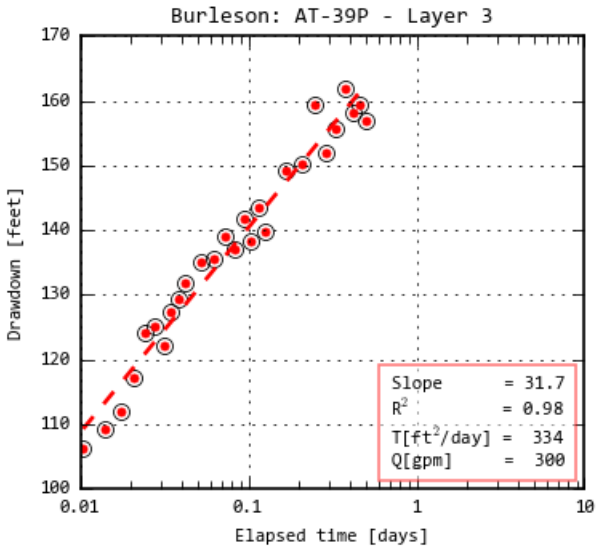
Burleson: AT-39P - Layer 3
Drawdown [feet]
Elapsed time [days]
Slope = 31.7
R² = 0.98
T[ft²/day] = 334
Q[gpm] = 300

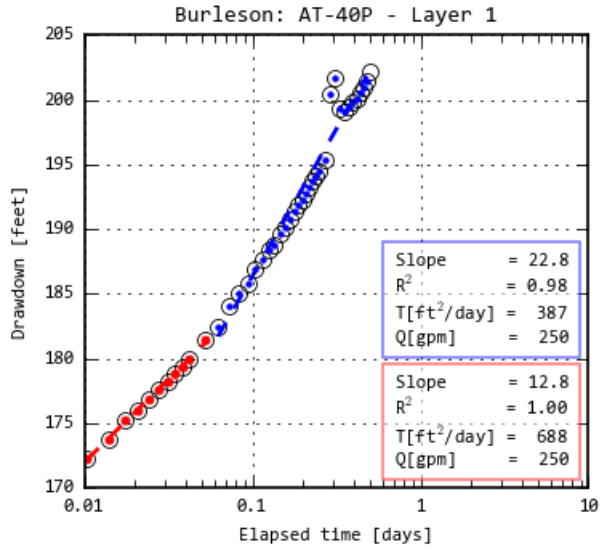
Burleson: AT-40P - Layer 1
Drawdown [feet]
Elapsed time [days]
Slope = 22.8
R² = 0.98
T[ft²/day] = 387
Q[gpm] = 250
Slope = 12.8
R² = 1.00
T[ft²/day] = 688
Q[gpm] = 250

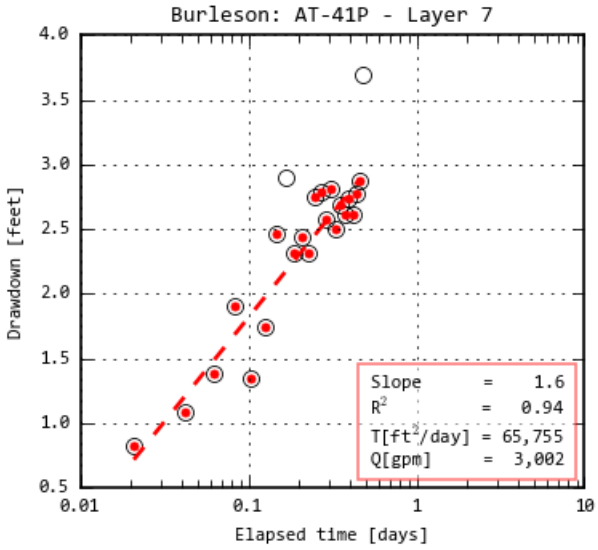
Burleson: AT-41P - Layer 7
Drawdown [feet]
Elapsed time [days]
Slope = 1.6
R² = 0.94
T[ft²/day] = 65,755
Q[gpm] = 3,002

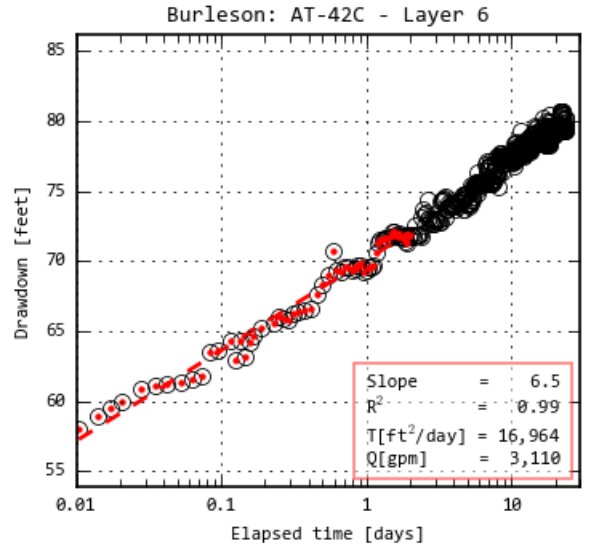
Burleson: AT-42C - Layer 6
Drawdown [feet]
Elapsed time [days]
Slope = 6.5
R² = 0.99
T[ft²/day] = 16,964
Q[gpm] = 3,110

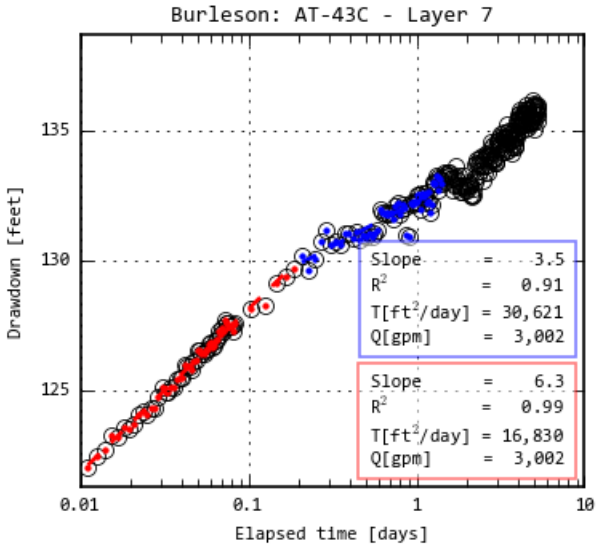
Burleson: AT-43C - Layer 7
Drawdown [feet]
Elapsed time [days]
Slope = 3.5
R² = 0.91
T[ft²/day] = 30,621
Q[gpm] = 3,002
Slope = 6.3
R² = 0.99
T[ft²/day] = 16,830
Q[gpm] = 3,002

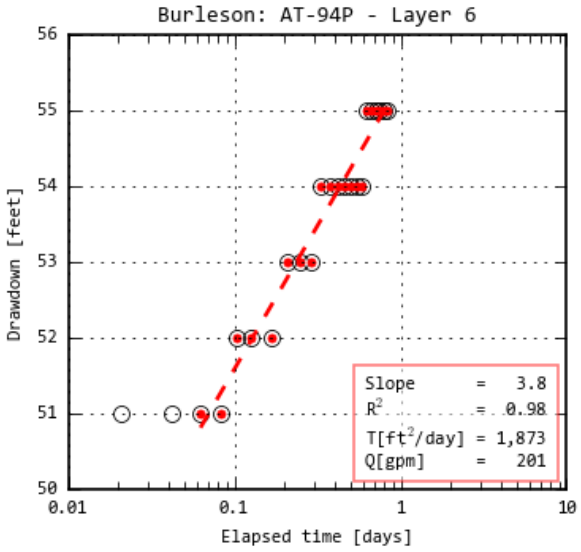
Burleson: AT-94P - Layer 6
Drawdown [feet]
Elapsed time [days]
56
55
54
53
52
51
50
0.01
0.1
1
10
Slope = 3.8
R2 = 0.98
T[ft2/day] = 1,873
Q[gpm] = 201

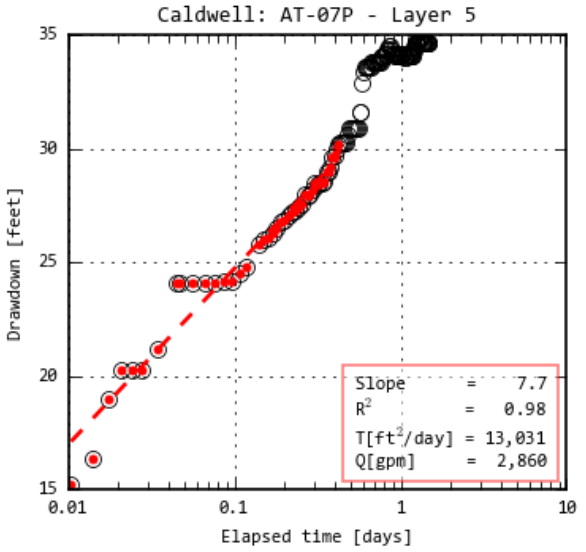
Caldwell: AT-07P - Layer 5
Drawdown [feet]
Elapsed time [days]
Slope = 7.7
R² = 0.98
T[ft²/day] = 13,031
Q[gpm] = 2,860

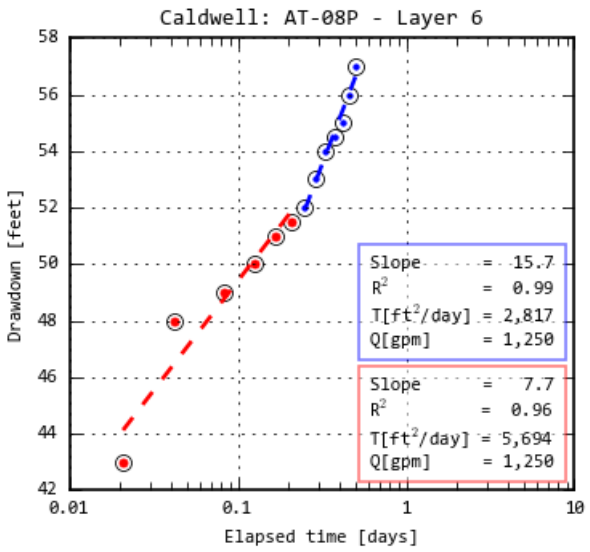
Caldwell: AT-08P - Layer 6
Drawdown [feet]
Elapsed time [days]
Slope = 15.7
R² = 0.99
T[ft²/day] = 2,817
Q[gpm] = 1,250
Slope = 7.7
R² = 0.96
T[ft²/day] = 5,694
Q[gpm] = 1,250

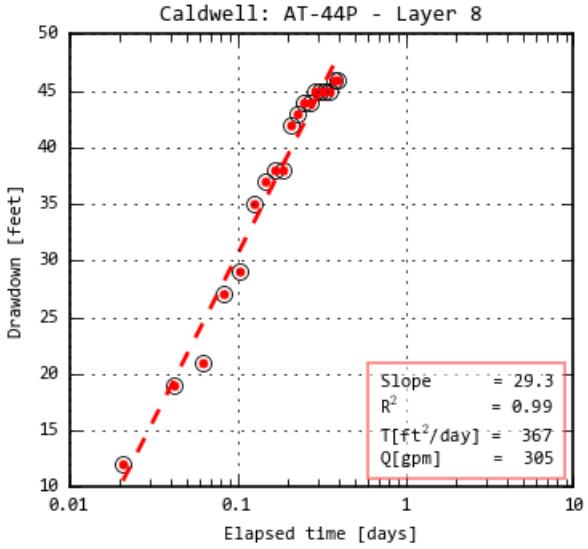
Caldwell: AT-44P - Layer 8
Drawdown [feet]
Elapsed time [days]
Slope = 29.3
R² = 0.99
T[ft²/day] = 367
Q[gpm] = 305

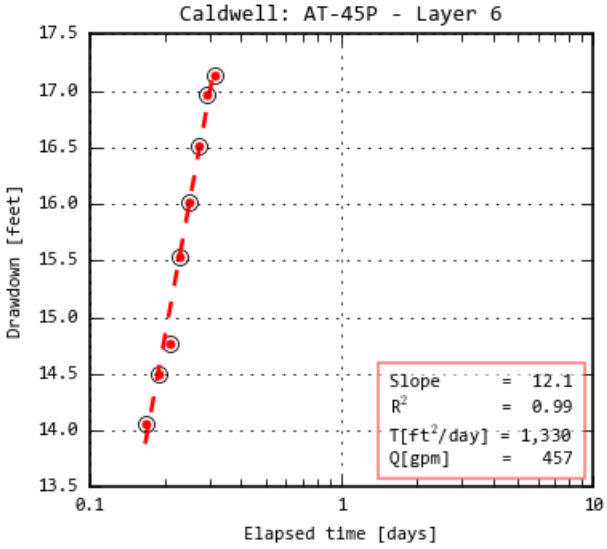
Caldwell: AT-45P - Layer 6
Drawdown [feet]
Elapsed time [days]
Slope = 12.1
R² = 0.99
T[ft²/day] = 1,330
Q[gpm] = 457

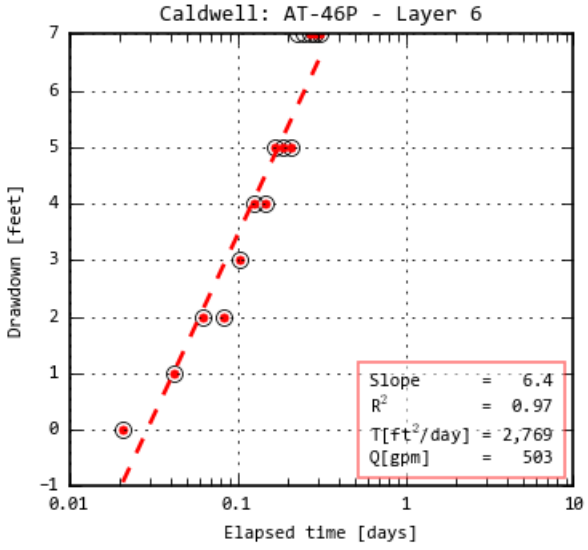
Caldwell: AT-46P - Layer 6
Drawdown [feet]
Elapsed time [days]
Slope = 6.4
R² = 0.97
T[ft²/day] = 2,769
Q[gpm] = 503

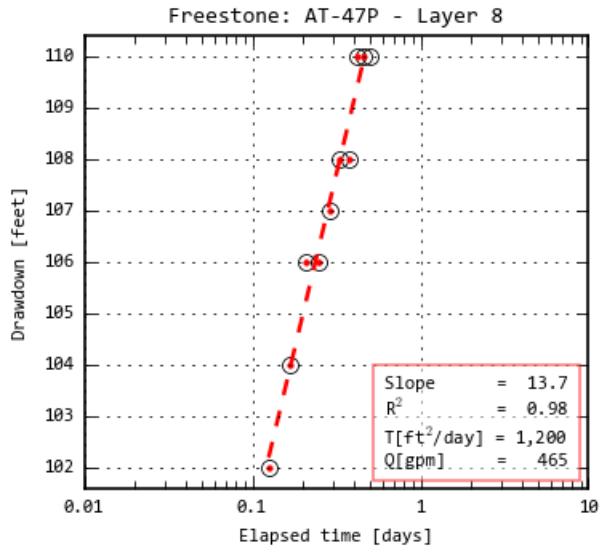
Freestone: AT-47P - Layer 8
Drawdown [feet]
Elapsed time [days]
Slope = 13.7
R² = 0.98
T[ft²/day] = 1,200
Q[gpm] = 465

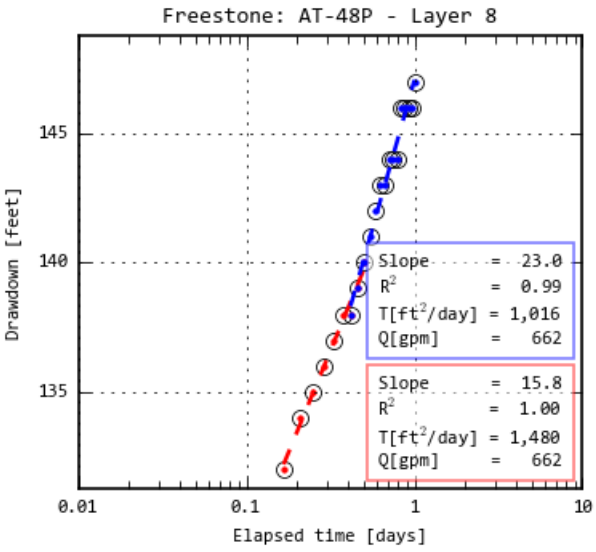
Freestone: AT-48P - Layer 8
Drawdown [feet]
Elapsed time [days]
Slope = 23.0
R² = 0.99
T[ft²/day] = 1,016
Q[gpm] = 662
Slope = 15.8
R² = 1.00
T[ft²/day] = 1,480
Q[gpm] = 662

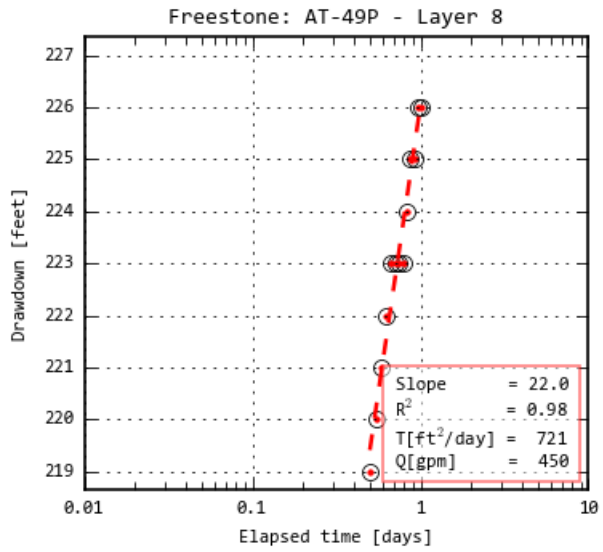
Freestone: AT-49P - Layer 8
Drawdown [feet]
Elapsed time [days]
Slope = 22.0
R² = 0.98
T[ft²/day] = 721
Q[gpm] = 450

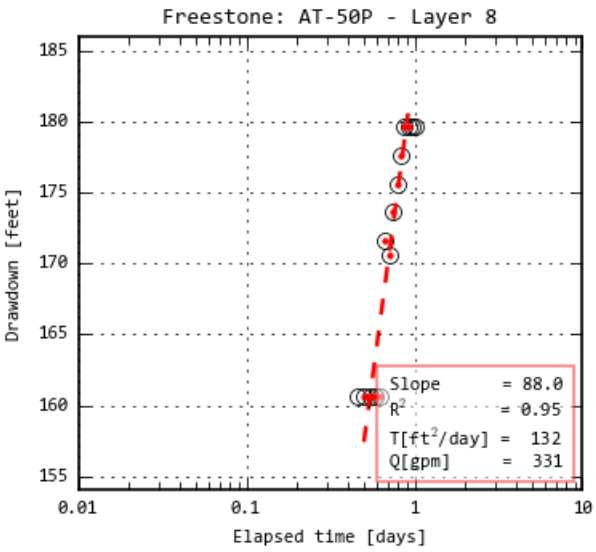
Freestone: AT-50P - Layer 8
Drawdown [feet]
Elapsed time [days]
Slope = 88.0
R² = 0.95
T[ft²/day] = 132
Q[gpm] = 331

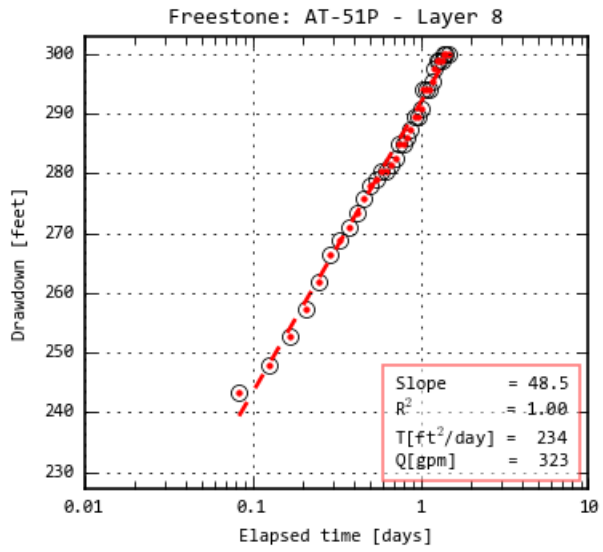
Freestone: AT-51P - Layer 8
Drawdown [feet]
Elapsed time [days]
Slope = 48.5
R² = 1.00
T[ft²/day] = 234
Q[gpm] = 323

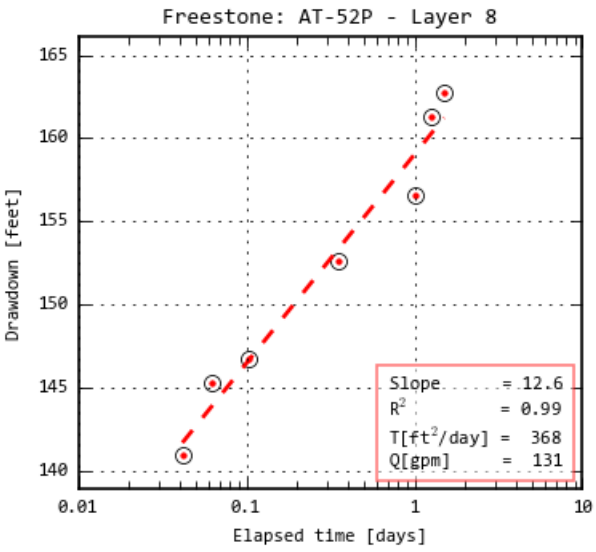
Freestone: AT-52P - Layer 8
Drawdown [feet]
Elapsed time [days]
Slope = 12.6
R² = 0.99
T[ft²/day] = 368
Q[gpm] = 131

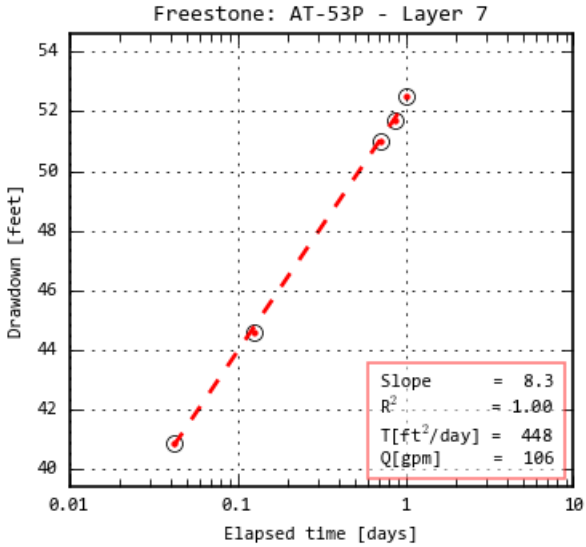
Freestone: AT-53P - Layer 7
Drawdown [feet]
Elapsed time [days]
Slope = 8.3
R² = 1.00
T[ft²/day] = 448
Q[gpm] = 106

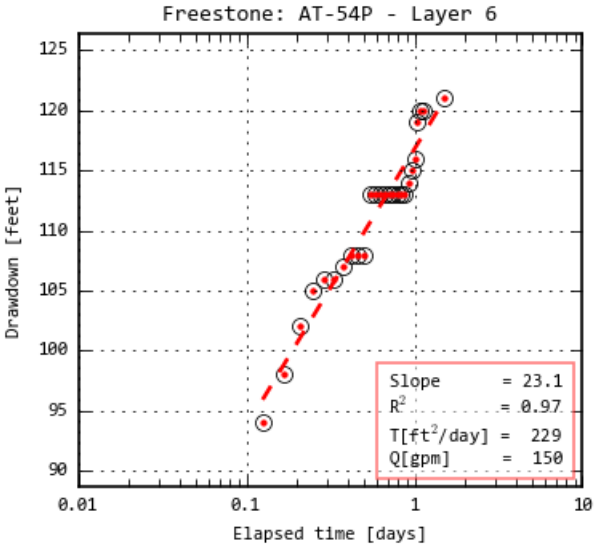
Freestone: AT-54P - Layer 6
Drawdown [feet]
Elapsed time [days]
Slope = 23.1
R² = 0.97
T[ft²/day] = 229
Q[gpm] = 150

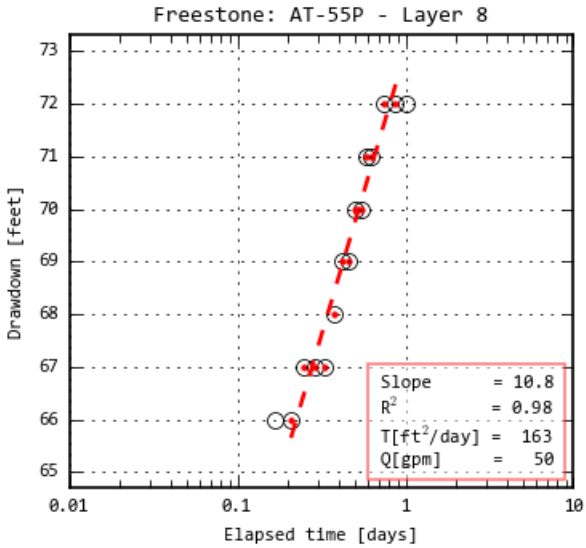
Freestone: AT-55P - Layer 8
Drawdown [feet]
Elapsed time [days]
Slope = 10.8
R² = 0.98
T[ft²/day] = 163
Q[gpm] = 50

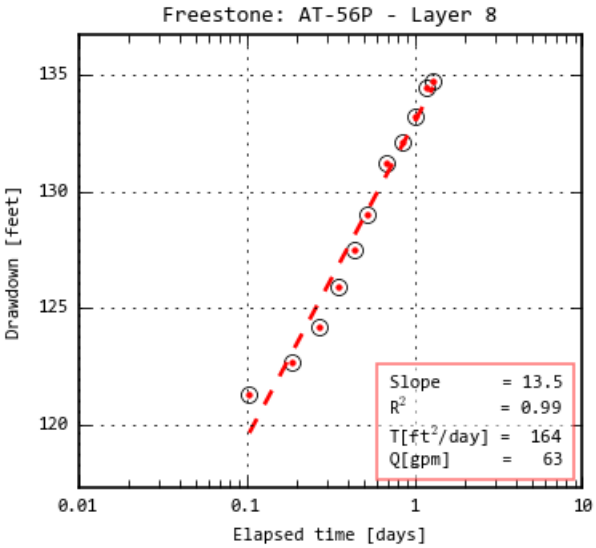
Freestone: AT-56P - Layer 8
Drawdown [feet]
Elapsed time [days]
Slope = 13.5
R² = 0.99
T[ft²/day] = 164
Q[gpm] = 63

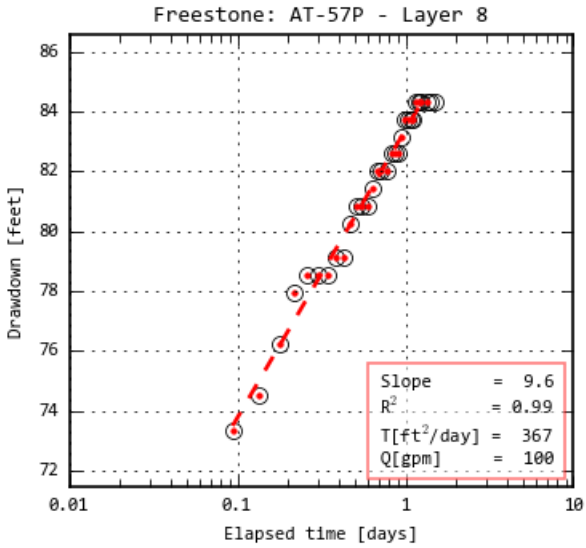
Freestone: AT-57P - Layer 8
Drawdown [feet]
Elapsed time [days]
Slope = 9.6
R² = 0.99
T[ft²/day] = 367
Q[gpm] = 100

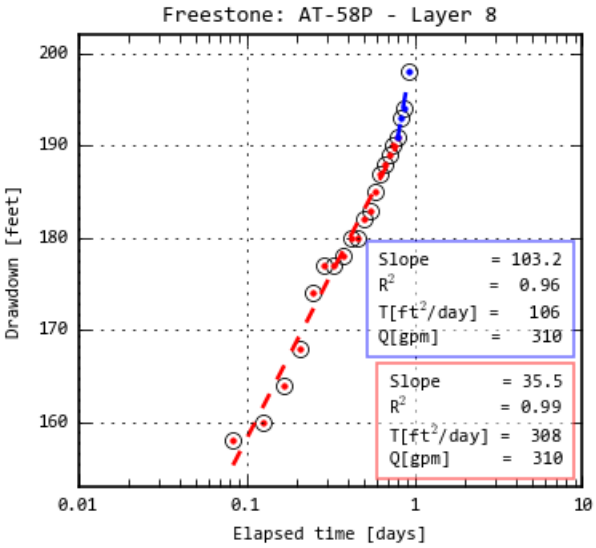
Freestone: AT-58P - Layer 8
Drawdown [feet]
Elapsed time [days]
Slope = 103.2
R² = 0.96
T[ft²/day] = 106
Q[gpm] = 310
Slope = 35.5
R² = 0.99
T[ft²/day] = 308
Q[gpm] = 310

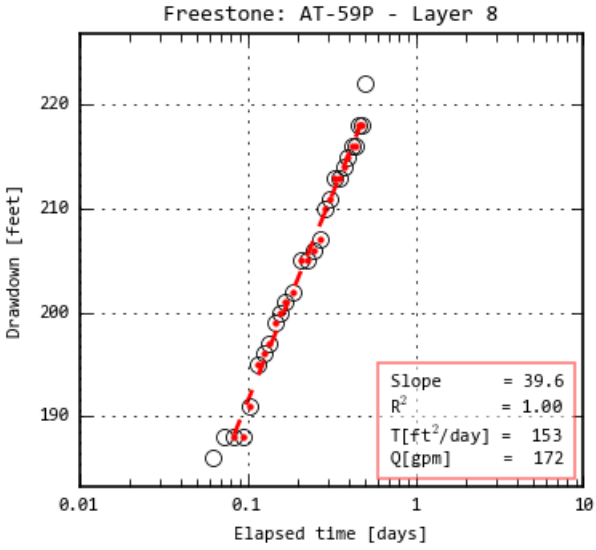
Freestone: AT-59P - Layer 8
Drawdown [feet]
Elapsed time [days]
Slope = 39.6
R² = 1.00
T[ft²/day] = 153
Q[gpm] = 172

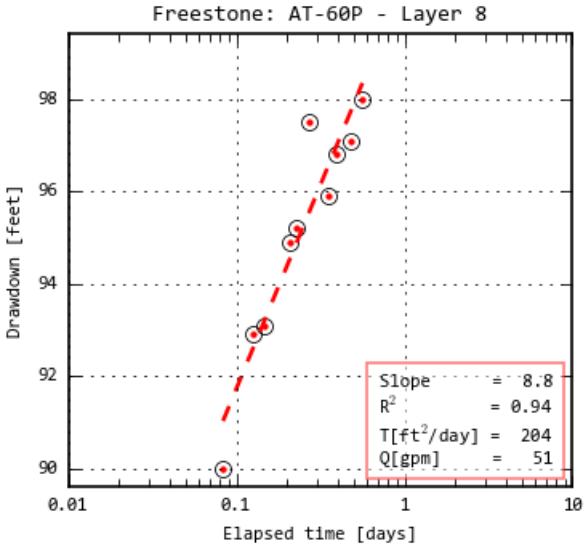
Freestone: AT-60P - Layer 8
Drawdown [feet]
Elapsed time [days]
Slope = 8.8
R² = 0.94
T[ft²/day] = 204
Q[gpm] = 51

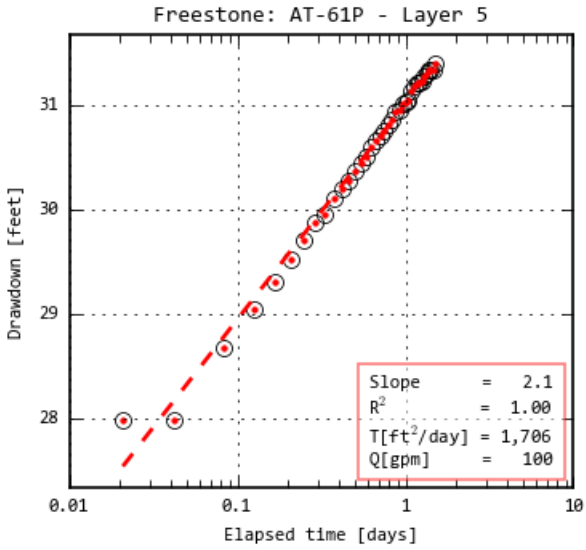
Freestone: AT-61P - Layer 5
Drawdown [feet]
Elapsed time [days]
Slope = 2.1
R² = 1.00
T[ft²/day] = 1,706
Q[gpm] = 100

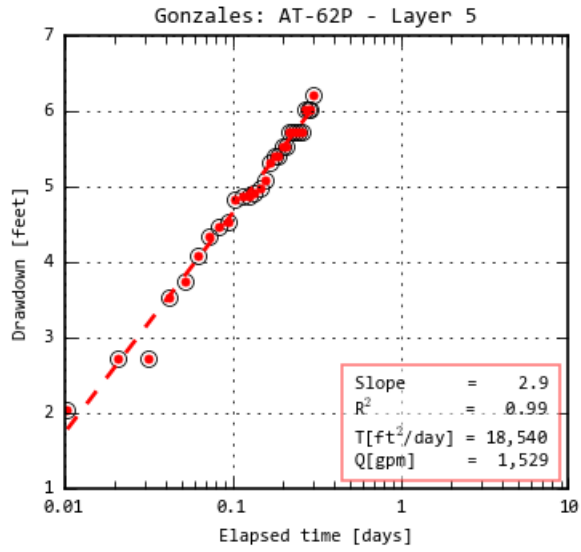
Gonzales: AT-62P - Layer 5
Drawdown [feet]
Elapsed time [days]
Slope = 2.9
R² = 0.99
T[ft²/day] = 18,540
Q[gpm] = 1,529

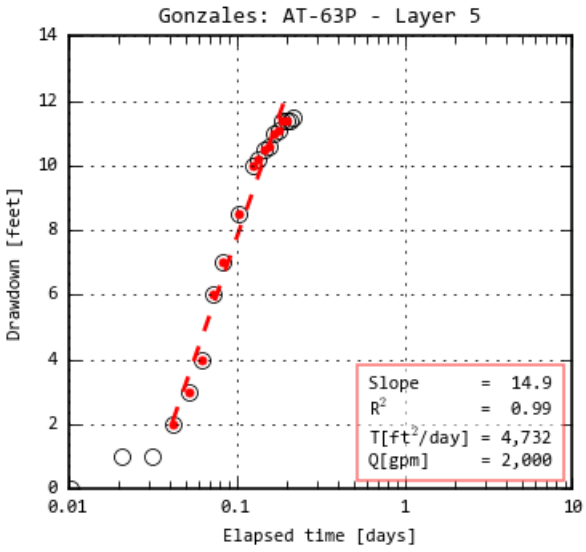
Gonzales: AT-63P - Layer 5
Drawdown [feet]
Elapsed time [days]
Slope = 14.9
R² = 0.99
T[ft²/day] = 4,732
Q[gpm] = 2,000

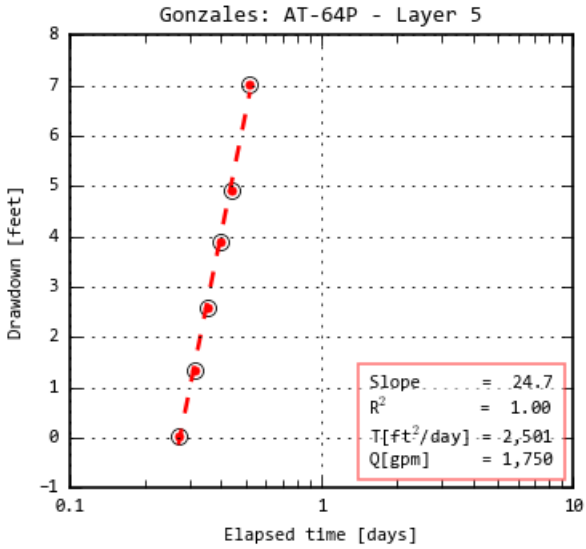
Gonzales: AT-64P - Layer 5
Drawdown [feet]
Elapsed time [days]
Slope = 24.7
R² = 1.00
T[ft²/day] = 2,501
Q[gpm] = 1,750

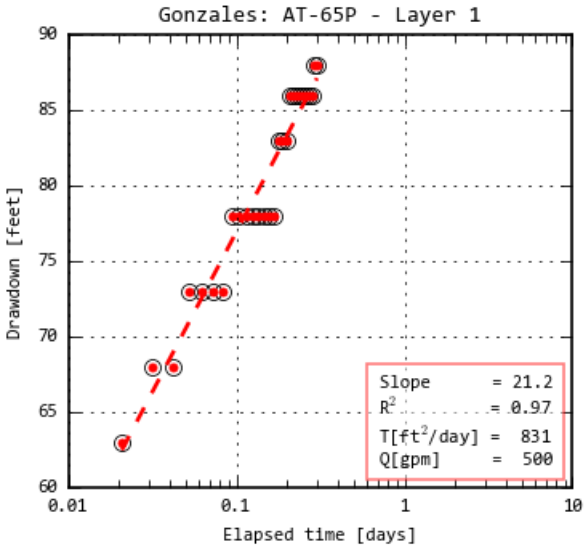
Gonzales: AT-65P - Layer 1
Drawdown [feet]
Elapsed time [days]
Slope = 21.2
R² = 0.97
T[ft²/day] = 831
Q[gpm] = 500

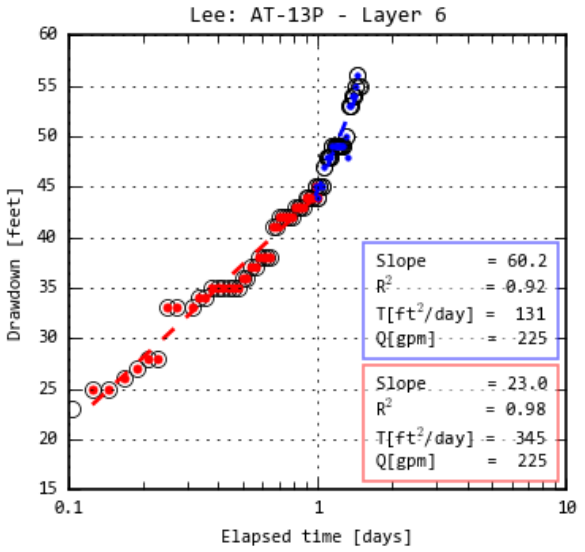
Lee: AT-13P - Layer 6
Drawdown [feet]
Elapsed time [days]
Slope = 60.2
R² = 0.92
T[ft²/day] = 131
Q[gpm] = 225
Slope = 23.0
R² = 0.98
T[ft²/day] = 345
Q[gpm] = 225

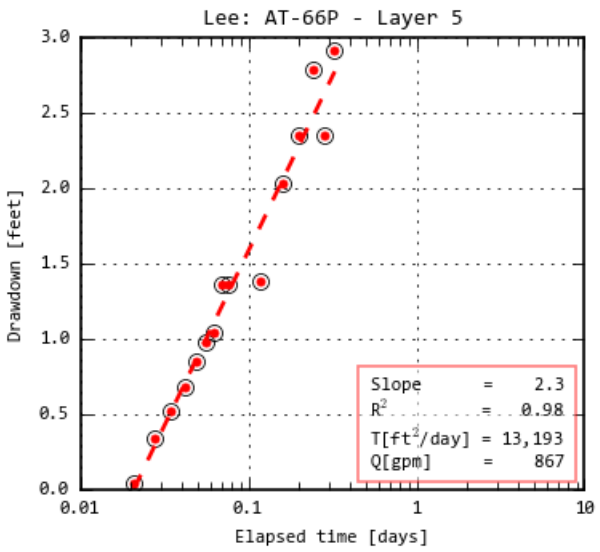
Lee: AT-66P - Layer 5
Drawdown [feet]
Elapsed time [days]
Slope = 2.3
R² = 0.98
T[ft²/day] = 13,193
Q[gpm] = 867

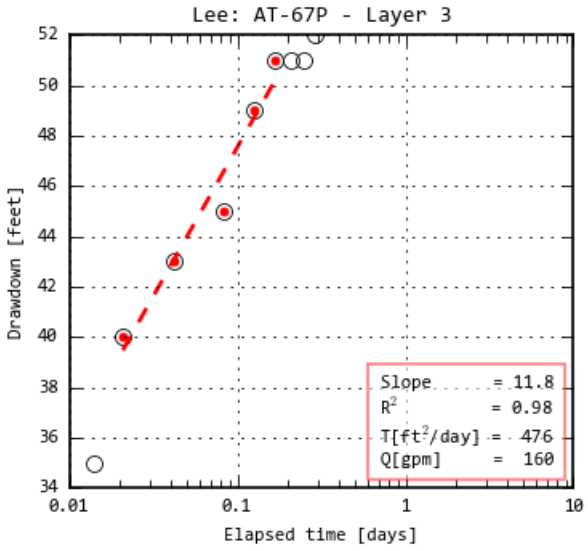
Lee: AT-67P - Layer 3
Drawdown [feet]
Elapsed time [days]
Slope = 11.8
R² = 0.98
T[ft²/day] = 476
Q[gpm] = 160

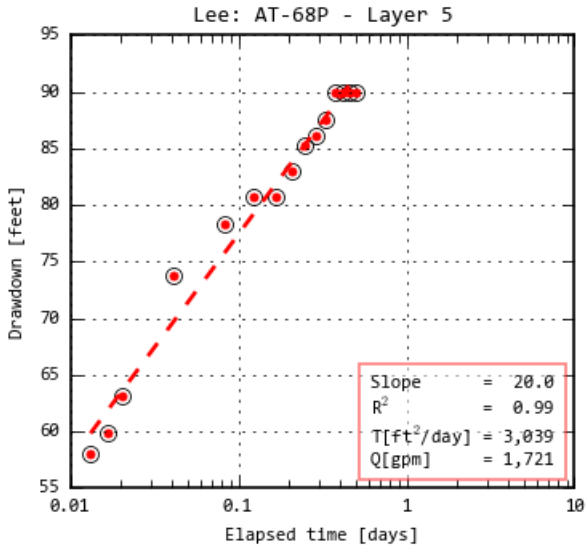
Lee: AT-68P - Layer 5
Drawdown [feet]
Elapsed time [days]
Slope = 20.0
R² = 0.99
T[ft²/day] = 3,039
Q[gpm] = 1,721

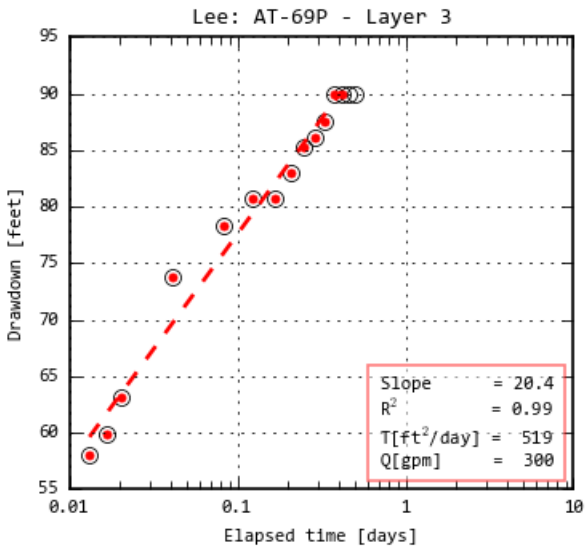
Lee: AT-69P - Layer 3
Drawdown [feet]
Elapsed time [days]
Slope = 20.4
R² = 0.99
T[ft²/day] = 519
Q[gpm] = 300

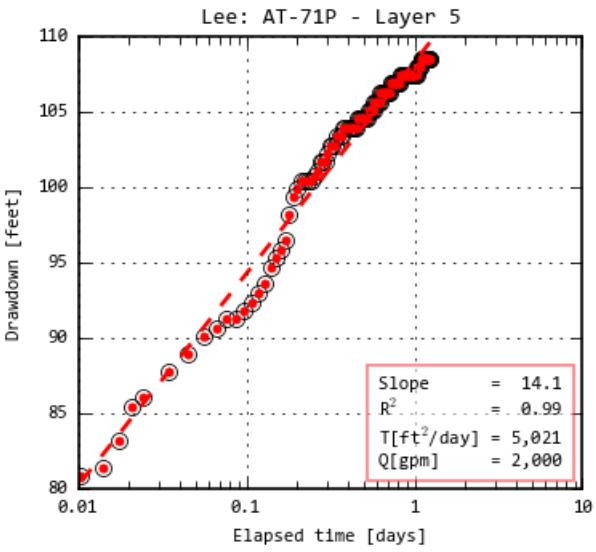
Lee: AT-71P - Layer 5
Drawdown [feet]
Elapsed time [days]
Slope = 14.1
R² = 0.99
T[ft²/day] = 5,021
Q[gpm] = 2,000

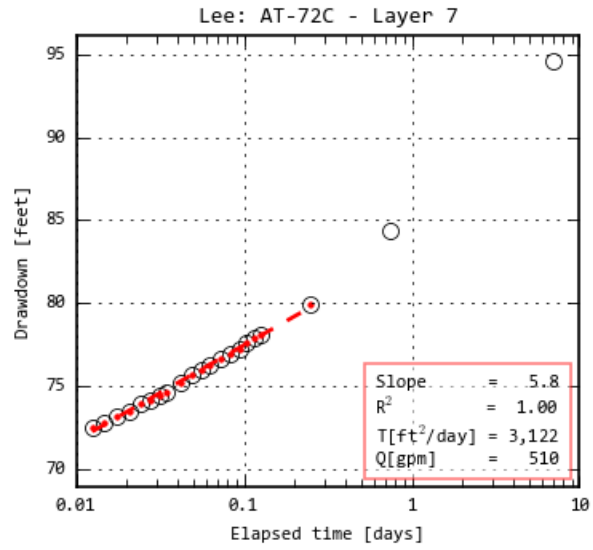
Lee: AT-72C - Layer 7
Drawdown [feet]
Elapsed time [days]
Slope = 5.8
R² = 1.00
T[ft²/day] = 3,122
Q[gpm] = 510

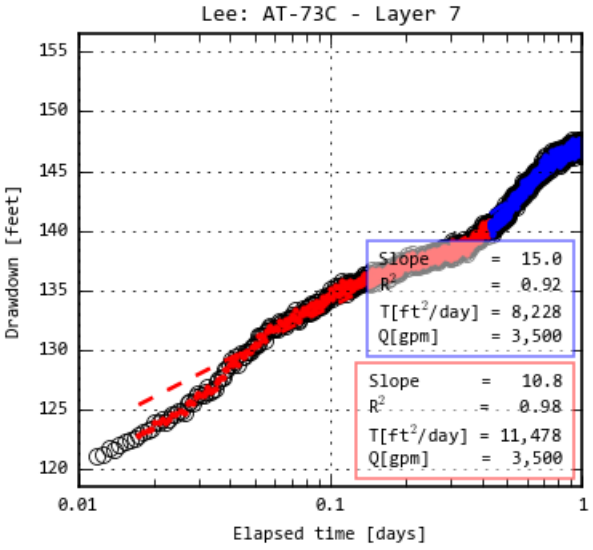
Lee: AT-73C - Layer 7
Drawdown [feet]
Elapsed time [days]
Slope = 15.0
R² = 0.92
T[ft²/day] = 8,228
Q[gpm] = 3,500
Slope = 10.8
R² = 0.98
T[ft²/day] = 11,478
Q[gpm] = 3,500

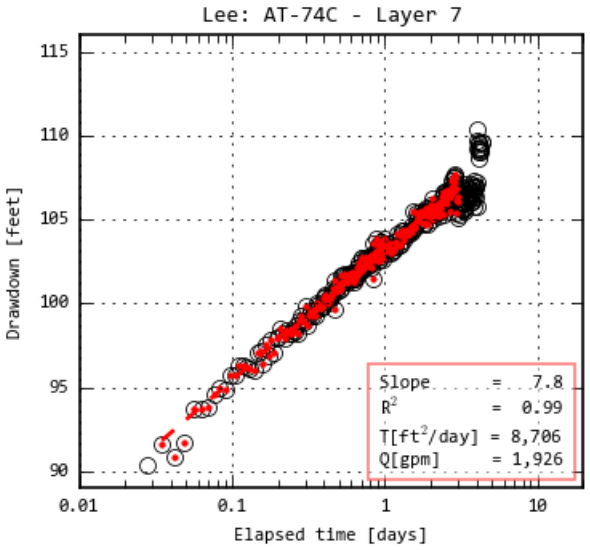
Lee: AT-74C - Layer 7
Drawdown [feet]
Elapsed time [days]
Slope = 7.8
R² = 0.99
T[ft²/day] = 8,706
Q[gpm] = 1,926

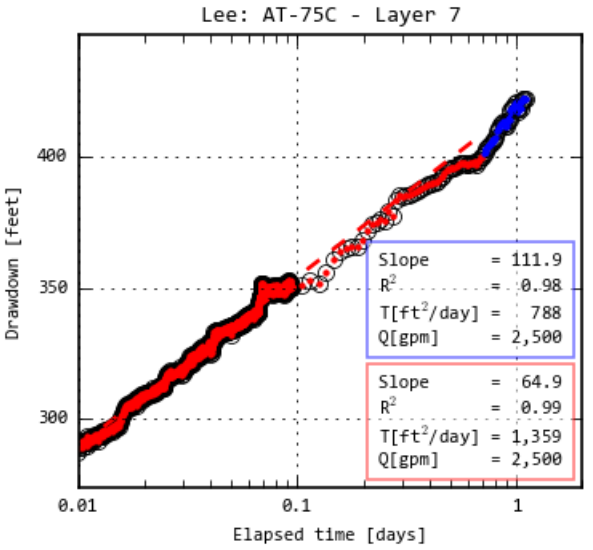
Lee: AT-75C - Layer 7
Drawdown [feet]
Elapsed time [days]
Slope = 111.9
R² = 0.98
T[ft²/day] = 788
Q[gpm] = 2,500
Slope = 64.9
R² = 0.99
T[ft²/day] = 1,359
Q[gpm] = 2,500

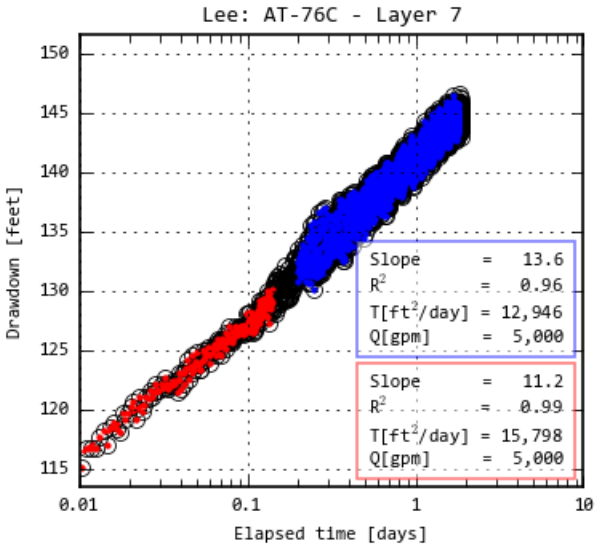
Lee: AT-76C - Layer 7
Drawdown [feet]
Elapsed time [days]
Slope = 13.6
R² = 0.96
T[ft²/day] = 12,946
Q[gpm] = 5,000
Slope = 11.2
R² = 0.99
T[ft²/day] = 15,798
Q[gpm] = 5,000

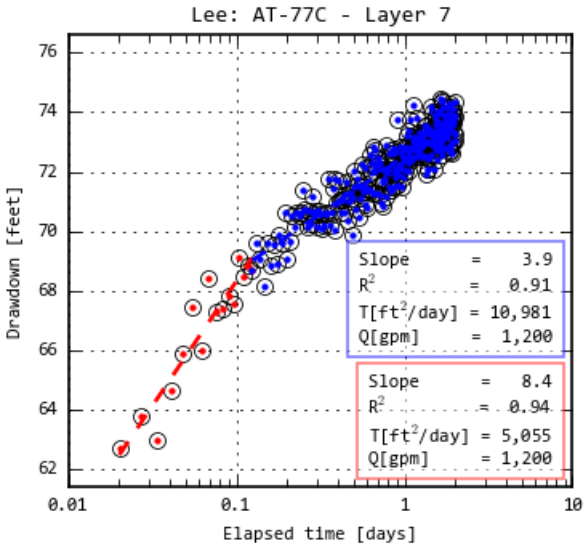
Lee: AT-77C - Layer 7
Drawdown [feet]
Elapsed time [days]
Slope = 3.9
R² = 0.91
T[ft²/day] = 10,981
Q[gpm] = 1,200
Slope = 8.4
R² = 0.94
T[ft²/day] = 5,055
Q[gpm] = 1,200

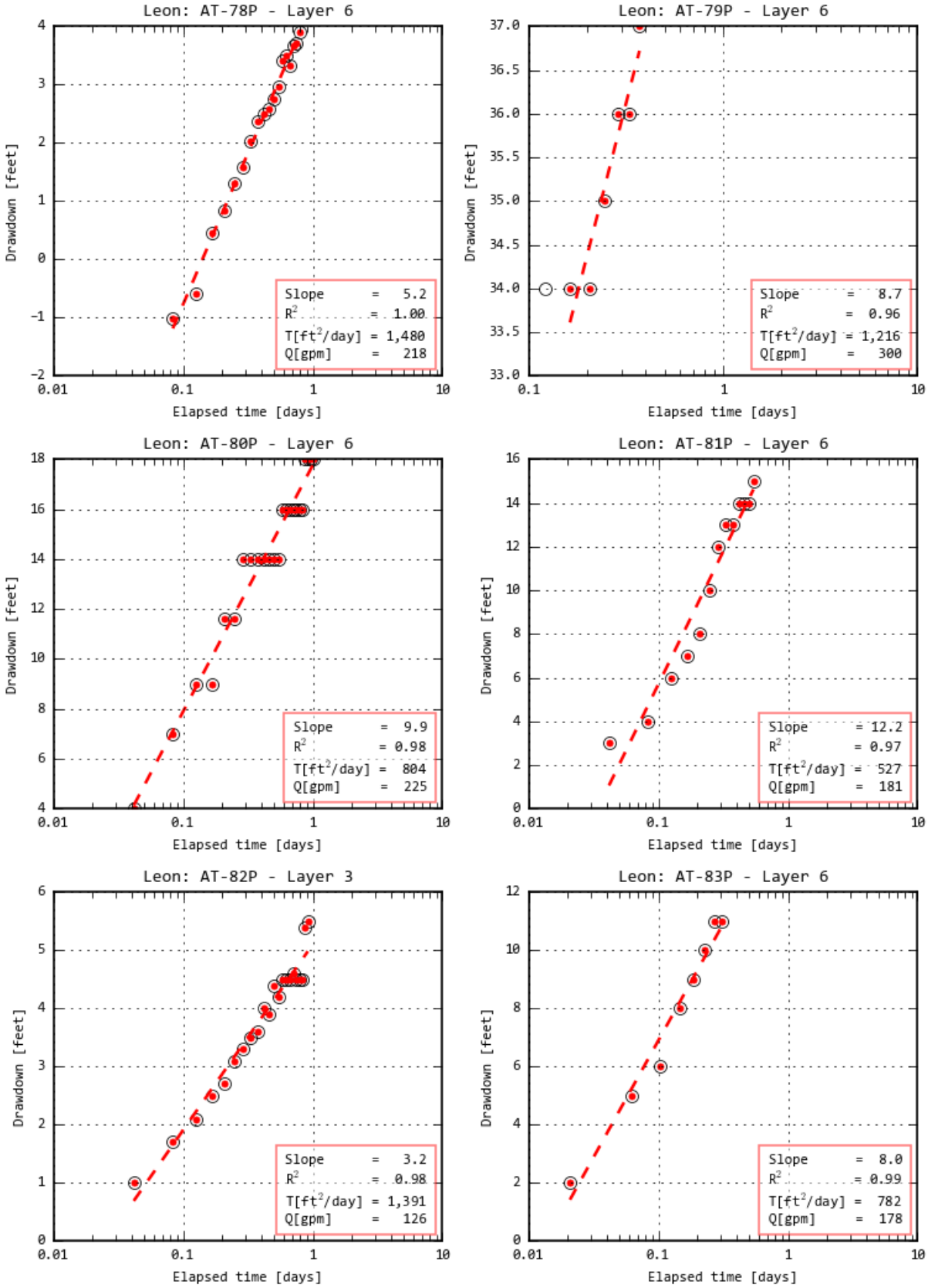
Leon: AT-78P - Layer 6
Slope = 5.2
R² = 1.00
T[ft²/day] = 1,480
Q[gpm] = 218
Leon: AT-79P - Layer 6
Slope = 8.7
R² = 0.96
T[ft²/day] = 1,216
Q[gpm] = 300
Leon: AT-80P - Layer 6
Slope = 9.9
R² = 0.98
T[ft²/day] = 804
Q[gpm] = 225
Leon: AT-81P - Layer 6
Slope = 12.2
R² = 0.97
T[ft²/day] = 527
Q[gpm] = 181
Leon: AT-82P - Layer 3
Slope = 3.2
R² = 0.98
T[ft²/day] = 1,391
Q[gpm] = 126
Leon: AT-83P - Layer 6
Slope = 8.0
R² = 0.99
T[ft²/day] = 782
Q[gpm] = 178
Drawdown [feet]
Elapsed time [days]

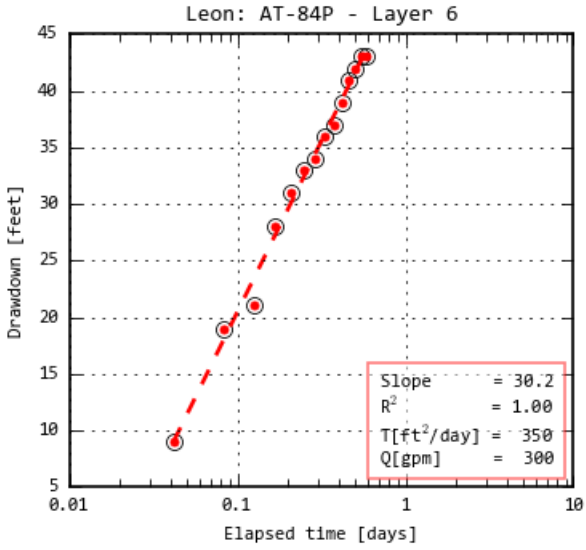
Leon: AT-84P - Layer 6
Drawdown [feet]
Elapsed time [days]
Slope = 30.2
R² = 1.00
T[ft²/day] = 350
Q[gpm] = 300

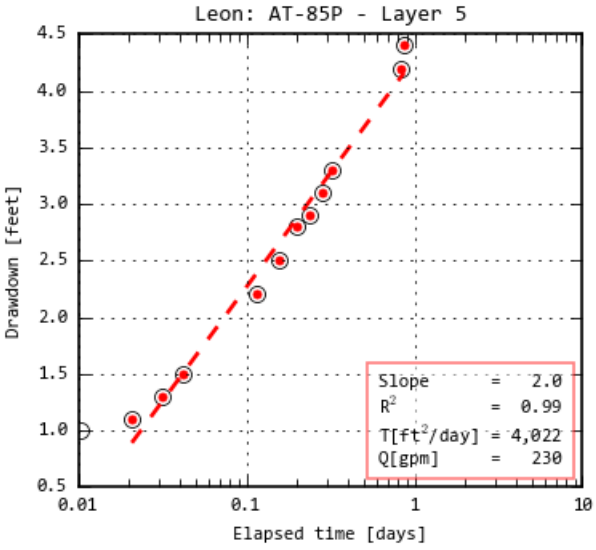
Leon: AT-85P - Layer 5
Drawdown [feet]
Elapsed time [days]
Slope = 2.0
R² = 0.99
T[ft²/day] = 4,022
Q[gpm] = 230

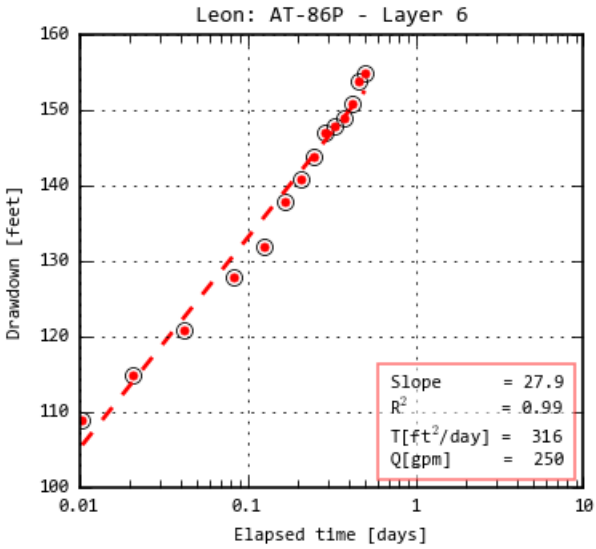
Leon: AT-86P - Layer 6
Drawdown [feet]
Elapsed time [days]
Slope = 27.9
R² = 0.99
T[ft²/day] = 316
Q[gpm] = 250

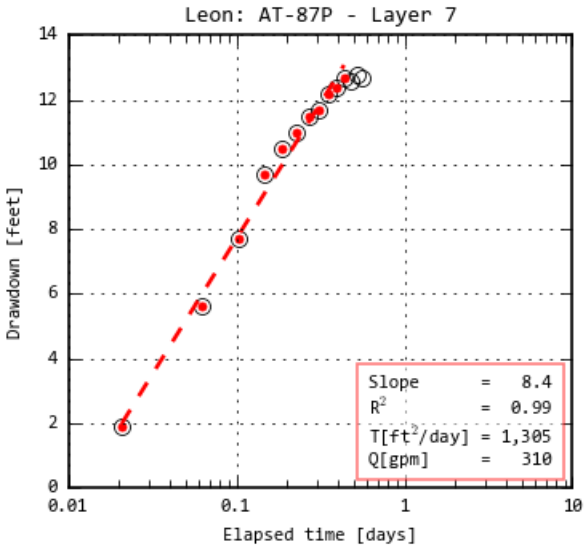
Leon: AT-87P - Layer 7
Drawdown [feet]
Elapsed time [days]
Slope = 8.4
R² = 0.99
T[ft²/day] = 1,305
Q[gpm] = 310

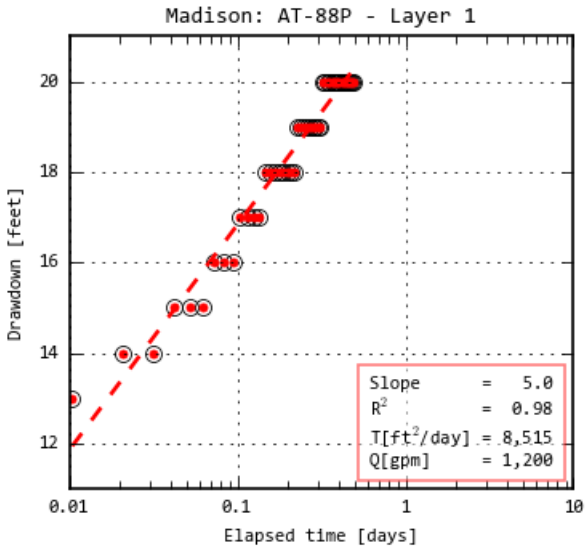
Madison: AT-88P - Layer 1
Drawdown [feet]
Elapsed time [days]
Slope = 5.0
R2 = 0.98
T[ft2/day] = 8,515
Q[gpm] = 1,200

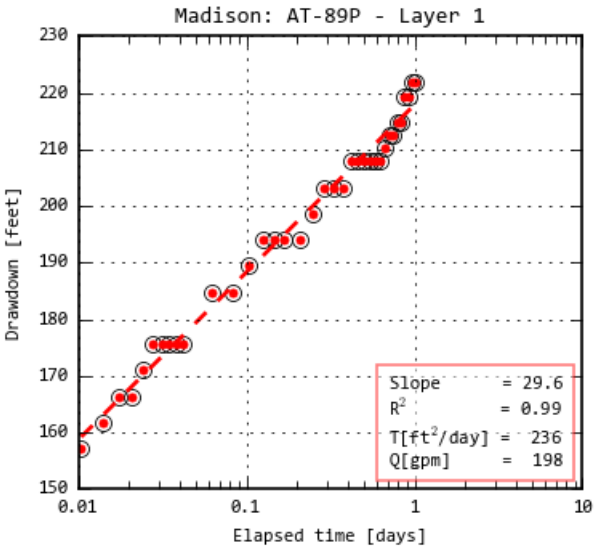
Madison: AT-89P - Layer 1
Drawdown [feet]
Elapsed time [days]
Slope = 29.6
R2 = 0.99
T[ft2/day] = 236
Q[gpm] = 198

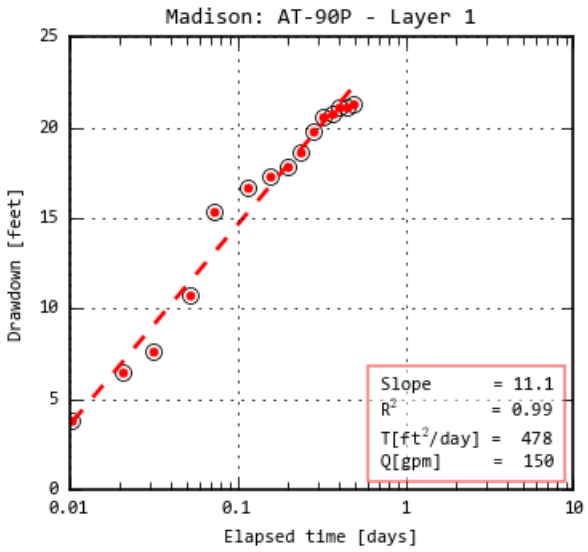
Madison: AT-90P - Layer 1
Drawdown [feet]
Elapsed time [days]
Slope = 11.1
R2 = 0.99
T[ft2/day] = 478
Q[gpm] = 150

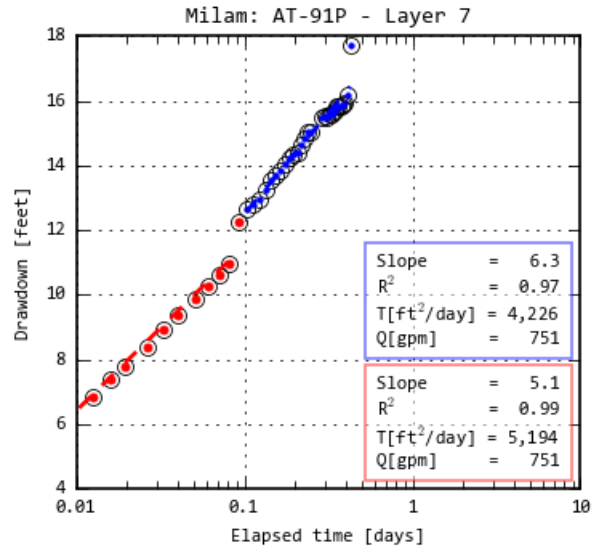
Milam: AT-91P - Layer 7
Drawdown [feet]
Elapsed time [days]
Slope = 6.3
R² = 0.97
T[ft²/day] = 4,226
Q[gpm] = 751
Slope = 5.1
R² = 0.99
T[ft²/day] = 5,194
Q[gpm] = 751

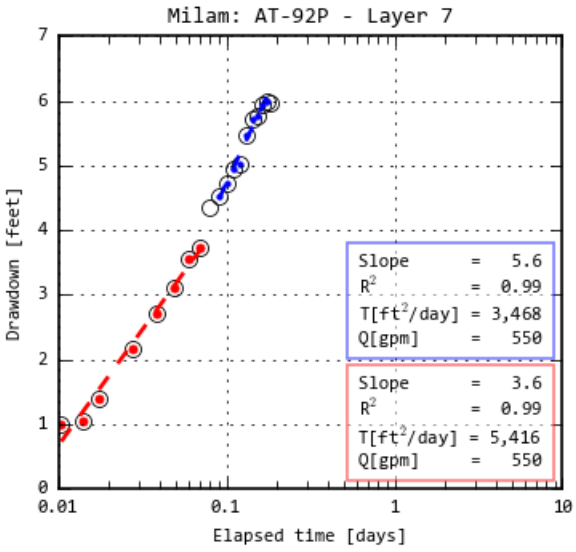
Milam: AT-92P - Layer 7
Drawdown [feet]
Elapsed time [days]
Slope = 5.6
R² = 0.99
T[ft²/day] = 3,468
Q[gpm] = 550
Slope = 3.6
R² = 0.99
T[ft²/day] = 5,416
Q[gpm] = 550

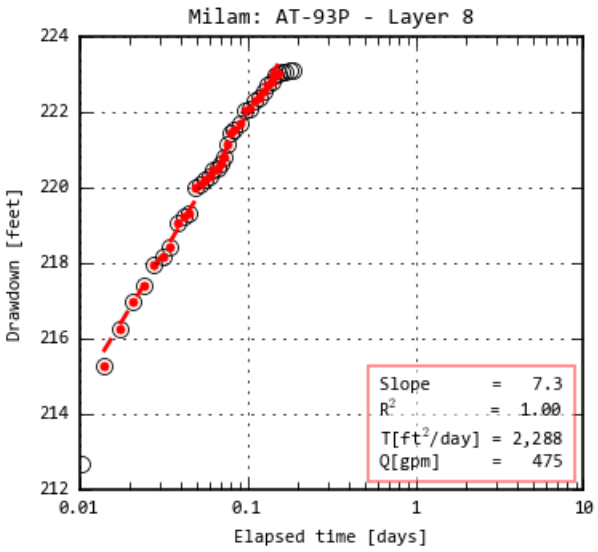
Milam: AT-93P - Layer 8
Drawdown [feet]
Elapsed time [days]
Slope = 7.3
R² = 1.00
T[ft²/day] = 2,288
Q[gpm] = 475

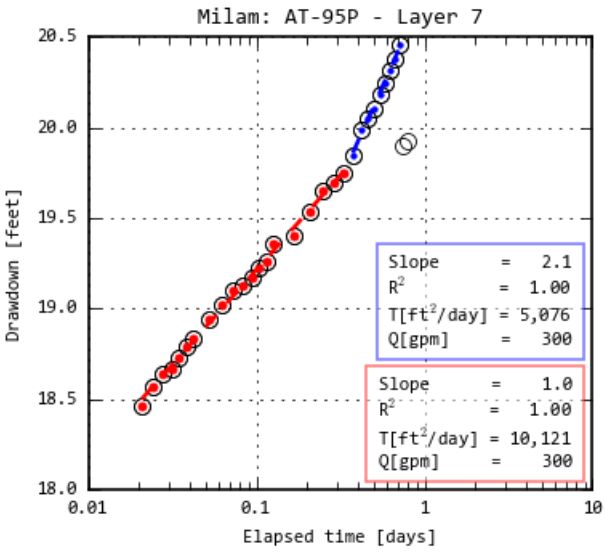
Milam: AT-95P - Layer 7
Drawdown [feet]
Elapsed time [days]
Slope = 2.1
R² = 1.00
T[ft²/day] = 5,076
Q[gpm] = 300
Slope = 1.0
R² = 1.00
T[ft²/day] = 10,121
Q[gpm] = 300

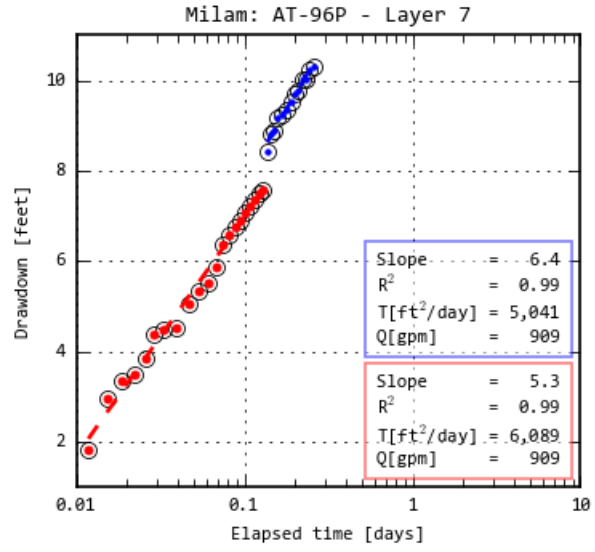
Milam: AT-96P - Layer 7
Drawdown [feet]
Elapsed time [days]
Slope = 6.4
R² = 0.99
T[ft²/day] = 5,041
Q[gpm] = 909
Slope = 5.3
R² = 0.99
T[ft²/day] = 6,089
Q[gpm] = 909

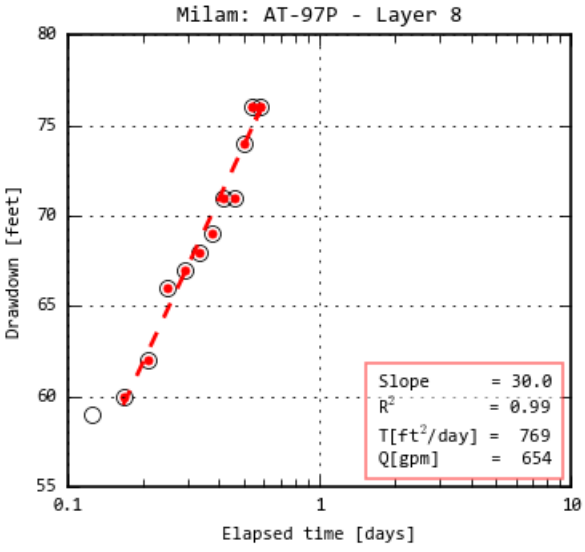
Milam: AT-97P - Layer 8
Drawdown [feet]
Elapsed time [days]
Slope = 30.0
R² = 0.99
T[ft²/day] = 769
Q[gpm] = 654

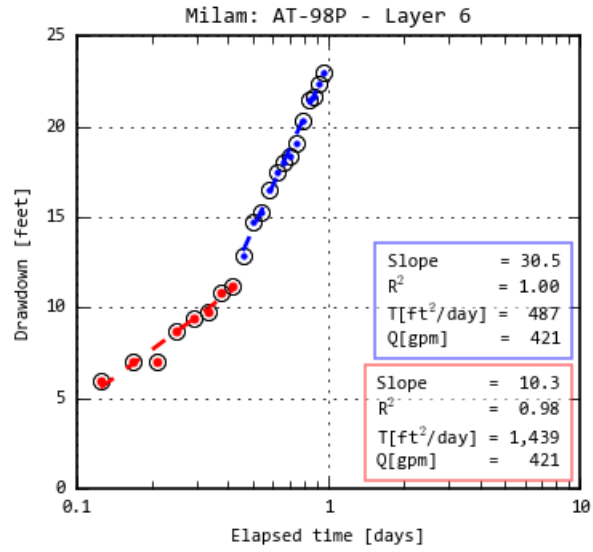
Milam: AT-98P - Layer 6
Drawdown [feet]
Elapsed time [days]
Slope = 30.5
R² = 1.00
T[ft²/day] = 487
Q[gpm] = 421
Slope = 10.3
R² = 0.98
T[ft²/day] = 1,439
Q[gpm] = 421

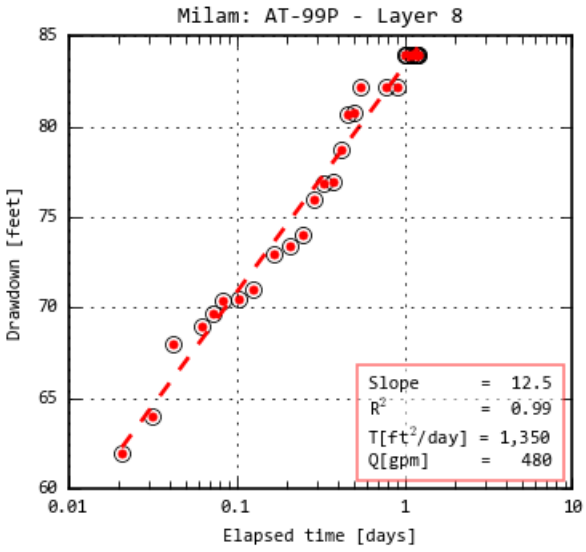
Milam: AT-99P - Layer 8
Drawdown [feet]
Elapsed time [days]
Slope = 12.5
R² = 0.99
T[ft²/day] = 1,350
Q[gpm] = 480

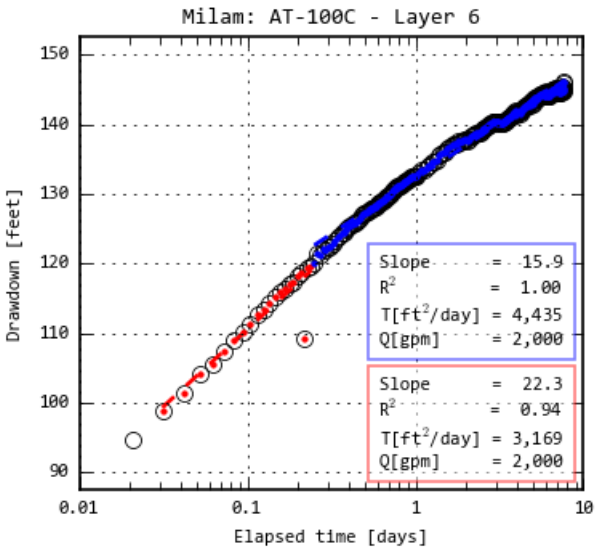
Milam: AT-100C - Layer 6
Drawdown [feet]
Elapsed time [days]
Slope = 15.9
R² = 1.00
T[ft²/day] = 4,435
Q[gpm] = 2,000
Slope = 22.3
R² = 0.94
T[ft²/day] = 3,169
Q[gpm] = 2,000

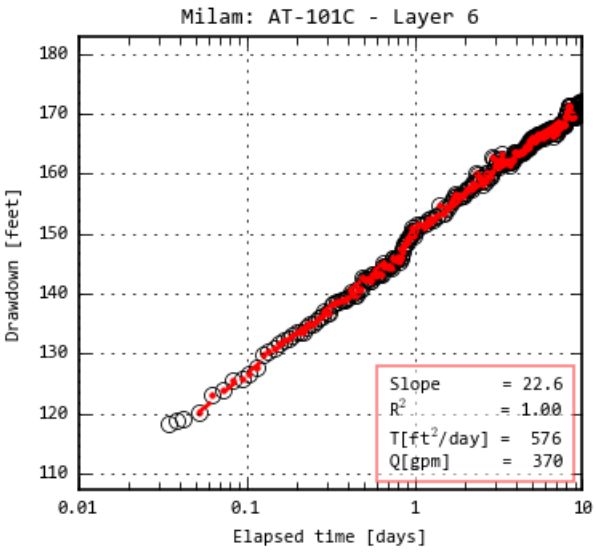
Milam: AT-101C - Layer 6
Drawdown [feet]
Elapsed time [days]
Slope = 22.6
R² = 1.00
T[ft²/day] = 576
Q[gpm] = 370

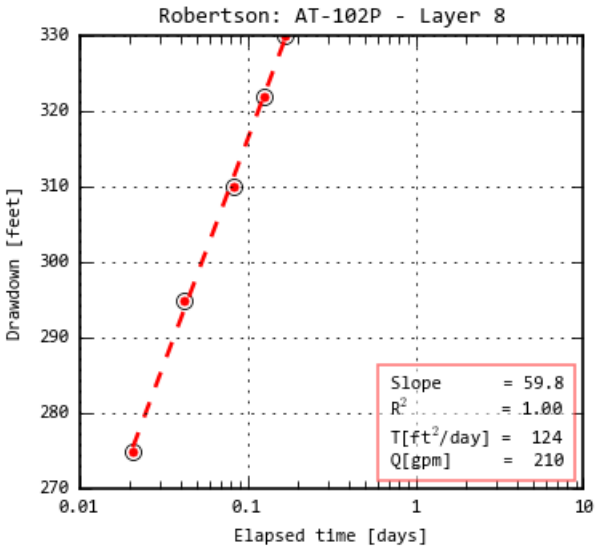
Robertson: AT-102P - Layer 8
Drawdown [feet]
Elapsed time [days]
Slope = 59.8
R² = 1.00
T[ft²/day] = 124
Q[gpm] = 210

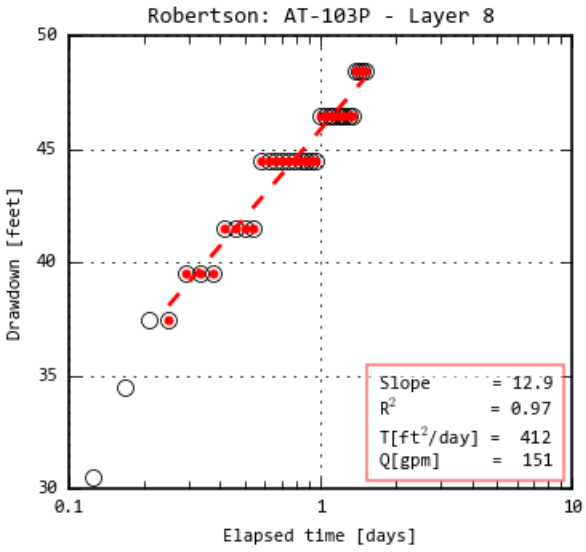
Robertson: AT-103P - Layer 8
Drawdown [feet]
Elapsed time [days]
Slope = 12.9
R² = 0.97
T[ft²/day] = 412
Q[gpm] = 151

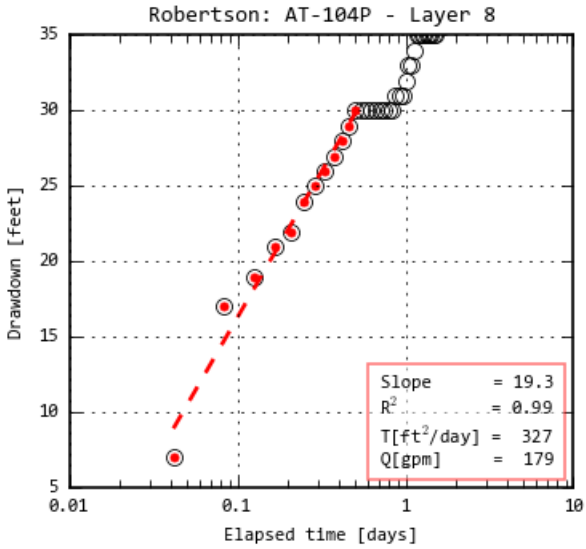
Robertson: AT-104P - Layer 8
Drawdown [feet]
Elapsed time [days]
Slope = 19.3
R² = 0.99
T[ft²/day] = 327
Q[gpm] = 179

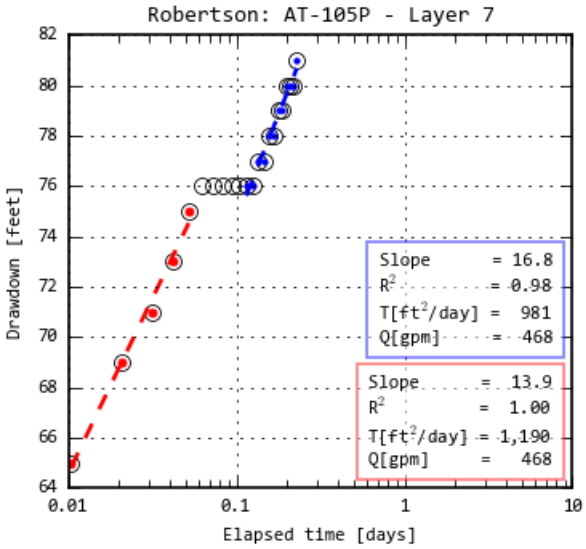
Robertson: AT-105P - Layer 7
Drawdown [feet]
Elapsed time [days]
Slope = 16.8
R² = 0.98
T[ft²/day] = 981
Q[gpm] = 468
Slope = 13.9
R² = 1.00
T[ft²/day] = 1,190
Q[gpm] = 468

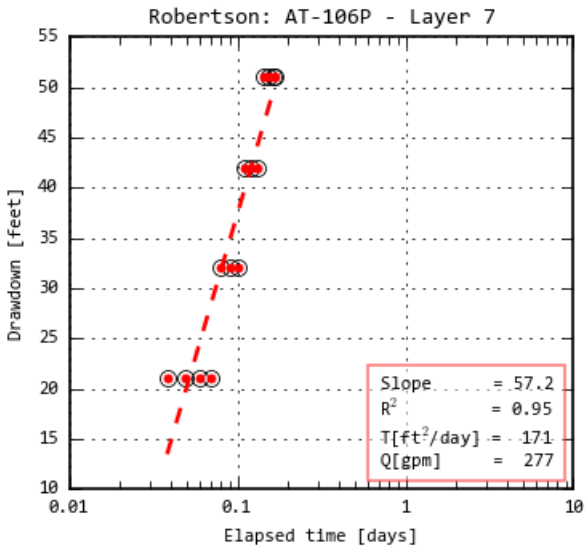
Robertson: AT-106P - Layer 7
Drawdown [feet]
Elapsed time [days]
Slope = 57.2
R² = 0.95
T[ft²/day] = 171
Q[gpm] = 277

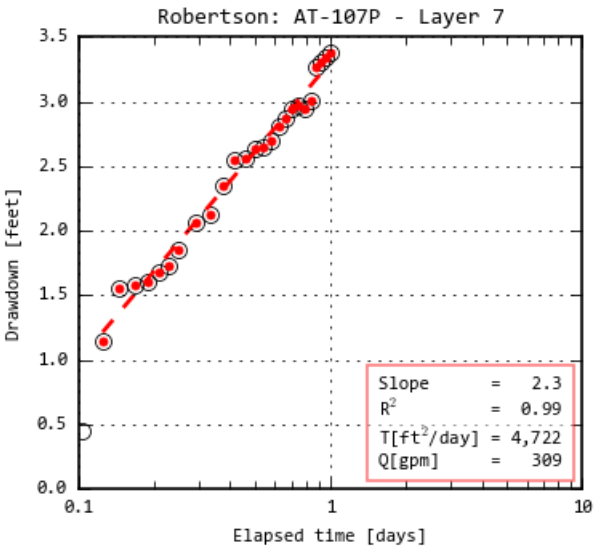
Robertson: AT-107P - Layer 7
Drawdown [feet]
Elapsed time [days]
Slope = 2.3
R² = 0.99
T[ft²/day] = 4,722
Q[gpm] = 309

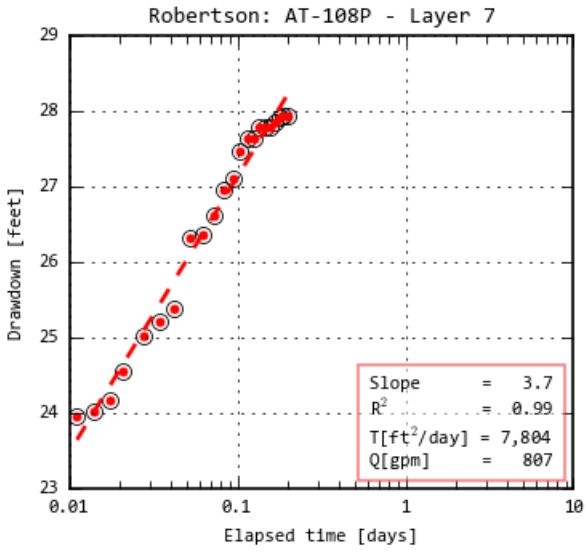
Robertson: AT-108P - Layer 7
Drawdown [feet]
Elapsed time [days]
Slope = 3.7
R² = 0.99
T[ft²/day] = 7,804
Q[gpm] = 807

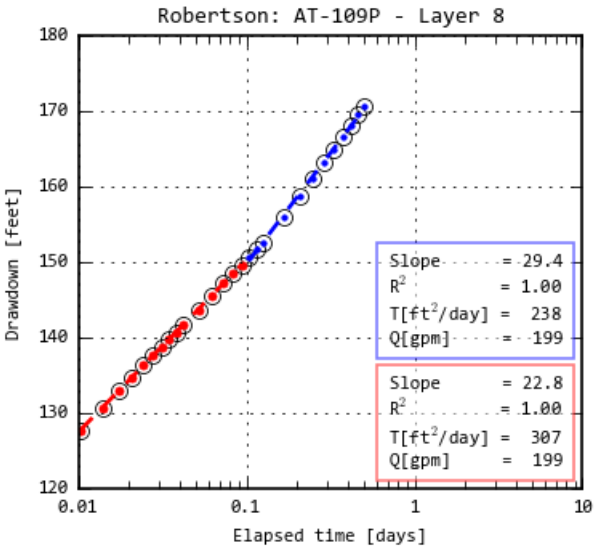
Robertson: AT-109P - Layer 8
Drawdown [feet]
Elapsed time [days]
Slope = 29.4
R² = 1.00
T[ft²/day] = 238
Q[gpm] = 199
Slope = 22.8
R² = 1.00
T[ft²/day] = 307
Q[gpm] = 199

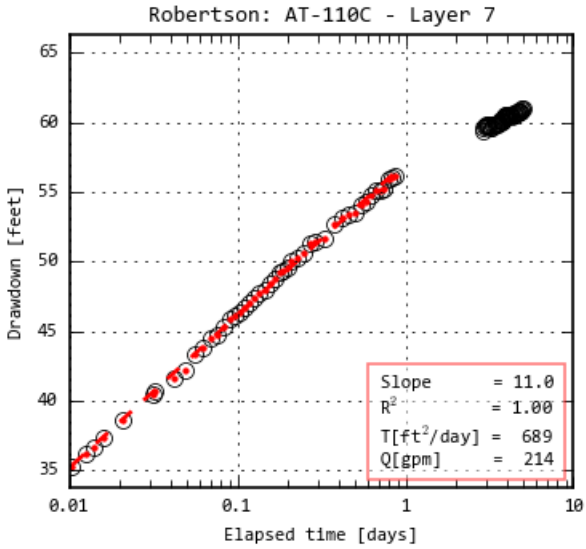
Robertson: AT-110C - Layer 7
Drawdown [feet]
Elapsed time [days]
Slope = 11.0
R² = 1.00
T[ft²/day] = 689
Q[gpm] = 214

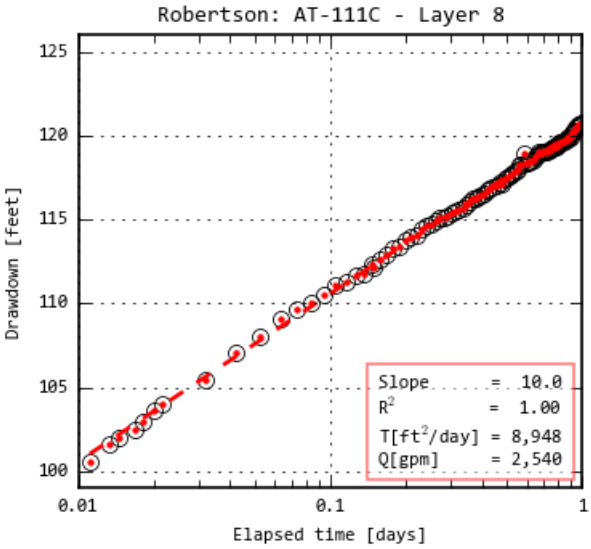
Robertson: AT-111C - Layer 8
Drawdown [feet]
Elapsed time [days]
Slope = 10.0
R² = 1.00
T[ft²/day] = 8,948
Q[gpm] = 2,540

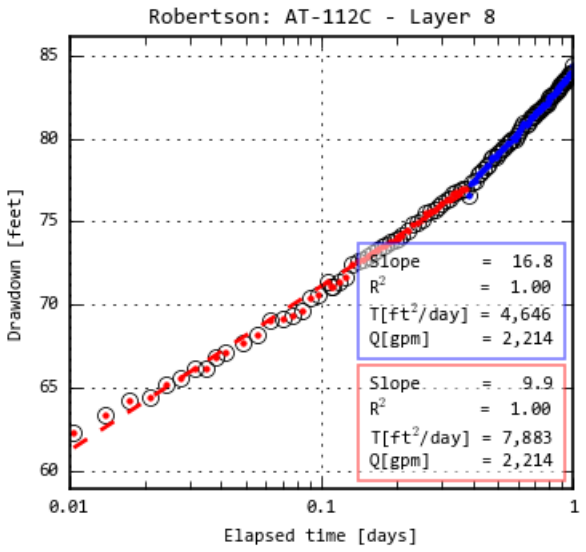
Robertson: AT-112C - Layer 8
Drawdown [feet]
Elapsed time [days]
Slope = 16.8
R² = 1.00
T[ft²/day] = 4,646
Q[gpm] = 2,214
Slope = 9.9
R² = 1.00
T[ft²/day] = 7,883
Q[gpm] = 2,214

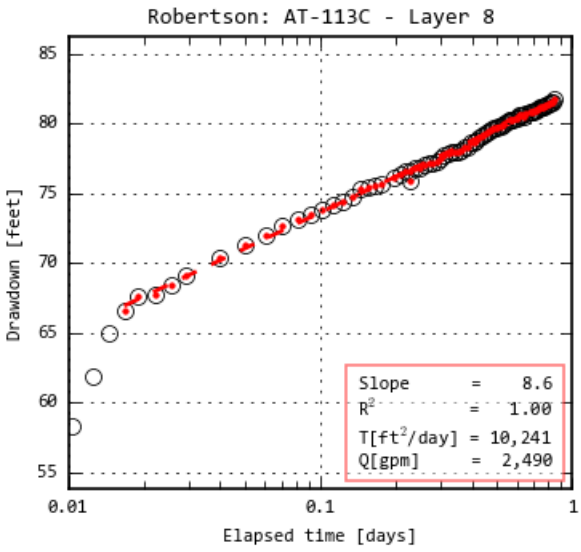
Robertson: AT-113C - Layer 8
Drawdown [feet]
Elapsed time [days]
Slope = 8.6
R² = 1.00
T[ft²/day] = 10,241
Q[gpm] = 2,490

This page is intentionally blank.

13 Appendix C

13.1 Introduction to MODFLOW USG

MODFLOW-USG (Panday and others, 2013; 2015) is an unstructured grid version of the MODFLOW family of codes developed and supported by the United States Geological Survey for simulating groundwater flow and tightly coupled processes. The following description of MODFLOW-USG was taken from United States Geological Survey (2017b). An underlying control volume finite difference formulation enables connection of grid cells to an arbitrary number of adjacent cells enabling a wide variety of structured and unstructured grid types to be supported. Benefits of a flexible grid design include focused horizontal and vertical grid refinement in areas of interest, such as along rivers or near wells or locations with hydraulic property variations over small horizontal and/or vertical distances.

Along with the Groundwater Flow Process in MODFLOW-2005, MODFLOW-USG also includes a new Connected Linear Network Process, which allows simulation of features such as multi-node wells, karst conduits, and tile drains. The equations for both processes are formulated into one matrix equation and solved simultaneously, resulting in tight coupling of the two processes and robustness from using an unstructured grid with unstructured matrix storage and solution schemes.

In addition, improved solution convergence is available with MODFLOW-USG through an optional Newton-Raphson formulation, which is based on the formulation in MODFLOW-NWT. Problems with the drying and wetting of grid cells is also avoided by this formulation. The existing MODFLOW solvers developed for structured and symmetric matrices were replaced in MODFLOW-USG with a new Sparse Matrix Solver Package. The flow equations and the Newton-Raphson formulation are solved with this new solver by several methods for resolving nonlinearities and multiple symmetric and asymmetric linear solution schemes, respectively.

The primary benefits of using MODFLOW-USG for the current effort include: (1) the ability for grid refinement in areas of interest in a computationally efficient manner, (2) the enhanced matrix solution, and (3) the ability to solve a steady-state solution. The MODFLOW-96 version of the central Queen City and Sparta aquifers groundwater availability model could not converge on a steady-state solution. Therefore, the ability to simulation steady-state conditions using MODFLOW-USG provides a significant benefit.

13.2 Development of the MODFLOW-USG Model

The MODFLOW-96 version of the Queen City-Sparta aquifers GAM was converted to MODFLOW-USG primarily with Groundwater Vistas (Environmental Simulations, Inc., 2011) by the following steps:

1) The MODFLOW-96 files were imported into Groundwater Vistas.
    a) MODFLOW-96 files were then generated from Groundwater Vistas and compared to the original model files. To verify that the import into Groundwater Vistas was correct, simulated results generated using the Groundwater Vista files were compared to the original model results for mass balance (cumulative and rates) at the first and last time step and visual inspection of the heads at the last time step. Mass balance results were identical and heads looked the same, indicating that import of the MODFLOW-96 model into Groundwater Vistas was successful.
2) Groundwater Vistas was used to generate MODFLOW-USG files.
    a) The MODFLOW-USG flag was turned on in Groundwater Vistas and the solver was converted to the Sparse Matrix Solver. Solver convergence criteria and settings are slightly different between the two MODFLOW versions, so those changes were also made.
3) Groundwater Vistas was used to run the MODFLOW-USG model.
    a) Comparison of the MODFLOW-USG results to the original model indicated similar mass balance results and heads, indicating that the conversion to MODFLOW-USG was successful.
4) Reduced inactive nodes in the domain for the MODFLOW-USG dataset to reduce the matrix and reran the model.
    a) Results were identical to the MODFLOW-USG model in step 3, indicating that the reduced matrix simulation was also successful.
5) Converted the MODFLOW-USG model to use the more robust options for unconfined flow provided by the upstream weighted scheme and Newton-Raphson linearization, and activated the AUTOFLOWREDUCE option for pumping so the pumping cannot extract water from below the bottom of a cell.
    a) Simulation results were somewhat similar to those for the MODFLOW-USG model in step 4. The primary source of the difference between the model results was due to higher

pumping in this model, which indicated that wells had gone dry and were eliminated from the step 4 model but were still active in this model.

6) Spot checks comparing water levels from both models identified some model parameters and values that were not implemented in the conversion using Groundwater Vistas. To resolve these issues, primarily associated with drain conductance, some manual changes were made outside of Groundwater Vistas in finalizing conversion of the model from MODFLOW-96 to MODFLOW-USG.

13.3 Validation of the MODFLOW-USG Model

The primary differences between the original MODFLOW-96 and new MODFLOW-USG models are:

- The solver and convergence criteria
- Solver settings related to how the drying of cells occurs
- Inactive nodes in the matrix equation
- Options for unconfined flow
- Extraction of water from below the bottom of a cell via pumping

The hydraulic properties for the two models were graphically displayed and compared by visual inspection. The properties looked the same for the two models, verifying that the conversion to MODFLOW-USG maintained the value and distribution of layer hydraulic properties.

A comparison of simulated hydraulic heads in 2000 for the two models was conducted to validate results for the MODFLOW-USG model. Scatter plots of MODFLOW-USG heads versus MODFLOW-96 heads for model layers representing the Sparta, Queen City, Carrizo, and Simsboro aquifers (model layers 1, 3, 5, and 7) are shown in Figure 12-1. These comparisons show some scatter on the order of about 25 feet from the one to one correlation line. In general, the greatest difference is observed for head values in the outcrop areas of the aquifers.

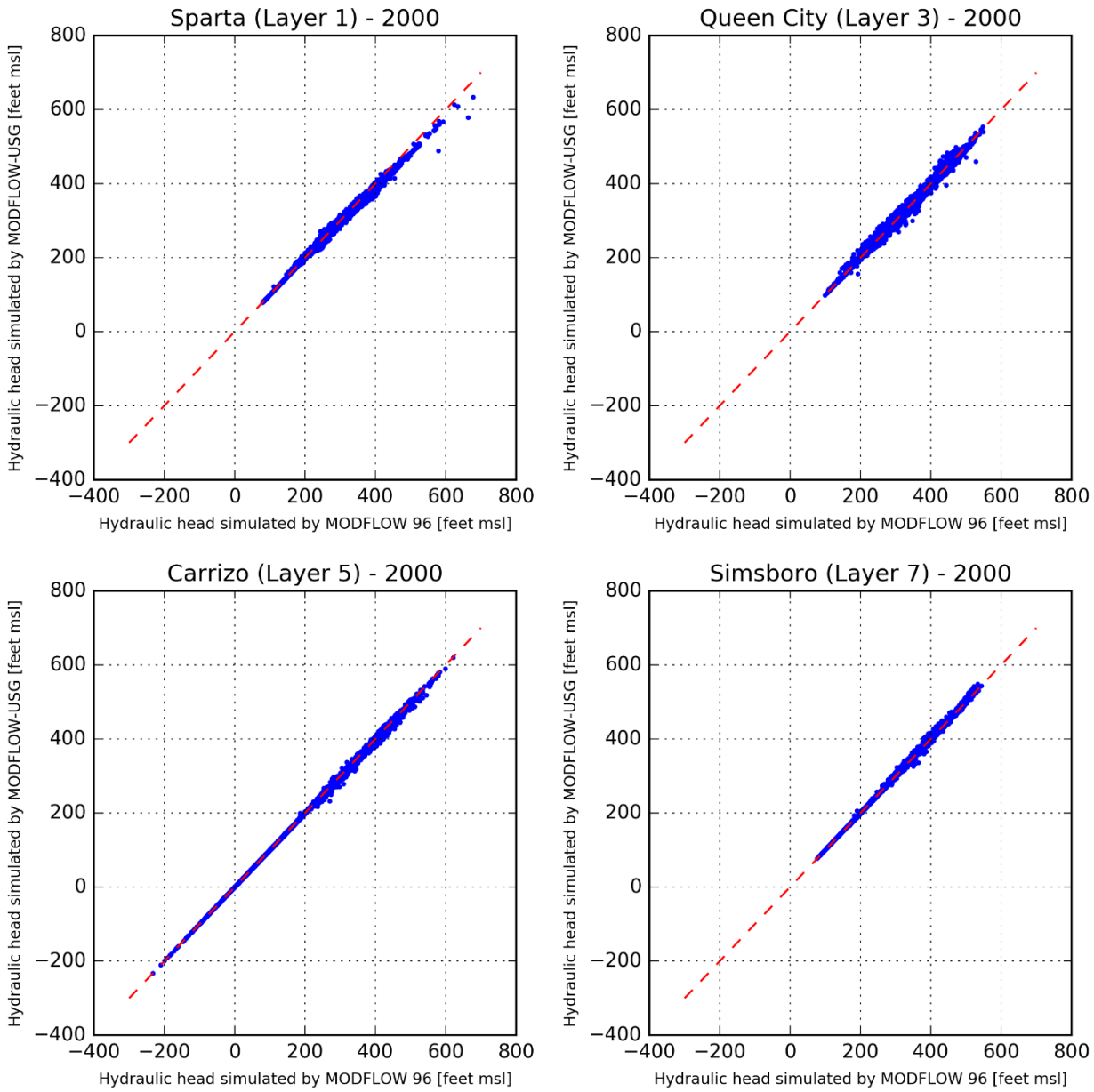

Figure 12-1. Comparison of 2000 heads from the original MODFLOW-96 and updated MODFLOW-USG models for the Sparta and Queen City (top) and Carrizo and Simsboro (bottom) aquifers.